Reversible electronic energy transfer in rotaxane architectures

Shilin Yu

université de BORDEAUX

THESIS

Presented at

UNIVERSITY OF BORDEAUX

DOCTORAL SCHOOL OF CHEMICAL SCIENCES

BY

Shilin YU

TO OBTAIN THE DEGREE OF

DOCTOR

SPECIALTY : ORGANIC CHEMISTRY

Reversible Electronic Energy Transfer in Rotaxane Architectures

---

Defence: 5th September 2018

In front of a jury composed of:

M. A. Jorge PAROLA	Professor Associado at Universidade NOVA de Lisboa	Reporter
Mme. Frédérique LOISEAU	Professor at Université Grenoble Alpes	Reporter
Mme. Stéphanie DELBAERE	Professor at Université de Lille	Président
M. Nathan D. MCCLENAGHAN	Directeur de Recherche CNRS	Supervisor
M. Jean-Luc POZZO	Professor at University of Bordeaux	Co-supervisor

Acknowledgements

Firstly I would like to thank my supervisors, Dr. Nathan D.McClenaghan and Professor Jean-Luc Pozzo, for not only giving me the opportunity to undertake this project, but also for their fantastic support and guidance throughout.

During this multidisciplinary thesis, it was my pleasure to collaborate with the group of Prof. Steve Goldup at the University of Southampton. I want to thank all collaboration partners for their contribution and the fruitful discussion concerning the work with them. Their patience and kindness to answer my questions are greatly appreciated.

I would like to thank all past and present members of the NEO group, especially to Arkadii Kupriakov, Mykhaylo Potopnyk and Sergey Denisov. They are not only my teachers but also good friends. The group is really an outstanding group of people and I feel privileged to have worked alongside them. I wish them all the very best in their future careers.

The CESAMO group and Dr. Isabelle Pianet (CNRS), who helped me with NMR samples and mass spectroscopy, is highly acknowledged. My acknowledgement also goes to Dr. Brice Kauffmann (IECB) for single crystal X-ray structure determination. Jinhua Wang and Yann Ferrand in IECB is also greatly appreciated, for their help and permission to use the gel permeation chromatography.

My deep gratitude goes in particular to China Scholarship Council (CSC) program for financing this research, as well as Université de Bordeaux for providing good working conditions.

Apart of said I would like say my tender thanks to Mom, Dad, Lili. Thanks also to my grandparents and my extended family for all their support and especially to my uncle and maternal grandparents, who unfortunately were unable to see me finish. Thanks to all my friends in China. A special thank you to Washington Shi, Shijian Ma, Jun Hu and Bin Zhu, who kept me going through the trickiest of times.

Table of Contents

General Introduction

With the development of supramolecular chemistry, the field of artificially constructed molecular machines (ACMMs) based on supramolecular self-assembly has attracted much attention during the past few decades. ACMMs was firstly considered by Richard Feynman's (Nobel physics laureate) seminal speech entitled "*There's Plenty of Room at the Bottom*" at the California Institute of Technology in 1959.[1] He inspired scientists to use bottom-up approach to construct nano-scale machines with atoms or molecules, instead of using traditional top-down miniaturization approach. Indeed, molecular motors and machines may be found in a range of biological processes: the exploitation of solar energy, the storage of energy, the ionic transport within the cell. For example, Yoshida and Futai reported their direct observation of the rotation of F_1-ATPase in 1997, as shown in Fig. 0-1.[2] More and more research is dedicated to constructing artificial molecular machines for biological or medical applications, even if it may take more decades, or even over a century.

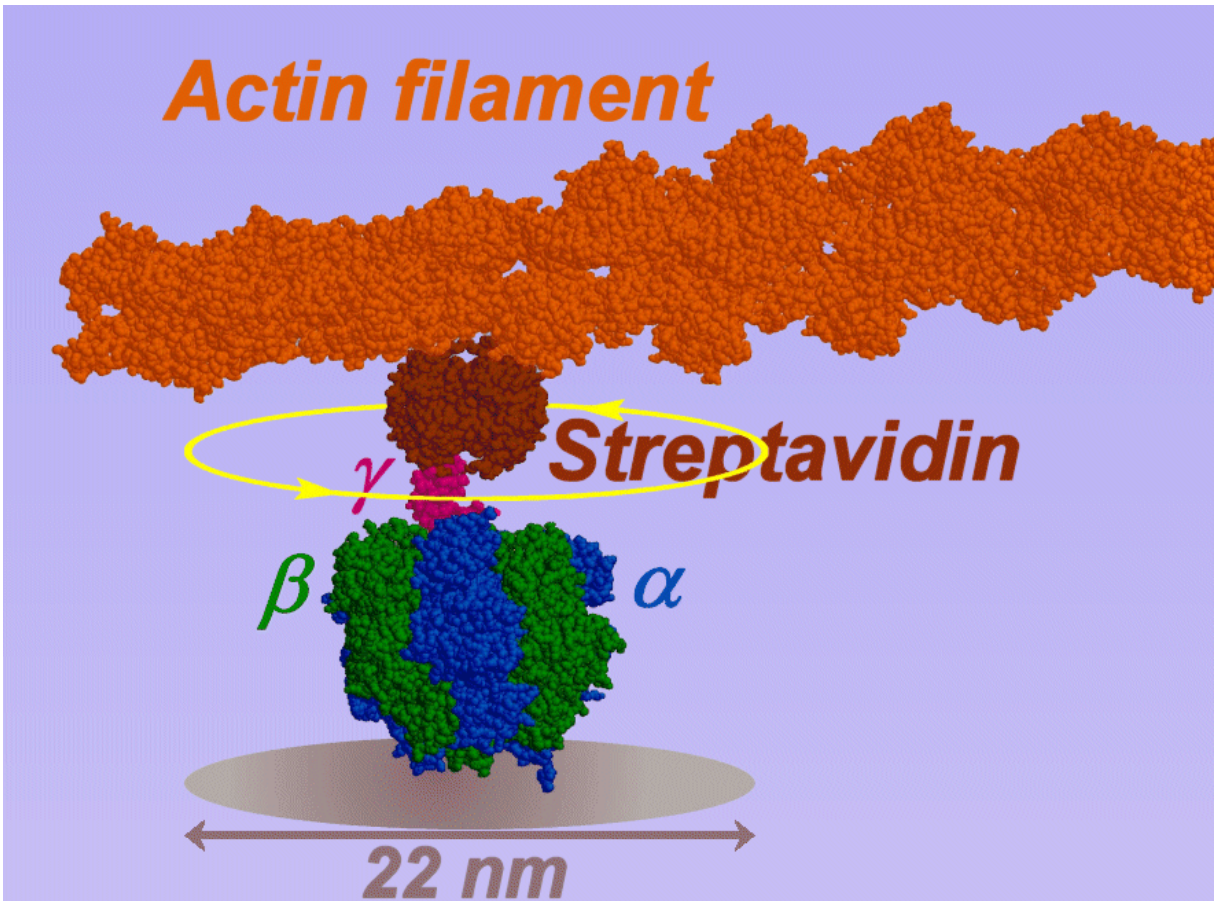

Figure 0-1 Schematic diagram of the rotation of F_1-ATPase.

Rotaxanes, constituted by molecular ring component interpenetrated by a dumbbell component, represent a promising class of molecular machine. Two stoppers on the ends of the dumbbell-

shaped component prevent the dissociation of the ring ensuring its structural integrity. In certain rotaxane designs, under a specific external stimulus, the ring component can move forth and back along the thread of the dumbbell component without separation. Rotaxanes represent ideal systems for the investigation of intermolecular weak interactions and state transitions, and provide model systems for the study of important physical and chemical processes between the components, for example, electronic energy transfer (EET) and electron transfer.

On the other hand, photochemistry studies the reaction or reactivity of molecules in their excited state after absorbing light. Reversible electronic energy transfer (REET) is a process which may occur in bichromophoric systems upon photoexcitation when the lowest-lying excited states between chromophores are quasi-isoenergetic and kinetics of interchromophore are favourable. REET can result in prolongation of the luminescence lifetime and change the nature of the excited state. REET processes have been well studied in covalent dyads. However, few examples of REET process were found in supramolecular systems, and none in kinetically-inert rotaxane systems.

The main objectives in this thesis are to design, construct and study rotaxane systems engineered with reversible electronic energy transfer processes. The main contents and results of this thesis are summarized as follows:

Chapter 1 describes the recent progress in the domain of interlocked molecules and notably molecular machines. A short history of molecular machine design and recent progress is given. The definition of three major classes of interpenetrating molecules (catenane, pseudorotaxane and rotaxane) are introduced and illustrated by examples. Several general strategies to construct rotaxanes are illustrated. Energy sources to power molecular machines, including chemical energy, electrochemical energy and photochemical energy and others are considered. The characterization methods of molecular machine states, including electronic absorption spectroscopy, NMR spectra, fluorescence spectroscopy, other methods are considered. In addition, the potential application of molecular machines in such areas as molecular nano-molecular valves, organic catalysts, organogelators, supramolecular polymers and biological/pharmaceutical potential applications are elaborated. Furthermore, a short introduction to photochemistry and REET process is also given.

In chapter 2, in order to construct a rotaxane based on REET processes, a synthetic strategy is

outlined. Active template metal catalysis (Huisgen and Cadiot-Chodkiewicz reactions) is chosen for the rotaxane formation. In this scenario, the metal ion, which is copper in the current case, serves the dual role of catalysis and template ensuring that the coupling reaction occurs within the macrocycle cavity. Pyrene and ruthenium(II) tris(bipyridine) were chosen to for the bichromophoric dyads to establish REET process as they were anticipated to offer matched energetic levels and appropriate kinetics. Decorated Ru complex can be designed and synthesized as a half thread and a donor group of REET; bipyridine-containing macrocycles with a pyrene group appendage, as an acceptor group of REET, will be designed and developed; half threads comprising trityl groups will be prepared. Rotaxanes engineered with potential REET process is predictable to be constructed by AT-CuAAC, firstly. Once the desired rotaxanes are afforded and confirmed using NMR spectra and HRMS, a series of spectroscopic methods (steady state and time-resolved spectroscopy) allow investigation of their photophysical properties, to show whether the REET process is instilled.

Chapter 3 evokes the possibility of using REET processes to track or control shuttling movements of the macrocycle on threads in rotaxanes. A series of REET rotaxanes with different thread lengths were designed and obtained by AT-CuAAC, confirmed using NMR spectra and HRMS. Different REET processes in these rotaxanes are anticipated to be seen by electronic absorption spectra, time-resolved spectroscopy and steady state spectroscopy. Two REET rotaxanes with different lengths will be also constructed by Cadiot-Chodkiewicz templated method, and confirmed by NMR spectra and HRMS. Due to a diynyl group directly connected to the Ru complex, which changes the MLCT states, different relationship of REET processes and the ring shuttling movements are anticipated.

In chapter 4, the influence of the coordination between Zn^{2+} and a REET [2]rotaxane on photophysical properties of a REET rotaxane is studied. A REET [2]rotaxane with a short thread comprising a triazole moiety was chosen as a rotaxane ligand for the coordination with Zn^{2+}. NMR spectra will be employed to confirm the formation of this rotaxane chelator. Titrations of Zn^{2+} to this REET rotaxane of electronic absorption spectra and luminescence emission spectra, could have a further vision into this coordination and give a binding constant. Transient absorption and luminescence kinetics of this REET rotaxane and its related chelator, will be compared to see how this coordination influence MLCT excited states and REET process. This result would give a deeper insight into the complexation between REET rotaxane and a metal ion, which might develop REET process in rotaxane systems. One approach to

reversible linear electronic energy hopping with varying number of acceptors at fixed distance in rotaxane systems is considered. The modular rotaxane synthesis approach towards a REET [3]rotaxane and its reference [2]rotaxane was designed and synthesized successfully, opening the way to future studies.

A general conclusion is given in chapter 5, while chapter 6 gives experimental details and characterisation of newly synthesized molecules.

[1] Feynman, R. P. Eng. Sci. 1960, 23, 22.

[2] Noji, H.; Yasuda, R.; Yoshida, M.; Kinosita Jr, K. Nature 1997, 386, 299.

Chapter 1 Introduction

1.1 A short introduction of the history of molecular machines

Chemistry is an ancient discipline, but like the development of human society, more and more branches are emerging from this ancient discipline. Supramolecular chemistry is one manifestation. The concepts of supramolecular chemistry, or more specifically host-guest interactions, were first described by Hermann Emil Fischer in 1894. This concept started to emerge as a new field of study in the late 1960's, and was acknowledged by the wider audience following the Nobel Prize awarded in 1987 to three of its pioneers, Donald J. Cram, Jean-Marie Lehn and Charles J. Pedersen, "*for their development and use of molecules with structure-specific interactions of high selectivity, awarded for syntheses of molecules that mimic important biological processes*". Supramolecular chemistry considers two or more chemical entities, which combine through molecular interactions and become a highly sophisticated and well-organized chemical entity. The aim of supramolecular chemistry is to study the structures, functions and properties of these chemical entities.[1] Their main feature is that all components combine through non-covalent molecular interactions. These interactions include: electrostatic interactions (electron-electron, electron-dipole and dipole-dipole), hydrogen bond, π-π stacking, diffusive forces, induction forces (van der Waals interactions), hydrophobic or solvophobic effect.[2] In nature, a wealth of supramolecular interactions are harnessed, which provide powerful biological catalysts for numerous functions within the metabolic processes of living-beings. Since crown ethers were reported in the 1970s,[3] many scientists have devoted themselves to probe and elucidate these non-covalent interactions in chemical and biological systems. As Lehn said, the interaction among the molecules in supramolecular chemistry is like the atoms and covalent bonds in the molecule. He described supramolecular chemisty as "*chemistry beyond the molecule*".[4]

The development of the nanosciences has a powerful influence on the progress of human society. In the last 50 years, the pieces used in machines and devices are becoming more and more miniaturized, which represents a major achievement in the technology field, especially in the information processing field. Chemists could produce nanoscale assemblies with different sizes, shapes, compositions, surface structures, charges and functions through organic synthesis. These assemblies can form structure systems with specific functions and usages after the self-assembly processes in supramolecular chemistry. These are deemed molecular devices or molecular machines.[5]

1.2 Definition of a molecular machine

Simply, a molecular machine could be defined as a rudimentary device[6,7], of nanoscopic size (1-100 nm). It is typically a molecular assembly combining two or more components through non-covalent bond interactions, or reversible covalent bonds. A molecular assembly could produce mechanical motion (output) like macroscopic machines, in response to some appropriate external stimulus (input). The mechanical motions often lead to physical or chemical changes in the system, and some signals can be detected to make a research on the movement of the molecular machine.

The concept of a molecular machine is not new, indeed our body can be regarded as a very sophisticated array of molecular machines. However, artificially constructed molecular machines (ACMMs) is a totally new area, which was firstly considered by Richard Feynman (Noble physics laureate)'s seminal speech entitled "*There's Plenty of Room at the Bottom*" at the California Institute of Technology in 1959.[8] In recent decades, due to the rapid development of scientific technology, our computers are becoming smaller and smaller, and cell phones are becoming smarter and smarter, but this traditional top-down miniaturization approach has been restricted by the physical scale limit. Hence, scientists reversed the thought, trying to use bottom-up approach to construct nano-scale machines with atoms or molecules. In 2016, The Nobel Prize in Chemistry was awarded jointly to Jean-Pierre Sauvage, Sir J. Fraser Stoddart and Bernard L. Feringa "*for the design and synthesis of molecular machines*".

At present, the study of molecular machine mainly includes:

1. types of external stimulus which run or trigger molecular machines;
2. types of molecular machine components' relative motions;
3. methods to detect or control the components' relative motions;
4. different synthetic methods of molecular machines;
5. functions of molecular machines;
6. approaches to computation with molecular machines.

1.3 Types of molecular machine

It is a huge challenge for supramolecular chemists to combine two, or more than two, assemblies to form molecular machines with specific functions through non-covalent bonds interactions. After decades of effort and innovations, chemists have reported many kinds of molecular machines, which have different shapes, use different driving forces to control every

kind of motion mode, in order to contribute different functions. Based on their constitutions, molecular machine topologies can be classified primarily as: pseudorotaxane, rotaxane and catenane, as described below.[9-12]

1.3.1 Molecular machines based on catenanes

Catenanes (*catena* is latin for chain) consist of two or more mechanically interlocked ring-shaped molecules that cannot be separated without breaking at least one covalent linkage, e.g., the [n]catenane (type A in Figure 1.1; n = 2 as it refers to the number of cyclic components). The interlocked macrocycles of catenanes can rotate and move within each other.[13]

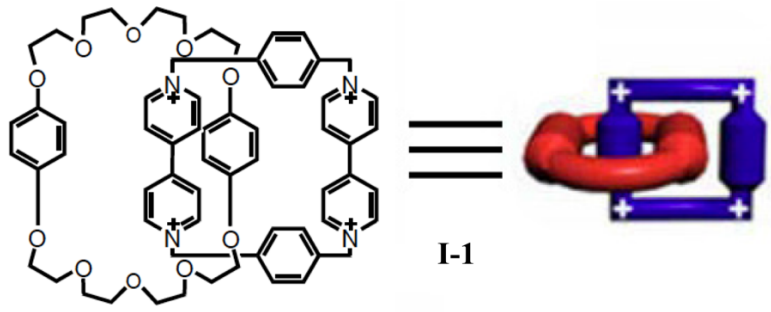

Figure 1.1 Example of a [2]catenane system.

In a [2]catenane, one cyclic component could slide or rotate relative to the other cyclic component. Schuster et al.[14] reported that they combined a cyclic component and a thread component by the coordination between the cuprous ion and phenanthroline ligands, then used a click reaction for cyclisation to afford a [2]catenane **I-2.Cu**. After removing the cuprous ion by adding KCN, the rotation of the macrocycle in [2]catenane **I-2** resulted (Fig. 1.2).

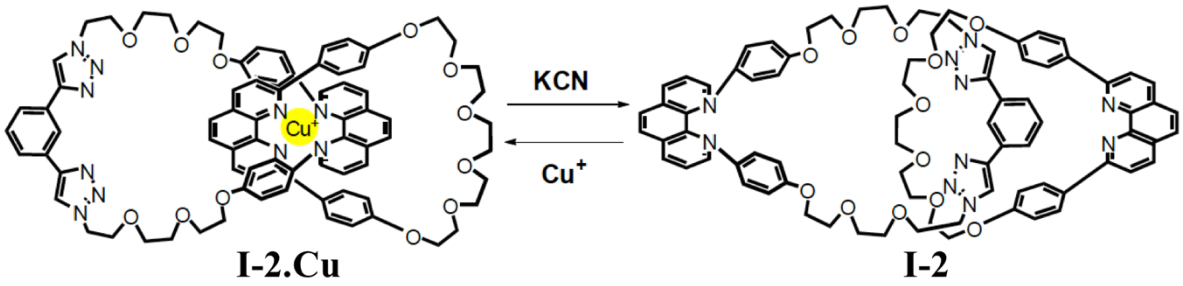

Figure 1.2 [2]Catenane system reported by Schuster et al.

Leigh et al.[15] reported a [2]catenane **I-3** which has 3 recognition stations, as in Fig. 1.3. **I-3**

consists of one large macrocycle and one small macrocycle. The small cyclic component has different binding constants with the three recognition stations, so the unidirectional rotation of the small cyclic component over the big cyclic component can be controlled.

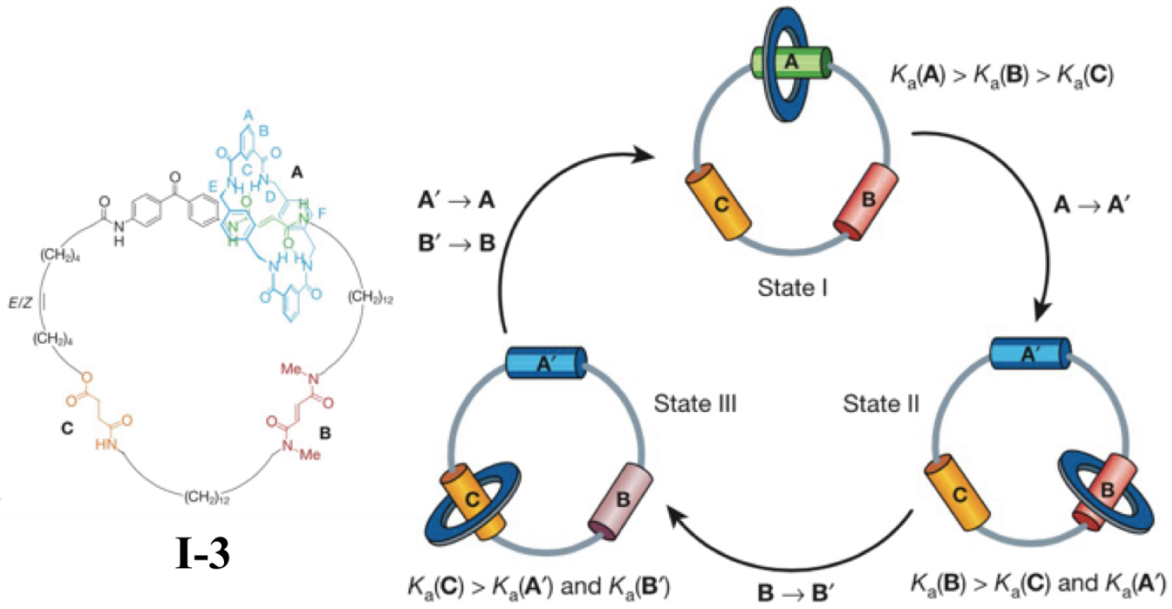

Figure 1.3 Catenane **I-3** containing three recognition sites reported by Leigh et al. Copyright (2003) Springer Nature.

1.3.2 Molecular machine based on pseudorotaxane

A pseudorotaxane is a supramolecular assembly, which consists of a ring component and an interpenetrating thread component (e.g., **I-4** in Fig. 1.4). As there are not the building blocks at two sides of the thread component, there exists the inclusion-dissociation balance between the ring component and the thread component, which is similar to the interposition-extraction motion.[16]

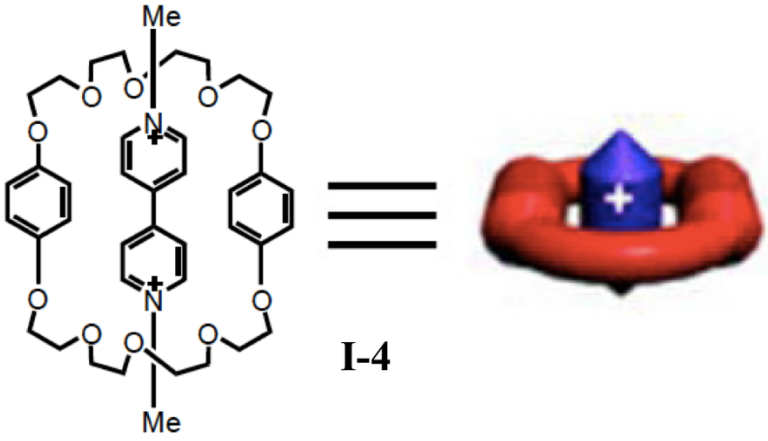

I-4

Figure 1.4 Example **I-4** of a [2]pseudorotaxane system.

Pseudorotaxane complexes can dissociate to give the free constituent molecular units under application of an external stimulus, and under the reversed stimulus, these units could combine with each other again. The pseudorotaxane's motion modes are shown in Fig. 1.5.[17] Further, chemists have found that pseudorotaxanes have the potential to be used with respect to drug release and antibacterial regulation.[18,19]

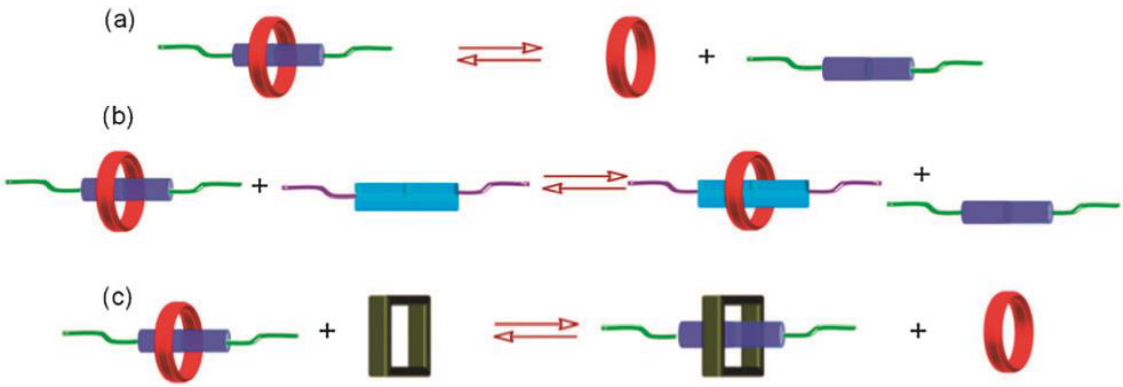

Figure 1.5 Schematic representations of a pseudorotaxane system. Copyright (2015) American Chemical Society.

A pseudorotaxane **I-5** in which dibenzo-24-crown-8 macrocycle (DB24C8) has a photo-induced directional movement through the thread component was reported by the Credi group in 2012.[20] As shown in Fig. 1.6, a thread compound **I-5T** was synthesized with a secondary amine salt part, where one side is a *trans*-azobenzene group, and the other side is cyclopentyl group. When the macrocyclic component and thread component are mixed, **I-5T** mainly crosses through the macrocycle from the *trans*-azobenzene part, and forms the pseudorotaxane. While under light irradiation at 365 nm, the *trans*-azobenzene group turns to be *cis*-form, and if a

certain amount of potassium ion is added into the pseudorotaxane system, dibenzo-24-crown-8 macrocycle would disassociate from the cyclopentyl group side of the secondary amine salt and combine with potassium ion, because the binding constant between DB24C8 and potassium ion is stronger than the binding constant between DB24C8 and the secondary amine salt. Then if the mixture is heated, the azobenzene group turns to be *trans*-form. A certain amount of dibenzo-18-crown-6 is added, since the binding constant between potassium ion and dibenzo-18-crown-6 is stronger, then the released DB24C8 can recombine with the secondary amine salt by crossing from the azobenzene side. Thus the directional movement of DB24C8 was achieved in the pseudorotaxane system.

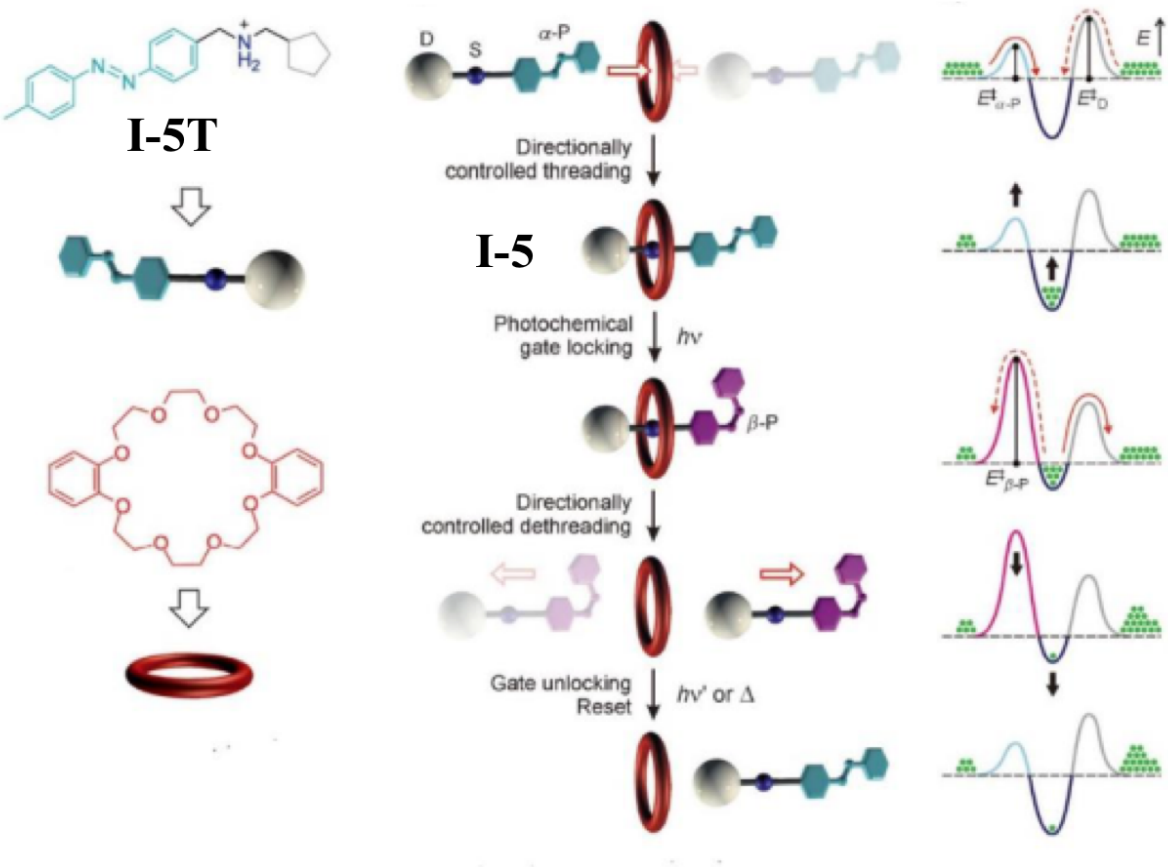

Figure 1.6 A pseudorotaxane **I-5** that photoactivated directionally controlled movement reported by Credi et al. Copyright (2012) John Wiley and Sons.

1.3.3 Molecular machine based on rotaxane

Rotaxane (*rota* is latin for wheel, and *axis* is Latin for axle), means "any compounds having a molecular structure in which a chain of atoms is threaded through a ring and, though not

chemically bonded to the ring, is mechanically constrained in position by the ring's structure", from the definition in the Oxford English dictionary. Usually, a rotaxane is composed of one "dumbbell" component (guest component) and one or more ring components (host components).[21] The ring component is crossed by the thread component and stopped by the two big building blocks, such that the ring component and the thread component have combined together with a non-covalent, mechanical bond. Concerning rotaxane nomenclature, *n* represents the number sum of components which combine with each other with non-covalent bonds in the rotaxane system. Apparently, when *n* is equal to 2, it will be the simplest rotaxane. Some of schematic representations of the rotaxane structures are shown in Fig. 1.7.

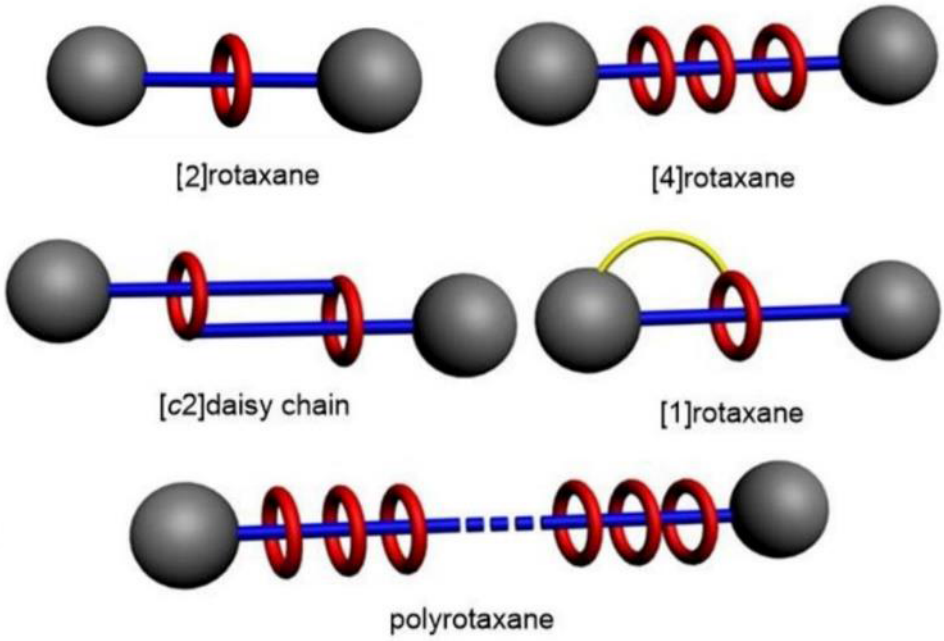

Figure 1.7. Schematic representation of the structures of rotaxanes. Copyright (2006) American Chemical Society.

In 1991, J. Fraser Stoddart reported the first molecular shuttle **I-6**,[22] as showed in Fig. 8. There are the same two recognition sites, hydroquinol with electron rich property, in the "dumbbell" component, which are separated by the polyether chain. Blocking groups are triisopropylsilyl groups, and the ring component is cyclobis(paraquat-p-phenylene) ($CBPQT^{4+}$). As the recognition stations are the same, the ring component is having the shuttling motion on the thread.

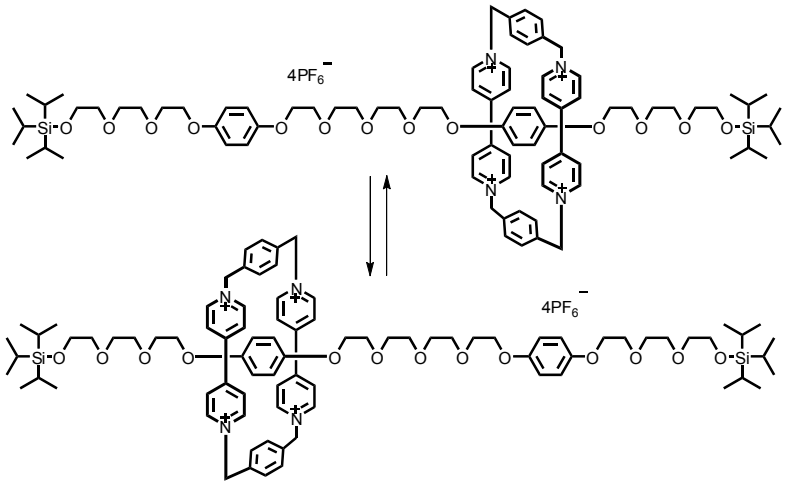

Figure 1.8. The first molecular shuttle **I-6** reported by Stoddart et al.

1.4 The synthesis of rotaxanes

There are several different strategies to synthesize rotaxanes, detailed below and illustrated in Figure 1.9.

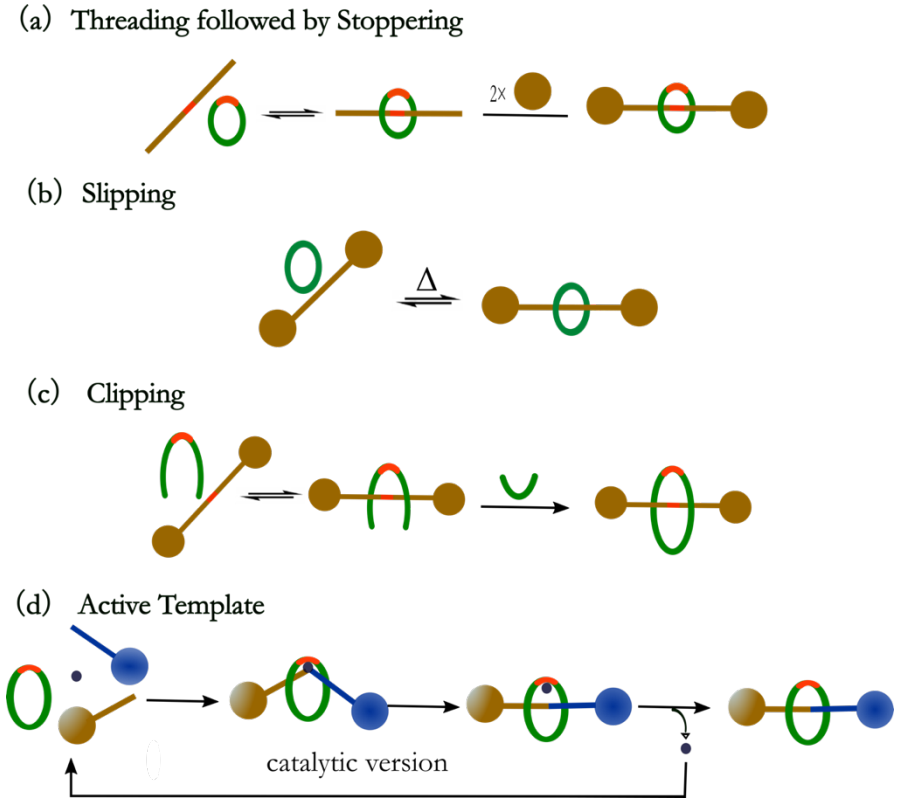

Figure 1.9 Schematic representation of the synthetic methods of rotaxanes.

The threading followed by stoppering approach involves mixing the ring component and thread

component to form a pseudorotaxane using specific interaction,[23] then using efficient covalent reactions to introduce bulky blocking groups at both ends of the thread component to form a kinetically-inert [2]rotaxane (Fig. 1.9a). The specific reactions to effect covalent capture include esterification,[24-29] Wittig reaction,[30-35] metal-catalytic olefin metathesis and so on.[36-42] The slippage approach consists in mixing the ring component and "dumbbell" component and heating, such that the ring component could overcome the potential energy barrier and slip over the stopper thereby entering onto the "dumbbell" component, the resulting rotaxane being formed. When the temperature is decreased, the ring component and "dumbbell" component could not separate from each other because of the significant energy barrier imposed by the bulky stoppers (Fig. 1.9b).[43,44] In the clipping approach, the macrocyclisation of the ring precursor is the last step to afford the rotaxane. During this step, the "dumbbell" component serves as a template for the ring precursor macrocyclisation (Fig. 1.9c). Beer has significantly contributed to this field.[45-47] Active template synthesis is a powerful recent strategy to construct rotaxanes. As shown in Fig. 1.9.d, the key feature is that the metal ion acts as both a template for entwining or threading the ring and the half-thread components and as a catalyst for capturing the mechanically-interlocked structures by covalent bond formation.[48-50] Since its inception in 2006, a lot of different metal-catalyzed reactions have been used in rotaxane synthesis, such as the copper(I)-catalyzed terminal alkyne-azide cycloaddition (the CuAAC ''click'' reaction),[51] copper(I)-mediated Cadiot–Chodkiewicz heterocoupling of a terminal alkyne with an alkyne halide[52], palladium-catalyzed oxidative Heck couplings,[53] and nickel- and copper-catalyzed alkyne homocouplings and heterocouplings.[54] Goldup recently reported a > 95% yield in rotaxane formation using the CuAAC ''click'' reaction.[55]

1.5 Energy sources of molecular machines

There has to be a dynamic aspect to the molecular machine, to let the machine run and perform a function, as in the macroscopic machine. An external stimulus should drive the rotaxane movement, marking a shift out of equilibrium, as a result of weakening or changing the interactions between the host part and guest part, so the choice of an appropriate external stimulus depends on the properties of the interactions. Chemical energy (such as acid/base), entropy change and solvent change could drive the hydrogen bond type rotaxane; Chemical energy (such as oxidizer/reducer), electrochemical energy (such as reduction/oxidation process), photochemical energy (such as photo-induced reduction/oxidation process) could be used in the rotaxane which is based on the electron donor/acceptor interaction. Furthermore, photo-

isomerization also could drive the rotaxane sub-component movement based on steric effects.

1.5.1 Chemical energy

There are lots of chemical energy driven molecular machines reported in the literature.[56-62] The most common way is acid/base driven, which features a high conversion rate, indeed even 100% conversion is possible.

Credi, Stoddart et al.[63] reported a molecular machine **I-7** that behaves in a manner reminiscent to a nanoscale elevator (Fig. 1.10), which is driven by acid/base regulation, and consists of a trifurcated drilling riglike component containing two different recognition sites at different levels in each of its three legs that are interlocked by a platform. In this nanoscale elevator **I-7**, the trifurcated host part is three DB24C8 rings fused together within a triphenylene core, the trifurcated guest contains two different stations namely, three dialkylammonium (-NH_2^+-) centers and three bipyridinium ($BIPY^{2+}$) units. The binding force between crown ether and dialkylammonium (-NH_2^+-) is from strong [N^+-H•••O] hydrogen bonding and weak [C-H•••O] interactions, while the DB24C8 and $BIPY^{2+}$ unit are stabilized by [C-H•••O] and [π- π] stacking interactions. On addition of a base (a tertiary amine) to a solution of the molecular elevator, the -NH_2^+- center deprotonates, which destroys the strong intercomponent hydrogen bonding, and DB24C8 ring moves to the $BIPY^{2+}$ unit; subsequent addition of acid restores the -NH_2^+- center, and DB24C8 ring could move back to encircle this recognition site. This chemically-driven operation of a two-component molecular machine behaves like a nanometer-scale elevator. This nanoactuator **I-7** is ca. 2.5 nm in height with diameter of ca. 3.5 nm. The energy supplied by an acid-base reaction could raise and lower the platform between the two levels on the rig's legs. The distance traveled by the platform is about 0.7 nm, and the elevator movement from the upper to lower level could generate a force of up to ca.200 pN.

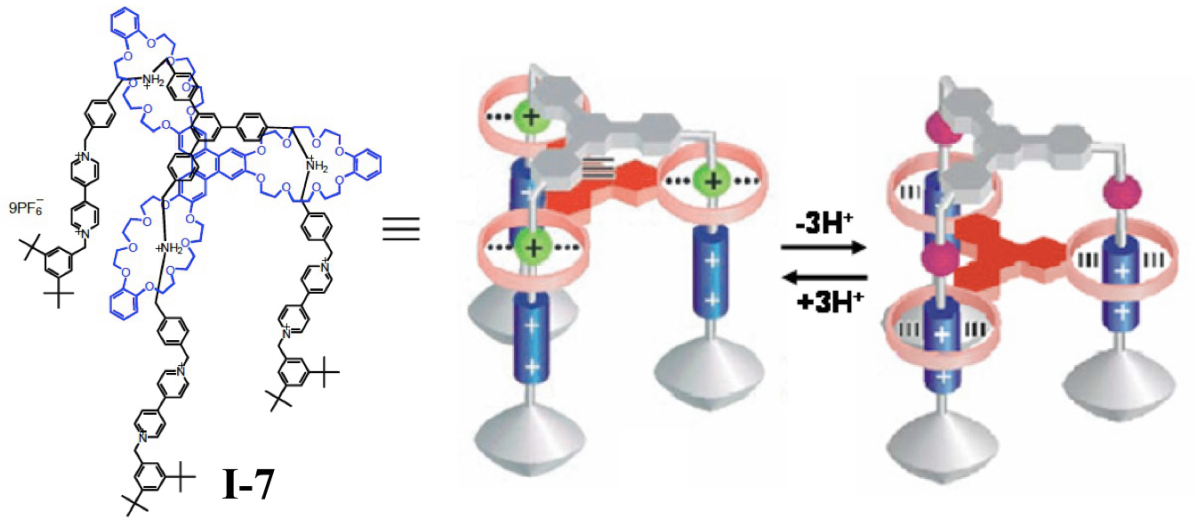

Figure 1.10 The acid-base driven molecular elevator **I-7** based on crown ether reported by Stoddart et al. Copyright (1998) American Chemical Society.

1.5.2 Electrochemical energy

Like the macroscopic machine, the electrochemical energy could also be used as the energy source of a rotaxane.[64-70] Molecular machines based on the π-electron acceptor/donor interaction could aid movements through oxidizing the electron donor or reducing the electron acceptor. These oxidation-reduction reactions could be contributed by changing the voltage.

Sauvage et al. reported a two-station [2]rotaxane **I-7** (Fig. 1.11) consisting of a dpbiiq-incorporating macrocycle (dpbiiq: 8,8'-diphen-yl-3,3'-bisisoquinoline) threaded by a coordinating fragment whose complexing units are a dpp and a terpy ligand (dpp: 2,9-diphenyl-1,10-phenanthro-line; terpy: 2,2',6',2''-terpyridine).[71] They found the oxidation/reduction of ions could change the coordination of ions, enabling the shuttling and rotate motion of the host molecule in **I-8**.

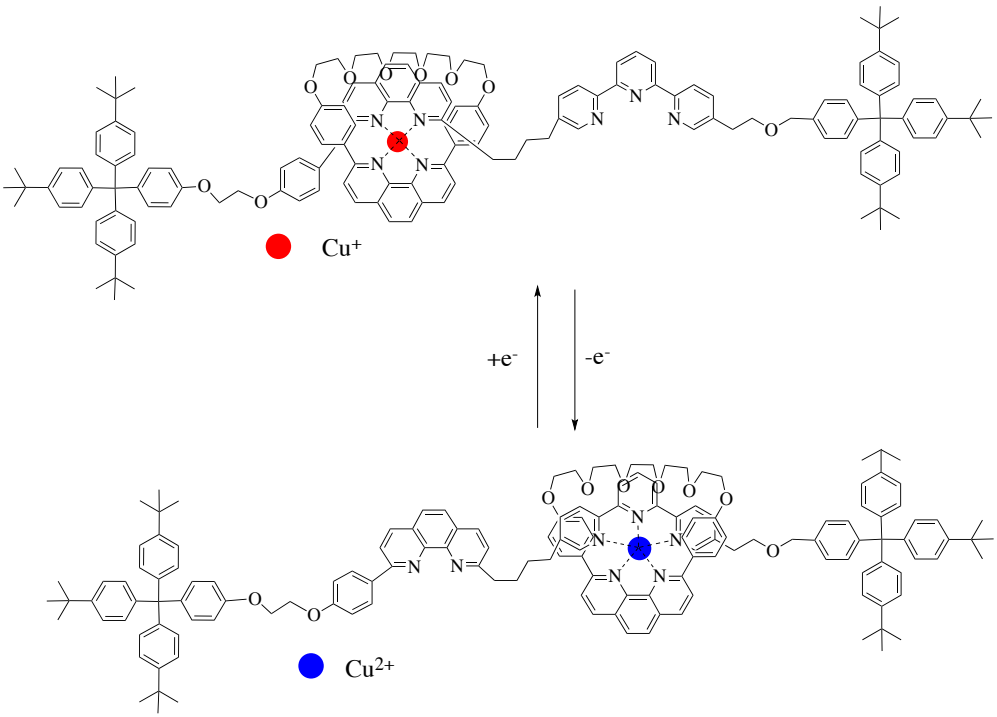

Figure 1.11 The electrochemically-driven rotaxane **I-8** reported by Sauvage et al.

1.5.3 Photochemical energy

Photochemical energy cannot produce mechanical movements directly, but it could trigger photochemical reactions, which could induce the movements of molecular machines.[72-77] Compared with other driven methods, optical energy is clean, the manipulation is simple and rapid, and it could be applied in very fast processes. A straightforward photochemical reaction is that light illumination drive conversion the -N=N- and -C=C- from *trans*-form (low energy) to *cis*-form (higher energy). Furthermore, this process can be reversible either thermally or photochemically, on irradiating with light of a different wavelength. A big polarity change of the photochromic group during color change plus the hydrogen-bond interaction is another popular way to drive the movements of rotaxanes.

Stoddart, Balzani et al.[78] reported a photochemically-driven molecular-level abacus **I-9**, which structure is shown in Fig. 1.12.a. Its thread contains ruthenium(II) complex $[Ru(bpy)_3]^{2+}$ ($\mathbf{P}^{2+}$) serving as a photosensitizer and as a stopper, the second stopper is tetraphenylmethane derivative group, as a classic stopper (**T**). The electron-accepting stations are 4,4'-bipyridinium unit($\mathbf{A_1}^{2+}$) and 3,3'-dimethyl-4,4'-bipyridinium unit ($\mathbf{A_2}^{2+}$). The rigid spacer **S** consists of three *p*-phenylene units, and the ring as a π-electron-donator is bis-*p*-phenylene[34]crown-10. The $\mathbf{A_1}$ unit is a stronger electron-acceptor station than $\mathbf{A_2}$, so the ring (**R**) encircles $\mathbf{A_1}$ unit at the ground state.

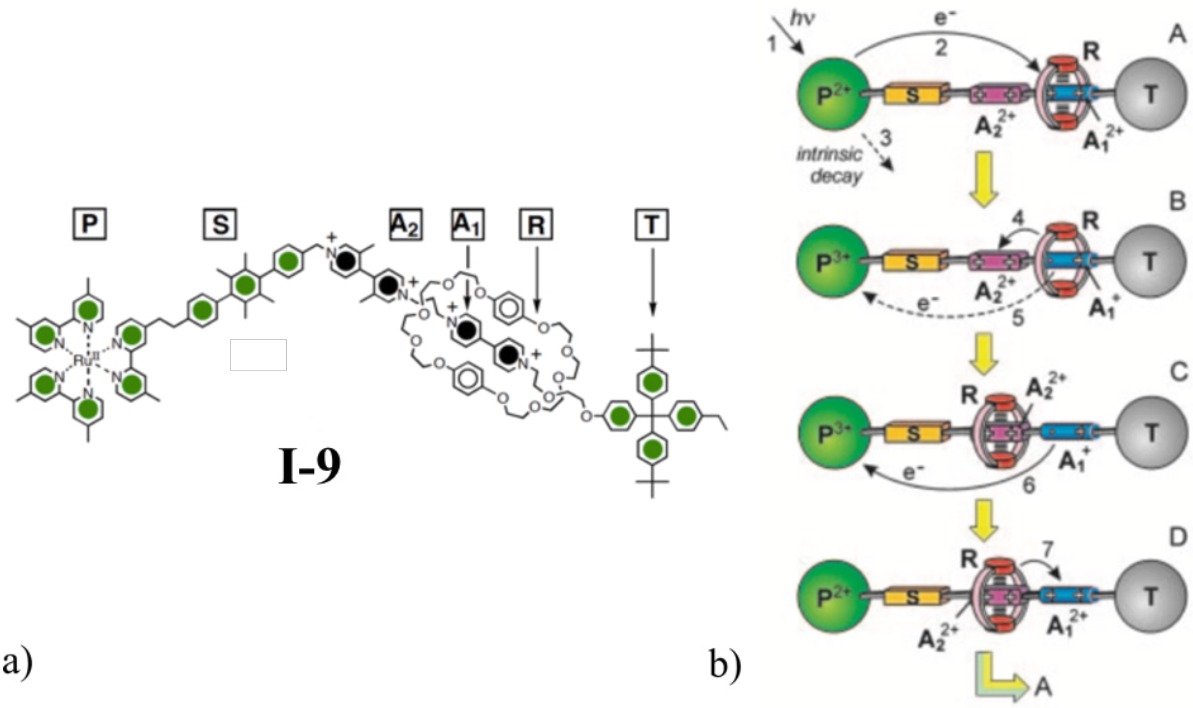

Figure 1.12 a) Structural formula of rotaxane **I-9**; b) mechanisms of the photochemically driven ring shuttling in rotaxane **I-9**. Copyright (2006) National Academy of Sciences, U.S.A.

The shuttling motion of **R** from $\mathbf{A_2}$ to $\mathbf{A_1}$ would occur (Fig. 1.12b) upon the one-electron reduction of $\mathbf{A_1}$ by visible light. Excitation of $\mathbf{P}^{2+}$ by light (step 1) results in the electron transfer from $\mathbf{P}^{2+}$ to $\mathbf{V_1}^{2+}$ (step 2), which competes with the intrinsic decay of the $\mathbf{P}^{2+}$ excited state (step 3). Upon reduction of $\mathbf{V_1}^{2+}$, deactivating $\mathbf{V_1}^{2+}$ by formation of $\mathbf{V_1}^{+\bullet}$, the ring moves to $\mathbf{V_2}^{2+}$ (step 4), which competes with the back electron transfer from $\mathbf{V_1}^{+\bullet}$ to the oxidized unit $\mathbf{P}^{3+}$ (step 5). The back electron transfer from the reduced station $\mathbf{V_1}^{+\bullet}$ to the oxidized unit $\mathbf{P}^{3+}$ (step 6) restores the electron-acceptor ability of $\mathbf{V_1}^{+\bullet}$ by formation of $\mathbf{V_1}^{2+}$. As a result, a back movement of the ring from $\mathbf{V_2}^{2+}$ occurs (step 7). The above forward and backward movement of the ring is driven by photochemical energy.

Leigh et al[79] reported a photoinduced reversible molecular shuttle **I-10** without the formation of any by-products, as is the case in chemically driven system. The system features a fast and reversible ring translocation between two hydrogen-bonding stations and a much slower back electron-transfer process after a nanosecond laser pulse. As shown in Fig. 1.13, [2]rotaxane **I-10** is composed of a benzylic amide macrocycle interlocked onto a thread, which has two potential hydrogen-bonding stations a succinamide (*succ*) station and a 3,6-di-*tert*-butyl-1,8-naphthalimide (*ni*) unit - separated by a $-(CH_2)_{12}-$ alkyl spacer. At room temperature, in a solution of acetonitrile, the macrocycle was held around the *succ* station by two sets of

bifurcated hydrogen bonds because the *ni* station is a poor H-bond acceptor. Laser excitation of the *ni* unit in the presence of an external donor led to the electron transfer process, and the *ni* unit was reduced to an anion radical, which binds more strongly with the macrocycle than the *succ* station; hence, the macrocycle moved to the $ni^{\bullet-}$ station. Remarkably the movement only took about 1 μs, and the charge recombination occurs after 100 μs, whereupon the oxidized donor recovered to its initial state and the macrocycle shuttled back to its original position.

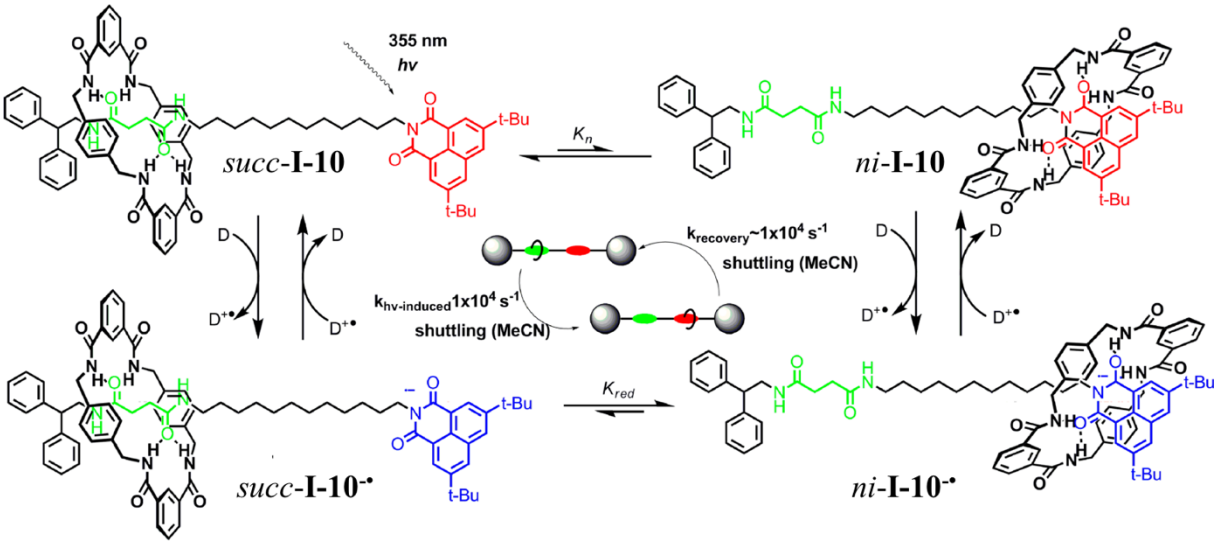

Figure 1.13 Photoinduced fast translational motion in the hydrogen-bonded molecular shuttle **I-10**. Copyright (2001) the American Association for the Advancement of Science.

Qu et al[80] reported a multistate [2]rotaxane **I-11** comprising an α-cyclodextrin (α-CD) macrocycle interlocked onto a dumbbell that has two different photoswitchable binding sites, namely an azobenzene site and a stilbene site, and is end-trapped by two fluorescent naphthalimide moieties, 4-amino-1,8 naphthalimide-3,6-disulfonic disodium salt (stopper A) and 1,8-naphthalimide-5-sulfonic sodium salt (stopper B; Fig.1.14). The photoactive units can be switched independently upon light irradiation at different wavelengths (UV/Vis). The multistate [2]rotaxane is converted between one dynamic state and three static states upon light irradiation. In a solution of [d_6]DMSO, the state (*E,E*)-**1** is the dynamic state in which the macrocycle moves forth and back between the azobenzene and stilbene sites. State (*E,E*)-**I-11** is converted into ($Z_{N=N}$,$E_{C=C}$)-**I-11** or ($E_{N=N}$,$Z_{C=C}$)-**I-11** by photoisomerization upon irradiation at the wavelength of 380 nm or 313 nm, respectively. Finally, further irradiation of isomer $Z_{N=N}$,$E_{C=C}$ at 313 nm or isomer $E_{N=N}$,$Z_{C=C}$ at 380 nm can generate (*Z,Z*)-**I-11**. Moreover, each photochemical reaction is fully reversible. The three Z isomers could be shifted back to the original state (*E,E*)-**I-11** by irradiation with UV light of another wavelength, as shown in Fig.

1.14. Most importantly, the multistate [2]rotaxane operations have pointed a way to design complicated logic circuits based on one molecule.

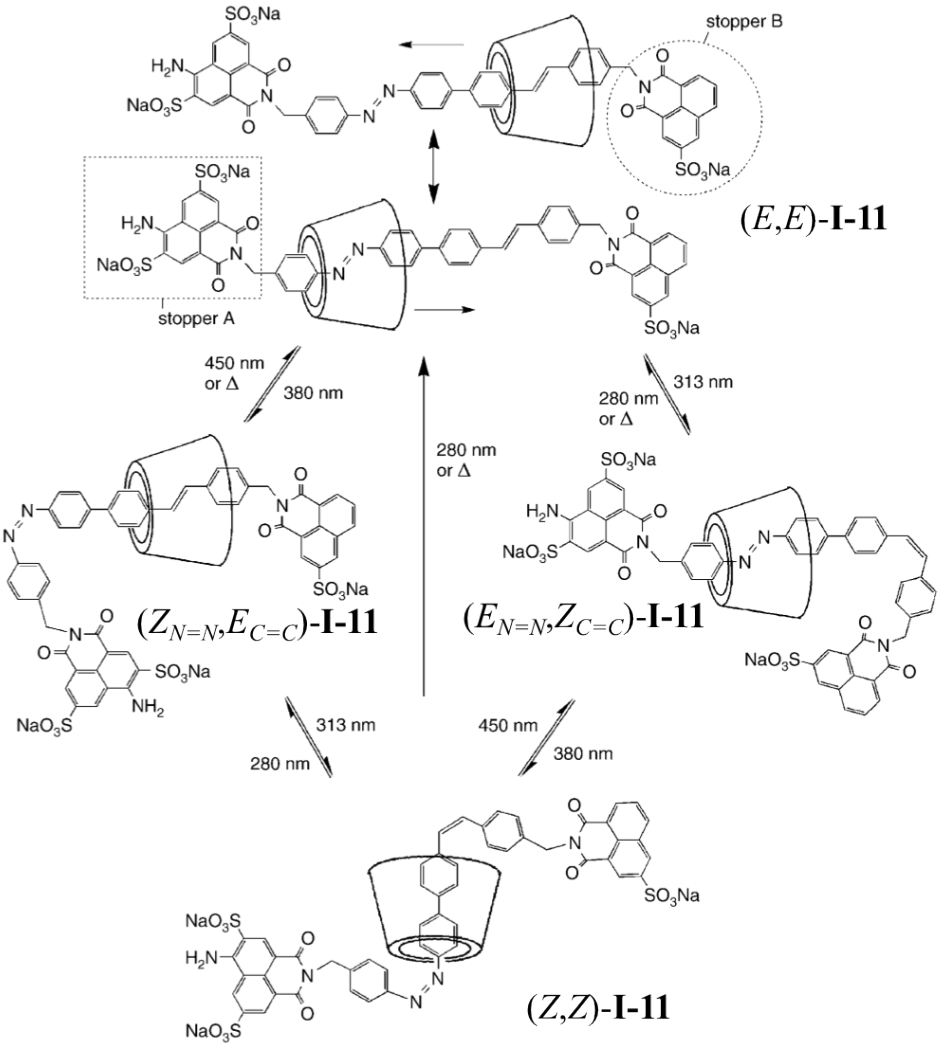

Figure. 1.14 The intrinsic interconversion network of the a-cyclodextrin/azobenzene–stilbene [2]rotaxane **I-11** between the four states: one E,E isomer ((*E*,*E*)-**I-11**), two E,Z isomers (($Z_{N=N}$,$E_{C=C}$)-**I-11**), ($E_{N=N}$,$Z_{C=C}$)-**I-11**), and one Z,Z isomer ((*Z*,*Z*)-**I-11**). Copyright (2012) John Wiley and Sons.

1.5.4 Other energy sources

Additionally, solvent change and changes in entropy[81-84] have also been used to drive molecular machines.

Aurelio et al[83] reported a solvent switchable rotaxane **I-12** comprising a macrocycle functionalized with two ferrocenyl units, a thread equipped with a pyrene unit, as a fluorophore

and a stopper, a diphenyl stopper, an alkyl station and a 1,4-diamide station. As shown in Fig. 1.15.a, this solvent switchable molecular shuttle has three different states, two non-degenerate and one degenerate states, which can be obtained in different solvents at room temperature. When the rotaxane is in chloroform/THF, it is at state **I-12A**, the ring encircles the 1,4-diamide station. Conversely, in DMSO, the macrocycle moves from 1,4-diamide station to alkyl station, due to the weakened hydrogen bonds between the macrocycle and 1,4-diamide staton, forming translational isomer **I-12B**; while in DMF, the macrocycle would occur a shuttling movement between two stations, affording a conformer **I-12A:B**. These three states can be tracked by ^{1}H NMR, and the comparison of fluorescence intensities of three conformers are shown in Fig. 1.15.b. Since the fluorescence of the pyrene moiety can be quenched by ferrocenyl units when it is close to ferrocenyl units, high contrast changes in fluorescence intensity of the pyrene stopper in the three conformers can be easily seen.

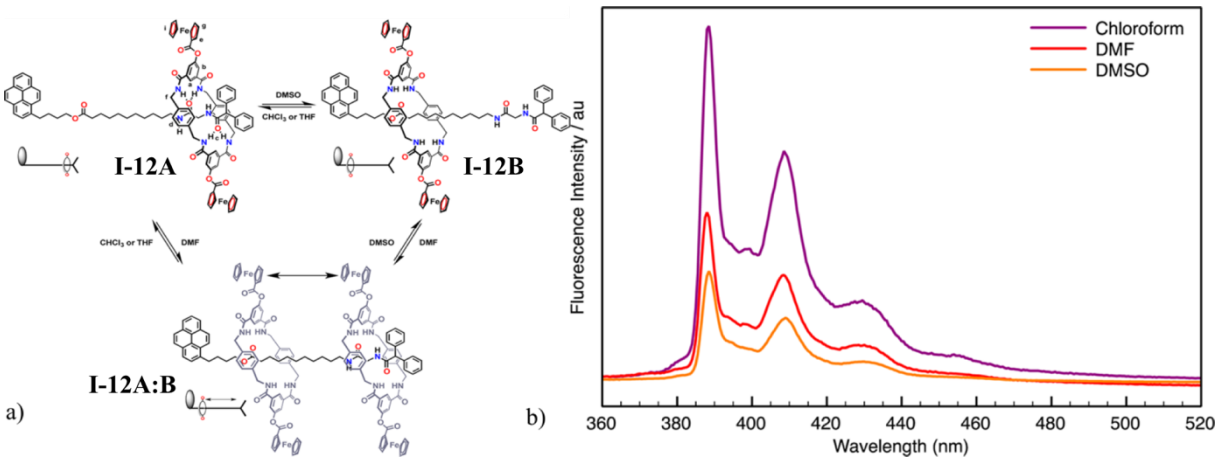

Figure. 1.15 a) Solvent switchable behavior of the studied molecular shuttle **I-12** in different solvents at room temperature; b) Comparison of the fluorescence intensities of the molecular shuttle in different solvents (λ_{ex} = 325 nm). Copyright (2013) American Chemical Society.

Kawai et al. constructed a molecular shuttle **I-13** with reversibly entropy-driven translational isomerism with accurate positional discrimination, the rotaxane structures and scheme are shown in Fig. 1.16.[84] When the sample is at low temperature, compound **I-13B** is formed; conversely, at high temperature, the formation of rotaxane **I-13R** was observed by ^{1}H NMR. In this reversible process, imine-bond formation and hydrogen-bond cleavage of rotaxane **I-13B** are thermodynamically matched processes (enthalpically favoured and entropically disfavoured processes), while imine-bond cleavage and hydrogen-bond formation of rotaxane **I-13R** are entropically favoured and enthalpically disfavoured processes. This discovery holds promise

for the further development of physical-driven molecular machines with an obvious transition responding to minor temperature changes.

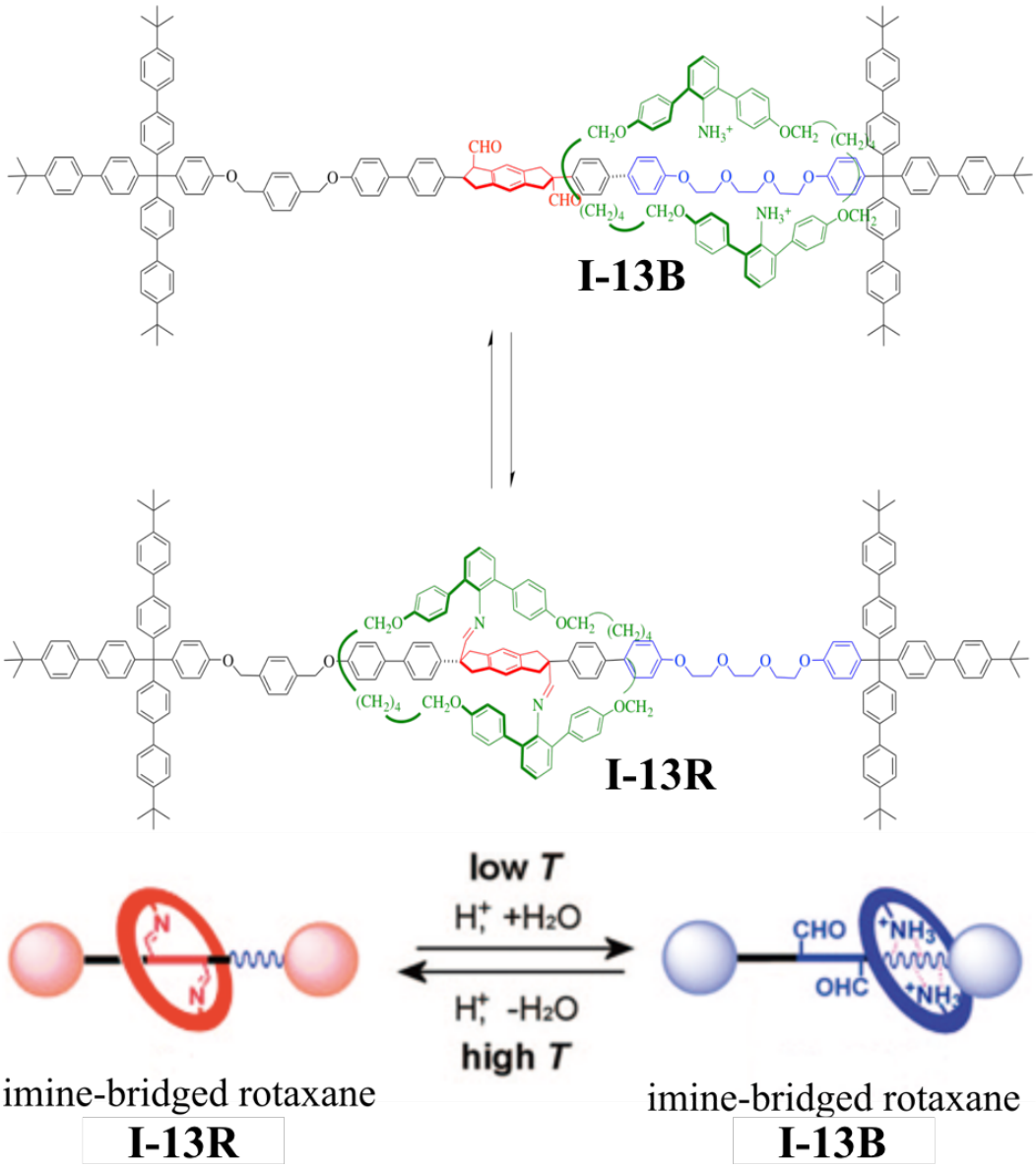

Fig. 1.16 An entropy-driven molecular shuttle **I-13** with reversible translational isomerisation. Copyright (2008) American Chemical Society.

1.6 Characterisation methods of molecular machine states

To verify every function and track state changes of molecular machines, we have to make a clear characterisation and identification of positions and states of molecular machines. Since the produced movements of host units caused by the conformation changes of molecular machines is very weak, there is a strong need to develop many kinds of tools and ways to detect

this weak change. Currently, methods and techniques to identify and detect positions and states of molecular machines mainly include: electronic absorption spectroscopy, Nuclear Magnetic Resonance (NMR), fluorescence, cyclic voltammetry, Induced Circular Dichroism Spectrum (*vide infra*).

1.6.1 Electronic absorption spectroscopy

Movements of host units in a molecular machine could weaken a specific interaction and produce a new interaction at the same time. So the host units' change in a molecular machine could cause an electronic change, which would show different absorption spectra.[85-88] UV-visible absorption spectroscopy is a rapid and straightforward way to detect operating states of molecular machines.

Goldup et al [89] reported a rotaxane (Fig. 1.17.a) based on a simple urea motif that binds F^- selectively as a separated ion pair with H^+ and reports the anion binding event through the absorption switch-on response. The host unit selectively binds F^- over more basic anions, which deprotonate the framework and less basic anions that bind more weakly. UV-vis titration measurement of rotaxane **I-14.HBF$_4$** with TBAF (0 - 12 eq.) in $CHCl_3/CH_3CN$ at 298 K showed the absorption intensity and shift change, which means the deprotonation of the host to regenerate **I-14** was slow.

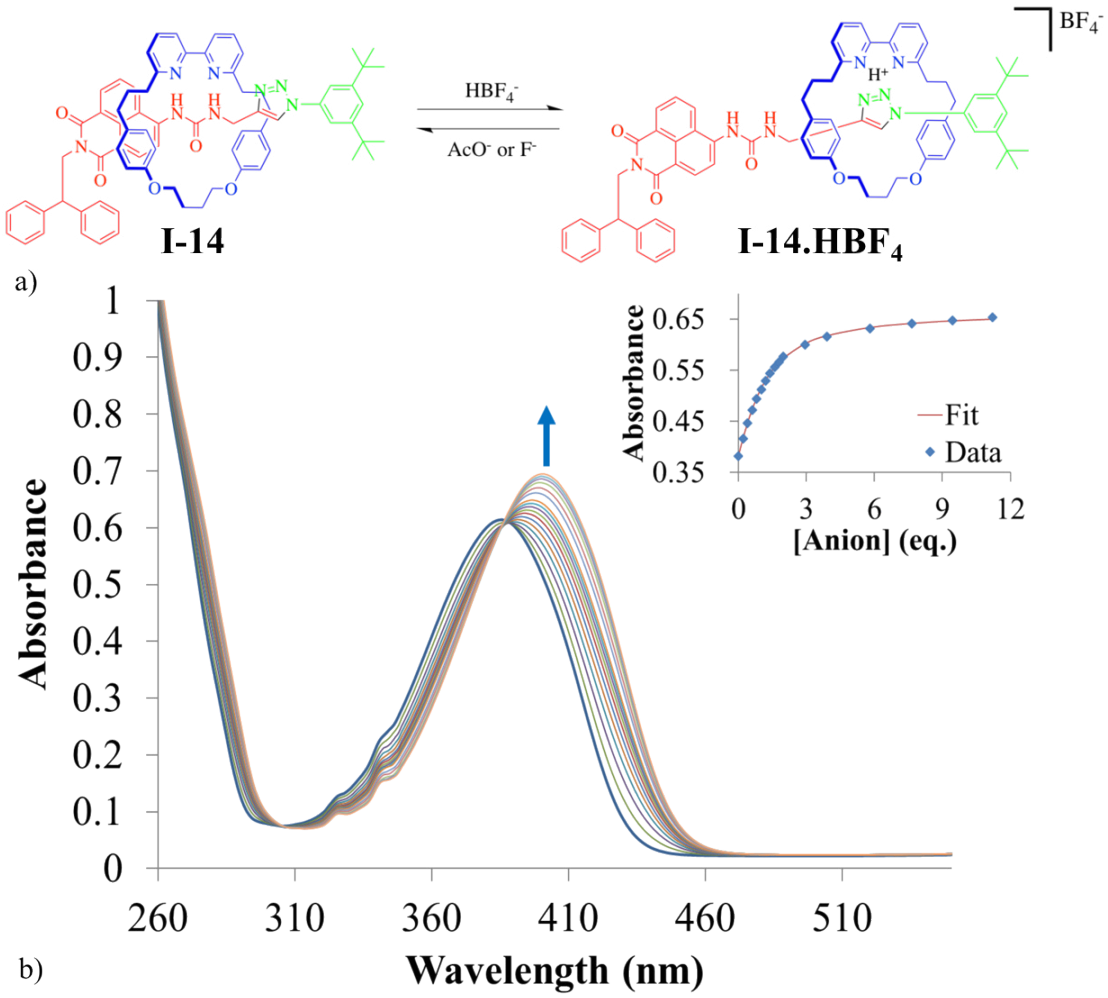

Figure. 1.17.a) Rotaxane structures reported by Goldup et al; b) UV-vis titration of **I-14** with TBAF (0 - 12 eq) in $CHCl_3/CH_3CN$ at 298 K.

1.6.2 Nuclear Magnetic Resonance spectra

A change of position, state of the host unit, or a change of components in molecular machines may cause relative motions of each component, which could influence the surrounding environment of each component. We can use Nuclear Magnetic Resonance Spectra technique to detect this influence. Nuclear Magnetic Resonance spectra play a very important role in detecting structures of organic compounds. Currently, Nuclear Magnetic Resonance spectra have become a main and irreplaceable tool to study complicated systems, like molecular machines.[90-92]

Coutrot et al reported a rotaxane molecular shuttle **I-15** with a sugar group as a building block.[93] As shown in Fig.1.18, [2]rotaxane is composed of a dibenzo-24-crown-8 macrocycle interlocked onto a thread, which has two recognition sites, a methyltriazolium (MTA) station

and a dialkylammonium(DAA) station. Since the crown ether has a stronger hydrogen bond interaction with station DAA than with station MTA, the ring would encircle the DAA site, which could be proven by NMR analysis. After the proton resonance comparison between rotaxane **I-15** and ring DB24C8, dumbbell component, it is found that the protons close to DAA station on the dumbbell component have signals which underwent a big shift from the NMR spectrum of the rotaxane **I-15**, while the shift of protons close to MTA station is small. From here we can see that the ring prefers to encircle DAA site, and it can be simple and easy to identify the position of ring components by 1D NMR.

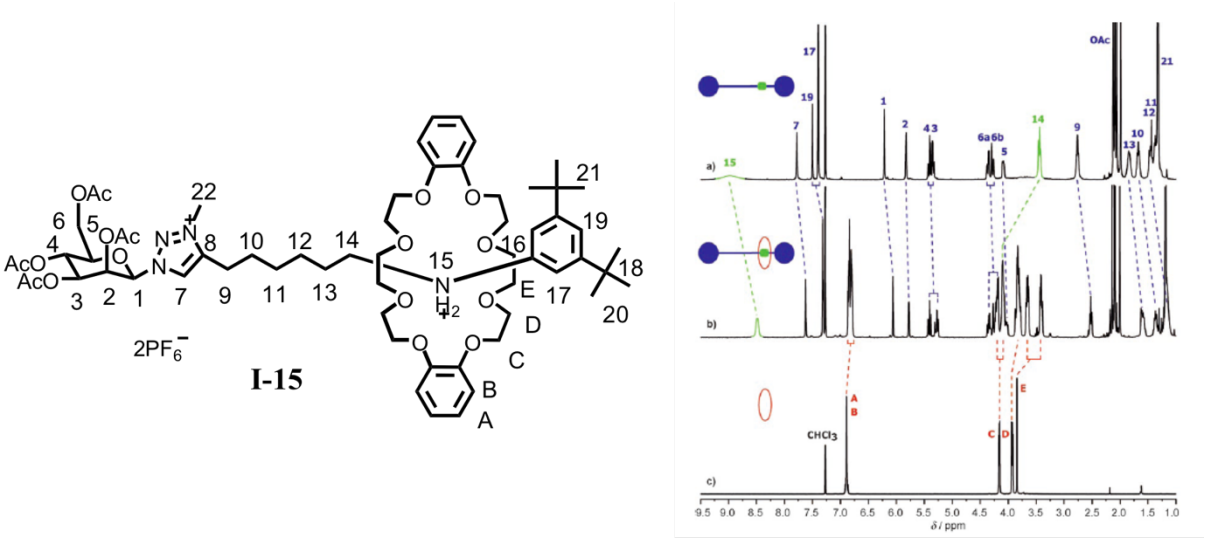

Fig. 1.18 The rotaxane **I-15** which can be investigated using ^{1}H NMR spectra reported by Coutrot et al. Copyright (2008) John Wiley and Sons.

Similarly, NMR techniques could also be used to study shuttling motions[94] of the ring component on the dumbbell component.

1.6.3 Fluorescence Spectroscopy

In some molecular machine systems, electron donor/acceptor units and fluorophore groups are engineered, sometimes when the conformation of molecular machine system changes, electron transfer process of donor/acceptor or energy transfer process can be influenced, and the luminescence properties of fluorophore can be changed. As a result, we can recognize positions of ring guest and states of molecular machine by detecting the fluorescent signal change in the molecular machine system.[95-97]

Zhang'Hui et al.[98] reported a [2]rotaxane **I-16** (Fig. 1.19.a) with dual-mode control of a PET

process using a ferrocene-functionalized dibenzo-24-crown-8 (DB24C8) macrocycle interlocked onto a dumbbell that has the dibenzylammonium (DBA) and the N-methyltriazolium (MTA) recognition sites, and 4-morpholine-naphthalimide (MA) stopper stays close to MTA station. The interactions between the functionalized DB24C8 macrocycle and two recognised stations can be affected by not only acid-base stimuli but also addition/removal of the fluoride anion. The fluorescence of MA stopper can be switched on and off by a tunable, distance-dependent photoinduced electron transfer (PET) process that occurs between the ferrocene electron donors and the excited MA fluorophore. Upon photoexcitation, when DB24C8 stays at MTA station, a highly efficient PET process is possible, which would quench MA fluorescence; but when DB24C8 stays at distant DBA station, fluorescence would not be quenched because of a less efficient PET process. As shown in Fig. 1.19.b and c, when the environment of **I-16** has been changed, we can track the ring positions or check how the new environment changes the rotaxane system by using fluorescence spectroscopy.

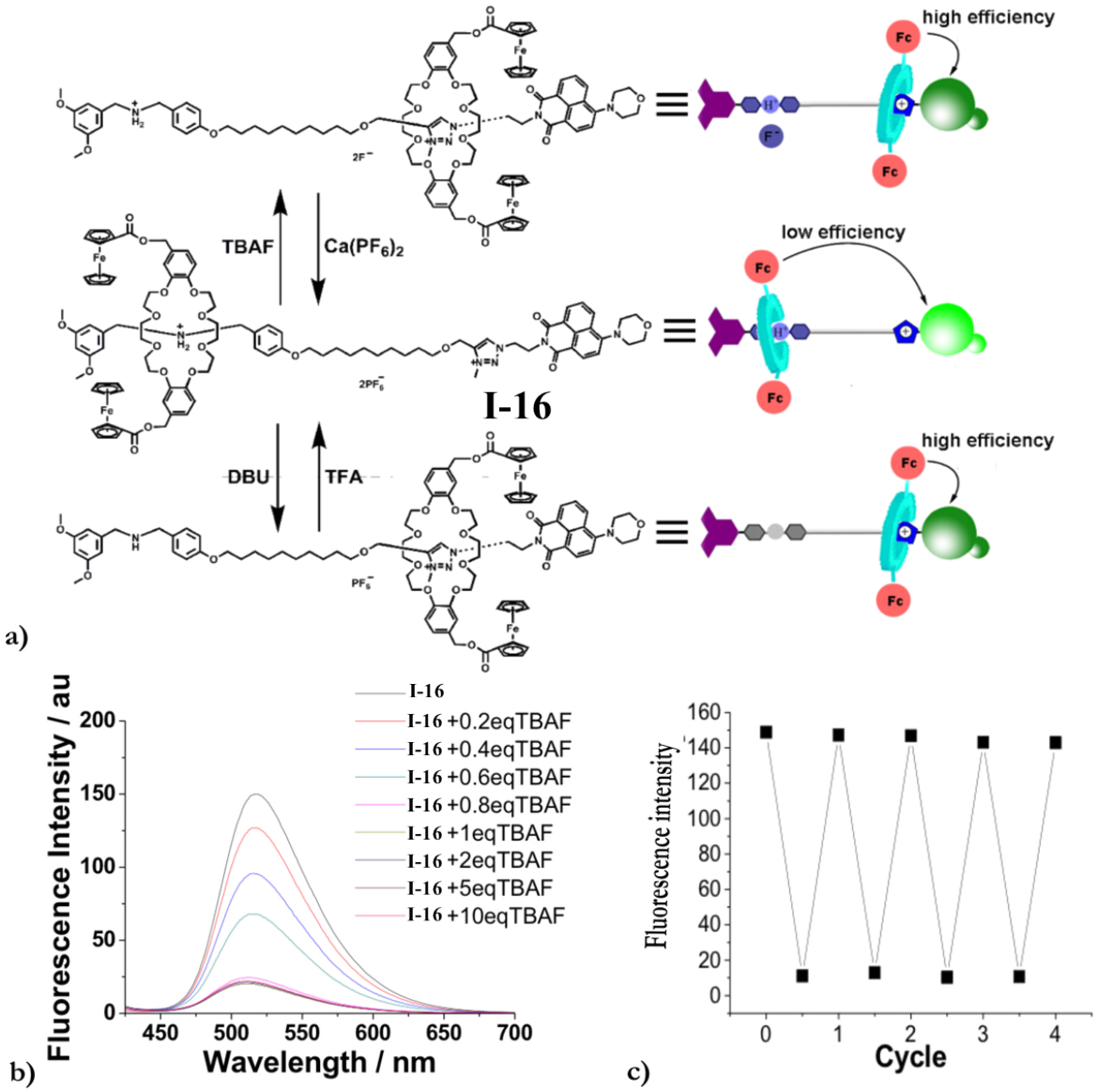

Figure 1.19 a) Schematic representation of the movement of **I-16** under the stimuli of DBU-TFA and TBAF-$Ca(PF_6)_2$; b) The fluorescence spectra of a DCM solution obtained after adding 0 - 10 equiv TBAF to the solution of [2]rotaxane **I-16** (1×10^{-5} M). The excitation wavelength is 398 nm; c) Fluorescence intensity of rotaxane **I-16** (10^{-5} M, CH_2Cl_2, r.t.) at 517 nm under addition of alternate compound (TBAF and $Ca(PF_6)_2$) for four cycles. The excitation wavelength is 398 nm. Copyright (2012) American Chemical Society.

Tucker, Credi, McClenaghan et al.[99] reported a photodriven [2]rotaxane **I-17R**-[2]catenane **I-17C** interconversion, which also could be detected or tracked by fluorescence spectroscopy technique. In this system (Fig.1.20.a), [2]rotaxane **I-17R** comprises a central dibenzylammonium group and two 9-alkoxyanthracene stoppers and is hosted by a 24-dibenzo-8-crown ring (DB24C8). The two terminal anthracene groups undergo a photodimerization

reaction fully completed after 1 hour of irradiation at 365 nm, which would result in a [2]catenane **I-17C** and decrease the fluorescent intensity of the system. The interconversion of the photodimer is thermally (Δ = 120 ˚C) and photochemically (λ = 280 nm) reversible. All these interconversion processes can be tracked with fluorescence spectroscopy, shown in Fig.1.20.

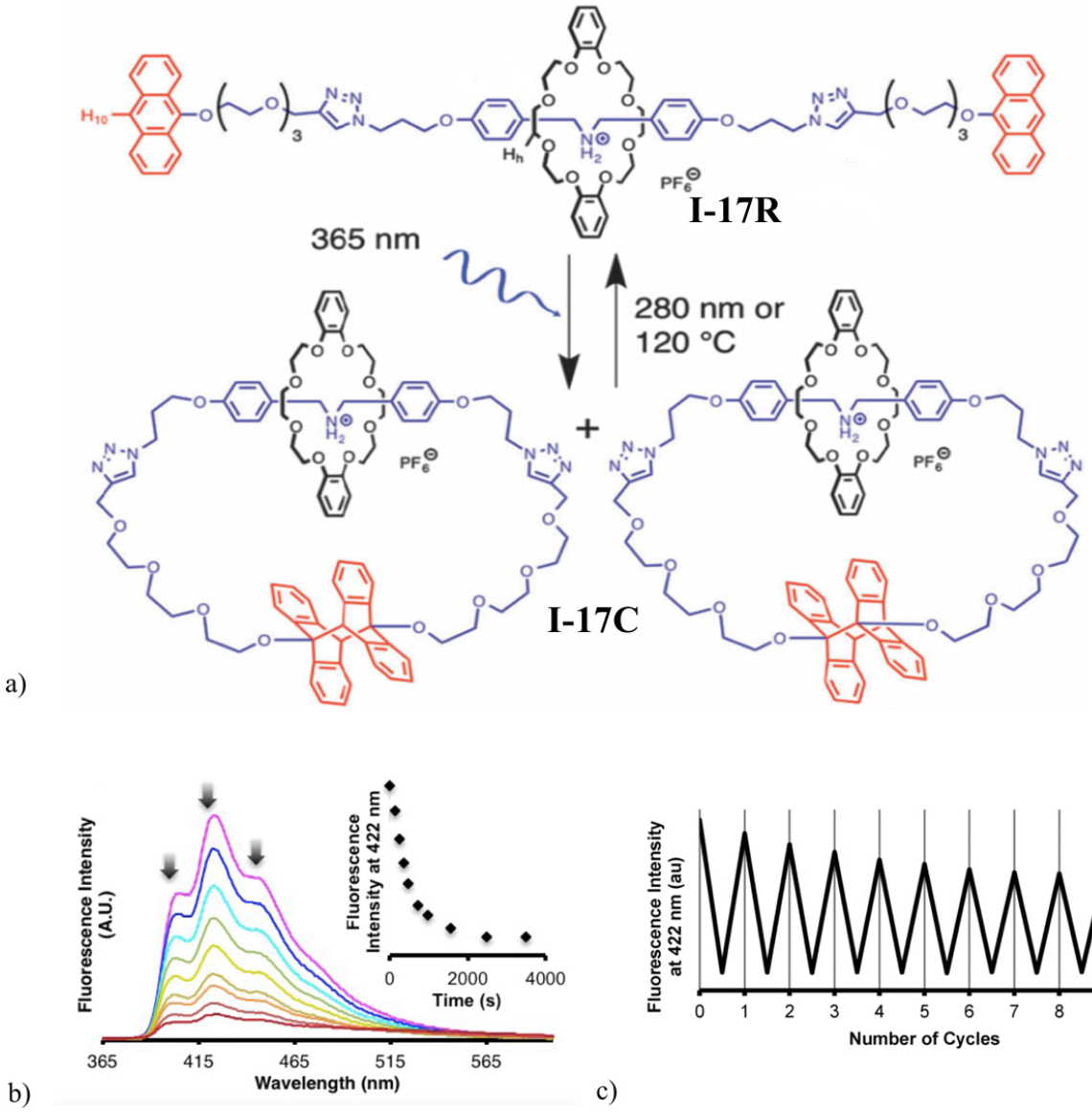

Figure 1.20 a) Schematic representation of [2]rotaxane **I-17R**-to-[2] catenane **I-17C** interconversion of; b) Fluorescence spectra of **I-17R** (2×10^{-5} M, CH_3CN) upon irradiation at 365 nm; c) Fluorescence intensity of interlocked system (2×10^{-5} M, CH_3CN) under alternate irradiation (365 nm and 280 nm) of 1 h for 10 cycles. Copyright (2015) the Royal Society of Chemistry.

1.6.4 Other methods and technologies

Besides the aforementioned methods, cyclic voltammetry[100,101] and induced circular dichroism [102,103] are also becoming popular tools to indicate the movement of molecular machines.

Li and coworkers synthesized and reported two-station-switching [1]rotaxane **I-18**, comprising a ferrocene-functionalised DB24C8, a DBA site and a MTA site, as shown in Fig. 1.21.a. In this system, upon external acid/base stimuli, rotaxanes **I-18N** and **I-18T** are reversibly switched, reversible inclusion and exclusion of the macrocycle on the amine group are adapted. These two different rotaxane states can be clearly identified by cyclic voltammetry (CV). When DB24C8 is included on the amine group, rotaxane **I-18N** has a reversible CV of the ferrocene unit, indicating a reversible oxidation and reduction process of ferrocene species. When DB24C8 is excluded from the amine group, affording rotaxane **I-18T**, whose CV shows an irreversible feature in that the oxidation and reduction peaks. They concluded that cyclic voltammetry method could be used to track or characterise states of such rotaxanes with electrochemical properties.

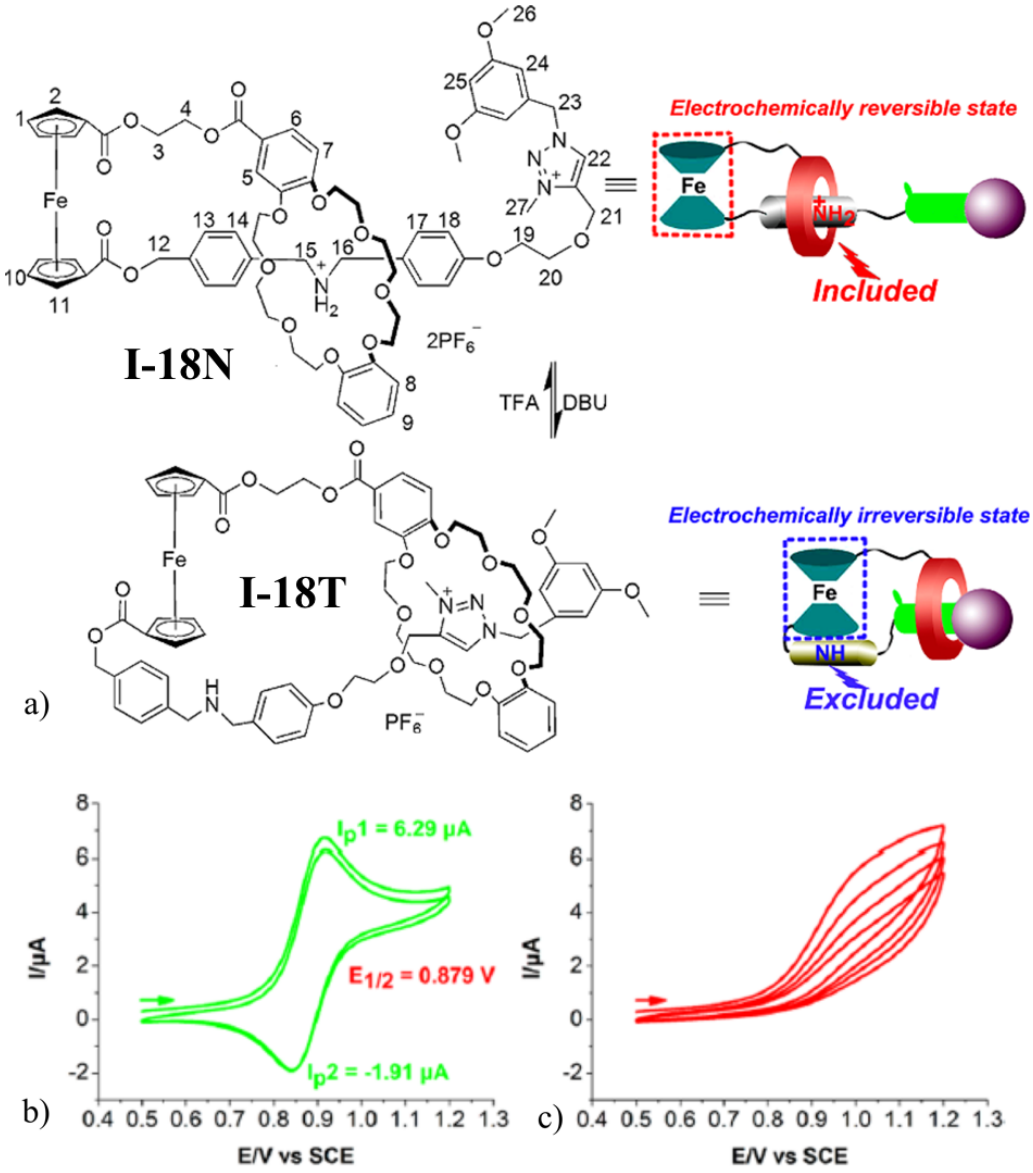

Figure 1.21 a) Switching process and schematic representation of rotaxane **I-18** that can switch between two different states. Evolution of the cyclic voltammetric curves of (b) **I-18N**, (c) **I-18T** in CH_3CN with $[(n\text{-}Bu)_4N]PF_6$ (0.1 M) as supporting electrolyte, scanned at 20 mV s^{-1}. The concentration of each compound is 1×10^{-3} M. Copyright (2012) American Chemical Society.

Gao and coworkers reported a light-induced cobalt coordinated [1]rotaxane **I-19** comprising two β-cyclodextrins, as shown in Fig. 1.22.a. Induced circular dichroism (ICD) spectra, as a fast and sensitive technology to monitor the molecular-scale motions, were used to indicate conformations of [1]rotaxane **I-19** irradiated by light. In Fig. 1.22.b, the peaks in the ICD spectrum respectively belong to four electric transition dipole moments: π-π*, n-π* of the Schiff base unit and π-π*, n-π* of the azobenzene moiety. Before the irradiation of *trans*- **I-19**,

the ICD spectrum of **I-19** shows two positive Cotton effect peaks at around 281 nm and 352 nm, and a negative Cotton effect peak at 232 nm. Upon irradiation with UV light of 365 nm for 10 min, a strong negative cotton effects at 314 nm is revealed, and two new strong positive Cotton effects peaks at 259 nm and 431 nm increases gradually, indicating the formation of *cis*-**I-19**. While upon irradiation of the sample at 430 nm, the spectrum changes shift back to a large extent, indicating the formation of *trans*-**I-19**. It is concluded that ICD spectrum is also an efficient approach to elaborate transformations of some molecular machines.

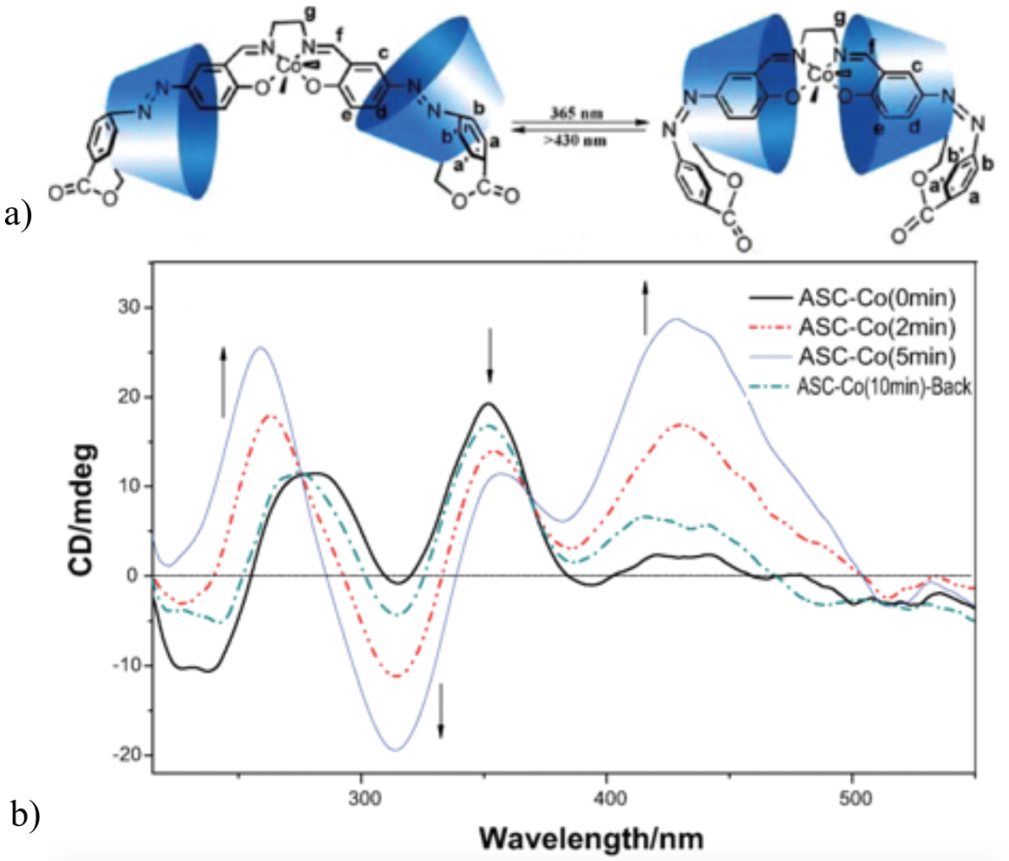

Figure 1.22 a) Structure of **I-19** from *trans*- to *cis*-form after the irradiations; b) ICD spectrum changes for **I-19** (25 °C, 1.2×10^{-4} mol.dm^{-3}) in aqueous solution by irradiation at 365 nm. And the spectrum changes shift back to a large extent by irradiation at 430 nm. Copyright (2011) the Royal Society of Chemistry.

1.7 Applications of molecular machines

While applications of molecular machines need to be further explored, potential applications in many fields, which include: nano-molecular valves, organocatalysts, organogelators, supramolecular polymers, biological/pharmaceutical potential applications are envisaged.

1.7.1 Nano-molecular valve

With the development of nanotechnology, scientists try to microminiaturize macroscopic machines, mimic or even copy functions of nano-scale bio-machines, which has become the chemist's motivation for constructing nanoscale molecular machines. As some components of mechanically interlocked molecules (MIMs) could be driven to move under external stimulus, this may be used to control opening and closing nanopores, thereby controlling storing/ releasing the dyes (or even drug molecules) in or from nanopores. If we combine rotaxanes, catenanes and pseudorotaxanes with silicon-based nanomaterials through covalent bonds, we might build some unique nanomolecular valves, which would be of major significance in drug release.

In 2008, Zink and Stoddart developed a nanomolecular valve[105] based on a pseudorotaxane and a mesoporous silicon-based nanomaterial. In this nanomolecular valve, [2]pseudorotaxanes consisting of cucurbit[6]uril (CB[6]) rings and bisammonium stalks were constructed (Fig. 1.23.a,b) on the surface of mesoporous silica nanoparticles, and CB[6] rings were used to catalyze alkyne-azide 1,3-dipolar cycloadditions, to bind bisammonium with ion-dipole interactions. At neutral pH condition, CB[6] rings encircle the bisammonium stalks tightly, thereby efficiently blocking the nanopores, which were loaded with fluorescent guest molecules (rhodamine B). Upon addition of base, the stalks are deprotonated, which results in spontaneous dethreading (Fig. 1.23.b,c) of the CB[6] rings and unblocking of the silica nanopores, thereby fluorochrome rhodamine B is released from the nanopores under efficient control. All processes are conducted in water, making this report an enabler for the development of drug delivery and release in living systems.

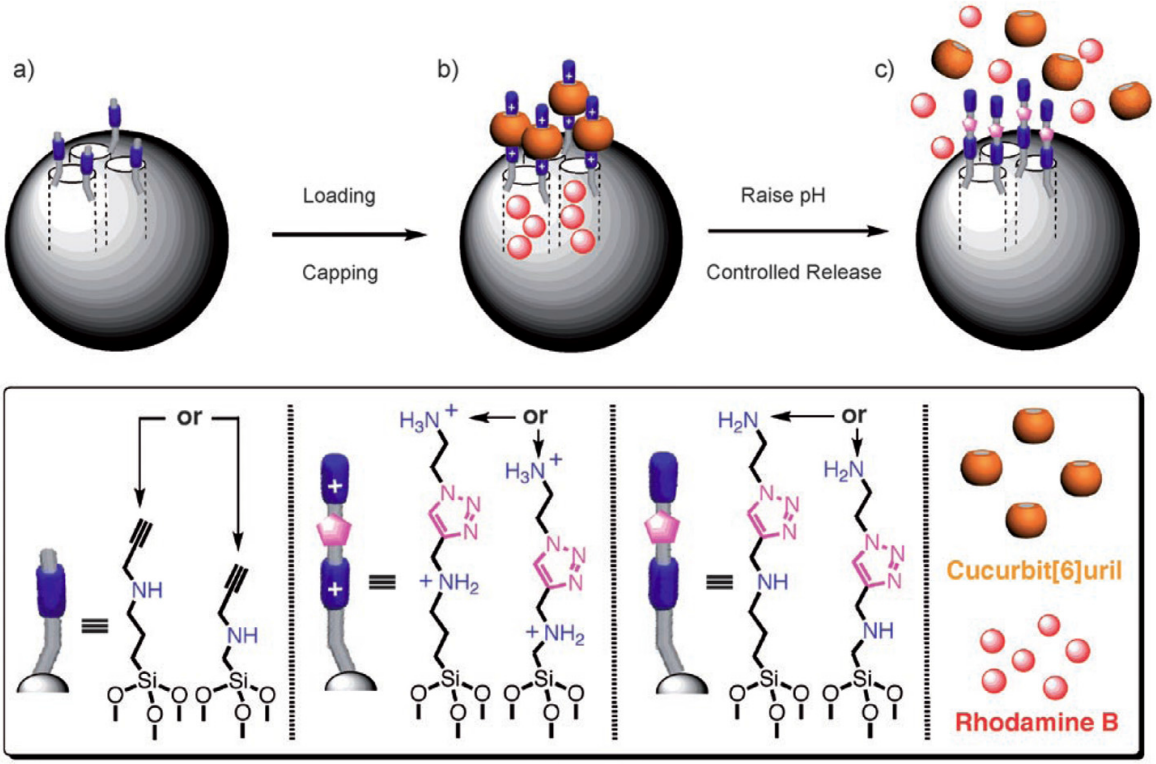

Figure 1.23 Graphical representations of operating supramolecular nanovalves. The alkyne-functionalized mesoporous silica nanoparticles MCM-41 are loaded (a, b) with rhodamine B molecules, and capped (a, b) with CB[6]. RhB molecules are released (c) by raising pH. Copyright (2008) John Wiley and Sons.

1.7.2 Organocatalysts

In 2012, Leigh et al.[106] reported a switchable organocatalyst based on a [2]rotaxane system **I-20**, which is exploited to conceal and reveal an organocatalytic site. It comprises a dibenzo[24]crown-8 macrocycle (DB24C8) and an axle containing both methyltriazolium (MTA) moiety and a dibenzylamine (DBA) moiety, as shown in Fig.1.24. As is known, the Michael addition of an aliphatic thiol, such as a fluorinated thiol, to trans-cinnamaldehyde is a class of reaction catalyzed by an iminium. When the rotaxane is protonated, DBA is a better binding site for DB24C8 than MTA site, the macrocycle encapsulates the central region of the axle. So the catalytic center is blocked, and the catalytic ability of [2]rotaxane **I-20** will be turned off. When DBA is not protonated, DBAs are the preferred binding sites for DB24C8 and DBA on the axle is exposed and the catalytic ability of [2]rotaxane **I-20** will be turned on.

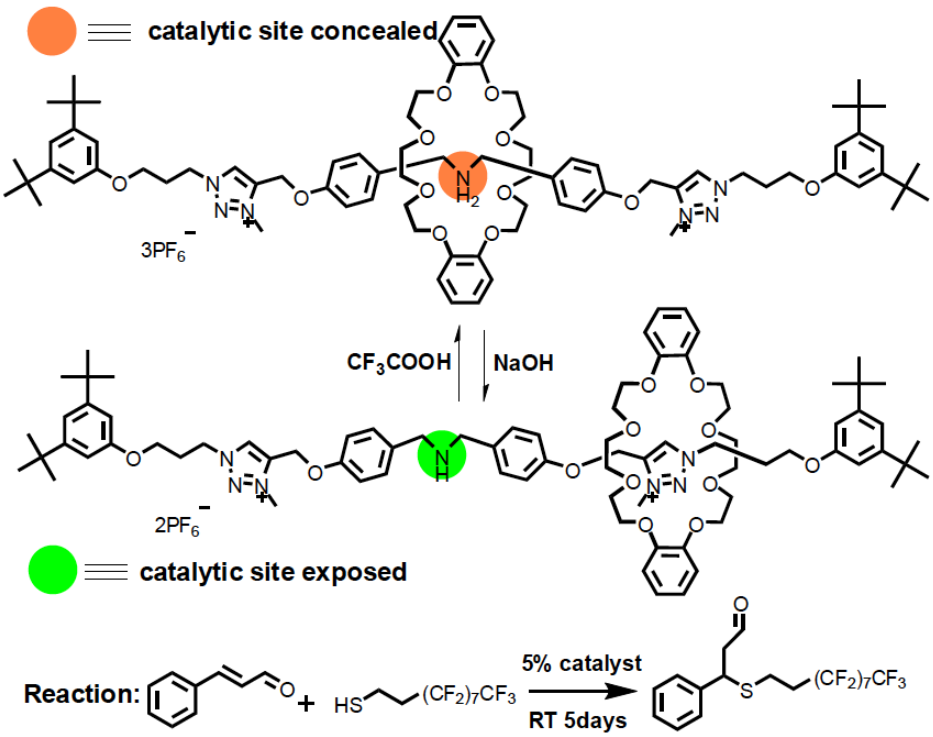

Figure 1.24 The rotaxane catalyst **I-20** reported by Leigh et al.

The group of Zhang'Xi developed a supramolecular strategy[107] to accelerate the Fenton reaction through the construction of a pseudorotaxane (Fig.1.25), which comprises two cucurbit[7]uril (CB[7]) rings and a derivative of 1,4-diketopyrrolo[3,4-c]pyrrole (DPP), a model dye for Fenton oxidation. The Fenton reaction is a complete oxidation of aromatic compounds by a combination of hydrogen peroxide (H_2O_2) and iron salts, and has importance in biology and been used to wastewater, contaminated soils and sludges. The DPP radical cation, the key intermediate in the oxidation process, can be activated by the electrostatically-negative carbonyl groups of CB[7] through the host–guest complexation between CB[7] and DPP. Owing to this supramolecular complexation, the activity of DPP radical cation improved greatly, thus induced a decrease in the apparent activation energy and significant promotion of the reaction rate. This supramolecular approach is highly efficient and facile, and hold promise to be extended to other kinds of radical reactions.

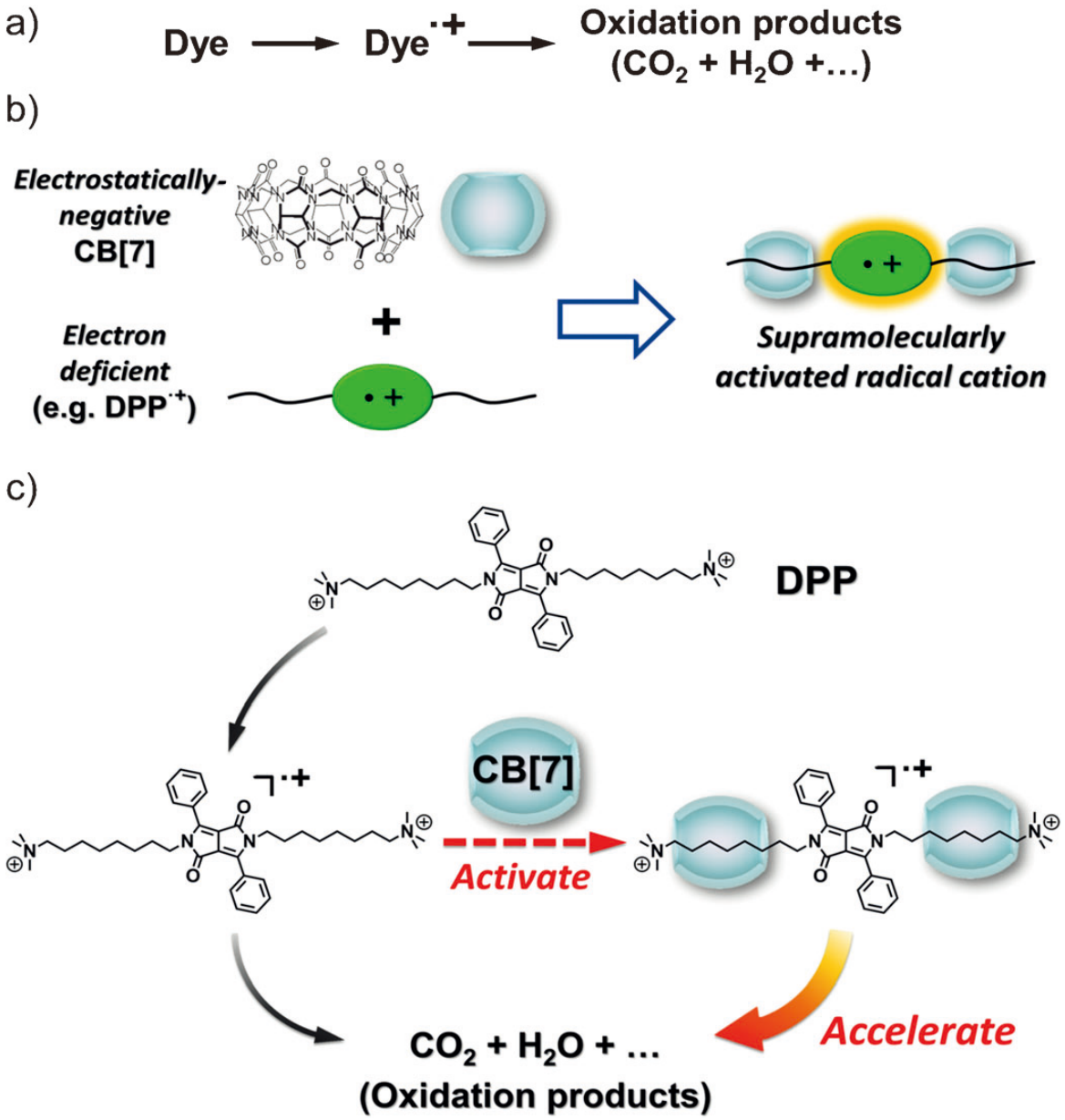

Figure 1.25 a) Possible mechanism of the Fenton reaction: a dye radical cation acts as an intermediate; b) Concept behind the design of a supramolecularly-activated radical cation; c) Proposed mechanism of an accelerated Fenton reaction. Copyright (2016) John Wiley and Sons.

1.7.3 Organogelator and superamolecular polymer

Hsueh et al. reported an organogelator system[108] based on a urea-based [2]rotaxane **I-21** (Fig.1.26), which does not feature long alkyl chains or gelation steroid units. This rotaxane consists of a benzylic diamide macrocycle mechanically interlocked on a thread, featuring two 3,5-di-*tert*-butylphenyl stoppers and two recognition sties-a DBA unit and a diphenylurea (DPU) unit. In a solution of **I-21** in 1-pentanol, on adding 1 equivalent of $HClO_4$ or $NaClO_4$ to

protonate the DBA site, the ring would prefer to encapsulate the DBA^+ station, and the organogelator was formed after sonification; while 2 equivalents of *t*BuOK or NBu_4OAc was added, the gelator returned to be in solution again. Furthermore, the same sol-gel phase transition of **I-21** in 1-pentanol was also achieved upon sequential addition of TBACl (1 equivalent) and $AgPF_6$ (1 equivalent). While from the comparison analysis of ^1H NMR, the writer found with the addition of equimolar amounts of these TBACl, the macrocycle did not move to the DPU station, which suggested anion Cl^- dissolved the organogel without changing the location of the macrocycle unit in **I-21**. On performing additional experiments, Cl^- was suggested to cause the amide NH units on the macrocycle to be stabilized to the NH_2^+ center through both hydrogen bonding and electrostatic attraction. It would hugely change the conformation of pyridinediamide units of [2]rotaxane **I-21**.

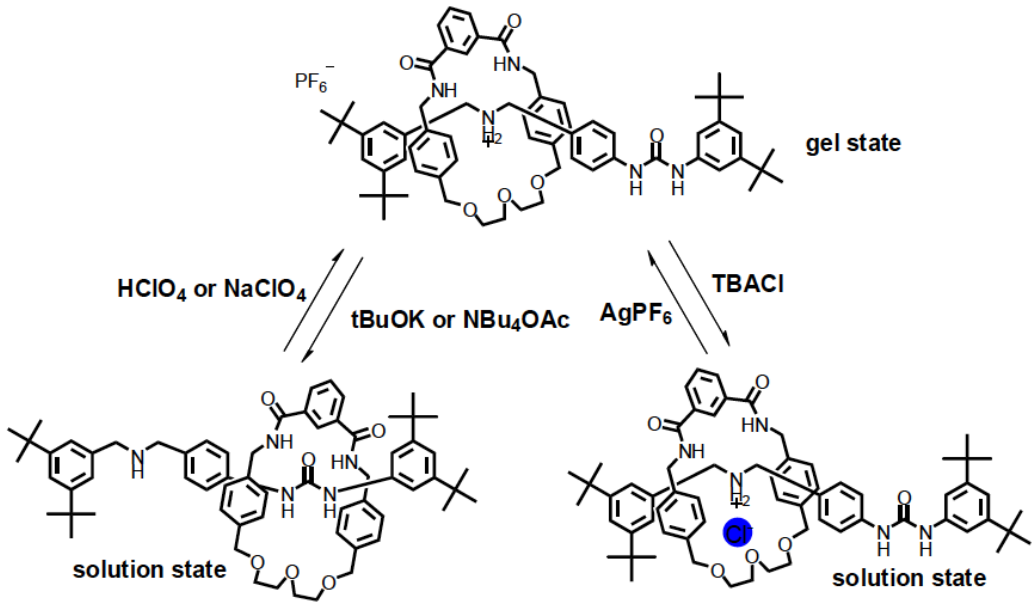

Figure 1.26 The acid/base- and anion-controllable organogel system based on [2]rotaxane **I-21** reported by Chiu et al.

Huang et al. [109] reported the design and synthesis of a novel dual-responsive supramolecular polymer gel, which is based on a crown ether-based pseudorotaxane **I-22**. Its monomer structure is shown in Fig. 1.27.a, on the left side, there is a DB24C8 ring forming a 1:1 threaded structure with the DBA salt on the right side through host-guest interactions. The flexible long alkyl chain in the middle favors the formation of linear supramolecular polymers. This monomer can form a supramolecular polymer gel in acetonitrile, and reversible sol-gel transitions can be realized by heating and cooling, or by adding base and acid, or by other stimulus (Fig. 1.27b).

The thermo- and pH-responsive gel-sol transition was also successfully employed for the controlled release of rhodamine B. This work demonstrated that the complex of DB24C8 and DBA is a good candidate as a building block to construct multiple supramolecular polymers, or even organogelators and transparent films.

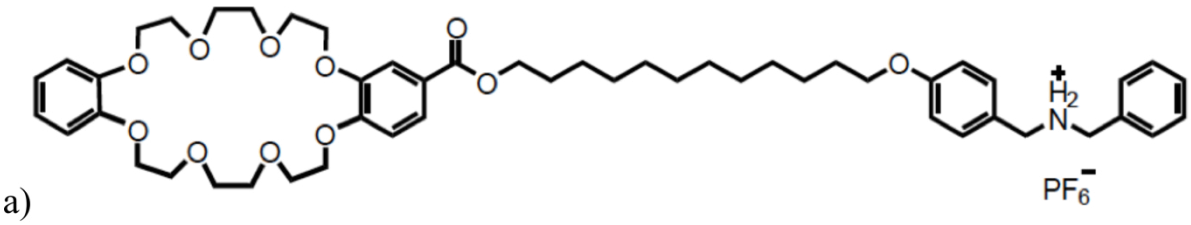

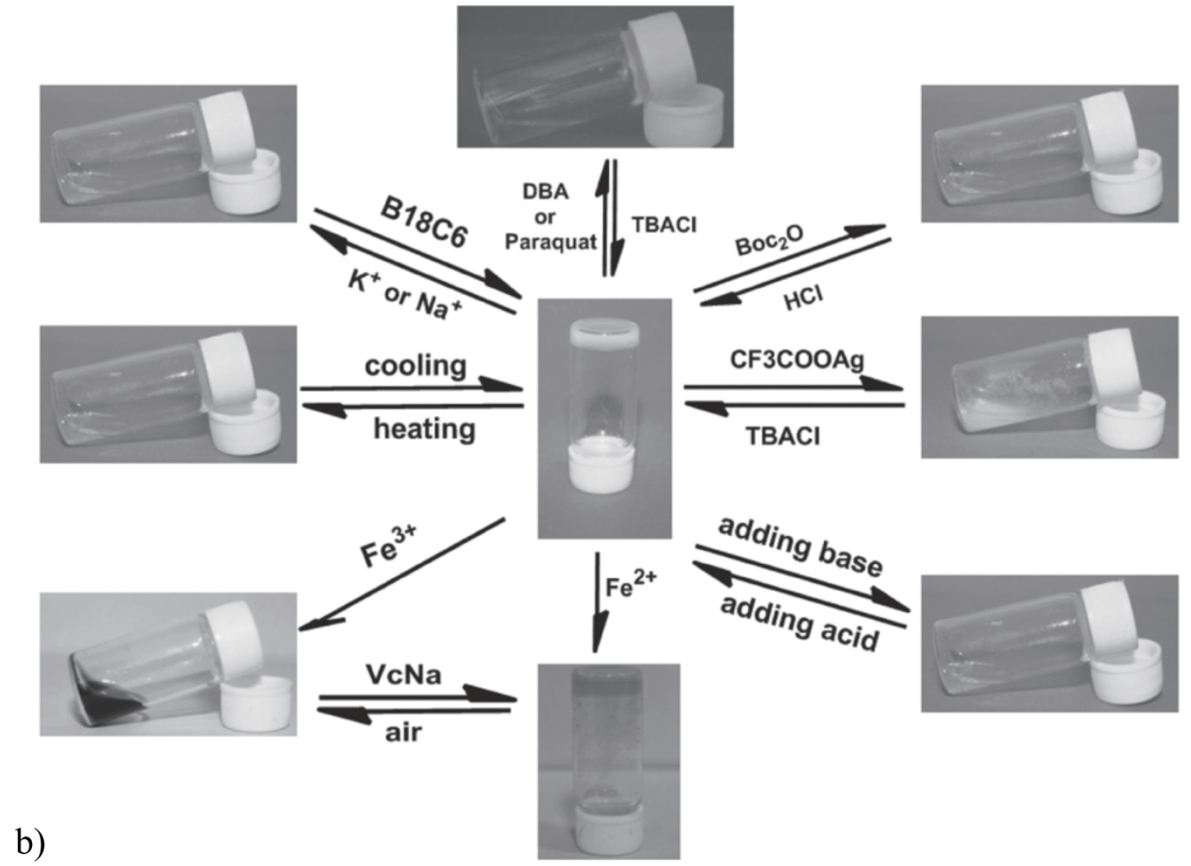

Figure 1.27 a) The monomer structure of the super-gel system reported by Huang et al; b) The reversible gel-sol transitions of the supramolecular polymer triggered by many different stimulus. Copyright (2011) John Wiley and Sons.

1.7.4 Biological/pharmaceutical potential applications

Thanks to efforts from chemists, molecular machines have been finding more and more potential applications in biological/pharmaceutical field. It is a big step for the molecular machines research to go back to the biological field, which is the origin of supramolecular

chemistry.

Huang et al[110] reported a novel pesudorotaxane system (Fig.1.28) based on a water-soluble pillar[6]arene (**I-23R**) and paraquat(**I-23V**). This new recognition motif in water not only has an extremely high binding constant (K_a = 1.02 × 10^8 M^{-1}), but also pH-responsiveness. This novel recognition motif was also used to control the self-assembly between **I-23R** and an amphiphilic paraquat derivative (**I-23L**) containing a hydrophilic 4,4′-bipyridinium unit. Due to the pH-responsiveness of **I-23R**, the reversible transitions between micelles formed by **I-23L** alone and vesicles formed by the complex of **I-23R** and **I-23L** could be achieved by adjusting pH in the solution. After some relative cell viability experiments, it was found the host-guest complexion limits the probability of paraquat to enter in contact with the reducers in the cell, which made the generation of its radical cation more difficult, resulting in the efficient decrease of paraquat toxicity. This result might enlighten chemists how to solve the problem in the toxic degradation field.

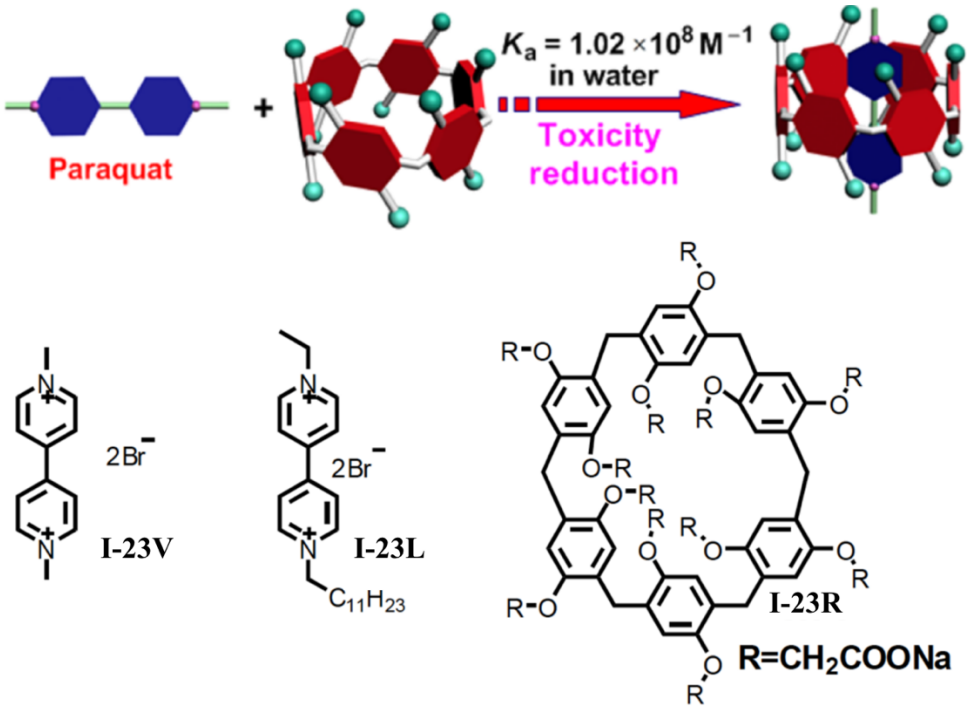

Figure 1.28 The pseudorotaxane based on **I-23R** and paraquat reported by Huang et al. Copyright (2012) American Chemical Society.

Basílio and Pischel developed a drug delivery system (Fig.1.29) by controlling a supramolecular host-guest assembly with a reversible photoswitch. Memantine, a widely prescribed Alzheimer's drug, could be encapsulated (K = 2.5 × 10^4 M^{-1}) by CB[7] in water.[111]

While a *trans*-chalcone derivative **I-24a** was added in the system, 80% memantine still complexed with CB[7], because **I-24a** does not have an efficient binding constant (K = 3.0 × 10^2 M^{-1}) with CB[7]. Furthermore, upon the irradiation of *trans*-chalcone at 366 nm, it afforded a flavylium ion, binding more strongly (K = 9.0 × 10^5 M^{-1}) with CB[7] than memantine. As a result, 90% memantine would be released from CB[7], proving that supramolecular system might be applied in the drug release field.

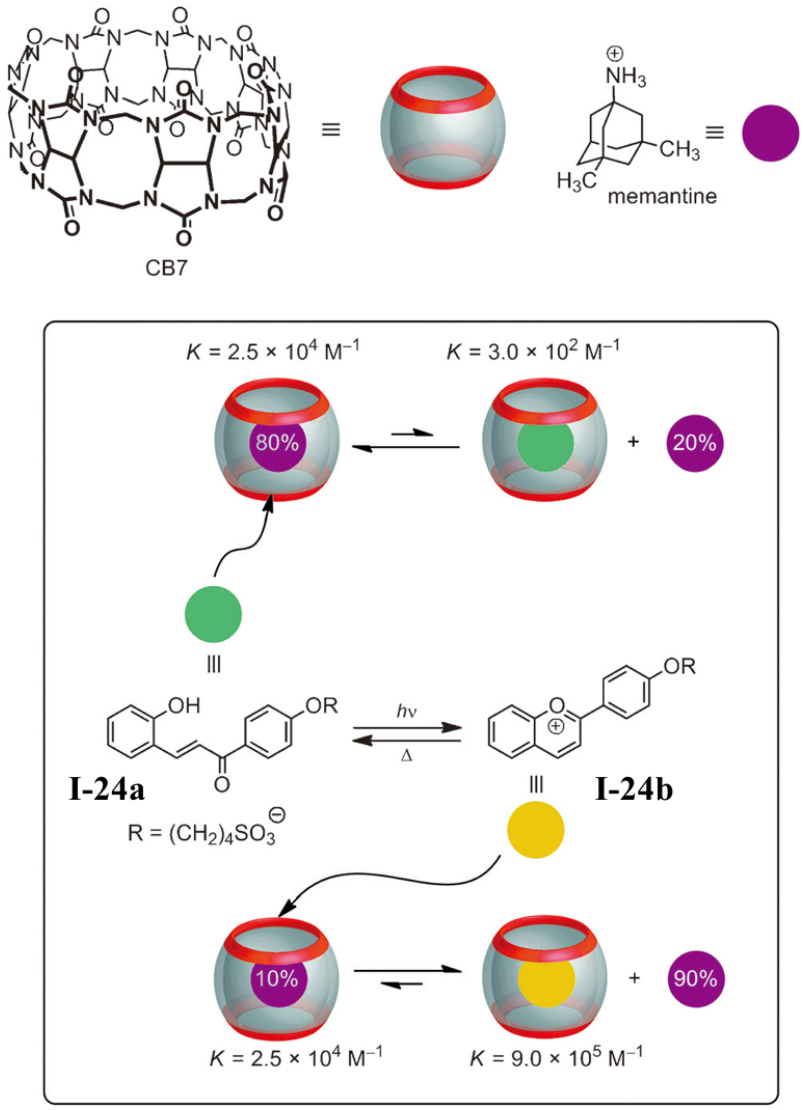

Figure 1.29 Coupling of a flavylium photoswitch with a memantine-CB[7] host-guest equilibrium for the phototriggered release of the drug (memantine). Copyright (2016) John Wiley and Sons.

The group of Zhang'Xi[112] described a supramolecular antibiotic switch (Fig.1.30), which relies on the supramolecular assembly/disassembly of cationic poly(phenylene vinylene) (PPV)

derivative with CB[7]. A PPV derivative with quaternary ammonium (QA) groups as side chains, which could bind and penetrate into the negatively charged membrane of bacteria (such as, *E. coli*) by electrostatic and hydrophobic interactions, was chosen as their antibacterial agent. When CB[7] was not added in the system of PPV and *E. coli*, PPV possessed the antibacterial activity; when CB[7] was added in the system, cationic PPV could form a non-covalent complex with CB[7], resulting in the encapsulation of QA groups in the hydrophobic cavity of CB[7], and turning off the antibacterial activity of PPV; reversibly, it could be turned on by adding amantadine (AD) to compete in binding with CB[7], releasing PPV to free QA groups. This reversible antibacterial activity "turned-on" and "turned-off" offers a proof-of-concept in antibacterial regulation by supramolecuelar assembly and disassembly processes.

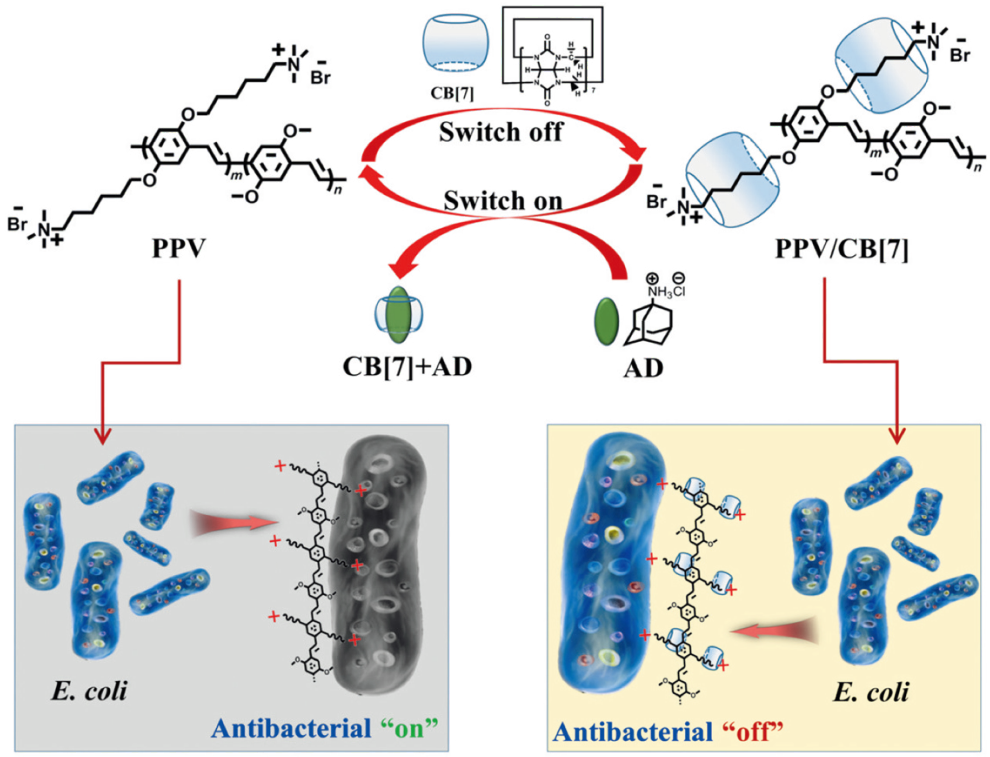

Figure 1.30 Supramolecular assembly of PPV with CB[7] and disassembly of PPV with CB[7] mediated by AD molecule for reversible control of antibacterial activity of PPV. Copyright (2015) John Wiley and Sons.

1.8 A short introduction to photochemistry

1.8.1 Absorption of light and electronic transitions

Photochemistry studies the changes in matter induced by light. In other words, it studies the

reaction or reactivity of molecules in their excited state after absorbing light. In modern physics, light, part of electromagnetic spectrum, is understood as a flux of photons.[113,114] The absorption of a UV photon by a molecule leads to an electronic transition, as one of the electrons in the molecule will be promoted from its occupied orbital to an unoccupied orbital of higher energy - e.g. from highest occupied molecular orbital (HOMO) to lowest unoccupied molecular orbital (LUMO). As a result, the total energy of the molecule would be increased, the molecule is in an excited state. A molecular orbital can be formed by a linear combination of two *s*, *s* and *p* or two p atomic orbitals when they have a collinear axis of symmetry. Those bonds are called σ orbitals. A π molecular orbital is formed from *p* atomic orbitals overlapping laterally, while non-binding electrons are in the *n* orbital.[115]

1.8.2 Excited state and deexcitation processes

Once a molecule absorbs light and forms an excited state, several different following processes could happen, as illustrated in a Perrin-Jablonski diagram (Fig. 1.31).[116] When an electron is promoted from the ground state to a higher energy level, its spin generally remains unchanged. The state where the total spin number is zero is called the singlet state. The ground state for most molecules is a singlet state (S_0), and the excited state formed initially by photon absorption is also a singlet state (S_1).

When the molecule is at the bottom of the singlet state after vibrational relaxation (2), it could go back to the ground state by emitting a photon, which is called fluorescence emission (3a); it could also undergo the internal conversion and vibrational relaxation(IC) back to the ground state (3b); and in the third case, it could be converted to a state where the electron spin has changed, and goes to a new excited state: triple state (T_1), this process (3c) is called intersystem crossing (ISC). At T_1, it can undergo vibrational relaxation, and go back to the ground state by emission of a photon, which in this case is called phosphorescence (4).

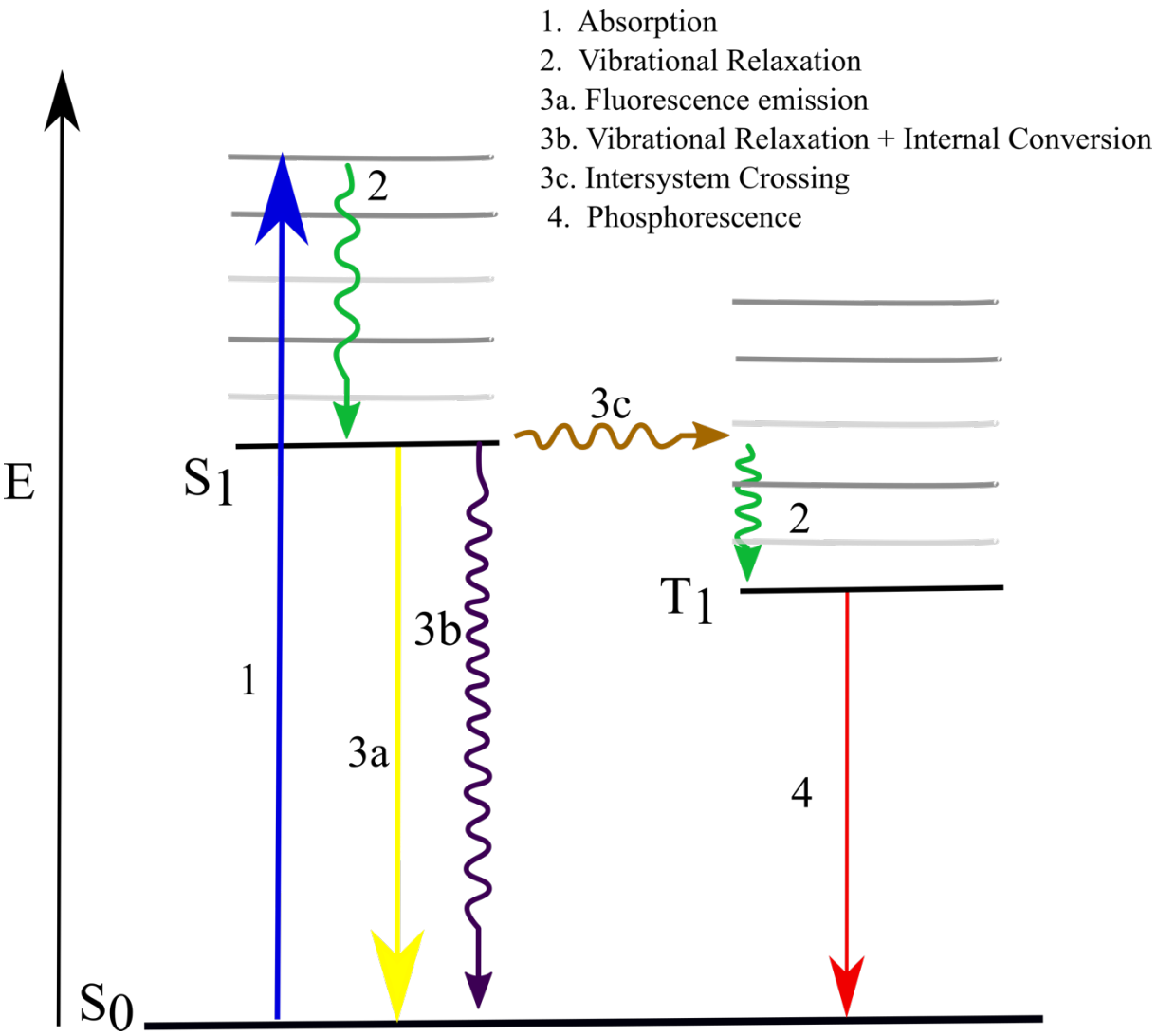

Figure 1.31 Perrin-Jablonski diagram.

Besides these intrinsic deexcitation processes, there are other processes that an excited state can undergo in the presence of another molecule. It also can transfer its charge either through photoinduced electron transfer (PET) or intra-(or inter-)molecular proton (ESIPT). Alternatively, it can also transfer the energy of its excited state to another molecule, either by emission and reabsorption, which is known as radiative energy transfer, or without emission of a photon, a process known as non-radiative energy transfer, which can occur either through dipole-dipole interaction or, through recovery of molecular orbitals of the donor and acceptor only at close distance. It has to be emphasized that this last process is by and large the only one that can happen when the excited state is a triplet state.

1.8.3 Characteristics of fluorescence emission

As molecules in the excited state are highly unstable and have a tendency to rapidly go back to the ground state, the excited state is normally short-lived. Different processes of deexcitation have been described above. The singlet excited state S_1 can deexcite by fluorescence, with a rate constant k_f; or by internal conversion and vibrational relaxation with a rate constant k_{IC}, or intersystem crossing with a rate constant k_{ISC}. Non-radiative processes are combined to get a rate constant k_{NR} (= k_{IC} + k_{ISC}), simplifying the calculation. In an example, a solution contains a fluorescent species M (concentration is noted (M_0)) which is excited by a short light pulse (t = 0) and a fraction of these molecules with the concentration noted (M^*) initially populates to the excited state S_1. It will follow equation 1 as in classical kinetics:

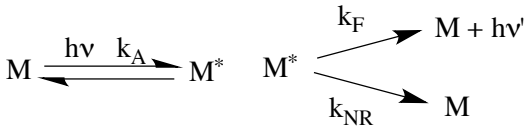

$$\frac{-d[M^*]}{dt} = (k_F + k_{NR}) \times [M^*] \qquad \text{equation 1}$$

τ is the lifetime of this excited state, given by the following equation:

$$\tau = \frac{1}{k_F + k_{NR}} \qquad \text{equation 2}$$

The fluorescence intensity $I_F(t)$ is then given by the following equation:

$$I_F(t) = k_F \times [M^*] \times e^{\frac{-t}{\tau}} \qquad \text{equation 3}$$

The quantum yield (Φ) of a process (fluorescence, photochemical reaction…) is defined as the number of photons emitted divided by the number of photons absorbed.[117] For example, the quantum yield of fluorescence Φ_F is given by the following equation:

$$\Phi_F = \frac{k_F}{k_F + k_{NR}} = k_F \times \tau \qquad \text{equation 4}$$

1.9 Introduction to reversible electronic energy transfer (REET)

Following the photoexcitation of a chromophore, the generated excited state has excess energy which can be dissipated in various ways both through radiative and non-radiative processes.[118] Assuming close approach of a second chromophore within the lifetime of the excited state, it can interact with a second, non-excited, chromophore. Indeed, a range of processes can occur on varying timescales, the ultimate outcome being determined by management of the excess energy according to kinetic and energetic considerations.

In a bichromophoric molecular system, electronic energy transfer (EET) can occur between chromophores, when spectral overlap and interchromophore distance conditions are satisfied (Fig. 1.32).[119] EET can occur between singlet states, between triplet states, as well as between singlet and triplet states.[120] Typically, this transfer is a unidirectional process when the energy difference (ΔE) > 5 kT. This unidirectional electronic energy transfer, such as Förster energy transfer, was applied in many fields: imaging, sensing and light-harvesting.[121] However, in some specific cases, when the lowest-lying excited states of the two chromophores are quasi-isoenergetic (ΔE ≤ 5 kT), reversible electronic energy transfer (REET) can be instilled, in other words the accepted energy of chromophore A from chromophore D can transfer back to chromophore A.[122]

$$D^* + A \rightarrow D + A^*$$

The rate of energy transfer depends primarily upon the extent of spectral overlap between the emission spectrum of the donor and the absorption spectrum of the acceptor, the quantum yield of the donor, the relative orientation of the donor and acceptor transition dipoles, and the distance between chromophores D and A. So as the energy gap between the two excited-states (energy difference between the low-lying interacting states) diminishes, the rate of back energy transfer is becoming faster.

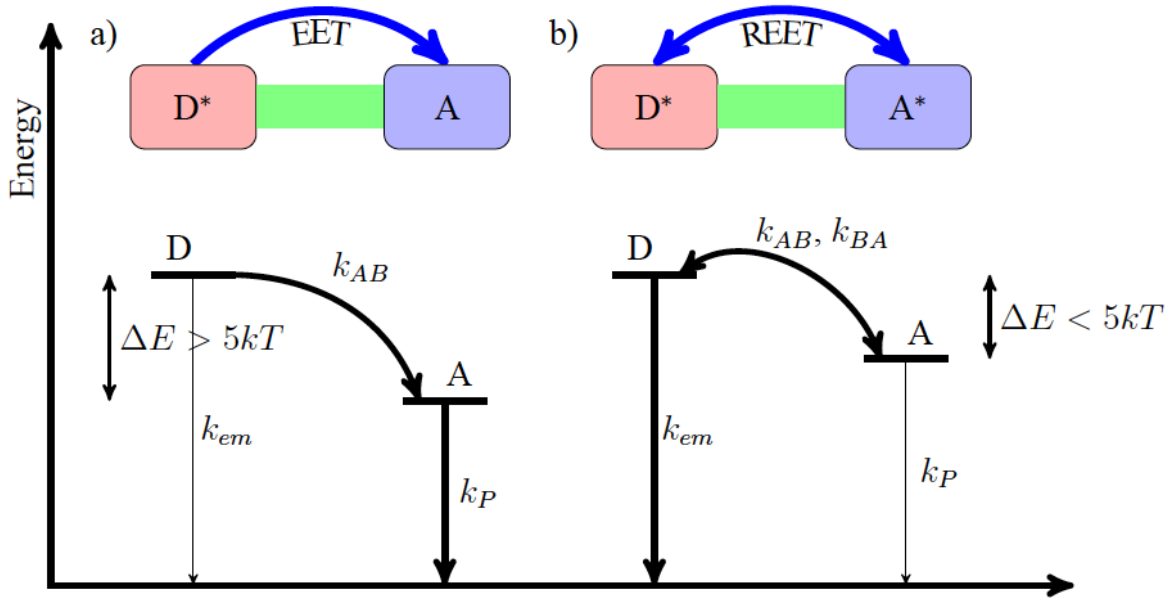

Figure 1.32 Schematic representation of bichromophoric system and pertinent excited states in molecular design “chromophore A-spacer-chromophore D”. a) Unidirectional electronic energy transfer; b) reversible electronic energy transfer between energetically close-lying excited-states.

Consider REET process between triplets as an example to see what will happen between two chromophores (Fig. 1.33): Upon photoexcitation, chromophore D singlet state is initially populated; then on the sub-picosecond timescale, an electron spin change occurs and the singlet state converts to be a new excited state: a triplet state, which is energetically more stable. When the distance between two matched chromophores is rather short (< 1 nm); when triplet-triplet energy gap (ΔE) ≤ 5 kT; and interchromophore electronic energy transfer rate (k_b, k_f) is faster than other relative chromophore deexcitation pathways, reversible interchromophore electronic energy transfer will occur, which competes with intrinsic decay pathways (fluorescence, internal conversion and vibrational relaxation). The weighted average distribution of energy between each chromophore and intrinsic chromophore decay rates govern observed lifetime, according to Equation 5. The observed luminescence lifetime of the whole system is prolonged as a result of the REET process. Since the lifetime of excited donor chromophore (τ_D) and acceptor group (τ_A) are known from the reference, the energy distributions between the two chromophores can be calculated upon establishing a dynamic equilibrium. (α corresponds to the percentage of energy which resides on the donor chromophore; while the remaining population 1- α corresponds to the percentage of energy which resides on the acceptor chromophore).

$$\frac{1}{\tau} = \alpha \left(\frac{1}{\tau_D}\right) + (1 - \alpha)\left(\frac{1}{\tau_A}\right) \qquad \text{Equation 5}$$

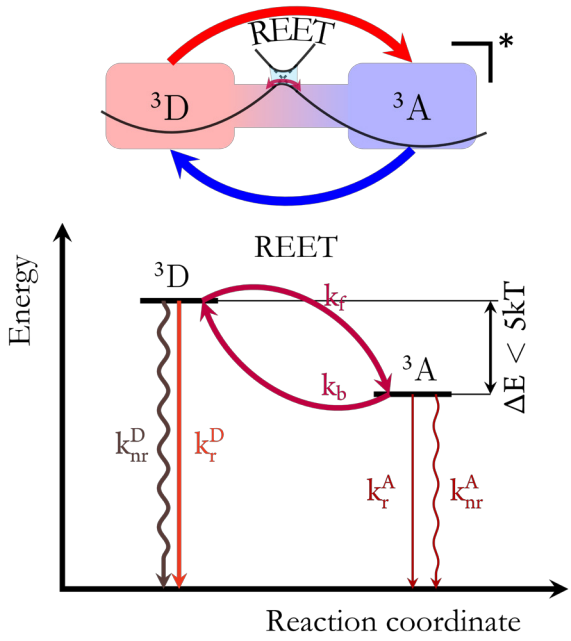

Figure 1.33 Schematic representation of reversible electronic energy transfer between matched chromophores (D and A) and key kinetic and energetic prerequisites.

Ruthenium polypyridine complexes have been frequently used in the general areas of photosensitizers, dyes, catalysts as well as nanotechnology.[123,124] Ru^{2+} has a d^6 electronic configuration and the polypyridine ligands possess σ donor orbitals localizing on the nitrogen atoms and π and π^* acceptor orbitals more or less delocalizing on aromatic rings. Following a single-configuration one electron description of the excited state in octahedral symmetry, promotion of an electron from a π_M orbital to the π^*_L ligand orbitals gives rise to Metal-to-Ligand Charge Transfer (MLCT) excited singlet state (^{1}MLCT), which populates a triplet state (^{3}MLCT). $Ru(bpy)_3^{2+}$ (bpy = 2,2'-bipyridine) has a luminescence quantum yield of 0.059 and luminescence lifetime 890 ns in degassed CH_3CN[125]. When $Ru(bpy)_3^{2+}$ is combined with organic chromophores which have triplet excited states energetically close to the triplet MLCT state of $Ru(bpy)_3^{2+}$ group, the excited-state lifetime is dramatically increased. This is of course beneficial in the realms of photosensitizers where a longer excited-state lifetime is conductive to bimolecular, diffusion-controlled processes.

Ford and Rodgers reported a bichromophoric system which comprises a $Ru(bpy)_3^{2+}$ group and a pyrene group separated by a short and flexible spacer (Fig. 1.34.a).[126] Using this compound, the first direct observation of a reversible intermolecular triplet-triplet energy transfer process was described. In a deoxygenated methanol solution, the writers observed that upon photoexcitation, a rapid intramolecular transfer of triplet energy (Ru→pyr) occurs with a forward rate constant of $(1.3 \pm 0.3) \times 10^8$ s^{-1} and a reverse transfer (Ru←pyr) occurs with a rate constant lower by a factor of 18 ± 3. When REET process leads to an excited-state equilibrium being established, on average most of the energy would stay on the pyrene group, as such it may be linked to an energy reservoir (Fig. 1.34.b). As the deactivation of the pyrene triplet state is a strongly forbidden process, the pyrene triplet state is much more persistent than the MLCT triplet state. As a result of this contribution, the system will give an observed lifetime of 11.2 ± 0.4 μs, which is much longer than the luminescence lifetime of the parent Ru complex.

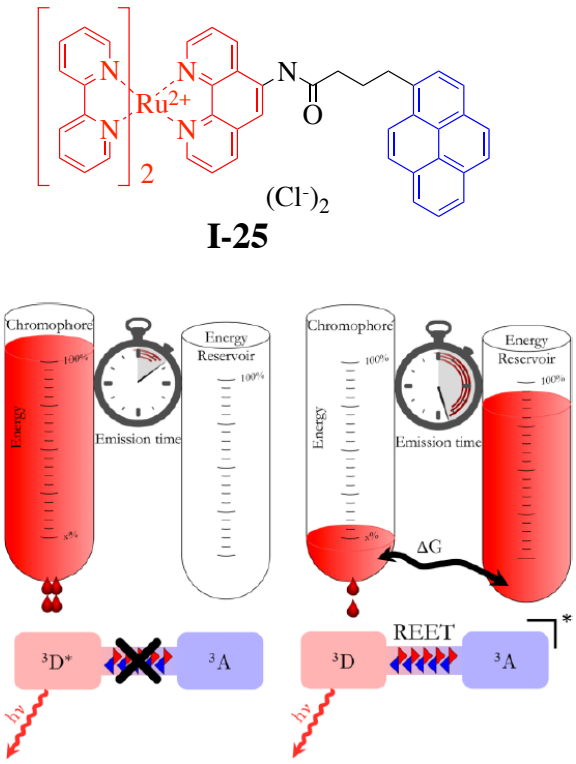

Figure 1.34 Structure of a bichromophore molecule **I-25** with REET process reported by Ford and Rodgers; Schematic cartoon representation of REET system and the notion of an energy reservoir.

In addition to covalent bichromophore dyads, non-covalent assemblies can be considered. In one example, REET processes on a bichromophoric molecular thread was investigated when free or integrated into a double-helix structure (Fig. 1.35). This allowed probing of conformational change upon host : guest complex formation. A bichromophoric, long and flexible saturated rod was synthesized, which comprises an inorganic $Ru(bpy)_3^{2+}$-like chromophore (bpy = 2,2'-bipyridine), whose emissive ^{3}MLCT state is quasi-isoenergetic with an organic triplet on a pyrene (^{3}Pyr) unit that is located at the opposite terminus of the thread.[127] In homogeneous solution, REET is instilled in the free rod, as evidenced through delayed luminescence, because these two chromophores can approach each other during the lifetime of the excited-state. While the abiotic aromatic oligoamide compound was added into the solution, a supramolecular dimer is formed resulting in the self-assembled antiparallel double helix, refolding the rod in its central void and forming a foldaxane **I-26**, i.e. a foldamer on an axel in analogy to the nomenclature employed for rotaxanes. Hence, the rod becomes effectively rigidified, increasing the distance between Ru complex and pyrene chromophore groups to at least 18.5 Å. This distance being very long for triplet-triplet transfer to occur,

consequently, the two chromophores display their individual photophysical characteristics, REET process is turned off. Thus in this example REET process can be used to probe conformation and distance with high sensitivity.

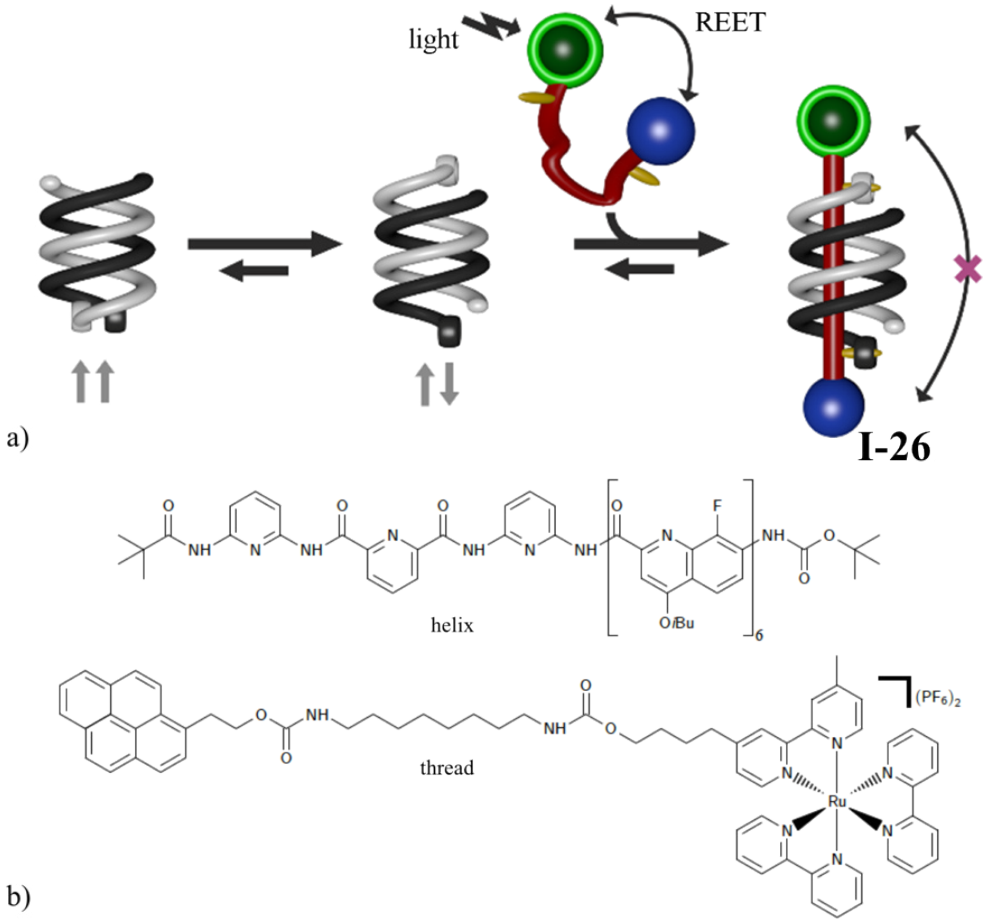

Figure 1.35 a) Representation of the parallel–antiparallel equilibrium of a double helix and the assembly-modulated photophysical properties; b) Structural formula of bichromophoric rod, and the aromatic oligoamide. Copyright (2016) John Wiley and Sons.

1.10 Overview of thesis projects

After more than 20 years of development, the field of artificial molecular machines, it is still in infancy. On the other hand, reversible electronic energy transfer (REET) process has been well studied, and is well-understood in covalent dyads and model systems. It will be interesting and feasible to engineer REET process into the system molecular machines. In the current work, approaches to engineer REET process into different mechanically-interlocked rotaxane systems will be investigated and discussed; studies of using relevant REET measurements to control or track the shuttling movements of the ring on thread will be explored; reversible linear electronic

energy hopping (varying number of acceptors at fixed distance) and rotaxanes as fluorescence sensors will be also investigated.

References

[1] Lehn J. M. Supramolecular Chemistry: Concepts and Perspectives. Wiley-VCH: Weinheim, 1995.

[2] Beer P. D., Gale P. A., Smith D. K. Supramolecular Chemistry. Oxford University Press: Great Britain, 1999.

[3] Pedersen C. J. Cyclic Polyethers and Their Complexes with Metal Salts. J. Am. Chem. Soc., 1967, 89(26), 7017-7036.

[4] Lehn J. M. Nobel Lecture, December 8, 1987.

[5] Balzani V., Nanochemistry: A Chemical Approach to Nanomaterials. small 2006, 2(5), 678-679.

[6] Balzani V., Venturi M., Credi A. Molecular Devices and Machines. Wiley-VCH, Weinheim, 2003.

[7] Balzani V., Credi A., Raymo F. M., Stoddart J. F. Artificial Molecular Machines. Angew. Chem. Int. Ed., 2000, 39(19), 3348-3391.

[8] Feynman R. P. There's Plenty of Room at the Bottom. Eng. Sci., 1960, 23(5), 22-36.

[9] Schill G. Catenanes, Rotaxanes and Knots. Academic Press, New York, 1971.

[10] Amabilino D. B., Stoddart J. F. Interlocked and Intertwined Structures and Superstructures. Chem. Rev., 1995, 95(8), 2725-2828.

[11] Sauvage J. P. Trasition Metal-Containing Rotaxanes and Catenanes in Motions: Toward Molecular Machines and Motors. Acc. Chem. Res., 1998, 31(10), 611-619.

[12] Balzani V., Credi A. Artificial Molecular-Level Machines. The Chemical Record, 2001, 1(6), 422-435.

[13] Balzani V., Credi A., Langford S. J., Raymo F. M., Stoddart J. F., Venturi M. Constructing Molecular Machinery: A Chemically-Switchable [2]Catenane. J. Am. Chem. Soc., 2000, 122(14), 3542-3543.

[14] Jackson D., Megiatto J., Schuster D. I. Alternative Demetalation Method for Cu(I)-Phenanthroline-Based Catenanes and Rotaxanes. Org. Lett., 2011, 13(7), 1808-1811.

[15] Leigh D. A., Wong J. K. Y., Dehez F., Zerbetto F. Unidirectional Rotation in a Mechanically Interlocked Molecular Rotor. Nature, 2003, 424(6945), 174-179.

[16] Vignon S. A., Stoddart J. F. Exploring Dynamics and Stereochemistry in Mechanically Interlocked Compounds. Collect. Czech. Chem. Commun., 2005, 70(10), 1493-1576.

[17] Xue M., Yang Y., Chi ., Yan X., Huang F.-H. Development of Pseudorotaxanes and

Rotaxanes: From Synthesis to Stimuli-Responsive Motions to Applications. Chem. Rev., 2015, 115(15), 7398-7501.

[18] Gao L., Han C., Zheng B., Dong S., Huang F. Formation of a Pillar [5] Arene-based [3]Pseudorotaxane in Solution and in the Solid State. Chem. Commun., 2013, 49(5), 472-474.

[19] Niu Z., Slebodnick C., Bonrad K., Huang F., Gibson H. W. The First [2]Pseudorotaxane and the First Pseudocryptand-type Poly [2]Pseudorotaxane Based on Bis(meta-phenylene)-32-crown-10 and Paraquat Derivatives. Org. Lett., 2011, 13(11), 2872-2875.

[20] Baroncini M., Silvi S., Venturi M., Credi A. Photoactivated Directionally Controlled Transit of a Non-Symmetric Molecular Axle Through a Macrocycle. Angew.Chem., 2012, 124(17), 4299-4302.

[21] Tian H., Wang Q. C. Recent Progress on Switchable Rotaxanes. Chem. Soc. Rev., 2006, 35(4), 361-374.

[22] Anelli P. L., Spencer N., Stoddart J. F. A Molecular Shuttle. J. Am. Chem. Soc., 1991, 113(13), 5131-5133.

[23] Gómez-López M., Preece J. A., Stoddart J. F. The Art and Science of Self-Assembling Molecular Machines. Nanotechnology, 1996, 7(3), 183-192.

[24] Watanabe N., Yagi T., Kihara N., Takata T. Highly Efficient Synthesis of [3] and [5] Rotaxanes Consisting of Crown Ether and a sec-Ammonium Salt. Chem. Comm., 2002, (22) 2720-2721.

[25] Nakazono K., Kuwata S., Takata T., Crown Ether-tert-Ammonium Salt Complex Fixed as Rotaxane and Its Derivation to Nonionic Rotaxane. Tetrahedron Lett., 2008, 49(15), 2397-2401.

[26] Tachibana Y., Kihara N., Furusho Y., Takata T., Is the tert-Butyl Group Bulky Enough to End-Cap a Pseudorotaxane with a 24-Crown-8-ether Wheel? Org. Lett., 2004, 6(24), 4507-4509.

[27] Tachibana Y., Kawasaki H., Kihara N., Takata T. Sequential O- and N-Acylation Protocol for High-Yield Preparation and Modification of Rotaxanes: Synthesis, Functionalization, Structure, and Intercomponent Interaction of Rotaxanes. J. Org. Chem., 2006, 71(14), 5093-5104.

[28] Zhang C. J., Li S. J., Zhang J. Q., Zhu K. L., Li N., Huang F. H. Benzo-21-Crown-7/Secondary Dialkylammonium Salt [2]Pseudorotaxane- and [2]Rotaxane-Type Threaded Structures. Org. Lett., 2007, 9(26), 5553-5556.

[29] Zhang C. J., Zhu K. L.; Li S. J., Zhang J. Q., Wang F., Liu M., Li N., Huang F. H.

Binding of Secondary Dialkylammonium Salts by Pyrido-21-Crown-7. Tetrahedron Lett., 2008, 49(48), 6917-6920.

[30] Jiang W., Winkler H. D. F., Schalley C. A., Integrative Self-Sorting: Construction of a Cascade-Stoppered Hetero[3]rotaxane. J. Am. Chem. Soc., 2008, 130(42), 13852-13853.

[31] Rowan S. J., Cantrill S. J., Stoddart J. F. Triphenylphosphonium-Stoppered [2]Rotaxanes. Org. Lett., 1999, 1(1), 129-132.

[32] Chang T., Heiss A. M., Cantrill S. J., Fyfe M.C.T., Pease A. R., Rowan S. J., Stoddart J. F., White A. J. P., Williams D. J. Ammonium Ion Binding with Pyridine-Containing Crown Ethers. Org. Lett., 2000, 2(19), 2947-2950.

[33] Elizarov A. M., Chiu S. H., Glink P. T., Stoddart J. F. Dendrimer with Rotaxane-Like Mechanical Branching. Org. Lett., 2002, 4(5), 679-682.

[34] Rowan S. J., Cantrill S. J., Stoddart J. F., White A. J. P., Williams D. J. Toward Daisy Chain Polymers: “Wittig Exchange” of Stoppers in [2]Rotaxane Monomers [J]. Org. Lett., 2000, 2(6), 759-762.

[35] Rowan S. J., Stoddart J. F. Precision Molecular Grafting: Exchanging Surrogate Stoppers in [2]Rotaxanes. J. Am. Chem. Soc., 2000, 122(1), 164-165.

[36] Kihara N., Motoda S., Yokozawa T., Takata T. End-Cap Exchange of Rotaxane by the Tsuji-Trost Allylation Reaction. Org. Lett., 2005, 7(7), 1199-1202.

[37] Tokunaga Y., Kawai N., Shimomura Y. Using Ruthenium-Catalysed Propargylic Substitutions for the Efficient Syntheses of Rotaxanes. Tetrahedron Lett., 2007, 48(29), 4995-4998.

[38] Giguère J. B., Thibeault D., Cronier F., Marois J. S., Auger M., Morin J. F. Synthesis of [2]- and [3]Rotaxanes through Sonogashira Coupling. Tetrahedron Lett., 2009, 50(39), 5497-5500.

[39] Trnka T. M., Grubbs R. H. The Development of L2X2Ru=CHR Olefin Metathesis Catalysts: An Organometallic Success Story. Acc. Chem. Res., 2001, 34(1), 18-29.

[40] Suzaki Y., Osakada K. End-capping of Pseudo[2]rotaxane Composed of Alkyl(ferrocenylmethyl)ammonium and Dibenzo[24]crown-8 via Cross Metathesis Reactions. Chem. Lett., 2006, 35(4), 374-375.

[41] Sasabe H., Kihara N., Mizuno K., Ogawa K., Takata T. Efficient Synthesis of [2]- and Higher Order Rotaxanes via the Transition Metal-Catalyzed Hydrosilylation of Alkyne. Tetrahedron Lett., 2005, 46(22), 3851-3853.

[42] Suzaki Y., Osakada K. Ferrocene-containing [2]- and [3]rotaxanes. Preparation via an

End-capping Cross-Metathesis Reaction and Electrochemical Properties. Dalton Trans., 2007, (23) 2376-2383.

[43] Ashton P. R., Fyfe M. C. T., Schiavo C., Stoddart J. F., White A. J. P., Williams D. J. A New Slippage Synthesis. Tetrahedron Lett., 1998, 39(31), 5455-5458.

[44] Ashton P. R., Baxter I., Fyfe M. C. T., Raymo F. M., Spencer N., Stoddart J. F., White A. J. P., Williams D. J. Rotaxane or Pseudorotaxane? That Is the Question! J. Am. Chem. Soc., 1998, 120(10), 2297-2307.

[45] Evans N. H., Beer P. D., A Janus [2]Rotaxane Synthesized by Using an Anion-Templated Clipping Methodology. Chem. Eur. J., 2011, 17(38), 10542-10546.

[46] Yin J., Dasgupta S., Wu J. S. Synthesis of [n]Rotaxanes by Template-Directed Clipping: The Role of the Dialkylammonium Recognition Sites. Org. Lett., 2010, 12(8), 1712-1715.

[47] Klivansky L. M., Koshkakaryan G., Cao D., Liu Y. Linear p-Acceptor-Templated Dynamic Clipping to Macrobicycles and [2]Rotaxanes. Angew. Chem. Int. Ed., 2009, 48(23), 4185-4189.

[48] Goldup S. M., Leigh D. A., Long T., McGonigal P. R., Symes M. D., Wu J. Active Metal Template Synthesis of [2]Catenanes. J. Am. Chem. Soc., 2009, 131, 15924-15929.

[49] Crowley J. D., Goldup S. M., Lee A. L., Leigh D. A., McBurney R. T. Active Metal Template Synthesis of Rotaxanes, Catenanes and Molecular Shuttles [J]. Chem. Soc. Rev., 2009, 38(6), 1530-1541.

[50] Lewis J. E. M., Galli M., Goldup S. M. Properties and Emerging Applications of Mechanically Interlocked Ligands. Chem. Commun., 2017, 53, 298-312.

[51] Aucagne V., Hanni K. D., Leigh D. A., Lusby P. J., Walker D. B. Catalytic “Click” Rotaxanes: A Substoichiometric Metal-Template Pathway to Mechanically Interlocked Architectures. J. Am. Chem. Soc., 2006, 128(7), 2186-2187.

[52] Berná J., Goldup S. M., Lee A.-L., Leigh D. A., Symes M. D., Teobaldi G., Zerbetto F. Cadiot-Chodkiewicz Active Template Synthesis of Rotaxanes and Switchable Molecular Shuttles with Weak Intercomponent Interactions. Angew. Chem. Int. Ed., 2008, 47, 4392-4396.

[53] Crowley J. D., Hanni K. D., Lee A. L., Leigh D. A. [2]Rotaxanes through Palladium Active-Template Oxidative Heck Cross-Couplings. J. Am. Chem. Soc., 2007, 129(40), 12092-12093.

[54] Crowley J. D., Goldup S. M., Gowans N. D., Leigh D. A., Ronaldson V. E., Slawin A. M. Z. An Unusual Nickel-Copper-Mediated Alkyne Homocoupling Reaction for the

Active-Template Synthesis of [2]Rotaxanes. J. Am. Chem. Soc., 2010, 132(17), 6243-6248.

[55] Lahlali H., Jobe K., Watkinson M., Goldup S. M. Macrocycle Size Matters: “Small” Functionalized Rotaxanes in Excellent Yield Using the CuAAC Active Template Approach. Angew. Chem. Int. Ed., 2011, 50, 4151-4155.

[56] Ashton P. R., Ballardini R., Balzani V., Baxter I., Credi A., Fyfe M. C. T., Gandolfi M. T., Gómez-López M., Martínez-Díaz M. V., Piersanti A., Spencer N., Stoddart J. F. Venturi M., White A. J. P., Williams D. J. Acid-Base Controllable Molecular Shuttles. J. Am. Chem. Soc., 1998, 120(46), 11932-11942.

[57] Rogez G., Ribera B. F., Credi A., Ballardini R., Gandolfi M. T., Balzani V., Liu Y., Northrop B. H., Stoddart J. F. A Molecular Plug-Socket Connector [J]. J. Am. Chem. Soc., 2007, 129(15), 4633-4642.

[58] Zheng H. Y., Zhou W. D., Lv J., Yin X. D., Li Y. J., Liu H. B., Li Y. L. A Dual-Response [2]Rotaxane Based on a 1,2,3-Triazole Ring as a Novel Recognition Station. Chem. Eur. J., 2009, 15(47), 13253-13262.

[59] Fang L., Hmadeh M., Wu J. S., Olson M. A., Spruell J. M., Trabolsi A., Yang Y. W., Elhabiri M., Albrecht-Gary A. M., Stoddart J. F. Acid-Base Actuation of [c2] Daisy Chains. J. Am. Chem. Soc., 2009, 131(20), 7126-7134.

[60] Romuald C., Busseron E., Coutrot F. Very Contracted to Extended co-Conformations with or without Oscillations in Two- and Three-Station [c2] Daisy Chains. J. Org. Chem., 2010, 75(19), 6516-6531.

[61] Busseron E., Romuald C., Coutrot F. Bistable or Oscillating State Depending on Station and Temperature in Three-Station Glycorotaxane Molecular Machines. Chem. Eur. J., 2010, 16(33), 10062-10073.

[62] Jiang Y., Guo J. B., Chen C. F. A New [3]Rotaxane Molecular Machine Based on a Dibenzylammonium Ion and a Triazolium Station. Org. Lett., 2010, 12(19), 4248-4251.

[63] Badjic J. D., Balzani V., Credi A., Silvi S., Stoddart J. F. A molecular elevator. Science, 2004, 303(5665), 1845-1849.

[64] Korybut-Daszkiewicz B., Wieckowska A., Bilewicz R., Domagała S., Wozniak K. An Electrochemically Controlled Molecular Shuttle. Angew. Chem. Int. Ed., 2004, 43(13), 1668-1672.

[65] Poleschak I., Kern J. M., Sauvage J. P. A Copper-Complexed Rotaxane in Motions Pirouetting of the Ring on the Millisecond Timescale. Chem. Commun., 2004, (4), 474-476.

[66] Wang C., Dyar S. M., Cao D., Fahrenbach A. C., Horwitz N., Colvin M. T., Carmieli R., Stern C. L., Dey S. K., Wasielewski M. R., Stoddart J. F. Tetrathiafulvalene Hetero Radical Cation Dimerization in a Redox-Active [2]Catenane. J. Am. Chem. Soc., 2012, 134(46), 19136-19145.

[67] Zhu Z. X., Fahrenbach A. C., Li H., Barnes J. C., Liu Z. C., Dyar S. M., Zhang H. C., Lei J. Y., Carmieli R., Sarjeant A. A., Stern C. L., Wasielewski M. R., Stoddart J. F. Controlling Switching in Bistable [2]Catenanes by Combining Donor-Acceptor and Radical-Radical Interactions. J. Am. Chem. Soc., 2012, 134(28), 11709-11720.

[68] Li H., Fahrenbach A. C., Coskun A., Zhu Z. X., Barin G., Zhao Y. L., Botros Y. Y., Sauvage J. P., Stoddart J. F. A Light-Stimulated Molecular Switch Driven by Radical-Radical Interactions in Water. Angew. Chem. Int. Ed., 2011, 50(30), 6782-6788.

[69] Olsen J. C., Fahrenbach A. C., Trabolsi A., Friedman D. C., Dey S. K., Gothard C. M., Shveyd A. K., Gasa T. B., Spruell J. M., Olson M. A., Wang C., Jacquot de Rouville H. P., Botros Y. Y., Stoddart J. F. A Neutral Redox-Switchable [2]Rotaxane. Org. Biomol. Chem., 2011, 9(20), 7126-7133.

[70] Trabolsi A., Khashab N., Fahrenbach A. C., Friedman D. C., Colvin M. T., Coti K. K., Benitez D., Tkatchouk E., Olsen J. C., Belowich M. E., Carmielli R., Khatib H. A., Goddard, W. A., Wasielewski M. R., Stoddart J. F. Radically Enhanced Molecular Recognition. Nature Chem., 2010, 2(1), 42-49.

[71] Durola F., Lux J., Sauvage J. P. A Fast-Moving Copper-Based Molecular Shuttle: Synthesis and Dynamic Properties. Chem. Eur. J., 2009, 15(16), 4124-4134.

[72] Stanier C. A., Alderman S. J., Claridge T. D. W., Anderson H. L. Unidirectional Photoinduced Shuttling in a Rotaxane with a Symmetric Stilbene Dumbbell. Angew. Chem. Int. Ed., 2002, 41(10), 1769-1772.

[73] Zhou W. D., Chen D. G., Li J. B., Xu J. L., Liu H. B., Li Y. L. Photoisomerization of Spiropyran for Driving a Molecular Shuttle. Org. Lett., 2007, 9(20), 3929-3932.

[74] Ma X., Cao J. J., Wang Q. C., Tian H. Photocontrolled Reversible Room Temperature Phosphorescence (RTP) Encoding beta-Cyclodextrin Pseudorotaxane. Chem. Commun., 2011, 47(12), 3559-3561.

[75] Silvi S., Venturi M., Credi A. Light Operated Molecular Machines. Chem. Commun., 2011, 47(9), 2483-2489.

[76] Zhu L. L., Yan H., Wang X. J., Zhao Y. L. Light-Controllable Cucurbit[7]uril-Based Molecular Shuttle. J. Org. Chem., 2012, 77(22), 10168-10175.

[77] Zhang T. P., Mu L. X., She G. W., Shi W. S. Light-Driven Molecular Shuttles Modified

on Silicon Nanowires. Chem. Commun., 2012, 48(3), 452-454.

[78] Balzani V., Clemente-León M., Credi A., Ferrer B., Venturi M., Flood A. H., Stoddart, J. F. Autonomous Artificial Nanomotor Powered by Sunlight. Proc. Natl. Acad. Sci. U. S. A. 2006, 103, 1178.

[79] Brouwer A. M., Frochot C., Gatti F. G., Leigh D. A., Mottier L., Paolucci F., Roffia S., Wurpel W. H. Photoinduction of Fast, Reversible Translational Motion in a Hydrogen-Bonded Molecular Shuttle. Science, 2001, 291, 2124-2128.

[80] Qu D.-H., Wang Q.C., Tian H. A Half Adder Based on a Photochemically Driven [2]Rotaxane. Angew. Chem. 2005, 117, 5430-5433.

[81] Wurpel G. W. H., Brouwer A. M., van Stokkum Ivo H. M., Farran A., Leigh D. A. Enhanced Hydrogen Bonding Induced by Optical Excitation: Unexpected Subnanosecond Photoinduced Dynamics in a Peptide-Based [2]Rotaxane. J. Am. Chem. Soc., 2001, 123(45), 11327-11328.

[82] Ros T. D., Guldi D. M., Morales A. F., Leigh D. A., Prato M., Turco R. Hydrogen Bond-Assembled Fullerene Molecular Shuttle. Org. Lett., 2003, 5(5), 689-691.

[83] Mateo-Alonso A., Ehli C., Guldi D. M., Prato M. A Three-Level Luminescent Response in a Pyrene/Ferrocene Rotaxane. Org. Lett., 2013, 15(1), 84-87.

[84] Umehara T., Kawai H., Fujiwara K., Suzuki T. Entropy-and Hydrolytic-Driven Positional Switching of Macrocycle Between Imine- and Hydrogen-Bonding Stations in Rotaxane-Based Molecular Shuttles. J. Am. Chem. Soc., 2008, 130(42), 13981-13988.

[85] Abraham W., Grubert L., Grummt U. W., Buck K. A Photoswitchable Rotaxane with a Folded Molecular Thread. Chem. Eur. J., 2004, 10(14), 3562-3568.

[86] Suhan N. D., Allen L., Gharib M. T., Viljoen E., Vella S. J., Loeb S. J. Colour Coding the Co-conformations of a [2]Rotaxane Flip-Switch. Chem. Commun., 2011, 47(21), 5991-5993.

[87] Ding Z. J., Zhang Y. M., Teng X., Liu Y. Controlled Photophysical Behaviors between Dibenzo-24-crown-8 Bearing Terpyridine Moiety and Fullerene-Containing Ammonium Salt. J. Org. Chem., 2011, 76(6), 1910-1913.

[88] Yamada Y., Okamoto M., Furukawa K., Kato T., Tanaka K. Switchable Intermolecular Communication in a Four-Fold Rotaxane. Angew. Chem. Int. Ed., 2012, 51(3), 709-713.

[89] Denis M., Qin L., Turner P., Jolliffe K. A., Goldup S. M. A Fluorescent Ditopic Rotaxane Ion Pair Host. Angew. Chem. Int. Ed., 2018, 57, 1- 6.

[90] Coutrot F., Romuald C., Busseron E. A New pH-Switchable Dimannosyl [c2]Daisy

Chain Molecular Machine. Org. Lett., 2008, 10(17), 3741-3744.

[91] Lin T. C., Lai, C. C., Chiu S. H. A Guanidinium Ion-Based Anion- and Solvent Polarity-Controllable Molecular Switch. Org. Lett., 2009, 11(3), 613-616.

[92] Zhang Z. J., Zhang H. Y., Wang H., Liu Y. A Twin-Axial Hetero[7]rotaxane. Angew. Chem. Int. Ed., 2011, 50(46), 10834-10838.

[93] Coutrot F., Busseron. E. A new glycorotaxane molecular machine based on an anilinium and a triazolium station. Chem. Eur. J., 2008, 14(16), 4784-4787.

[94] Young P. G., Hirose K., Tobe Y. Axle Length Does Not Affect Switching Dynamics in Degenerate Molecular Shuttles with Rigid Spacers. J. Am. Chem. Soc. 2014, 136, 7899-7906.

[95] Qu D. H., Wang Q. C., Ren J., Tian H. A Light-Driven Rotaxane Molecular Shuttle with Dual Fluorescence Addresses. Org. Lett., 2004, 6(13), 2085-2088.

[96] Prez E. M., Dryden D. T., Leigh D. A., Teobaldi G., Zerbetto F. A Generic Basis for Some Simple Light-Operated Mechanical Molecular Machines. J. Am. Chem. Soc., 2004, 126(39), 12210-12211.

[97] Yang W. L., Li Y. J., Zhang J. H., Yu Y. W., Liu T. F., Liu H. B., Li Y. L. Synthesis of a [2]Rotaxane Operated in Basic Environment. Org. Biomol. Chem., 2011, 9(17), 6022-6026.

[98] Yang W. L., Li Y. J., Zhang J. H., Chen N., Chen S. H., Liu H. B., Li Y. L., Directed Synthesis of [2]Catenanes Incorporating Naphthalenediimide and Crown Ethers by Associated Interactions of Templates. J. Org. Chem., 2011, 76(19):7750-7756.

[99] Zhang H., Hu J., Qu D.-H. Dual-Mode Control of PET Process in a Ferrocene-Functionalized [2]Rotaxane with High-Contrast Fluorescence Output. Org. Lett., 2012, 14(9), 2334-2337.

[100] Tron A., Jacquot H.-P., Ducrot A., Tucker J. H. R., Baroncini M., Credi A., McClenaghan N. D. Photodriven [2]rotaxane–[2]catenane interconversion. Chem. Commun., 2015, 51, 2810-2813.

[101] Li H., Zhang H., Zhang Q., Zhang Q. W., Qu D. H. A Switchable Ferrocene-Based [1]Rotaxane with an Electrochemical Signal Output. Org. Lett., 2012, 14(23), 5900-5903.

[102] Li H., Zhu Z. X., Fahrenbach A. C., Savoie B. M., Ke C. F., Barnes J. C., Lei J. Y., Zhao Y. L., Lilley L. M., Marks T. J., Ratner M. A., Stoddart J. F. Mechanical Bond-Induced Radical Stabilization. J. Am. Chem. Soc., 2013, 135(1), 456-467.

[103] Gao C., Ma X., Zhang Q., Wang Q. C., Qu D. H., Tian H. A Light-Powered Stretch-

Contraction Supramolecular System Based on Cobalt Coordinated [1]Rotaxane. Org. Biomol. Chem., 2011, 9(4), 1126-1132.

[104] Di Motta S., Avellini T., Silvi S., Venturi M., Ma X., Tian H., Credi A., Negri F. Photophysical Properties and Conformational Effects on the Circular Dichroism of an AzobenzeneCyclodextrin [1]Rotaxane and Its Molecular Components. Chem. Eur. J., 2013, 19(9), 3131-3138.

[105] Angelos S., Yang Y. W., Patel K., Stoddart, J. F., Zink J. I. pH-Responsive Supramolecular Nanovalves Based on Cucurbit[6]uril Pseudorotaxanes. Angew. Chem. Int. Ed., 2008, 47(12), 2222-2226.

[106] Blanco V., Carlone A., Hanni K. D., Leigh D. A., Lewandowski B. A Rotaxane-Based Switchable Organocatalyst. Angew. Chem. Int. Ed., 2012, 51(21), 5166-5169.

[107] Jiao Y., Li W.-L., Xu J.-F., Wang G.-T., Li J., Wang Z.-Q., Zhang X. A Supramolecularly Activated Radical Cation for Accelerated Catalytic Oxidation. Angew. Chem. Int. Ed. 2016, 55, 1-6.

[108] Hsueh S.-Y., Kuo C.-T., Lu T.-W., Lai C.-C., Liu Y.-H., Hsu H.-F., Peng S.-M., Chen C.-H., Chiu S.-H. Acid/Base- and Anion-Controllable Organogels Formed From a Urea-Based Molecular Switch. Angew. Chem. Int. Ed. 2010, 49, 9170-9173.

[109] Dong S., Luo Y., Yan X. Z., Zheng B., Ding X.,Yu Y. H., Ma Z., Zhao Q. L., Huang F. H. A Dual-Responsive Supramolecular Polymer Gel Formed by Crown Ether Based Molecular Recognition. Angew. Chem. Int. Ed. 2011, 50, 1905-1909.

[110] Yu G. C., Zhou X. Y., Zhang Z. B., Han C. Y., Mao Z. W., Gao C. Y., Huang F. H. Pillar[6]arene/Paraquat Molecular Recognition in Water: High Binding Strength, pH-Responsiveness, and Application in Controllable Self-Assembly, Controlled Release, and Treatment of Paraquat Poisoning. J. Am. Chem. Soc., 2012, 134(47), 19489-19497.

[111] Basílio N., Pischel U. Drug Delivery by Controlling a Supramolecular Host-Guest Assembly with a Reversible Photoswitch. Chem. Eur. J. 2016, 22, 15208-15211.

[112] Bai H. T., Yuan H. X., Nie C. Y., Wang B., Lv F. T., Liu L. B., Wang S. A Supramolecular Antibiotic Switch for Antibacterial Regulation. Angew. Chem. Int. Ed. 2015, 54, 13208-13213.

[113] Coyle J. D., John. Wiley & Sons Inc 1988.

[114] Williams A. T., Winfield S. A., Miller J. N. Analyst 1983, 108, 1067-1071.

[115] Valeur B. Wiley-VCH Verlag GmbH 2001.

[116] Birks J. B. Organic Molecular Photophysics. Wiley-VCH., 1975.

[117] Lakowicz J. Principles of Fluorescence Spectroscopy. Principles of Fluorescence

Spectroscopy. New York: Kluwer Academic, 1999.

[118] Valeur B. Molecular Fluorescence: Principles and Applications. Wiley-VCH, 2002, 387.

[119] Rajapakse H. E., Miller L. W. Time-resolved Luminescence Resonance Energy Transfer Imaging of Protein-Protein Interactions in Living Cells. Proc. Natl. Acad. Sci., 2010, 107, 13582-13587.

[120] Peng H.-Q., Niu L.-Y., Chen Y.-Z., Wu L.-Z., Tung C.-H., Yang Q.-Z. Biological Applications of Supramolecular Assemblies Designed for Excitation Energy Transfer. Chem. Rev., 2015, 115, 7502-7542.

[121] Wu P. G., Brand L. Resonance Energy Transfer: Methods and Applications“. Anal. Biochem., 1994, 218, 1–13.

[122] McClenaghan N. D., Barigelletti F., Maubert B., Campagna S. Chem. Commun., 2002, 602.

[123] Imahori H., Mori Y., Matano Y. Nanostructured Artificial Photosynthesis. J. Photochem. Photobiol., 2003, 4, 51-83.

[124] Balzani V., Credi A., Venturi M. Molecular Devices and Machines: Concepts and Perspectives for the Nanoworld, Second Edition. Wiley-VCH Verlag GmbH & Co. KGaA, 2008.

[125] Montalti M., Credi A., Prodi L., Gandolfi M. T. Handbook of Photochemistry, Third Edition. London: CRC/Taylor & Francis, 2006, 633.

[126] Ford W. E., Rodgers M. A. J. Reversible Triplet-Triplet Energy Transfer within a Covalently Linked Bichromophoric Molecule. J. Phys. Chem., 1992, 96, 2917–2920.

[127] Denisov S. A., Gan Q., Wang X., Scarpantonio L., Ferrand Y, Kauffmann B., Jonusauskas G., Huc I., McClenaghan N. D. Electronic Energy Transfer Modulation in a Dynamic Foldaxane: Proof-of-Principle of a Lifetime-Based Conformation Probe. Angew. Chem., 2016, 128, 1350-1355.

Chapter 2 Prototype [2]Rotaxanes Engineered with Reversible Electronic Energy Transfer Processes

2.1 Introduction

2.1.1 Introduction to rotaxanes formation by AT-CuAAC

Concerning rotaxane construction, the active template Cu-mediated alkyne-azide cycloaddition reaction (AT-CuAAC)[1,2] has rapidly become one of the tools of choice for the synthesis of rotaxanes. In this approach, the copper ion plays the dual role of template and catalyst. The Cu-catalysed mechanism of rotaxane formation is illustrated in Fig. 2.1, using a bidentate macrocycle as an example. Firstly, a Cu(I) ion coordinates with two nitrogens of the bidentate macrocycle. Then coordination of the azide and terminal alkyne to the copper can occur through opposite faces of the macrocycle, completing the preferred tetrahedral primary coordination sphere of Cu(I). Finally, after reaction and demetalation with a suitable ligating base (such as: KCN, EDTA/$NH_{3\ sat}$, or TBACN), a [2]rotaxane is obtained. Employing AT-CuAAC to construct rotaxanes has several advantages: its broad substrate scope; high synthetic yield; mild reaction conditions and facile separation of products.

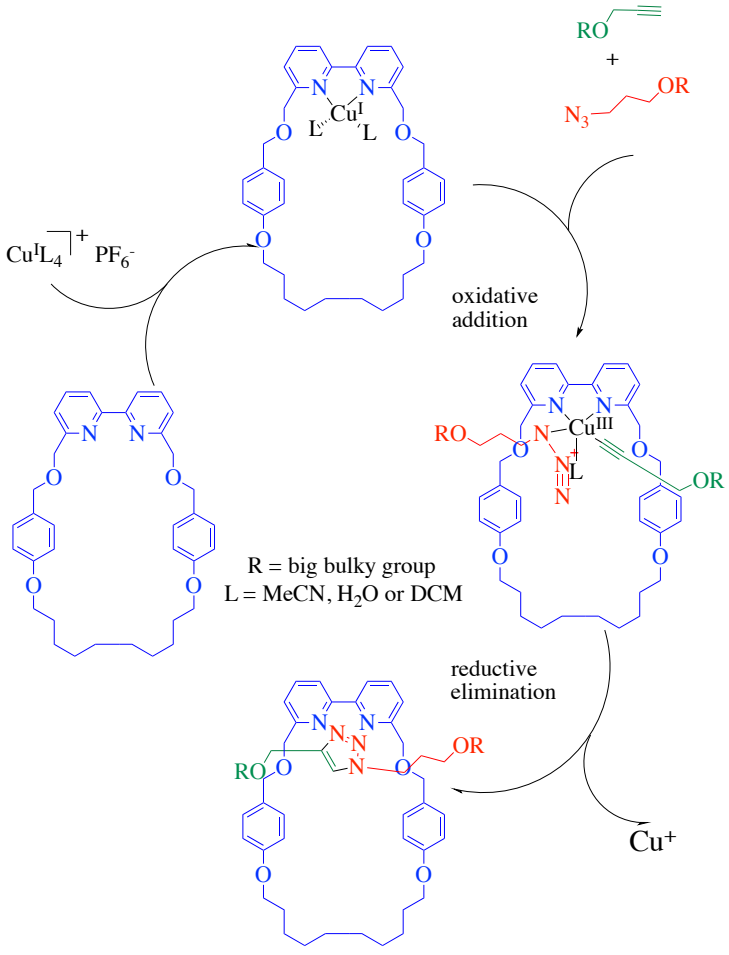

Figure 2.1 Mechanism of rotaxane formation by AT-CuAAC reaction.

By varying the reaction conditions and reactant stoichiometry, the desired rotaxane can be obtained in good yields (80% - 98%) via the AT-CuAAC method. As shown in Fig. 2.2.a, Leigh and co-workers found the yield of such rotaxanes (based on the quantity of macrocycle) was increased to 94% by adding 5 equivalents of azide and alkyne.[3] Furthermore, the yield based on half-threads increased to > 95% with using 10 equivalents of macrocycle to decrease the quantity of uncoordinated Cu^{I} ion.[4] In 2011, the group of Goldup found that the macrocycle size affected the yield of AT-CuAAC rotaxane formation[5]. In all investigated macrocycles, the smallest macrocycle (Fig. 2.2.b) was > 99% consumed, with just one equivalent of half short threads. In 2013, they also observed the formation of a rotaxane Cu^{I} triazolide **28-Cu** (Fig. 2.2.c) as judged by NMR, MS and single-crystal X-ray diffraction analysis.[6] Furthermore, it was the first observation of the triazolide intermediate of rotaxane formation by AT-CuAAC, which also verifies the aforementioned mechanism.

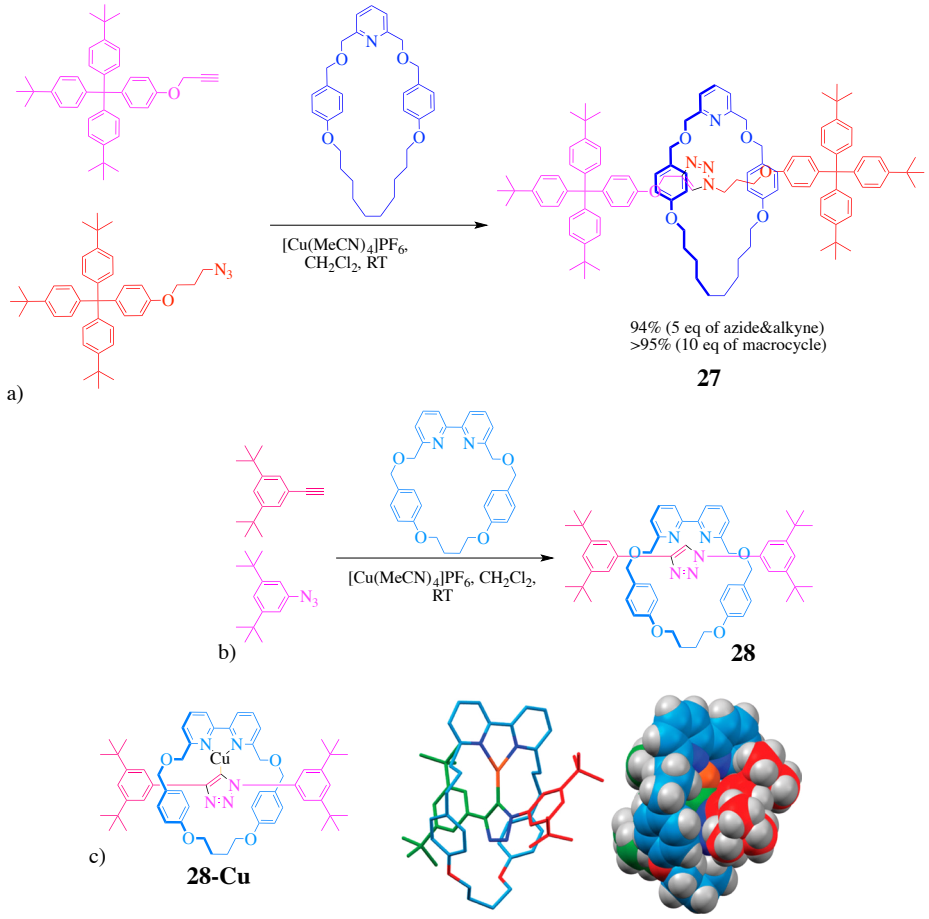

Figure 2.2 a) Leigh's original active template CuAAC reaction; b) Goldup's active template CuAAC reaction with smallest macrocycle investigated; c) The chemical structure and X-ray diffraction representation of the first observed triazolide intermediate **28-Cu** through CuAAC by Goldup et al.

2.1.2 Formation of bipyridine-containing macrocycles

Formation of rotaxanes incorporating bipyridine macrocycles using AT-CuAAC reactions are often high yielding. However, macrocyclisations involving bipyridine precursors, typically via a double Williamson etherification, are extremely inefficient: 5-20 % yield. That is partly due to the fact that the bipyridine unit preferentially adopts a trans-rotamer form, which hinders the desired macrocyclisation, leading to a low yield. In 2016, the group of Goldup developed a new strategy for macrocyclisation: forming the ligand during the macrocyclisation process.[7] The desired macrocycle precursor (Fig. 2.3), a thread bearing a 2-bromopyridine unit on each side, was prepared. Following the intramolecular coupling mediated by Ni(0), the ligand was formed; after EDTA/$NH_{3\ sat}$ washing to break the ligand-metal adduct, the corresponding bipyridine macrocycle was successfully afforded in high yield.

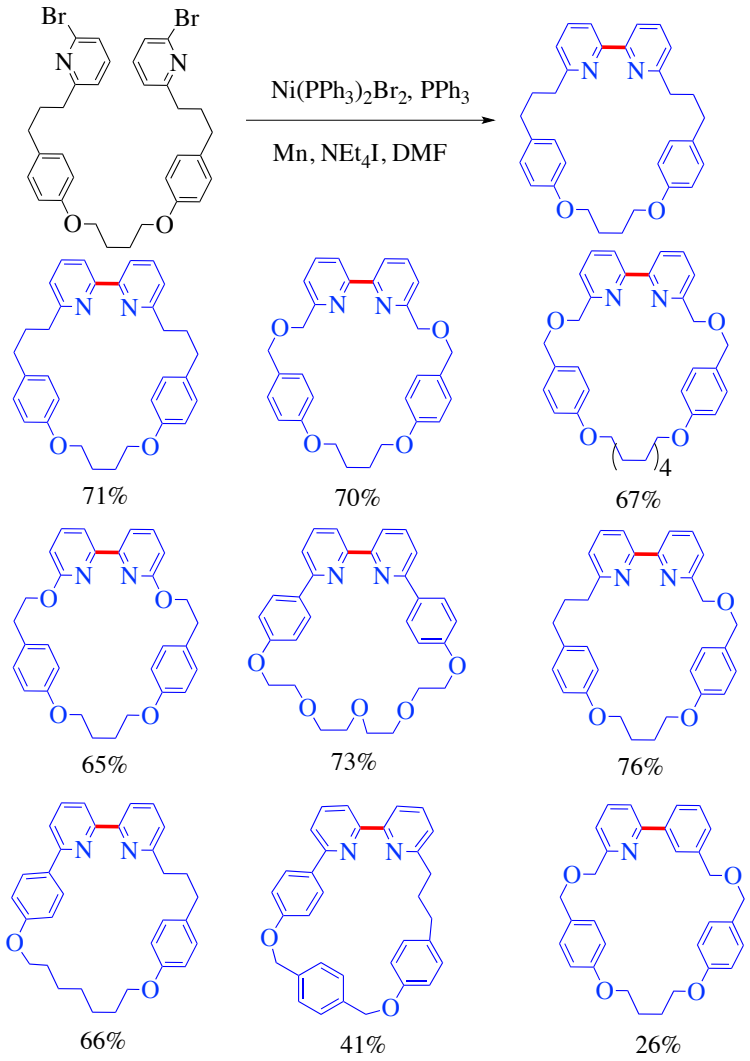

Figure 2.3 Ni-mediated synthesis of macrocycles developed by Goldup et al.

2.2 Strategy for development of rotaxanes exhibiting REET

Based on all revealed reports, a fine design of mechanically-interlocked rotaxane formation is possible. In particular, the incorporation of functional sub-components opens the possibility to investigate a range of processes in a well-defined architecture. In the current project, the formation of rotaxanes by the AT-CuAAC reaction with potential REET processes was proposed, as illustrated in Fig. 2.4. The red half rod (**P**) represents a Ru-complex alkyne as a stopper and a donor group of REET process, the grey half rod (**T**) represents a classic trityl group with an azide as a stopper, the torus part represents a bipyridine macrocycle with a pyrene group or a pyrene derivative as a tail. Under copper(I) catalysed condition, when the macrocycle size is suitable, AT-CuAAC rotaxane formation with potential REET process is possible.

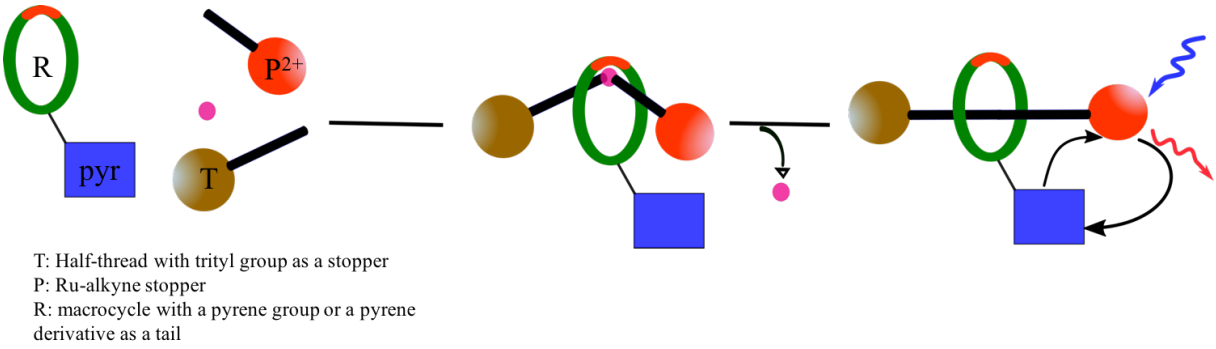

Figure 2.4 Strategy to construct rotaxanes displaying REET processes by AT-CuAAC reactions, **P** represents a Ru-complex alkyne, **T** represents a trityl group with an azide, **R** represents a macrocycle functionalized by a pendant pyrene group.

2.3 Synthesis of trityl stoppers functionalized by an azide terminal group

The tetraphenylmethane trityl group and its derivatives represent a popular choice of the stoppers in rotaxane formation, because of their large size and classical synthesis route. Two trityl stoppers functionalized by terminal azide groups were synthesized, following the literature procedure set out by Li Hai-Gen,[8] and their scheme is shown in Fig. 2.5. Commercially-available 1-bromo-4-*tert*-butylbenzene (**II-1**) was used to form a Grignard reagent, using magnesium with a catalytic amount of iodine. The following reaction gave tris(4-(*tert*-butyl)phenyl)methanol (**II-3**) by using methyl 4-*tert*-butylbenzoate (**II-2**) to attack the Grignard reagent. A Friedel-Crafts reaction of **II-3** in phenol using HCl as a catalyst provided

4-tris(4-*tert*-butylphenyl)phenol (**II-4**), which was monosubstituted by a large excess of the dibromoalkane compounds with different chain lengths, using a Williamson etherification reaction. The final steps were the substitutions of bromides by azide groups, affording trityl stoppers (**T_1**, **T_2**) functionalized by reactive terminal azide group.

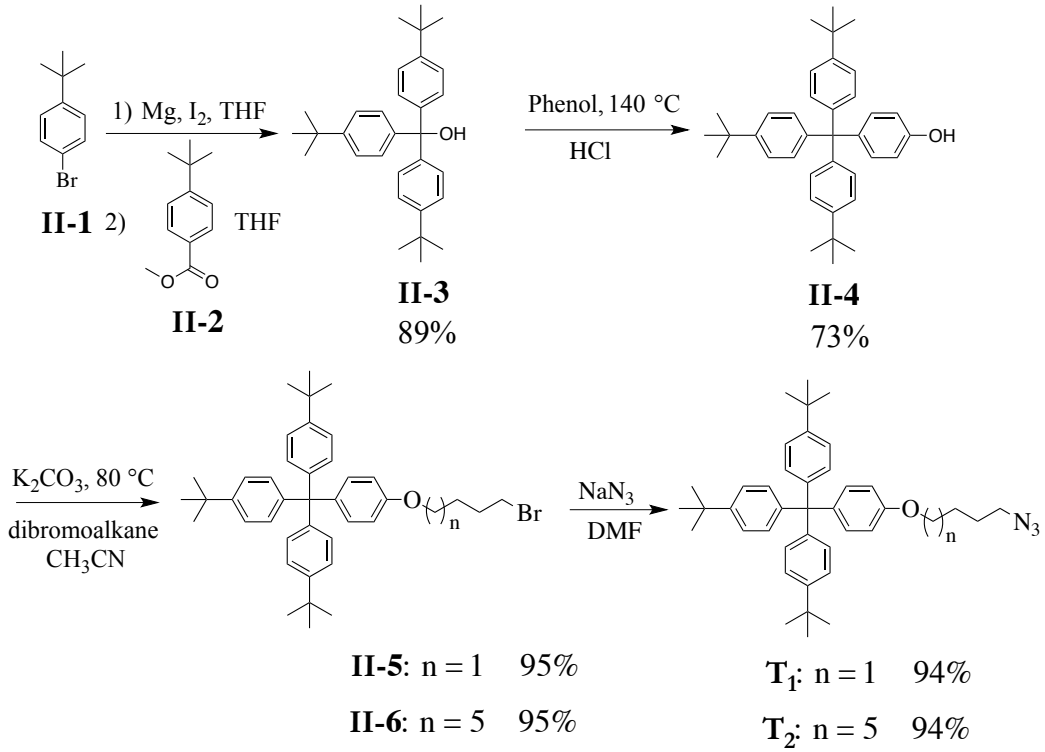

Figure 2.5 Synthetic scheme of two trityl stoppers functionalized by terminal azide group.

2.4 Synthesis of Ru complex stopper functionalized by a terminal alkyne group

When a Ru complex, a photosensitizer, is engineered into a rotaxane system, it also can be used as a stopper.[9] Following the literature procedure set out by Baron et al.,[10] the scheme for synthesizing a Ru complex stopper (**P_1**) functionalized by a terminal alkyne group was shown in Fig. 2.6. One nitrogen of commercially-available 2,2'-bipyridine (**II-7**) was reacted with hydrogen peroxide in a solution of TFA to afford the corresponding N-oxide compound, namely 2,2'-bipyridine-1-oxide (**II-8**). Reaction with KNO_3 in the concentrated H_2SO_4 introduced a $-NO_2$ group, which was subsequently replaced by bromine in the presence of acetyl bromide, and deprotected using PBr_3. Following the Sonogashira coupling reaction with (trimethylsilyl)acetylene and deprotection of trimethylsilyl group by treatment with potassium

carbonate, compound **II-11** was transformed into compound **II-13**. After the complexation of compound **II-13** with $[Ru(bpy)_2Cl_2]$, and workup, the Ru complex stopper (**P_1**) functionalized by a terminal alkyne group was obtained.

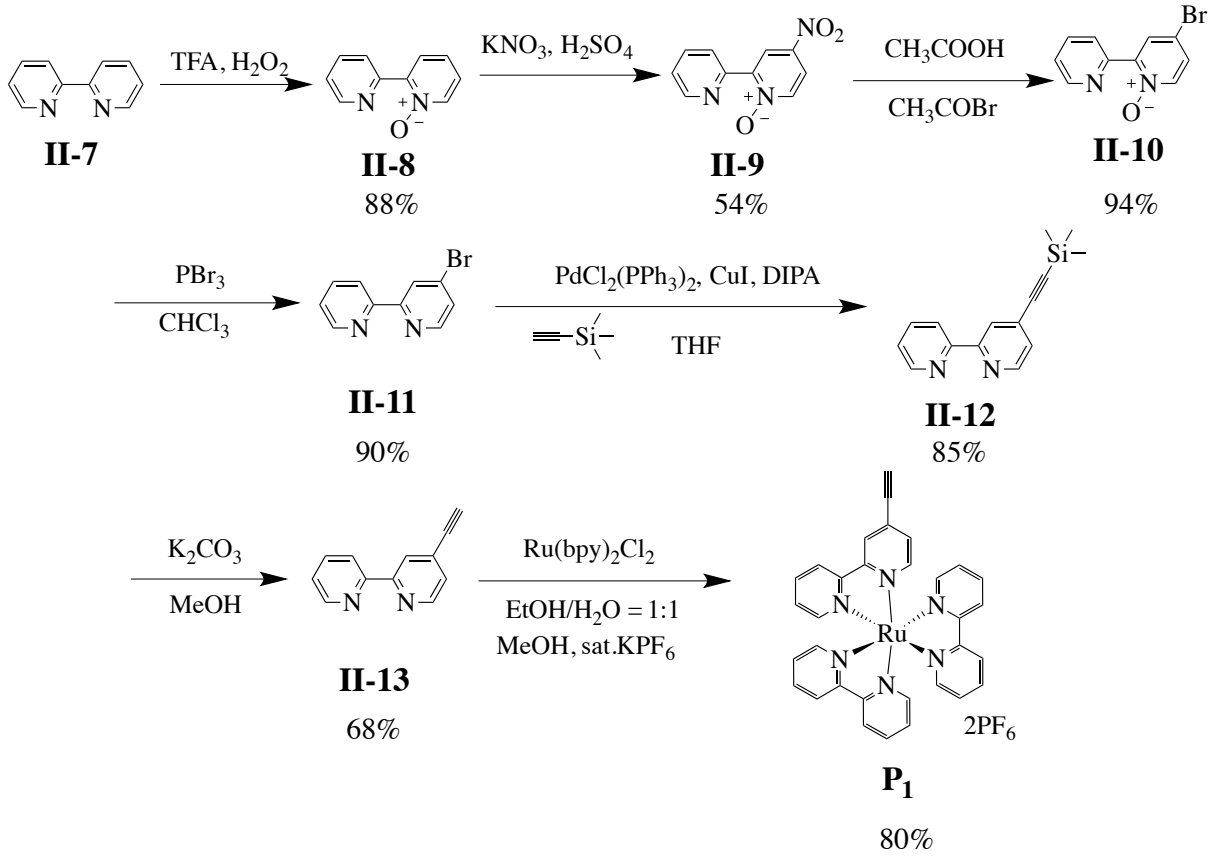

Figure 2.6 Synthesis scheme of Ru(bipyridine)$_2$(bipyridine-CCH) hexafluorophosphate (**P_1**).

2.5 Formation of rotaxanes M_1&M_2

2.5.1 Synthesis of macrocycles functionalized by a pendant pyrene group

Owing to the high yield of macrocyclisation using Ni-mediated coupling, the favoured synthetic scheme for the first pyrene-macrocycle is shown in Fig. 2.7. The short arm **II-15** was afforded in two steps: mono-Suzuki coupling reaction of (4-methoxyphenyl)boronic acid and 2,6-dibromopyridine, and deprotection of the methoxy-group by treatment with HBr. On the other hand, compound 4-(1-pyrene)catechol (**II-17**) was obtained by a Suzuki coupling reaction of 1-pyrene boronic acid and 4-bromo-1,2-dimethoxybenzene, and deprotection of methoxyl groups by BBr_3 treatment. This catechol was then reacted with 3-bromopropanol to afford two arms, which were then tosylated by TsCl in the presence of TEA. A pyrene-macrocycle-

precursor was synthesized by the Williamson etherification of 1 equivalent of tosylate **II-19** and 2 equivalents of phenol. Using the Ni-mediated coupling method in a highly diluted solution, a first bipyridine macrocycle functionalized by a pendant pyrene group was afforded in 50% yield.

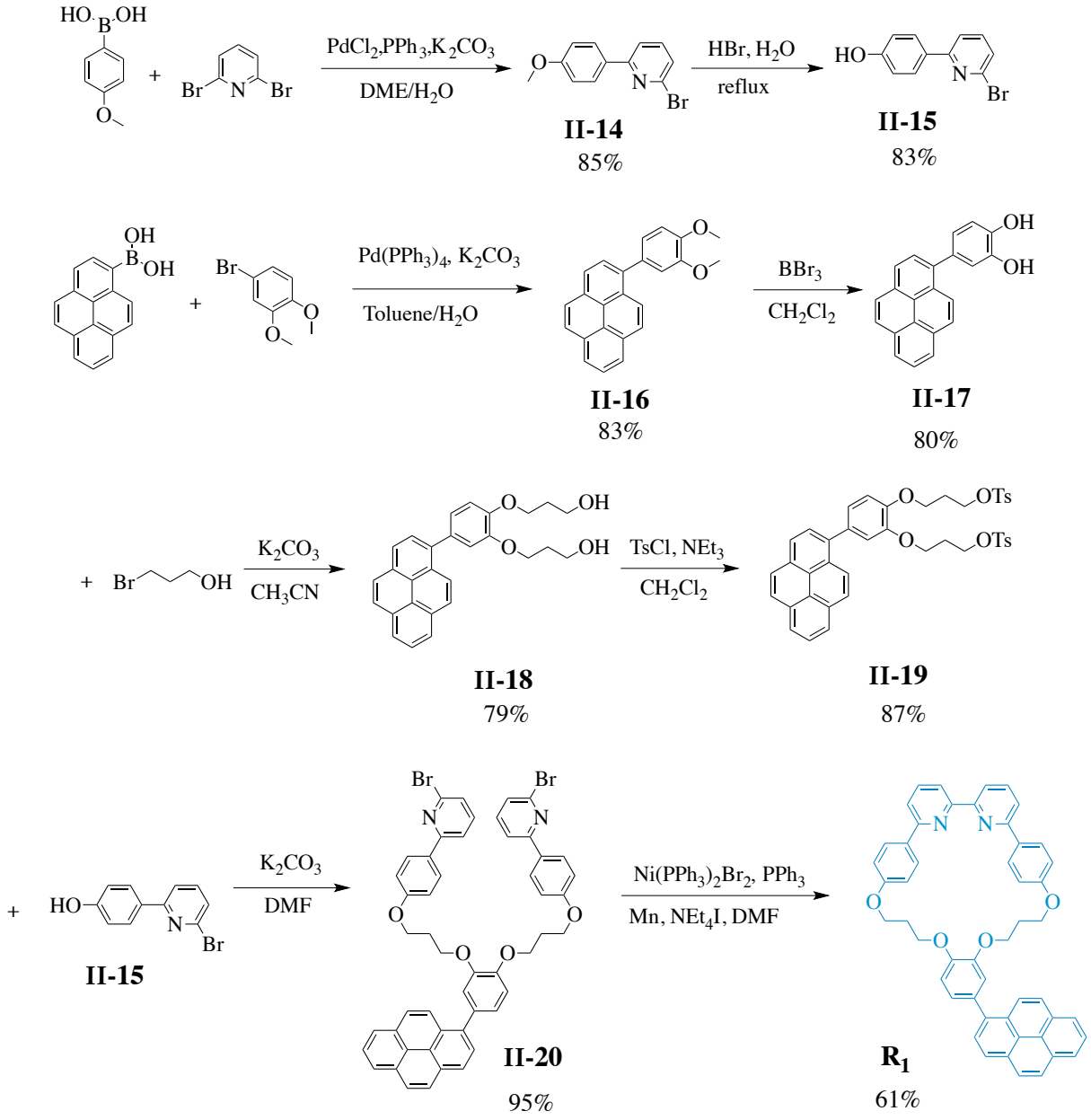

Figure 2.7 Synthetic scheme of a rigid pyrene-macrocycle $\mathbf{R_1}$.

2.5.2 Rotaxane formation test

Instead of using the more precious pyrene-macrocycle to try the rotaxane synthesis directly, a classical small macrocycle **R$_0$** reported by Goldup's group was used to make a rotaxane formation test with 1.5 equivalents of stopper **T$_1$** and **P$_1$**, as shown in Fig. 2.8. It is noteworthy that the weighing of the Cu(I) is very important, as even a small excess will significantly reduce the rotaxane yields.

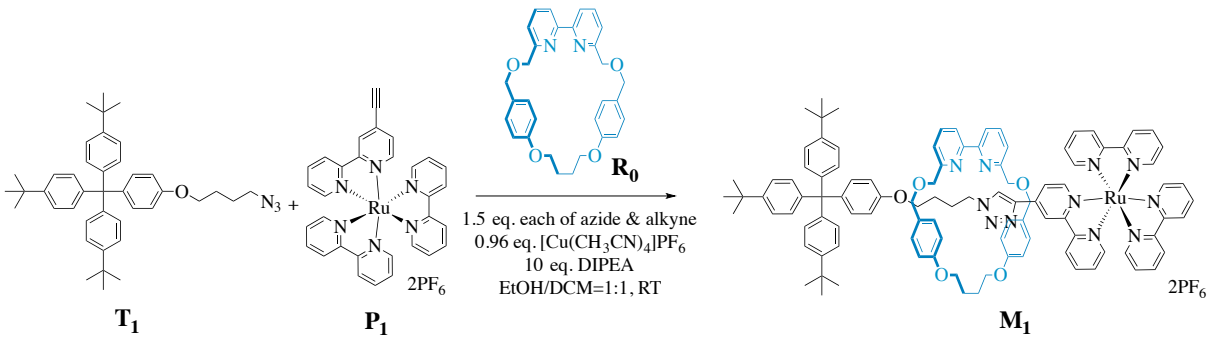

Figure 2.8 Synthetic scheme of rotaxane **M$_1$**.

Compared with ^{1}H NMR of free **R$_0$**, ^{1}H NMR spectrum of an aliquot of the reaction mixture forming rotaxane **M$_1$** (Fig. 2.9.a) showed the macrocycles were almost totally consumed, and the mass spectrum of the mixture also showed the formation of the desired [2]rotaxane ((**M$_1$**-2PF$_6$)/2 = 838.8).

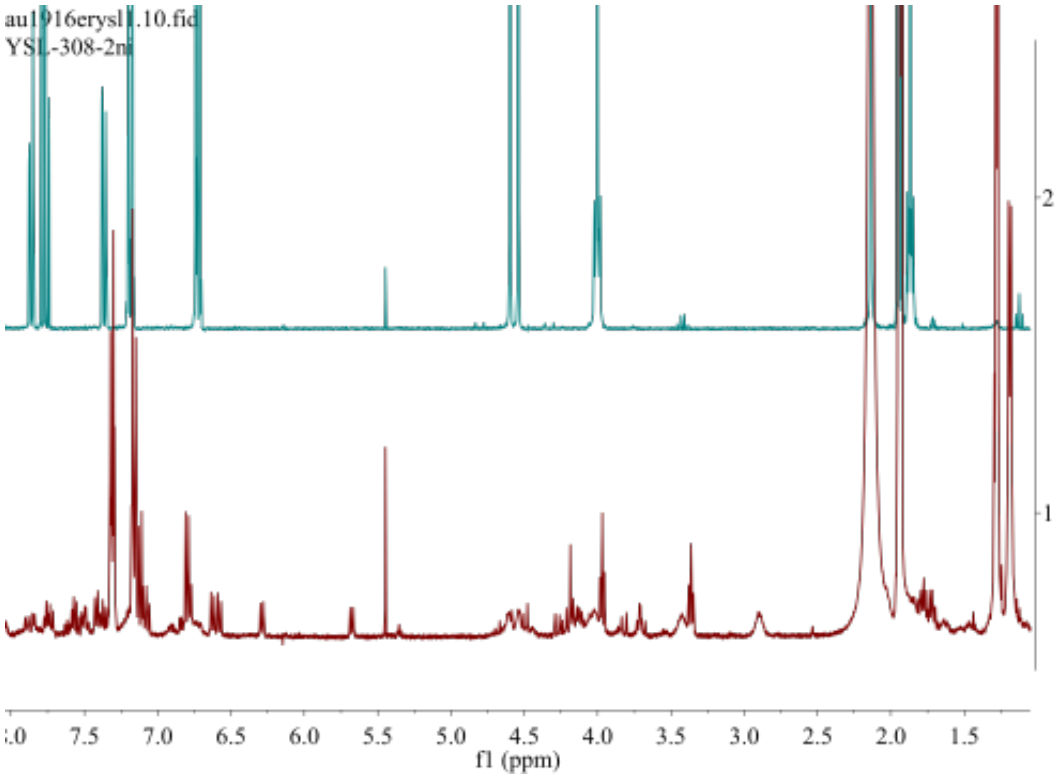

a)

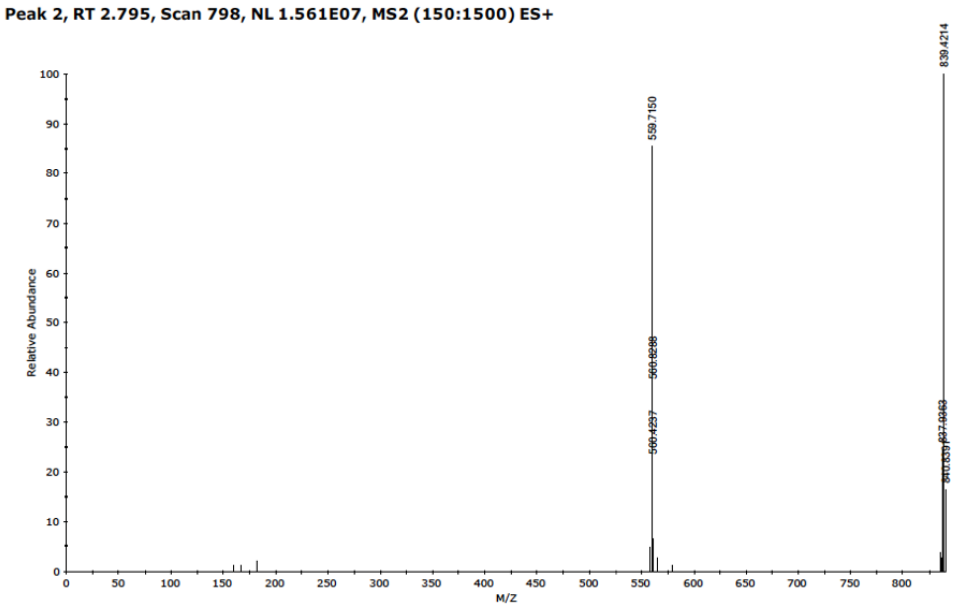

b)

Figure 2.9 a) ^{1}H NMR spectra of Goldup-type macrocycle (top) and mixture $\mathbf{M_1}$ in CD_3CN (bottom) after reaction; b) Mass spectrum of the mixture $\mathbf{M_1}$ in MeCN.

After the purification by column chromatography on silica and ion-exchange, a pure potential [2]rotaxane fraction was obtained in high yield (80%) from the mixture, whose ^{1}H NMR is shown in Fig. 2.10. This test showed that rotaxane formation by AT-CuAAC reaction is possible with the Ru complex stopper $\mathbf{P_1}$ as the alkyne group.

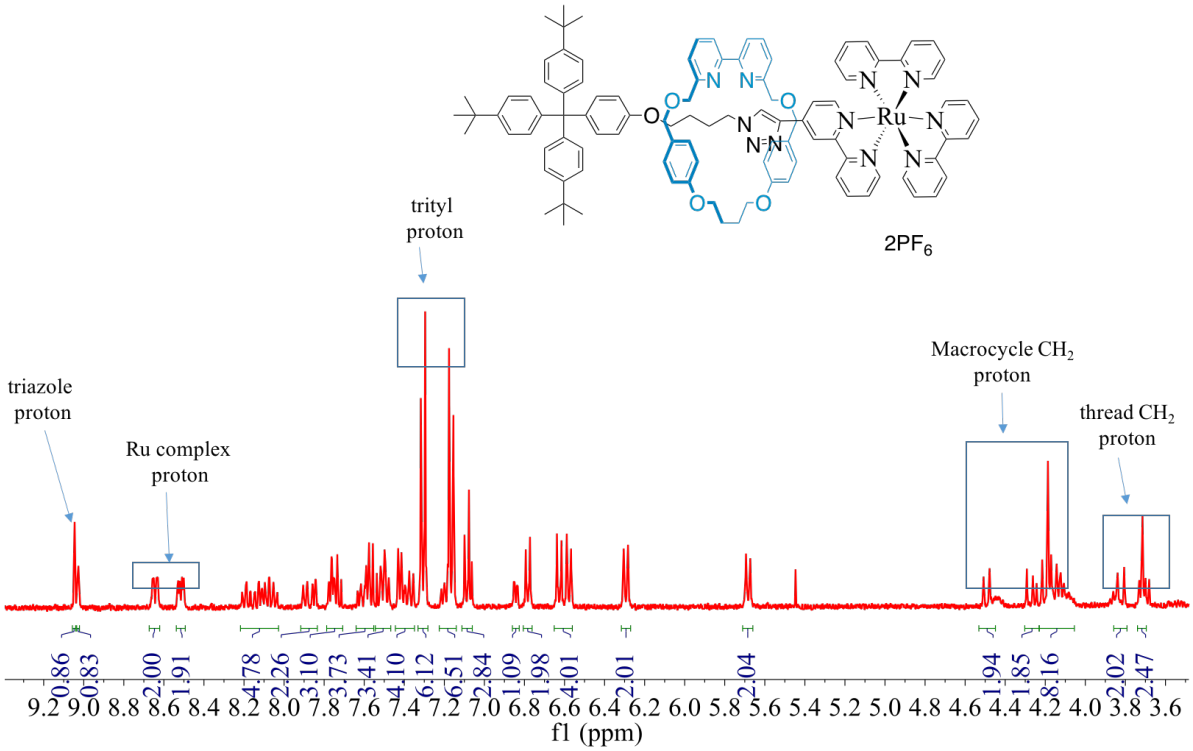

Figure 2.10 ^{1}H NMR of product **M$_1$** in CD_3CN.

2.5.3 Formation of rotaxane M$_2$

The first rotaxane formation (see conditions in Fig. 2.11) to yield a product potentially engineered with REET processes was attempted, using pyrene-macrocycle **R$_1$**. Unfortunately, very few new peaks, mostly the signals of the original free macrocycle and the empty thread, were seen in the ^{1}H NMR of an aliquot of mixture, which was taken after 3 days stirring at room temperature under nitrogen atmosphere. That is due to the small cavity of the macrocycle **R$_1$** and the steric hinderance of the bis-phenyl bipyridine head unit, which greatly impeded the formation of rotaxane.

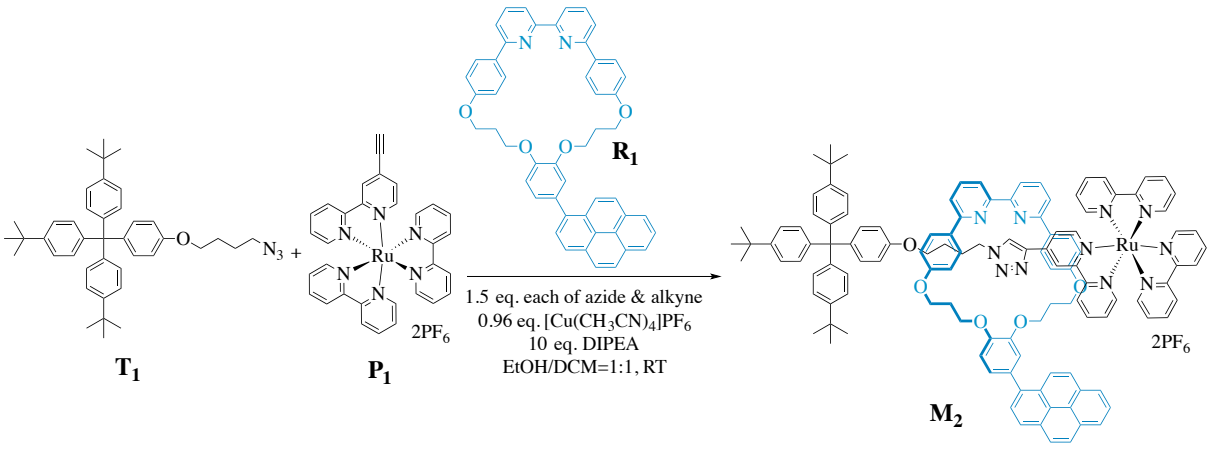

Figure 2.11 Synthetic scheme of macrocycle **M_2**

2.6 Formation of rotaxane M_3 with a flexible macrocycle

It was considered a logical progression to test a less sterically-hindered macrocycle, like macrocycle **R_2** which is shown in Fig. 2.12. A short arm 6-bromo-2-pyridinemethanol (**II-21**) was synthesized by the reduction of ethyl 6-bromo-2-picolinate, using sodium borohydride. The second pyrene-macrocycle-precursor was afforded by a Williamson etherification reaction with 1,4-bis(chloromethyl)benzene and **II-21** in two steps. Using the Ni-mediated coupling method in a highly diluted solution, a more flexible pyrene-macrocycle (**R_2**) was afforded in 70% yield. This flexible macrocycle was used to construct a new rotaxane **M_3** with 1.5 equivalents of stopper **T_2** and **P_1**. From the crude ^{1}H NMR of mixture **M_3**, most of the free **R_2** was consumed, the peaks belonged to the -CH_2- of **R_2** shifted and split, and the triazole peak was appeared at 9.55 – 9.75 ppm.

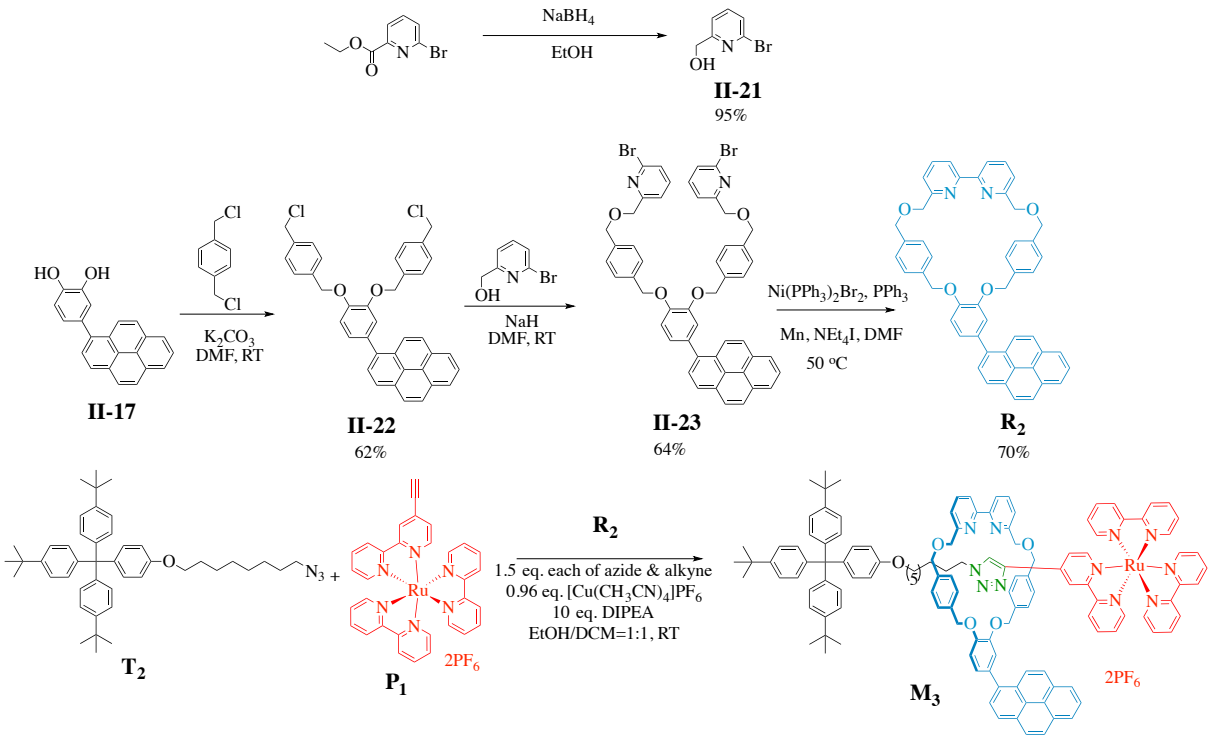

Figure 2.12 Synthesis scheme of rotaxane **M_3**.

After the standard work-up, the crude product was purified by column chromatography and GPC to afford the major fraction, whose ^{1}H NMR spectrum is shown in Fig. 2.13, at 9.55 – 9.75 ppm, two triazole peaks were found. On analyzing this NMR spectrum, specific peaks were attributed to the trityl group, many specific multiplet peaks correspond to the Ru^{2+} complex, a triplet peak at 3.86 ppm belong to the thread component and some shifted and split macrocycle peaks were found, which are consistent with the formation of the desired compound. However in this ^{1}H NMR spectra, many peaks doubled up because of the chirality influence of the asymmetrical pyrene-macrocycle and Λ&Δ stereoisomers of the ruthenium moiety. Owing to the complexity in detailed attribution, more symmetrical variants were sought.

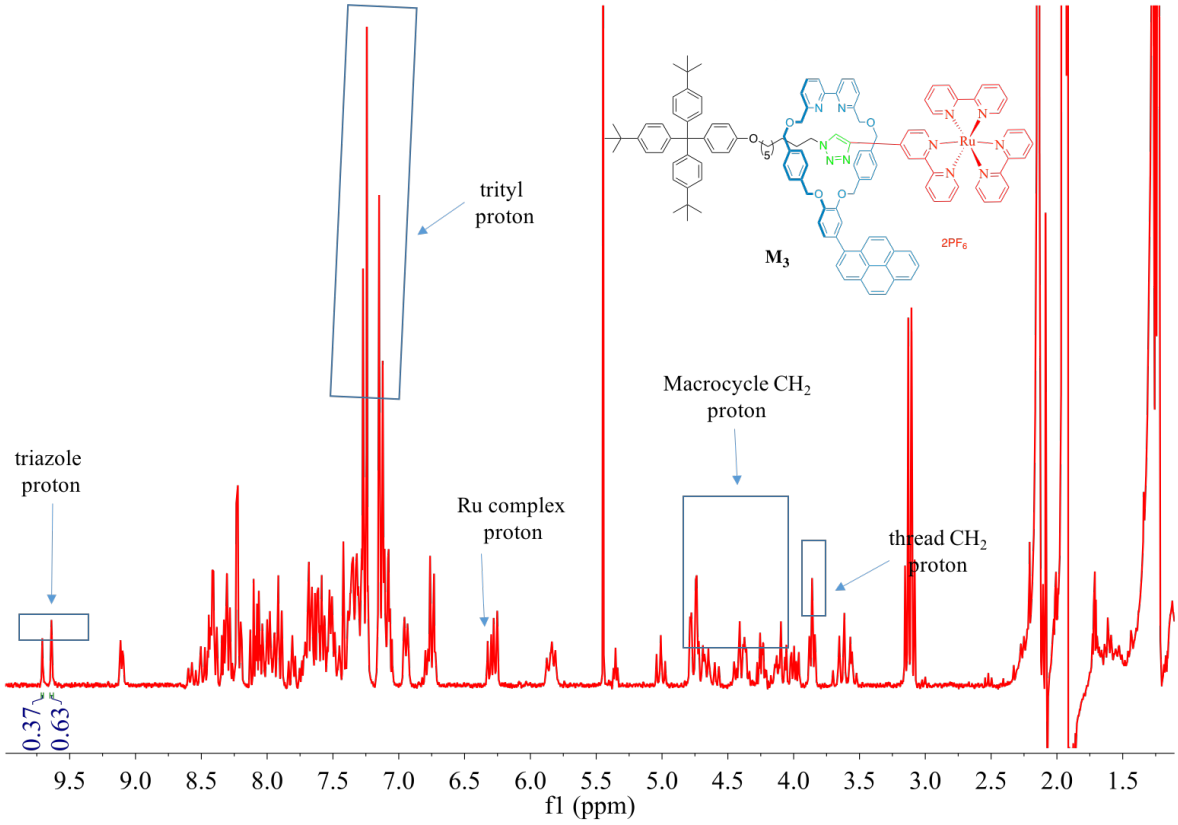

Figure 2.13 ^{1}H NMR of product **M$_3$** in CD_3CN.

2.7 Formation of rotaxane M$_4$ with a symmetrical macrocycle

2.7.1 Synthesis and characterization of rotaxane M$_4$

Taking into account the role of isomers, a symmetrical pyrene-macrocycle was designed with only a small modification and synthesized using the same method and route as the previous one, as shown in Fig. 2.14. To minimize the consumption of the precious pyrene moiety, a convergent approach was adopted, where an arm (**II-24**) was obtained before being attached to the pyrene moiety. In order to avoid getting an asymmetrical pyrene-macrocycle, 3,5-dimethoxybromobenzene was chosen as the starting material, and to obtain 3,5-dimethoxy-(1-pyrene)benzene (**II-25**), which was deprotected by BBr_3 affording 5-pyrene-resorcinol (**II-26**). A Williamson etherification of **II-26** and **II-24** provided the macrocycle precursor **II-27**, which was coupled to give a symmetrical macrocycle **R$_3$**. **R$_3$** was used to construct a new rotaxane **M$_4$** with 1.5 equivalents of stoppers **T$_2$** and **P$_1$**.

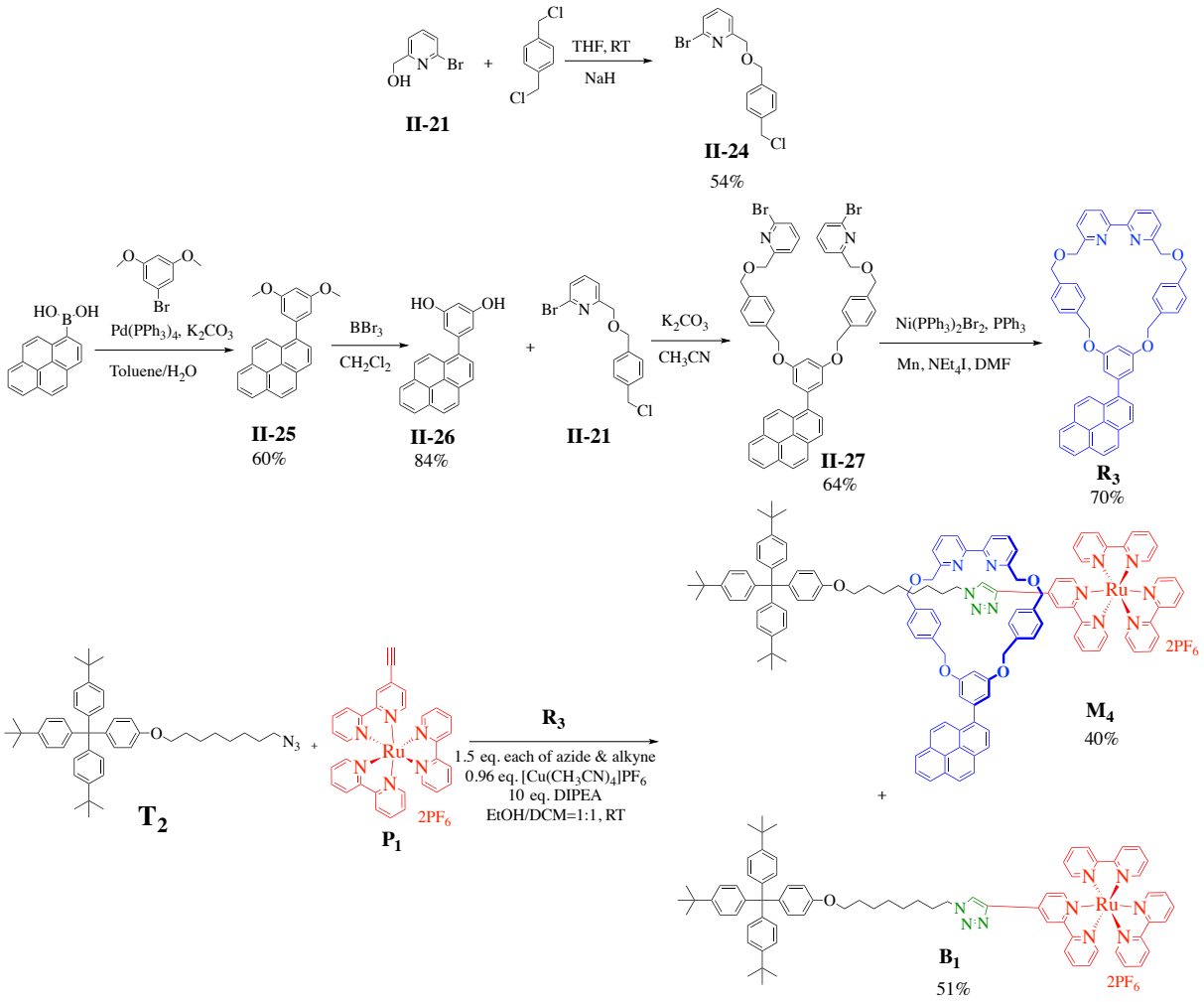

Figure 2.14 Synthesis scheme of **M4**.

After the standard work-up, the crude product was purified by column chromatography and GPC to afford the largest fraction, whose ^{1}H NMR spectrum is shown in Fig. 2.15. A singlet peak at 8.87 ppm could be attributed to the triazole proton, two specific multiplet peaks at 7.30 – 7.10 ppm could be attributed to the trityl group, a multiplet peak at 7.85 – 7.63 ppm corresponds to the Ru complex, two triplet peaks at 3.76 – 3.56 ppm are associated to the thread component and some specific peaks at 5.19 – 4.13 ppm belong to the macrocycle -CH_2- groups and so on, with the corresponding integration values. When taken in conjunction with the ^{13}C NMR spectrum and HRMS, this fraction could be unambiguously identified as the target rotaxane.

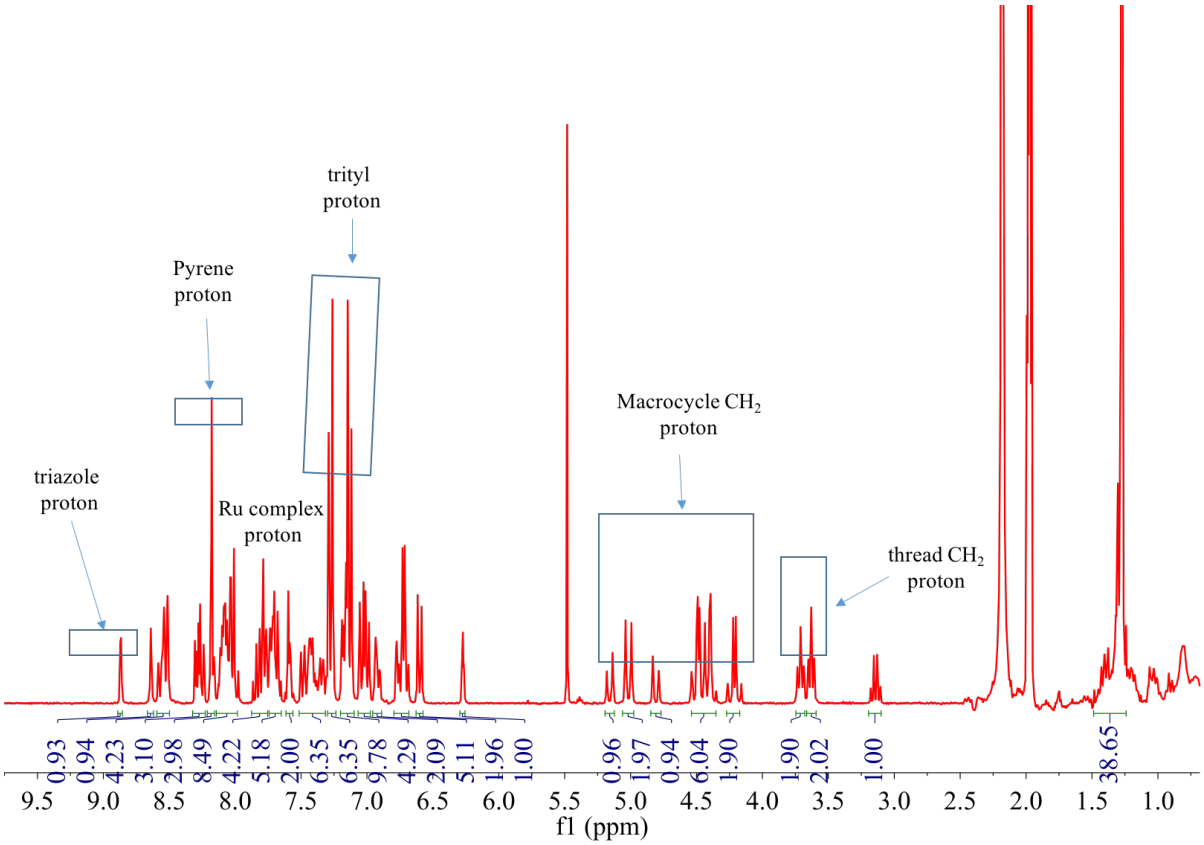

Figure 2.15 ^{1}H NMR of product **M$_4$** in CD_3CN.

2.7.2 Electronic absorption spectroscopy of rotaxane M$_4$

The electronic absorption spectra of rotaxane **M$_4$** and pyrene-containing macrocycle **R$_3$** in acetonitrile, with thread **B$_1$** and the pyrene as references, are shown in Fig. 2.16. In the visible region, similar MLCT absorption bands for rotaxane **M$_4$** and thread **B$_1$** were found in the range of 400 - 500 nm; similar phenyl-pyrene absorption bands for rotaxane **M$_4$** and macrocycle **R$_3$** were found in the range of 320 - 360 nm. Compared with the absorption of pyrene, the phenyl-pyrene clearly behaves differently, which is consistent with the triplet states of pyrene and phenyl-pyrene interacting. Although the absorption spectrum of phenyl-pyrene absorption is not affected by the presence of Ru^{2+} complex in the rotaxane **M$_4$**, a luminescence decay was measured to see if REET process can be still instilled in this system.

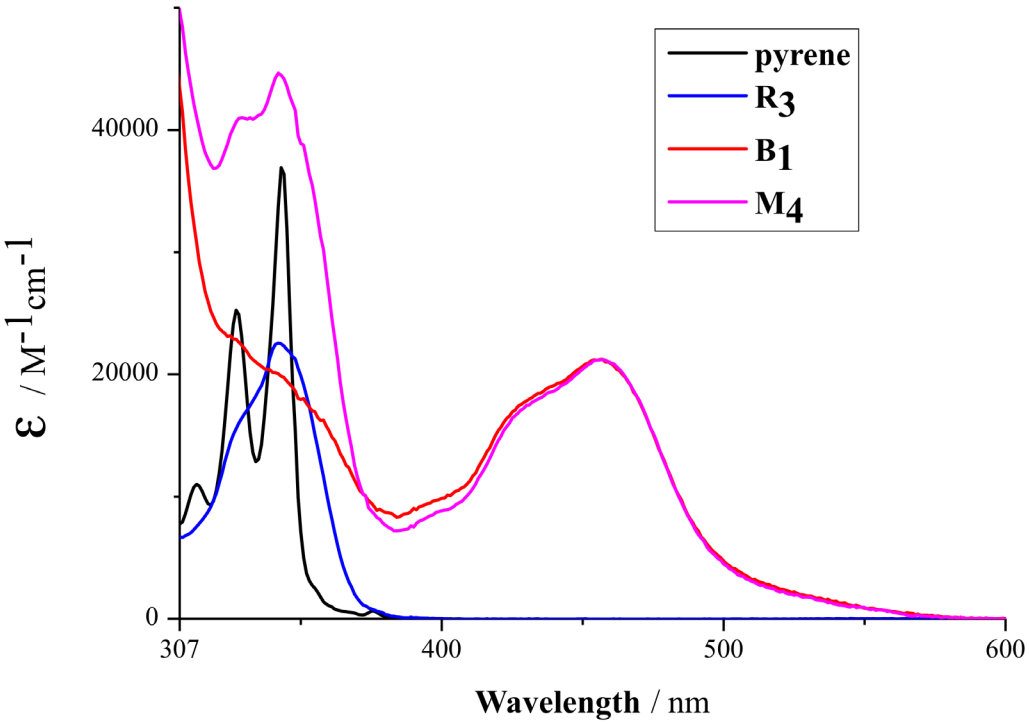

Figure 2.16 UV-vis absorption spectra of rotaxane **M**$_4$, thread **B**$_1$ and pyrene-containing macrocycle **R**$_3$ in acetonitrile.

2.7.3 Luminescence decays of rotaxane M$_4$

As shown in Fig. 2.17, free thread **B**$_1$ shows typical MLCT luminescence in degassed acetonitrile ($\Phi = 0.10$, $\tau = 1.2$ μs), while rotaxane **M**$_4$ shows a prolonged luminescence lifetime ($\tau_1 = 1.2$ μs, 6.4%; $\tau_2 = 14.0$ μs, 93.6%) with similar quantum yield and enhanced sensitivity to molecular oxygen. As we can see in the spectrum, 2 decay components are observed. This effect can be attributed to differing effects. REET process may not operational in a small amount of rotaxanes because the distance between pyrene moiety and Ru complex is not short enough, or due to a conformational effect. Another possibility can be due to slow forward electronic energy transfer with respect to the intrinsic ruthenium complex decay. Extensive purification allows us to discount the presence of impurity, unless the rotaxane were to lose a small fraction of the pyrene-appended macrocycle.

Globally, this system holds promise in the tracking of sub-molecular movement in molecular machines using measures of REET.

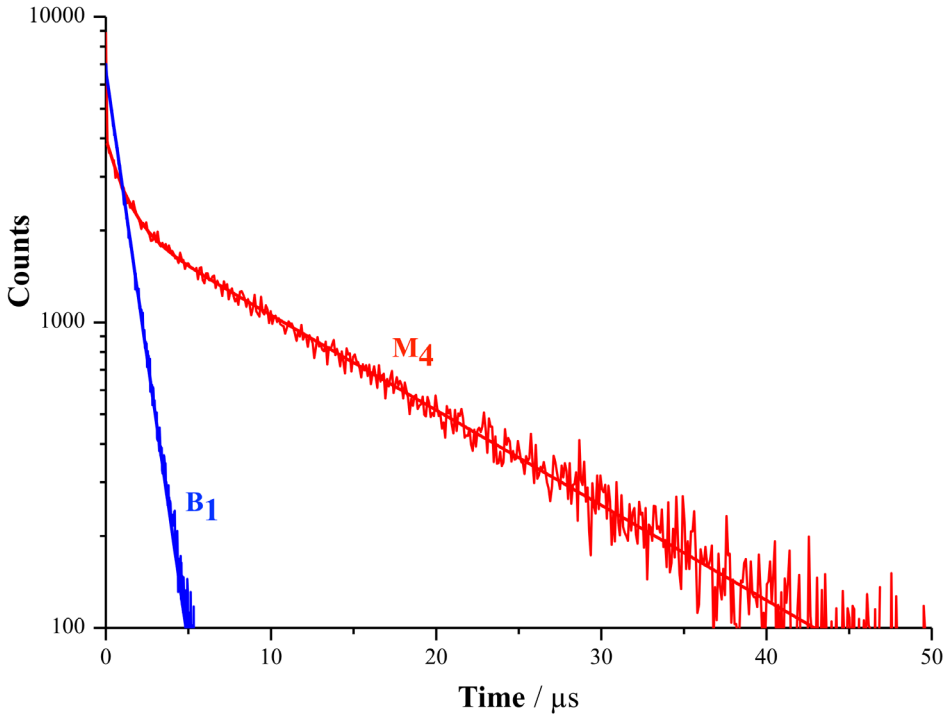

Figure 2.17 Luminescence decays of rotaxane **M_4** & thread **B_1** (λ_{ex} = 450 nm, λ_{em} = 620 nm) in degassed MeCN.

2.8 Formation of rotaxane M_5 with a symmetrical pyene-methylene-macrocycle

2.8.1 Synthesis and characterization of rotaxane M_5

In the meantime, another type of symmetrical pyrene-macrocycle was also designed and synthesized, as shown in Fig. 2.18. Commercially-available 1-bromopyrene was used to form a Grignard reagent, using magnesium with a catalytic amount of iodine. The following reaction obtained (3,5-dimethoxylphenyl)pyren-1-ylmethanol (**II-28**) by reacting 3,5-dimethoxybenzaldehyde with a Grignard reagent. Me_2SiHCl, as a Lewis acid, was added in the solution of **II-28**, in the presence of indium(III) chloride catalyst. As a result, the deoxygenation of the secondary alcohol was fulfilled in mild conditions, affording 1-(3,5-dimethoxylbenzyl)pyrene (**II-29**) with a good yield. After deprotection of **II-29** by BBr_3, 1 equivalent of the obtained resorcinol derivative (**II-30**) was used to have a Williamson etherification with 2 equivalents of arms **II-21**, affording a macrocycle precursor (**II-31**). Using

the Ni-mediated coupling method to **II-31** in a highly diluted solution, a pyrene-methylene-macrocycle $\mathbf{R_4}$ was afforded in 70% yield.

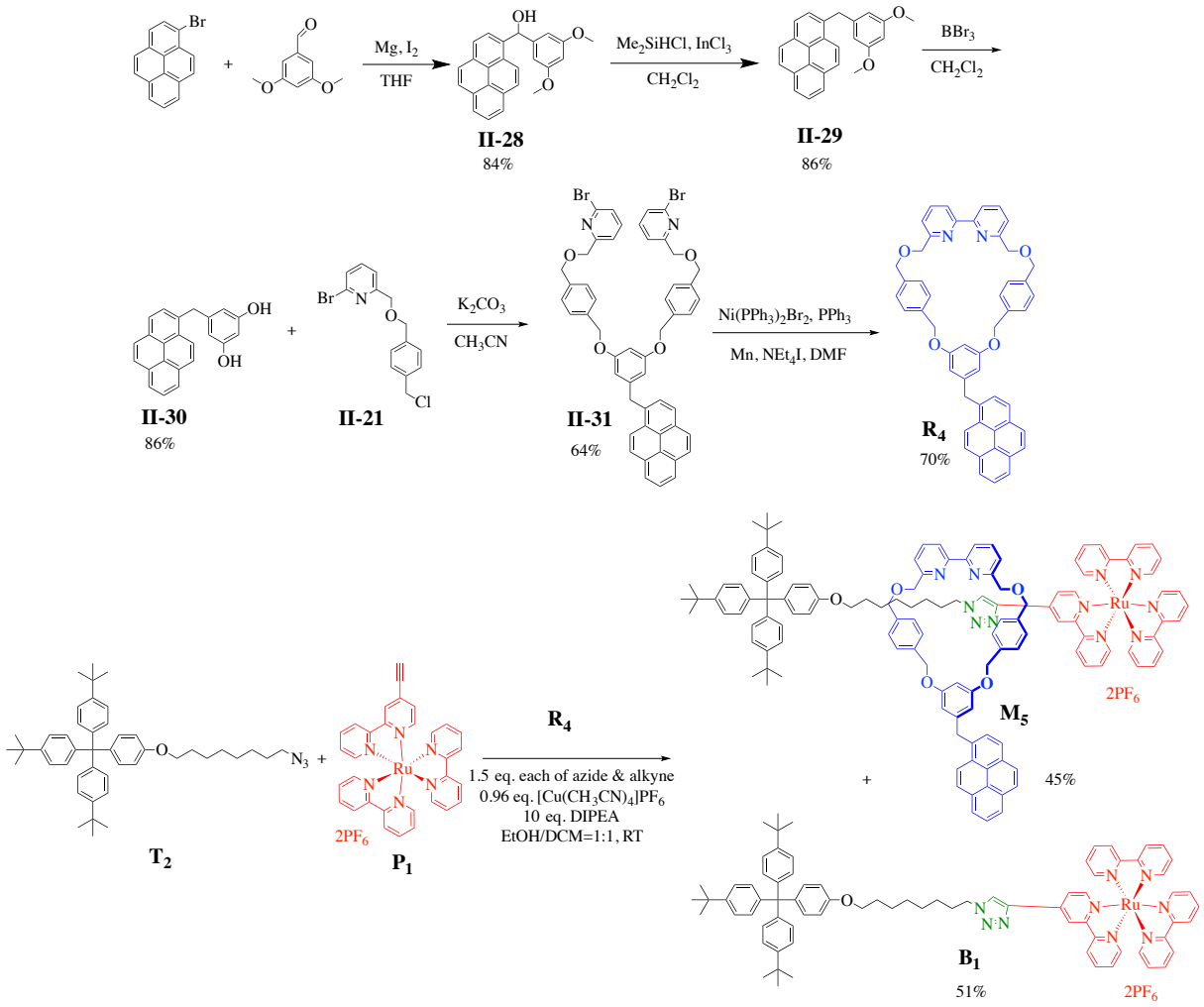

Figure 2.18 Synthesis scheme of rotaxane $\mathbf{M_5}$.

By a vapor diffusion of diethyl ether into a solution of $\mathbf{R_4}$ in chloroform, single crystals were grown of sufficient quality to permit X-ray crystallographic analysis. The single crystal structure is shown in Fig. 2.19. As we can see, the bipyridine unit is in the trans-rotamer form, which may explain why the bipyridine macrocycle precursor disfavors the macrocyclisation by a double-Williamson etherification.

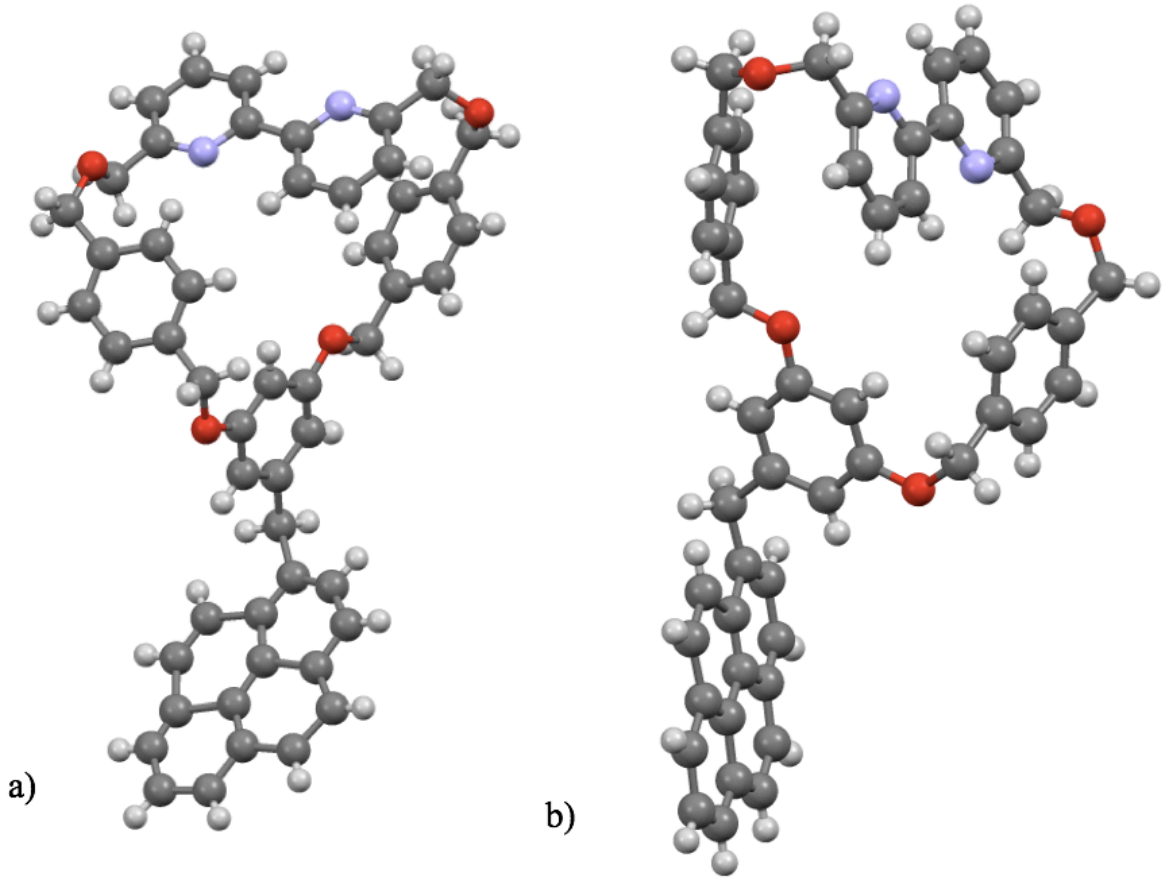

Figure 2.19 Single-crystal X-ray structures (ball and stick shape) of macrocycle **R_4** from a) the front; b) the side-on view.

Rotaxane **M_5** was constructed based on macrocycle **R_4** and half threads **T_2&P_1** by AT-CuAAC reaction. After the standard work-up, the crude product was purified by column chromatography and GPC to afford the largest fraction. On analyzing this ^{1}H NMR spectrum (Fig. 2.20), a singlet resonance at 8.62 ppm could be attributed to the triazole proton; two specific multiplet peaks at 7.28 – 7.09 ppm could be attributed to the trityl group; a multiplet at 8.55 – 8.48 ppm corresponds to the Ru complex; a triplet peak at 6.27 ppm is associated to the proton of the benzene group, as a part of the macrocycle, which is attached to the methylene-pyrene group; two triplets at 3.88 – 3.66 ppm belong to the thread component and some peaks at 4.90 – 4.33 ppm could be attributed to the macrocycle -CH_2- groups and so on; and the integration is as anticipated. Taken in conjunction with ^{13}C NMR spectrum and HRMS, it could be ascertained that this fraction is the target rotaxane.

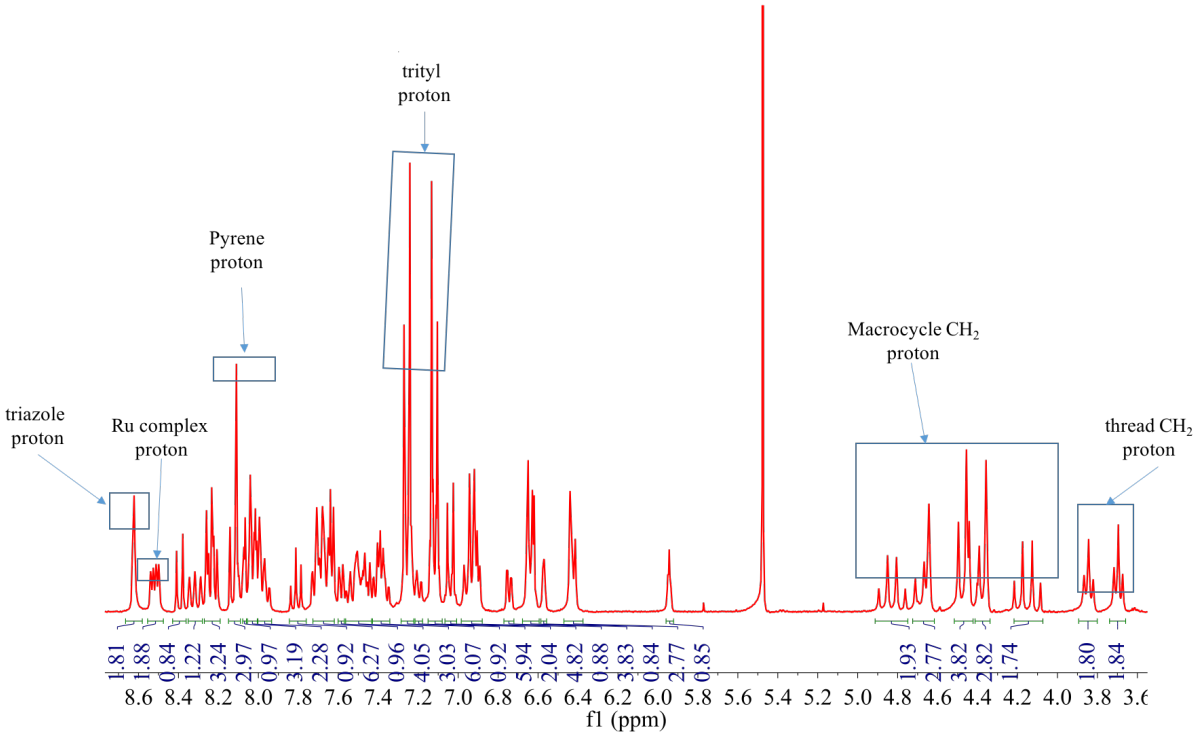

Figure 2.20 ^{1}H NMR of product **M$_5$** in CD_3CN.

2.8.2 Electronic absorption spectroscopy of rotaxane M$_5$

The electronic absorption spectra of rotaxane **M$_5$**, thread **B$_1$** and pyrene-containing macrocycle **R$_4$** in acetonitrile are shown in Fig. 2.21. In the visible region, similar MLCT absorption bands for rotaxane **M$_5$** and thread **B$_1$** were found in the range of 400 - 500 nm; the pyrene absorption bands for rotaxane **M$_5$** were found not to change in the range of 320 - 360 nm. The vibronic fine structure of pyrene absorption is not affected by the presence of Ru complex in the rotaxane **M$_5$**, which implies that there is only a weak ground-state coupling between two chromophores.

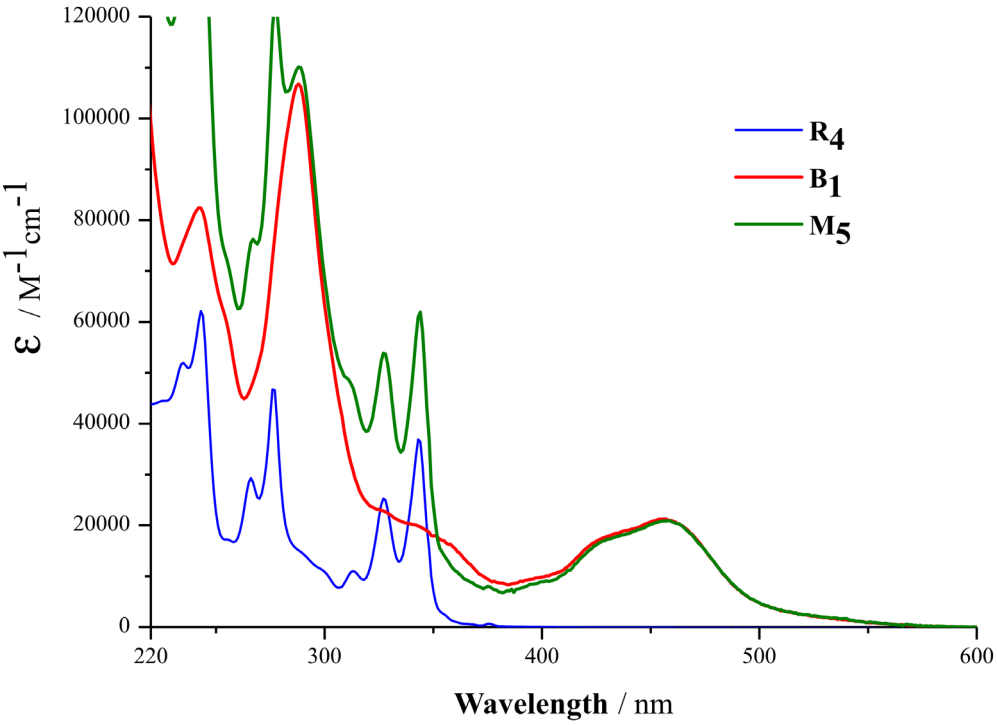

Figure 2.21 UV-vis absorption spectra of rotaxane **M$_5$**, thread **B$_1$** and pyrene-containing macrocycle **R$_4$** in acetonitrile.

2.8.3 Luminescence spectroscopy of rotaxane M$_5$

In Fig. 2.22, the photoluminescence spectra are presented of **M$_5$** at different temperatures. At room temperature, a broad structureless red MLCT-based emission for **M$_5$** ($\lambda_{em.max}$ = 620 nm, λ_{ex} = 450 nm) in degassed acetonitrile is presented. Low temperature phosphorescence measurements were undertaken to gain further insight into the energies of the pertinent states and relative energy levels of **M$_5$** and macrocycle **R$_4$**. Indeed, the highest energy feature is taken as the energy of the excited state. At 77 K, slightly blue-shifted ^{3}MLCT structured phosphorescence ($\lambda_{em.max}$ = 589 nm) could be observed with respect to room temperature for **M$_5$**, (due to three different energies of MLCT states in emission spectrum being easily separated in low temperature). The energy of the lowest-lying ^{3}MLCT ($\lambda_{em.max}$ = 589 nm) is calculated to be 2.11 eV, which is slightly different from the energy (2.07 eV) of the lowest-lying triplet pyrene ($\lambda_{em.max}$ = 600 nm, λ_{ex} = 342 nm). A small energy gap value between two chromophores assumes the possible establishment of REET processes in rotaxane **M$_5$**.

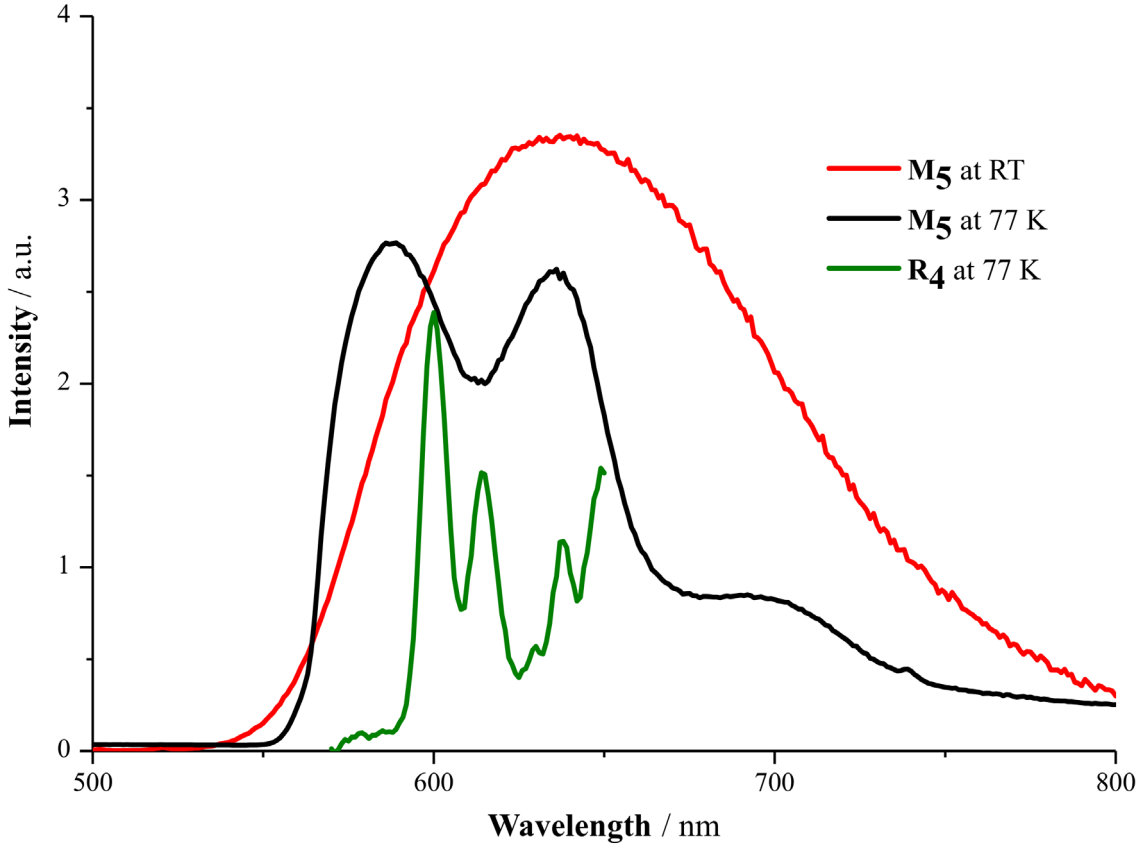

Figure 2.22 Luminescence (293 K, red) and phosphorescence (77 K, black) spectra of **M$_5$** in degassed acetonitrile (λ_{ex} = 450 nm). Phosphorescence (77 K, green) spectrum of macrocycle **R$_4$** is given (λ_{ex} = 342 nm).

2.8.4 Luminescence decays of rotaxane M$_5$

As shown in Fig. 2.23, free thread **B$_1$** shows typical MLCT luminescence in degassed acetonitrile (Φ = 0.08, τ = 1.2 μs), while rotaxane **M$_5$** shows a prolonged luminescence with a lifetime of 5.6 μs with a similar quantum yield and enhanced sensitivity to molecular oxygen. In the first 200 ns, the luminescence intensity of **M$_5$** decreases faster than the one of **B$_1$**, this could arise because energy transfer occurs, part of the energy is transferred from the Ru^{2+} complex to the pyrene moiety and stored there. This indicates that no additional loss pathways are introduced compared with the free thread and that the pyrene is a key in prolonging the excited-state lifetime. Compared with the structure of rotaxane **M$_4$**, rotaxane **M$_5$** only contains one more methylene group between pyrene-moiety and a phenyl-moiety of the ring. While from the luminescence decays of rotaxane **M$_5$**, it seems that all rotaxanes in the solution could establish REET process after photoirradiation. One explanation for this behavior may be the

additional methylene group between pyrene-moiety and a phenyl-moiety of the ring in rotaxane **M$_5$** could render the pyrene linkage more flexible, which increases the possibility of it being close to the Ru complex, allowing REET process. Further studies were undertaken to gain further insight into a possible shuttling movement of rotaxanes and the origin of the prolonged luminescence.

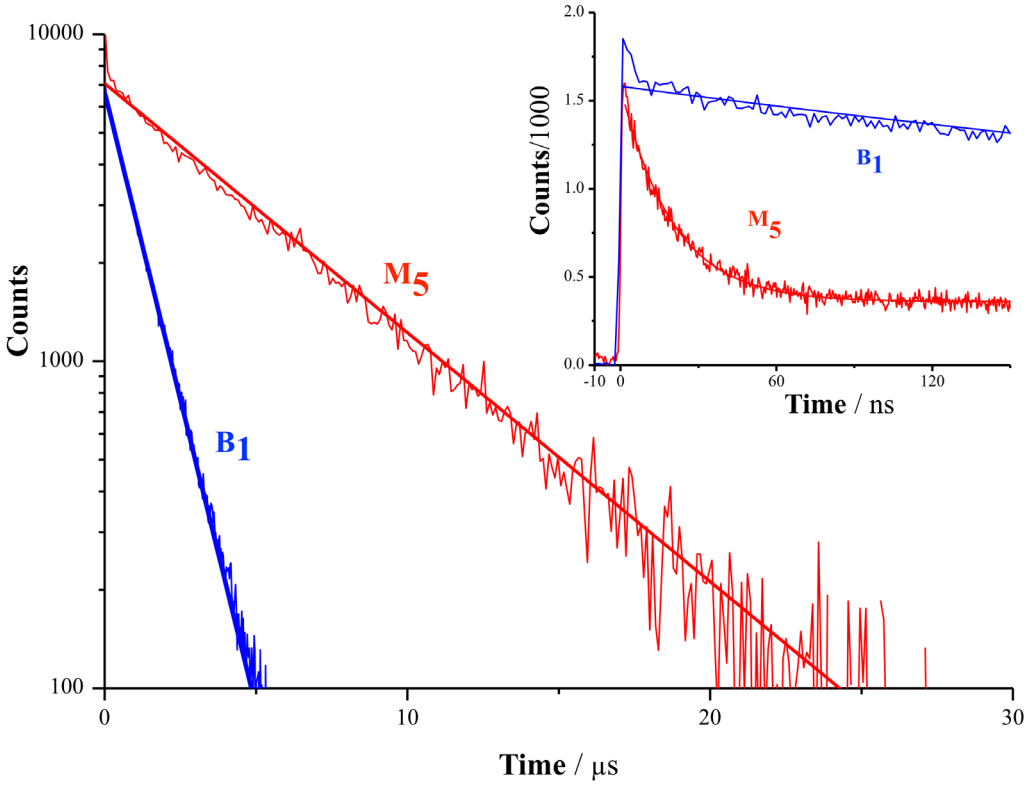

Figure 2.23 Luminescence decays of rotaxane **M$_5$** & thread **B$_1$** in degassed acetonitrile (λ_{ex}=450 nm, λ_{em}=620 nm).

2.8.5 Time-resolved transient absorption spectroscopy of rotaxane M$_5$

Luminescence decays give information on the ultimate fate of the excited molecule, e.g. by delivering information on the enhanced emission lifetime of the system, while transient absorption spectroscopy elucidates the management of energy by excited molecules before emission occurs and how this large lifetime enhancement resulted in the system. A pump-probe experiment was performed on rotaxane **M$_5$**, whose 3D representation is shown in Fig. 2.24.a. Following MLCT excitation of rotaxane **M$_5$**, energy is effectively redistributed between the two chromophores. The pyrene triplet state absorption band with maximum at 410 nm gradually

grows and the Ru^{2+} complex triplet state absorption at 370 nm gradually decreased (Fig.2.24.b). After 15 ns, the synchronous decay of the pyrene $T_1 \rightarrow T_n$ transient and excited MLCT signals confirmed a dynamic excited state equilibrium is established between the two chromophores. The energy is predominantly localised on the pyrene unit (78%), as the rate of back transfer from pyrene unit to inorganic unit is less than forward transfer rate ($1.8 \cdot 10^7$ s^{-1} *vs.* $6.7 \cdot 10^7$ s^{-1}). The rate constant of luminescence decay is a weighted average of MLCT and pyrene unit contributions (see equation below: α means the population of luminescence decays of Ru complex part; τ_{Ru} means the lifetime of Ru-complex, eg., $\mathbf{B_1}$; τ_{pyr} means the lifetime of pyrene-moiety.). Since the pyrene triplet state is much more persistent than the MLCT triplet state, a lifetime elongation is observed. This observed result confirms the presence of quasi-isoenergetic excited states on the two adjacent chromophores, thus permitting rapid REET.

$$1/\tau = \alpha\,(1/\tau_{Ru}) + (1-\alpha)\,(1/\tau_{pyr})$$

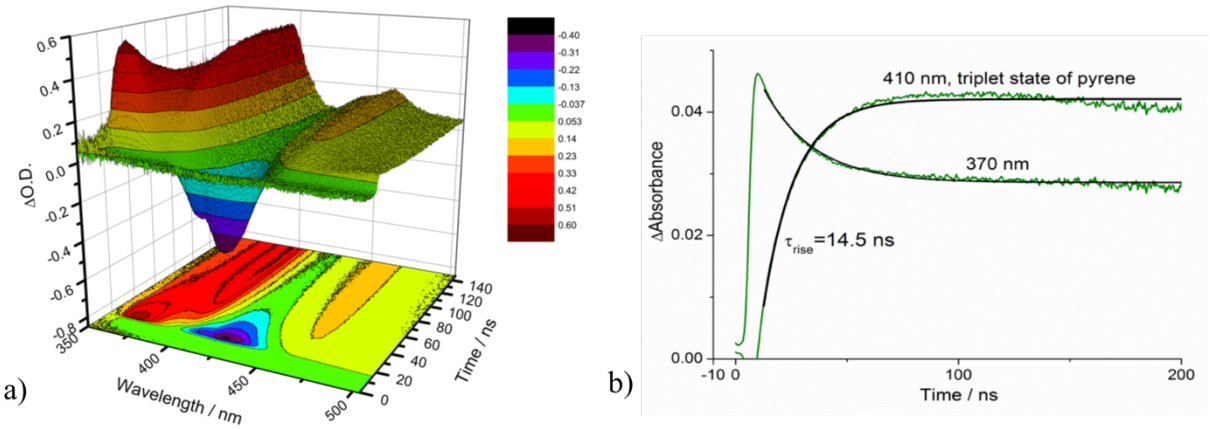

Figure 2.24 a) Transient absorption map of rotaxane $\mathbf{M_5}$ showing equilibration of REET in CH_3CN (λ_{ex} = 450 nm). b) Transient absorption kinetics at 370 and 410 nm of $\mathbf{M_5}$ in degassed acetonitrile (λ_{ex} = 450 nm). The kinetics at 370 nm corresponds to the superposition of decrease of ruthenium complex in ^{3}MLCT state and grow-in of pyrene in triplet state. The kinetics at 410 nm only corresponds to grow-in of pyrene in triplet state. Black solid line – the fitting. Rise time of kinetics at 410 nm is 14.5 ns.

2.8.6 Variable temperature luminescence of rotaxane $\mathbf{M_5}$

In addition to the aforementioned measurements, luminescence decays of $\mathbf{M_5}$ based at two different temperatures, were measured. As shown in Fig. 2.25, dashed lines are the computational results, which take into account temperature dependent viscosity, and solid lines

show the experimental results. From the primary investigation, viscosity affects the rate of luminescence decay of rotaxane **M$_5$**. The influence might be the movement of rotaxane affected by the viscosity. In order to get more and clear information about luminescence decays of **M$_5$** based on different temperatures, a more complete fitting model needs to be tuned and will be reported in due course.

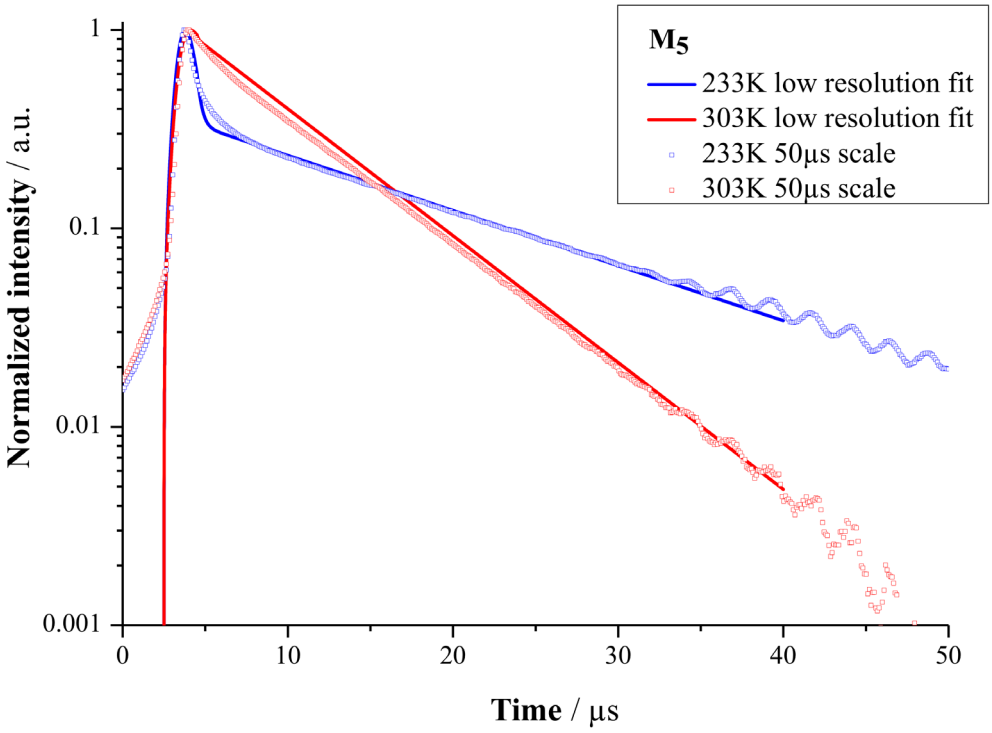

Figure 2.25 Luminescence decays of rotaxane **M$_5$** in degassed acetonitrile (λ_{ex}=450 nm, λ_{em}=620 nm) at 233 K and 303 K.

2.9 Conclusion

Several half-threads were synthesized for the preparation of rotaxane construction, four different pyrene-type macrocycles were designed and developed to build a rotaxane system with an integrated bidirectional electronic energy transfer process. It was found that two symmetrical pyrene-macrocycles (phenyl pyrene **R$_3$**, and methylene pyrene **R$_4$**) were good candidates as ring components to primarily investigate the REET process in the rotaxane system. Two rotaxanes (**M$_4$**, **M$_5$**) comprising different symmetrical pyrene-macrocycles (**R$_3$**, **R$_4$**) were constructed by an active template Cu-catalyzed alkyne-azide cycloaddition reaction. The

constitution of the rotaxanes was confirmed by NMR, HRMS and electronic absorption spectroscopy. Time-resolved spectroscopy and steady state spectroscopy showed that unprecedented reversible electronic energy transfer processes were instilled in rotaxane systems (**M_4**, **M_5**) and prolonged luminescence lifetimes were observed. Comparison of luminescence decays of **M_5** (or **M_4**) and thread **B_1** showed the prolonged luminescence lifetime of rotaxane caused by the in-built REET process in the system. Transient absorption of **M_5** demonstrated the REET process between pyrene group in the ring part and Ru-complex moiety in the thread part and explained why the luminescence lifetime was prolonged, primary variable temperatures luminescence decays of **M_5** disclosed more information of REET process in a rotaxane system. It is noteworthy that the MLCT luminescence lifetime (14 μs) of **M_4** was much longer than that (5.6 μs) of **M_5**, this is attributed largely to the different energy gaps of ^{3}MLCT-**M_4** *vs* ^{3}pyr-**R_3** and ^{3}MLCT-**M_5** *vs* ^{3}pyr-**R_4**.

References

[1] Crowley J. D., Goldup S. M., Lee A. L., Leigh D. A., McBurney R. T. Active Metal Template Synthesis of Rotaxanes, Catenanes and Molecular Shuttles. Chem. Soc. Rev., 2009, 38, 1530-1541.

[2] Denis M., Goldup S. M. the Active Template Approach to Interlocked Molecules. 2016, 1, 61

[3] Aucagne V., Hänni K. D., Leigh D. A., Lusby P. J., Walker D. B. Catalytic "Click" Rotaxanes: A Substoichiometric Metal-Template Pathway to Mechanically Interlocked Architectures. J. Am. Chem. Soc., 2006, 128, 2186-2187.

[4] Aucagne V., Berná J., Crowley J. D., Goldup S. M., Hanni K. D., Leigh D. A., Lusby P. J., Ronaldson V. E., Slawin A. M. Z., Viterisi A., Walker D. B. Catalytic 'Active-Metal' Template Synthesis of [2]Rotaxanes, [3]Rotaxanes, and Molecular Shuttles, and Some Observations on the Mechanism of the Cu(I)-Catalyzed Azide-Alkyne 1,3‑Cycloaddition. J. Am. Chem. Soc., 2007, 129, 11950-11963.

[5] Lahlali H., Jobe K., Watkinson M., Goldup S. M. Macrocycle Size Matters: "Small" Functionalized Rotaxanes in Excellent Yield Using the CuAAC Active Template Approach. Angew. Chem. Int. Ed., 2011, 50, 4151-4155.

[6] Winn J., Pinczewska A., Goldup S. M. Synthesis of a Rotaxane Cu^{I} Triazolide under Aqueous Conditions. J. Am. Chem. Soc. 2013, 135, 13318-13321.

[7] Lewis J. E. M., R. Bordoli J., Denis M., Fletcher C. J., Galli M., Neal E. A., Rochettea E. M., Goldup S. M. High Yielding Synthesis of 2,2'-Bipyridine Macrocycles, Versatile Intermediates in the Synthesis of Rotaxanes. Chem. Sci., 2016, 7, 3154-3161.

[8] Li H.-G., Wang G.-W. Liquid-Assisted One-Pot Mechanosynthesis and Properties of Neutral Donor-Acceptor [2]Rotaxanes. J. Org. Chem., 2017, 82 (12), 6341-6348.

[9] Balzani V., Clemente-León M., Credi A., Ferrer B., Venturi M., Flood A. H., Stoddart, J. F. Autonomous Artificial Nanomotor Powered by Sunlight. Proc. Natl. Acad. Sci. U. S. A. 2006, 103, 1178.

[10] Baron A., Herrero C., Quaranta H., Charlot M.-F., Leibl W., Vauzeilles B., Aukauloo A. Click Chemistry on a Ruthenium Polypyridine Complex. An Efficient and Versatile Synthetic Route for the Synthesis of Photoactive Modular Assemblies. Inorg. Chem., 2012, 51, 5985-5987.

Chapter 3 Energy Shuttling / REET in Molecular Shuttles with Varying Threads

3.1 Introduction

3.1.1 Progress of research in molecular shuttles

Molecular shuttles based on [2]rotaxanes possessing at least two recognition sites for the moving macrocyclic ring have attracted much attention in terms of potential applications[1-3] in molecular switches and molecular machines. In such molecular shuttles, the control or tracking of the ring shuttling motion along the dumbbell components, which is mostly affected by noncovalent binding interactions between two recognition sites, is of crucial importance. The switching rate of the ring shuttling movement may directly determine the effectiveness of a device[4]. It is noteworthy that a better understanding of shuttling motion is an indispensable requirement for the rational design of nanomaterials.

In the research of ring shuttling motion of molecular shuttles, dynamic ^{1}H NMR spectroscopy is often used. Günbas et al. used dynamic ^{1}H NMR spectroscopy to calculate the populations of different co-conformers of a molecular shuttle (Fig. 3.1), and found a weaker binding of the macrocycle to a recognition site could accelerate the switching of molecular shuttles.[5] In rotaxane **29**, there are two recognition sites: the *succ* station and the *ni-gly* station, the latter is slightly less favourable for the binding of Leigh-type macrocycle. From the primary comparison of ^{1}H NMR spectra of **29** and the corresponding thread **30** in $CDCl_3$, the H_d protons in rotaxane **29** are markedly shielded, which shows that a significant fraction of rotaxane **29** exists as the *ni*-co-conformer. In order to get the populations of these two co-conformers, a model rotaxane **31** and thread **32** consisting of two *ni-gly* units were synthesized. The population (α) of the *ni*-co-conformer in rotaxane **29** was calculated from an equation ($\alpha = \frac{\delta_1 - \delta_3}{2(\delta_4 - \delta_5)}$). The δ's refer to the chemical shifts of H_d in compounds **29**, **30**, **31** and **32**. Since the macrocycle mostly stays on the two recognition sites, so the population of the *succ*-co-conformer is 1 - α.

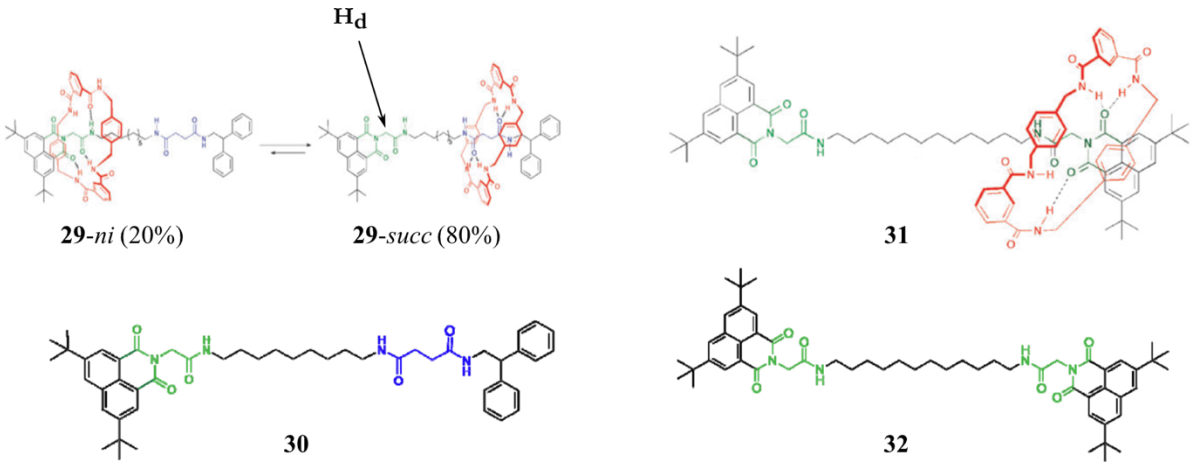

Figure 3.1 Structures of rotaxanes **29&31** and related threads **30&32** reported by Günbas et al Copyright (2010) the Royal Society of Chemistry.

Furthermore, they synthesized four different degenerate molecular shuttles **33**, **34**, **35** and **36** in which *ni-gly* units are as stoppers and recognition sites.[6] Three of them contain alkyl flexible spacers with different lengths: C_9, C_{12} and C_{26}; the fourth one contains a rigid spacer: a diphenylethyne unit, as shown in Fig. 3.2.a. With the analysis of NMR experiments at variable temperatures, it was found that the shuttling rates of macrocycle in rotaxanes **33**, **34**, **35** with flexible spacers were extremely close, the rigid diphenylethyne spacer does not highly hinder the shuttling of the macrocycle between the two *ni-gly* sites. It is noteworthy that the flexible spacer can be appropriately folded, which makes the possibility that the macrocycle can interact with the other *ni-gly* station through one of its amide groups that is not interacting with the encircled *ni-gly* station (Fig. 3.2.b). This kind of folded *ni-gly* coconformer cannot exist in a rotaxane with rigid spacer.

a)

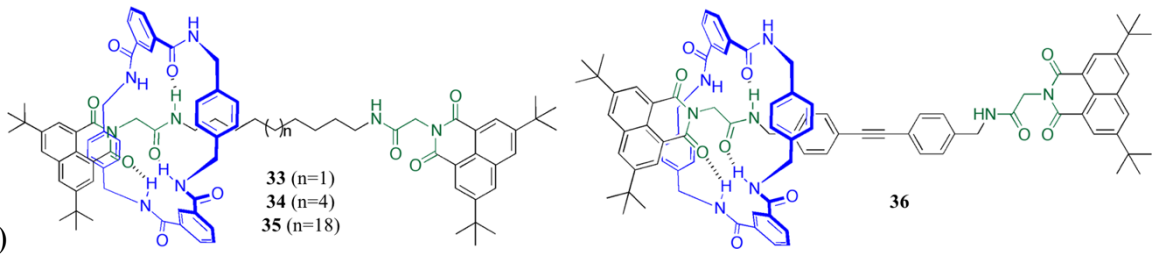

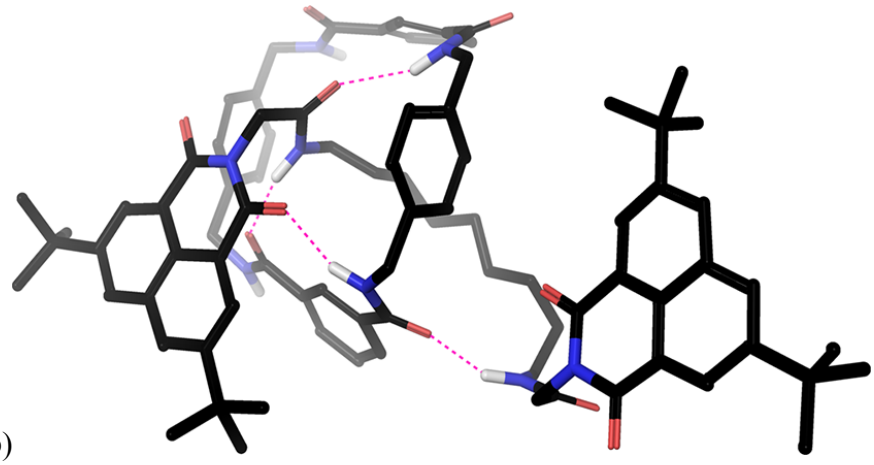

b)

Figure 3.2 a) Structures of degenerate molecular shuttles with flexible and rigid spacers synthesized by Günbas et al.; b) Snapshot from an MD simulation of rotaxane **33** illustrating possibility of macrocycle interacting with two stations at one state. Copyright (2012) American Chemical Society.

Hirose et al. built a series of [2]rotaxane molecular shuttles **37^{n}** possessing different numbers of phenylene units as spacers between two DBA recognition sites of DB24C8, as shown in Fig. 3.3.a.[7] They found from the ^{1}H NMR spectra of rotaxanes at 303 K, slow shuttling of the DB24C8 ring between two DBA stations on the NMR time scale was revealed. However, deeper investigations showed the free energies of activation ($\Delta G^{\ddagger}$) for ring shuttling remained constant regardless of the length of the rigid rod-like spacers, like the cartoon illustration in Fig. 3.3.b.

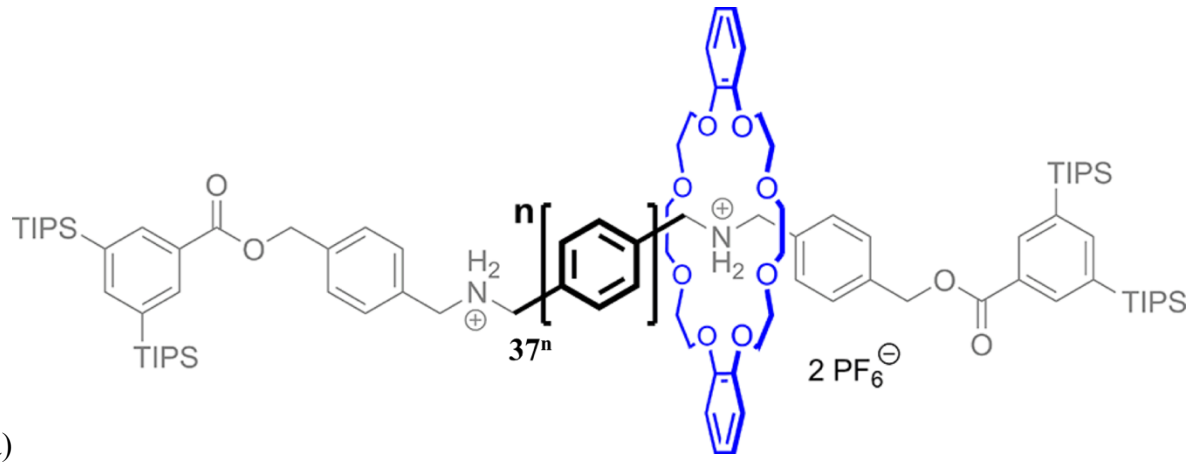

a)

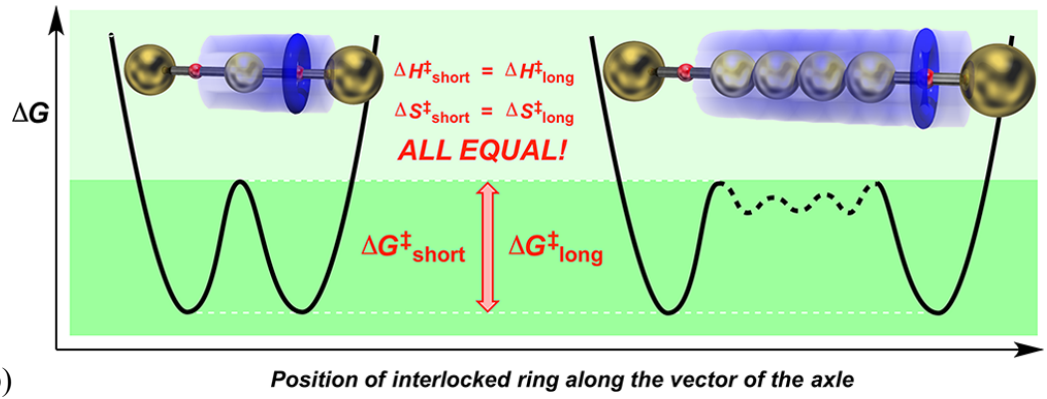

b)

Figure 3.3 a) Structures of degenerate molecular shuttles with rigid spacers synthesized by Hirose et al.; b) Cartoon illustration of axle length not affecting switching dynamics in degenerate molecular shuttles with rigid spacers. Copyright (2014) American Chemical Society.

Equally, Qu et al. developed a symmetrical molecular shuttle **38**, in which a macrocycle DB24C8 encircles on a thread possessing two DBA stations on each end and two triazole groups between the DBA stations, as shown in Fig. 3.4.[8] The writers found in the obtained molecular shuttle **39** by the deprotonation of **38**, the ring DB24C8 in **39** can migrate much faster along the thread than in **38** ($k_2 >> k_1$). This is because the specific NH group-DB24C8 interaction is much weaker than the DBA-DB24C8 interaction. While the methylation of triazole groups to **38** can introduce two more recognition sites MTA, whose interactions with DB24C8 are much weaker than DBA-DB24C8 interactions. Variable temperature and dynamic EXSY NMR experiments show the rate of ring migration in **40** (k_3) is faster than the rate of ring migration in **38** (k_1). They concluded a step-by-step ring movement is preferable to a large amplitude movement in a molecular shuttle.

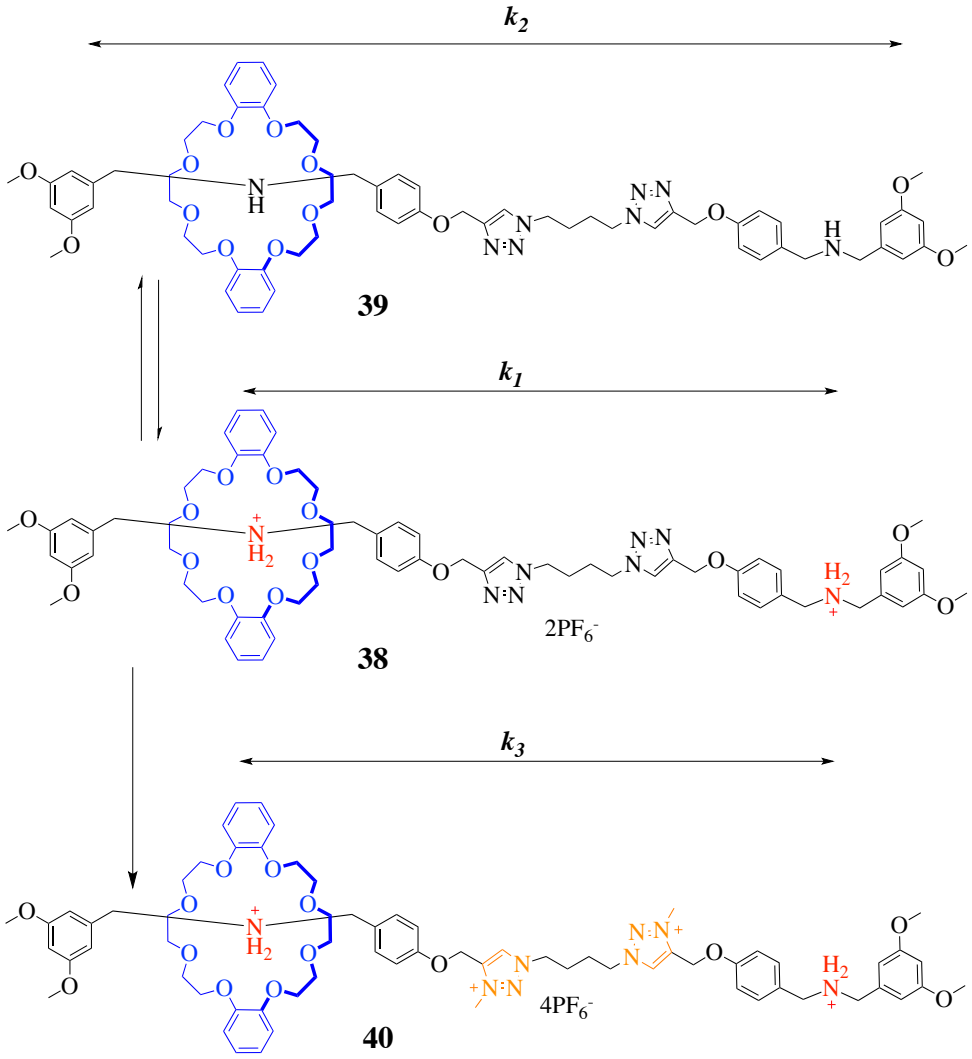

Figure 3.4 Three molecular shuttles with different recognition sites developed by Qu and coworkers.

3.1.2 Introduction to rotaxane constructions by templated Cadiot-Chodkiewicz method

The aforementioned molecular shuttles all include at least two strong recognition sites, which are used to bind the ring and localize the position of the ring on the axle. As shown in the paper of Hirose and coworkers, these strong non-covalent interactions often provide the major contribution to the activation energy to shuttling. This would also slow down the rate of shuttling movement, reported by Qu et al. In order to establish molecular shuttles with much weaker intercomponent interactions and faster ring shuttling movements, the templated Cadiot-Chodkiewicz approach can be considered, whose mechanism is illustrated in Fig. 3.5. Firstly, a tetrahedral Cu(I) ion coordinates to two nitrogens, as binding sites of the bidentate macrocycle.

Then under basic conditions, the coordination of the bromoalkyne and terminal alkyne to the copper through opposite faces of the macrocycle will occur, producing a Cu^{III} intermediate. Finally, after demetalation with a suitable base (such as: KCN, EDTA/$NH_{3\ sat}$, or TBACN), a [2]rotaxane without strong intercomponent binding motifs is obtained.

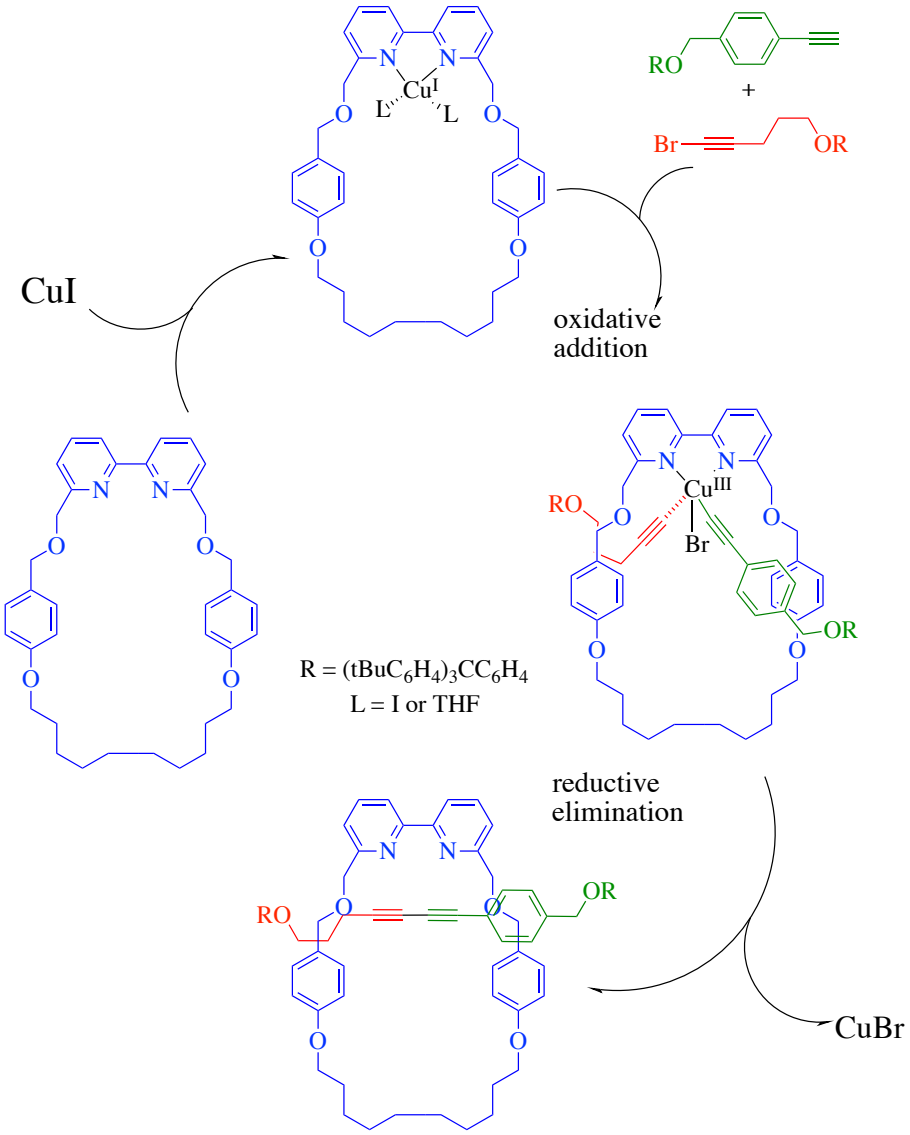

Figure 3.5 Mechanism of rotaxination of bidentate macrocycle by Cadiot-Chodkiewicz template method.

Leigh and coworkers firstly introduced the Cadiot-Chodkiewicz template method into synthesis of rotaxanes, as shown in Fig.3.6.a.[9] In order to maximally avoid the formation of homocoupled rotaxane, copper acetylide was preferentially preformed from the treatment of alkyne with n-BuLi and transmetalation with CuI. After introducing bromoalkyne to produce a Cu^{III} intermediate and demetalation with a suitable strong base, a desired heterocoupled

rotaxane **41** was furnished with 80% yield. Following the same idea, Goldup and Leigh constructed a [2]catenane **42** using Cadiot-Chodkiewicz reaction, in Fig. 3.6.b.[10] Due to the decomposition of bromoalkyne during the treatment of terminal alkyne of compound alkyne-bromoalkyne with LiHMDS, prior to the transmetalation with CuI, 5 equivalent of alkyne-bromoalkyne was employed. Finally, a desired [2]catenane **42** was obtained (yield = 21%). Considering the mechanisms of Cadiot-Chodkiewicz and Glaser reactions,[11] and the simplicity of separating undesired homocoupled and their targeted heterocoupled rotaxanes, Anderson and coworkers chose a milder condition to afford the non-symmetrical rotaxane (Fig. 3.6.c).[12] Firstly, a CuI•Macrocycle complex was obtained and two half threads – alkyne and bromoalkyne were added to give heterocoupling. With this procedure, some homocoupled rotaxanes may be formed, but they will be easily separated from the targeted heterocoupled rotaxane **43** (yield: 19%).

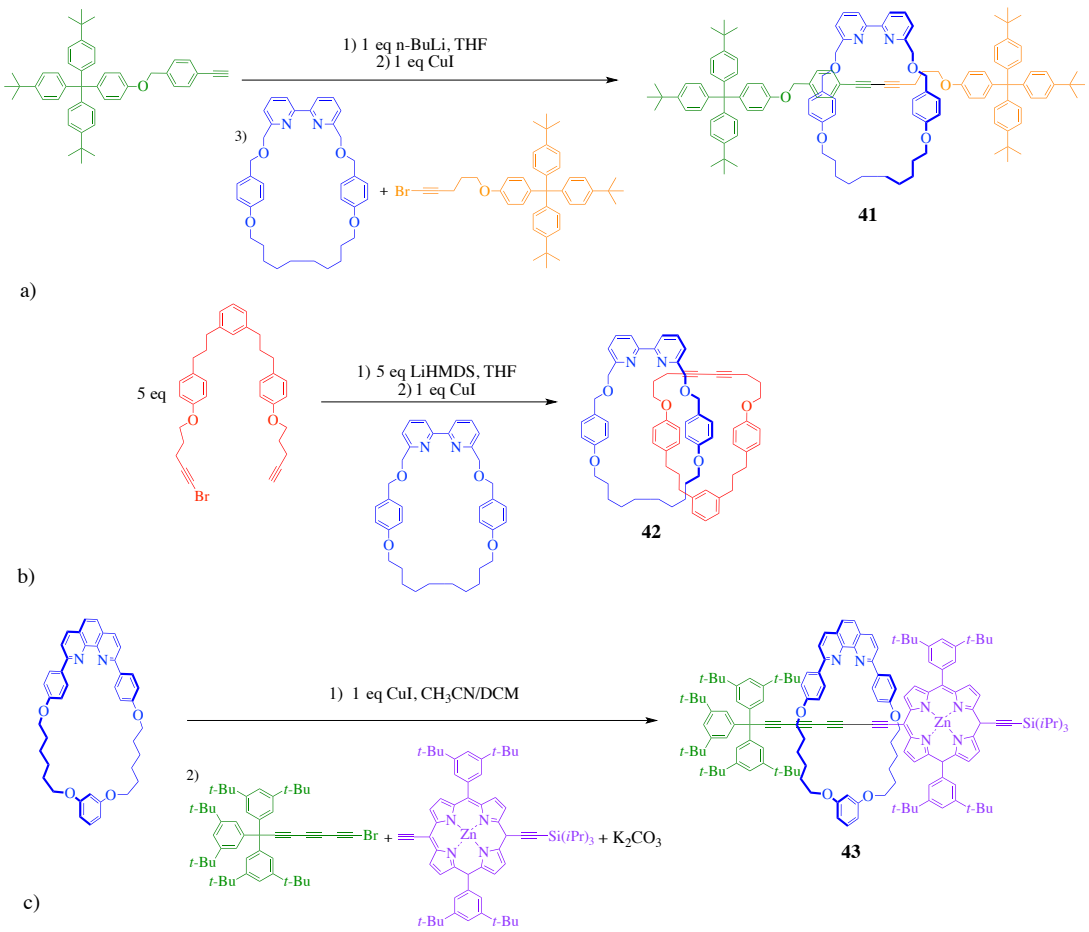

Figure 3.6 a) First Cadiot-Chodkiewicz template synthesis of heterocoupled rotaxane **41** reported by Leigh et al.; b) Goldup's [2]catenane **42** by Cadiot-Chodkiewicz reaction; c) A Cadiot-Chodkiewicz template synthesis of heterocoupled rotaxane **43** under mild condition reported by Anderson and coworkers.

3.2 Formation and spectroscopic studies of rotaxane M_6

All aforementioned studies of ring shuttling movements in molecular shuttles are based on the analysis of variable temperature and dynamic EXSY NMR experiments. In this chapter, REET processes will be engineered into molecular shuttles to investigate the ring shuttling movements. As discussed in chapter 2, from the luminescence decays of rotaxane $\mathbf{M_5}$, it seems that all tested rotaxanes in solution could establish REET processes after photo-irradiation. It would be interesting to design and construct another rotaxane with a shorter thread, tracking the difference of shuttling movements by some relevant REET techniques.

3.2.1 Synthesis and characterization of rotaxane M_6

Rotaxane $\mathbf{M_6}$ was designed and constructed based on macrocycle $\mathbf{R_4}$ and half threads $\mathbf{P_1}$ and $\mathbf{T_1}$ with $-(CH_2)_4-$ chain by AT-CuAAC reaction. After the normal work-up procedure, the crude product was purified by column chromatography and GPC to afford the major fraction. The ^1H NMR spectrum (Fig. 3.7), showed a singlet peak at 8.59 ppm which could be attributed to the triazole proton; two specific multiplet peaks at 7.28 – 7.22 and 7.14 – 7.08 ppm could be attributed to the trityl group; three multiplet peaks at 8.49 – 8.44, 7.72 – 7.60 and 7.40 – 7.29 ppm correspond to the Ru complex; a triplet peak at 5.91 ppm is associated to the proton of the benzene group, as a part of the macrocycle, which is attached to the methylene-pyrene group; two triplet peaks at 3.83 – 3.75 and 3.52 – 3.46 ppm could be attributed to the thread component and some peaks at 4.90 – 4.02 ppm belong to the macrocycle $-CH_2-$ groups and so on; and the integration is as anticipated. Taken in conjunction with ^{13}C NMR spectrum and HRMS, it could be ascertained that this fraction is the desired rotaxane.

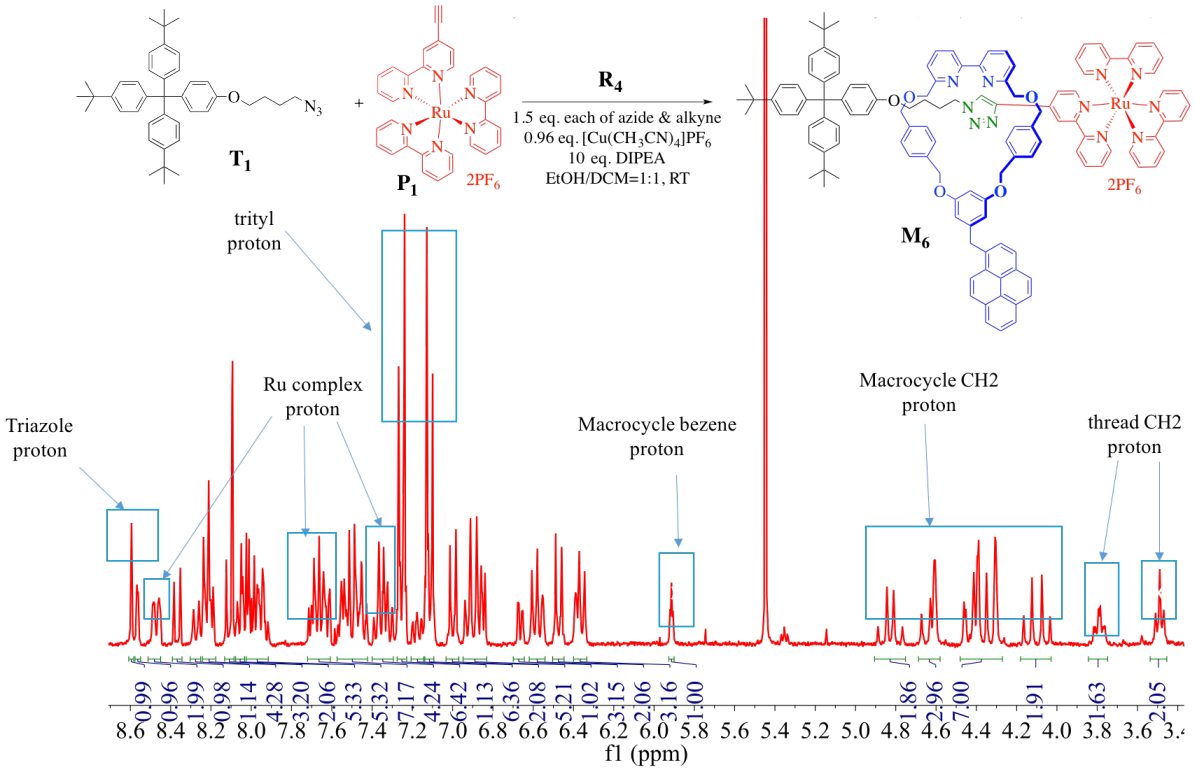

Figure 3.7 Synthetic scheme and ^{1}H NMR of rotaxane **M$_6$** in CD_3CN.

3.2.2 Electronic absorption comparison of rotaxanes M$_5$&M$_6$

The UV-vis absorption spectra of rotaxanes **M$_5$&M$_6$**, thread **B$_1$** and pyrene-containing macrocycle **R$_4$** in acetonitrile are shown in Fig. 3.8. In the visible region, similar MLCT absorption bands for rotaxane **M$_6$** and rotaxane **M$_5$**, or thread **B$_1$** were found in the range of 400 - 500 nm; similar pyrene absorption bands for rotaxane **M$_6$** and rotaxane **M$_5$**, or macrocycle **R$_4$** were found at the range of 320 - 360 nm. It is also concluded that there is only a weak ground-state coupling between the two chromophores in rotaxane **M$_6$**. In the whole observed visible region, the absorption of rotaxane **M$_5$** was almost the same as rotaxane **M$_6$**, this is because that rotaxanes **M$_5$** and **M$_6$** just have a difference of four –CH_2– in the thread of rotaxanes.

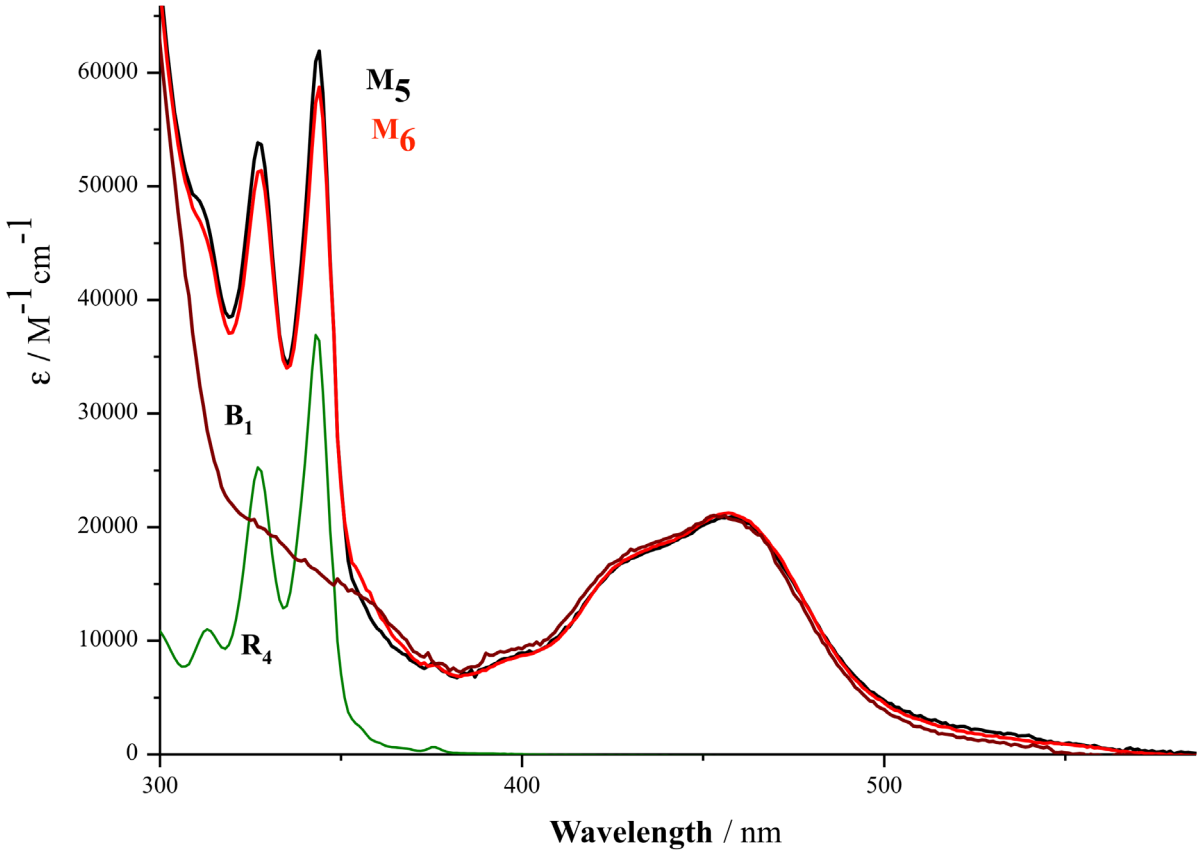

Figure 3.8 UV-vis absorption spectra of rotaxanes **M$_5$**& **M$_6$**, thread **B$_1$** and pyrene-containing macrocycle **R$_4$** in acetonitrile.

3.2.3 Comparison of luminescence decays of rotaxanes M$_5$&M$_6$

As shown in Fig. 3.9, rotaxane **M$_6$** shows almost the same prolonged luminescence lifetime (τ = 5.6 μs) of rotaxane **M$_5$** in degassed ACN. In the first 200 ns following excitation (i.e. pre-equilibration time) and during the whole process of luminescence decays, the luminescence intensity of rotaxane **M$_6$** decreases with a similar rate to that of rotaxane **M$_5$**. This result shows there is not an obvious difference of the REET process observed between rotaxanes **M$_6$** and **M$_5$** despite the longer thread in one case (**M$_5$**). One explanation for this behavior may be that the triazole moiety in the thread has a strong non-covalent host-guest interaction with the bipyridyl moiety on the macrocycle, causing the pyrene-macrocycle to predominantly encircle the triazole moiety, which is close to the Ru^{2+} complex moiety. Some DFT calculations on relevant rotaxanes (see below) were undertaken to gain further insight into the host-guest interactions which would impact shuttling movements in rotaxanes.

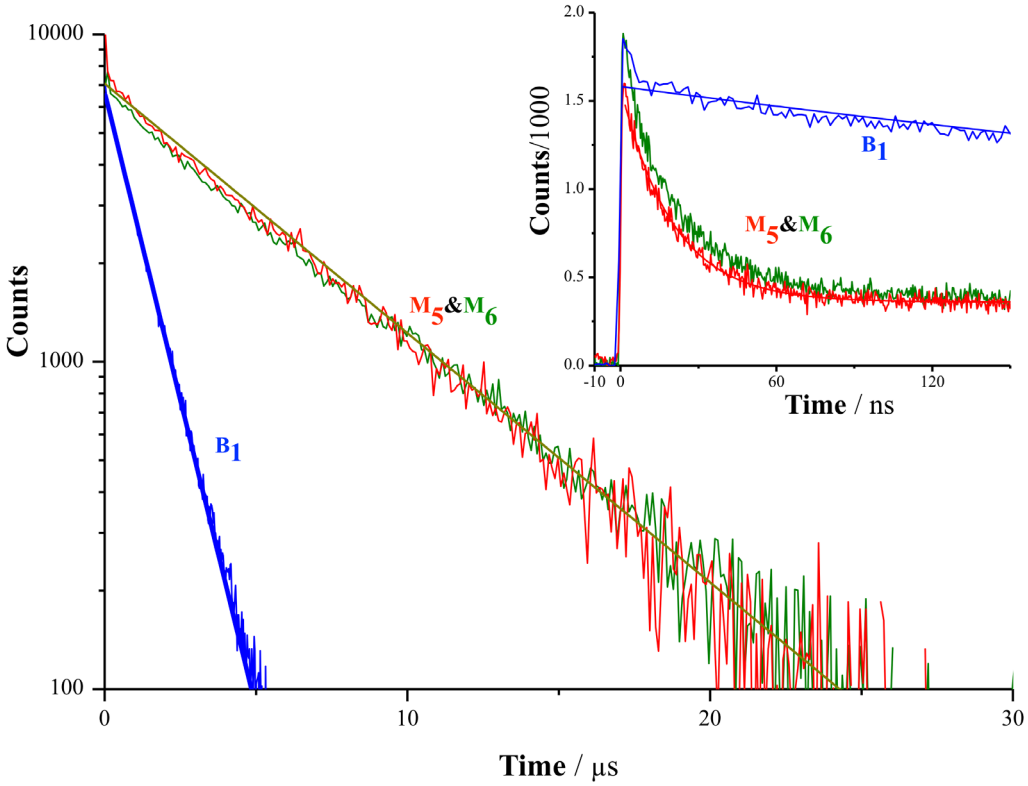

Figure 3.9 Luminescence decays of rotaxanes **M$_5$&M$_6$** and thread **B$_1$** in degassed acetonitrile (λ_{ex} = 450 nm, λ_{em} = 620 nm).

3.2.4 DFT calculations of rotaxane M$_5$

More information about REET processes in molecular shuttles was obtained by carrying out DFT calculations on rotaxane **M$_5$** using with the Gaussian (G16) program package.[13] Two initial structures were prepared, in which the ring has been placed around the triazole moiety (position **1**, Fig. 3.10.a) or around the oxygen atom close to the trityl group (position **2**, Fig. 3.10.b). Geometries were optimized at the b3lyp/6-311g(d) level, including Grimme's D3 dispersion correction,[14] with the LanL2DZ pseudopotential and basis set to describe the Ru atom.[15] Relative energies of the two conformations differed by 4.83 kcal/mol, with position **1** being the most stable structure.

As we know, for an unsymmetrical thread featuring two different stations, a 2 kcal/mol difference in binding affinity is sufficient to ensure 95% occupancy of the preferred binding site at room temperature, according to a Boltzman distribution.[16] This seems to predict that during the ring shuttling process, the ring with a pyrene moiety is almost exclusively around the triazole moiety, close to the Ru complex. Considering that REET can be instilled when the

distance between chromophore Ru complex and chromophore pyrene moiety must be short enough (< 1 nm), more than 95% of rotaxane molecules in the solution can build REET process upon photoexcitation. This seemingly big ΔΔG value between the two positions seems to imply that there exits an intercomponent interaction between triazole moiety and bipyridyl moiety of the ring. No matter if it is an absolute value, there is no doubt that the ring with a pyrene moiety would predominantly occupy position **1** and be close to the Ru complex. This might be why there is no difference of relevant luminescence decays between rotaxane $\mathbf{M_5}$ and $\mathbf{M_6}$, which just have four $-CH_2-$ difference in structures.

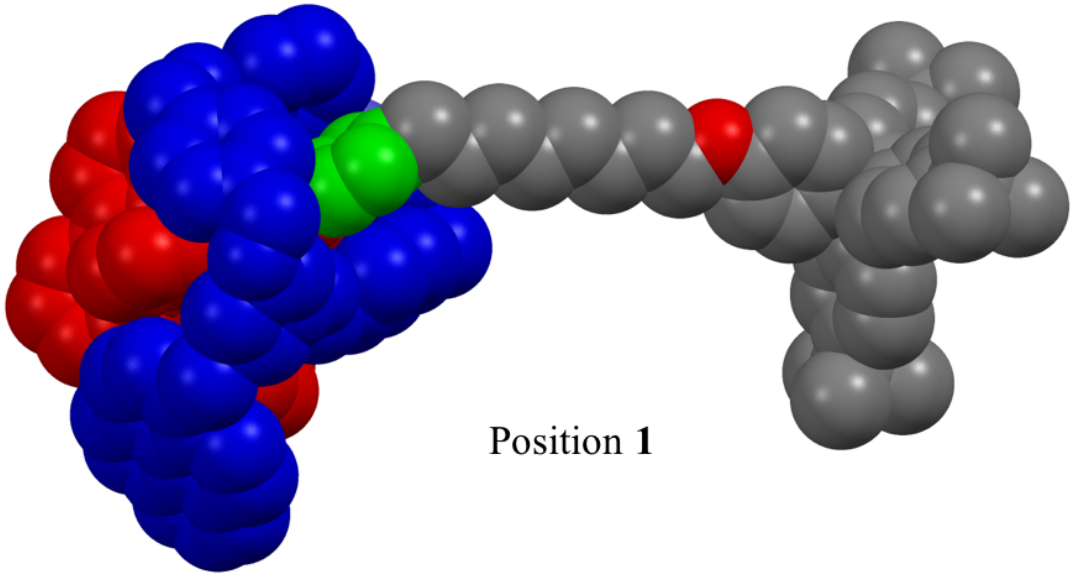

a)

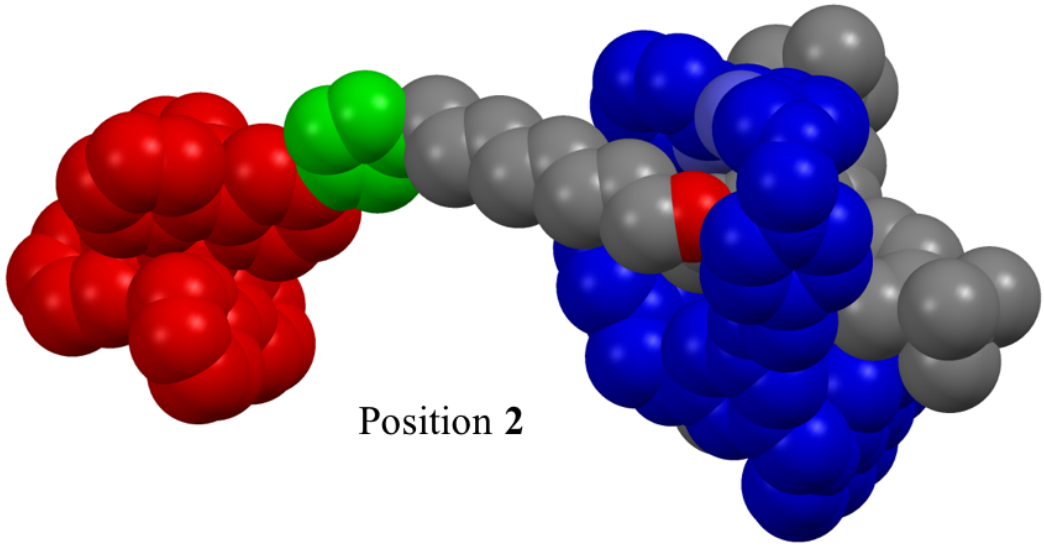

b)

Figure 3.10 DFT optimised geometries of rotaxane $\mathbf{M_5}$ in which a) the ring encircles the triazole moiety close to the Ru complex (position **1**), b) the ring encircles the oxygen close to the trityl group (position **2**).

3.3 Formation and spectroscopic studies of rotaxane M_7

To verify the assumption of the strong interaction between triazole moiety and bipyridyl moiety, and introduce a possible 2 station system, a [2]rotaxane with two triazole moieties at opposing ends of the thread was designed and constructed, as shown in Fig. 3.11.

3.3.1 Synthesis and characterization of rotaxane M_7

Commercially-available 1,8-dibromooctane was reacted with sodium azide to afford 1,8-diazidooctane (**III-1**). Through mono-CuAAC reaction, obtaining alkyne **III-2** from phenol **II-4** through Williamson etherification and excess of **III-1** produced single azide $\mathbf{T_3}$, which is a half thread for rotaxane formation. Rotaxane $\mathbf{M_7}$ with two triazole groups at each end of the thread was constructed based on macrocycle $\mathbf{R_4}$ and half threads $\mathbf{T_3}$&$\mathbf{P_1}$ by AT-CuAAC reaction. After the standard work-up, the crude product was purified by GPC to afford the major fraction.

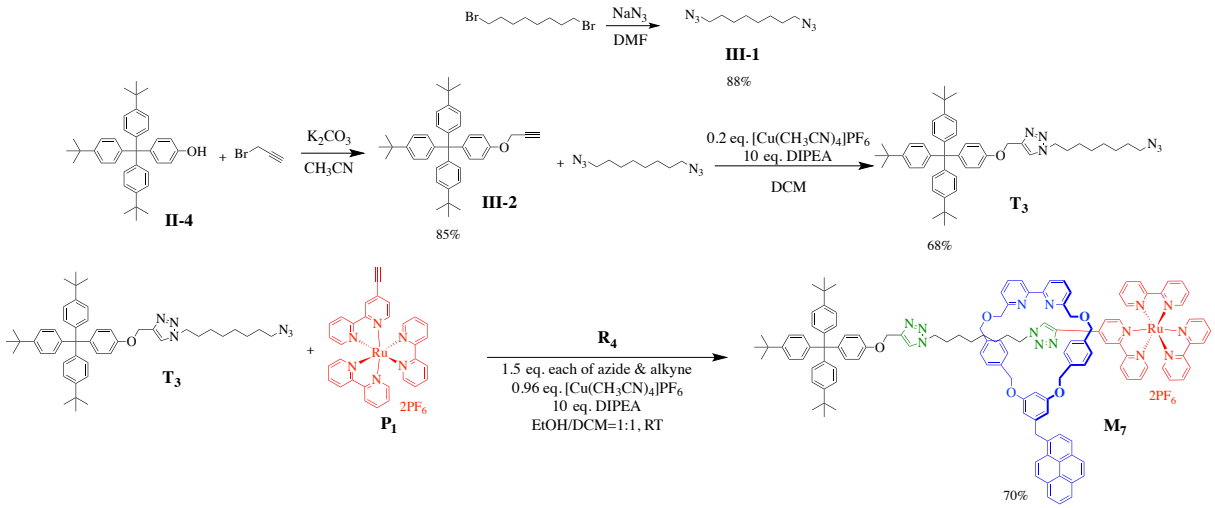

Figure 3.11 Synthesis of rotaxane $\mathbf{M_7}$.

On analyzing the NMR spectrum (Fig. 3.12), two multiplet specific peaks at 7.25 – 7.18 ppm and 7.11 – 7.05 ppm could be attributed to the trityl group; two multiplet peaks at 8.49 – 8.40 ppm, and 7.40 – 7.30 ppm correspond to the Ru complex; a triplet peak at 5.92 ppm is associated to the proton of the benzene group, as a part of the macrocycle, to which the methylene-pyrene group is attached; two triplet peaks at 4.00 ppm and 3.84 ppm and a singlet peak at 5.00 ppm belong to the thread component and some peaks at 4.88 – 4.05 ppm belong to the macrocycle -

CH_2- groups and so on; and the integration is as anticipated. Taken in conjunction with ^{13}C NMR spectra and HRMS, it could be ascertained that this fraction is the desired rotaxane.

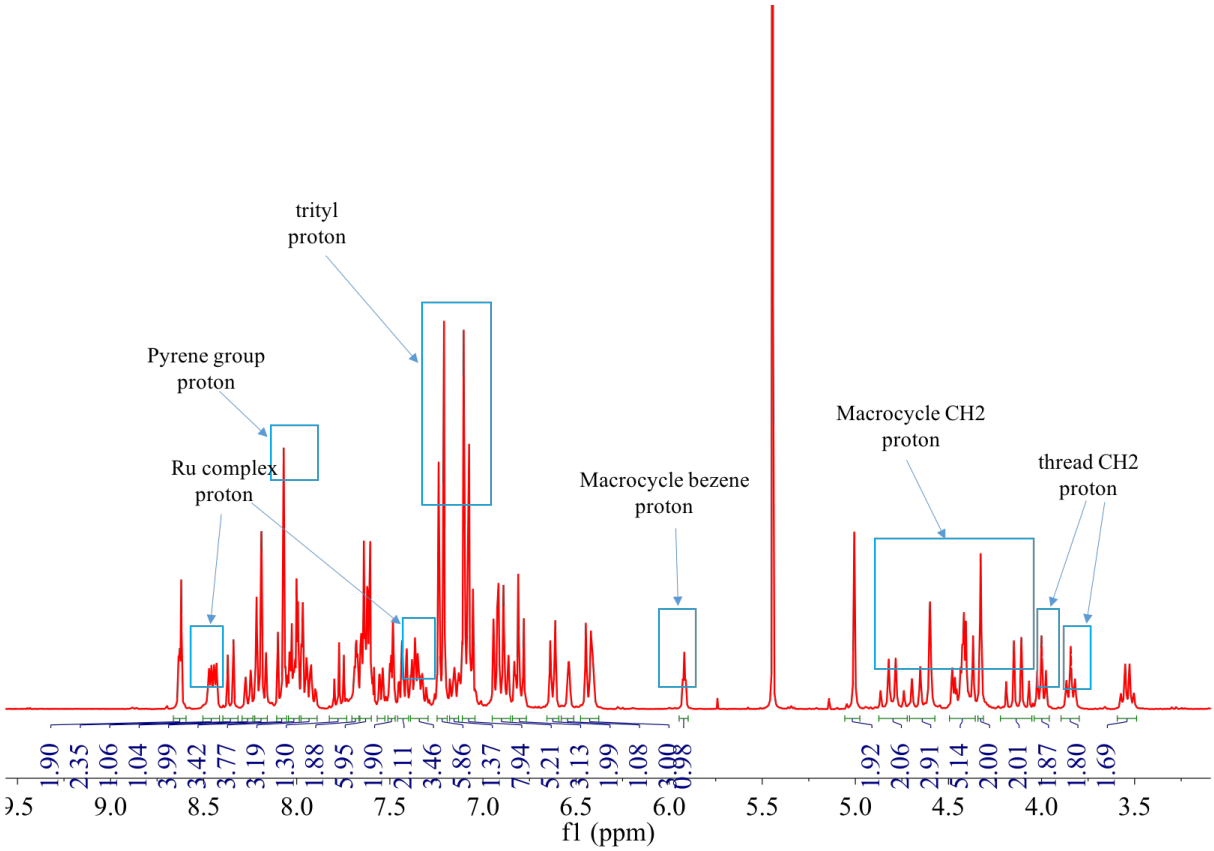

Figure 3.12 ^1H NMR of product $\mathbf{M_7}$ in CD_3CN.

3.3.2 UV-vis spectroscopy comparison of rotaxanes $\mathbf{M_5}$&$\mathbf{M_6}$&$\mathbf{M_7}$

The UV-vis absorption spectra of rotaxanes $\mathbf{M_5}$&$\mathbf{M_6}$&$\mathbf{M_7}$, thread $\mathbf{B_1}$ and pyrene-containing macrocycle $\mathbf{R_4}$ in acetonitrile are shown in Fig. 3.13. In the visible region, compared with other rotaxanes, or the thread and the macrocycle, similar MLCT absorption bands and pyrene absorption bands for rotaxane $\mathbf{M_7}$ were observed. It is also concluded that there only exits a weak ground-state coupling between two chromophores in rotaxane $\mathbf{M_7}$.

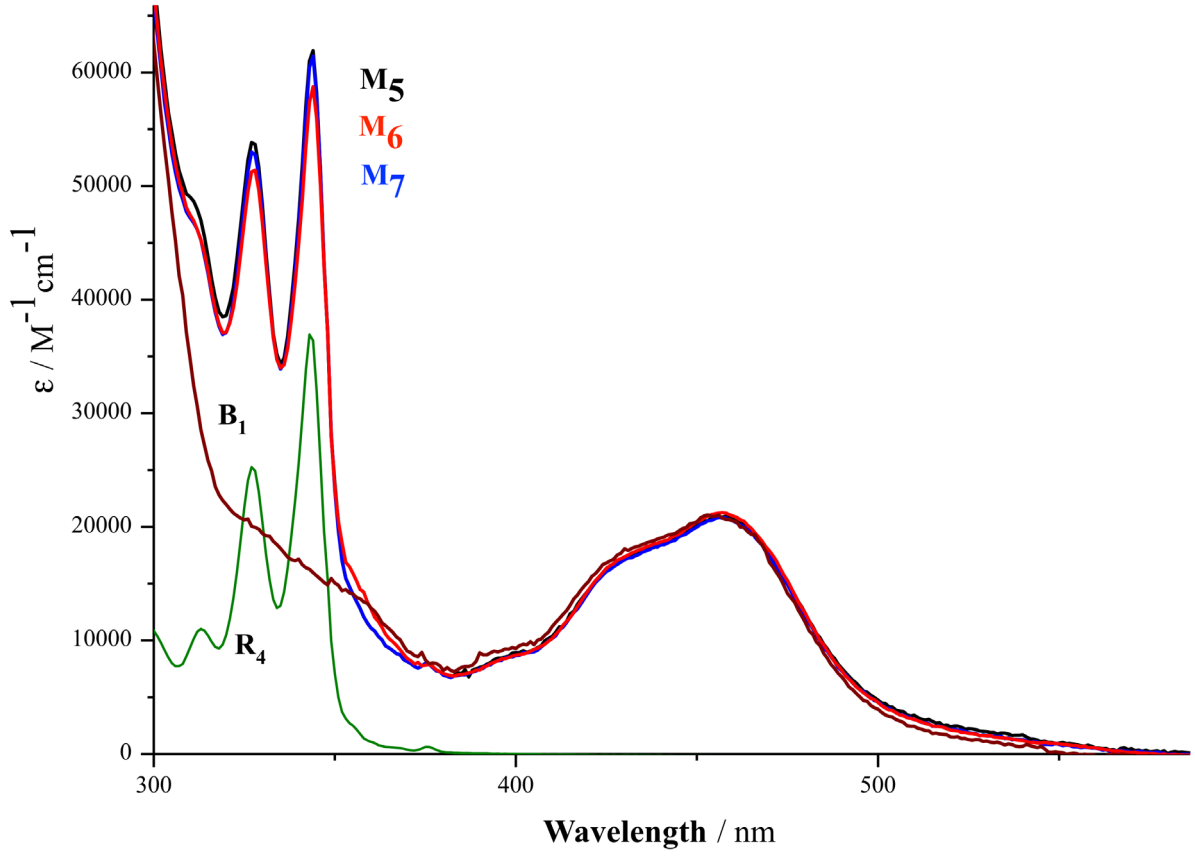

Figure 3.13 UV-vis absorption spectra of rotaxanes **M$_5$**&**M$_6$**&**M$_7$**, thread **B$_1$** and pyrene-containing macrocycle **R$_4$** in acetonitrile.

3.3.3 Luminescence spectroscopy comparison of rotaxanes M$_5$&M$_7$

In Fig. 3.14, the photoluminescence spectrum at room temperature and the phosphorescence spectrum of rotaxane **M$_7$** ($\lambda_{em.max}$ = 637 nm, λ_{ex} = 450 nm) in degassed acetonitrile are the same as the relative ones of rotaxane **M$_5$**. So the energy difference (ΔE = 0.04 eV) between the close-lying states of two chromophores in rotaxane **M$_7$** is also very small, which assumes the possible establishment of REET processes in rotaxane **M$_7$**.

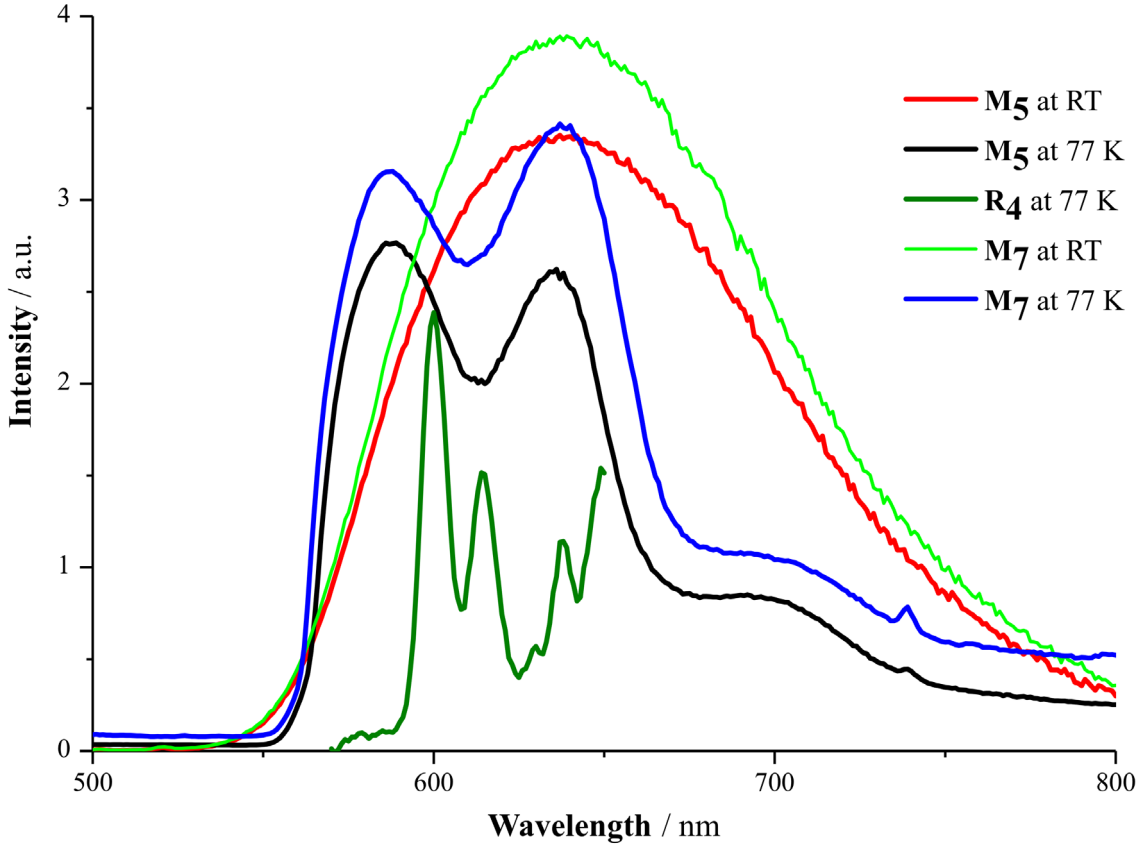

Figure 3.14 Fluorescence (293 K) and phosphorescence (77 K) spectra of **M_5&M_7** (with one triazole) in degassed acetonitrile (λ_{ex} = 450 nm). For comparison of energies triplet states phosphorescence (77 K) spectrum of macrocycle **R_4** is given (λ_{ex} = 342 nm).

3.3.4 Comparison of luminescence decays of rotaxanes M_5&M_7

Luminescence decays of rotaxanes **M_5&M_7** and thread **B_1** are shown in Fig. 3.15. There is a slight difference between rotaxanes **M_5&M_7**: at 60 - 200 ns, the luminescence intensity of rotaxane **M_7** decreases much faster than the one of thread **B_1**, but a little slower than the one of rotaxane **M_5**; at 0.2 - 20 μs, the luminescence intensity of rotaxane **M_7** decreases much slower than the one of thread **B_1**, but obviously faster than the one of rotaxane **M_5**. As analyses of rotaxane **M_7** proved that the sample was pure, we could assume, only a small fraction (11%) of rotaxanes in degassed ACN did not give rise to REET processes from a biexponential curve fit of luminescence decays of rotaxane **M_7**. This seems to indicate that the second, distant triazole moiety in the thread does not have a strong host-guest non-covalent interaction with the bipyridyl moiety in the macrocycle, otherwise a significant portion of rotaxanes could not give

the REET process. Therefore, some DFT calculations on relevant rotaxanes (see below) were undertaken to test this assumption.

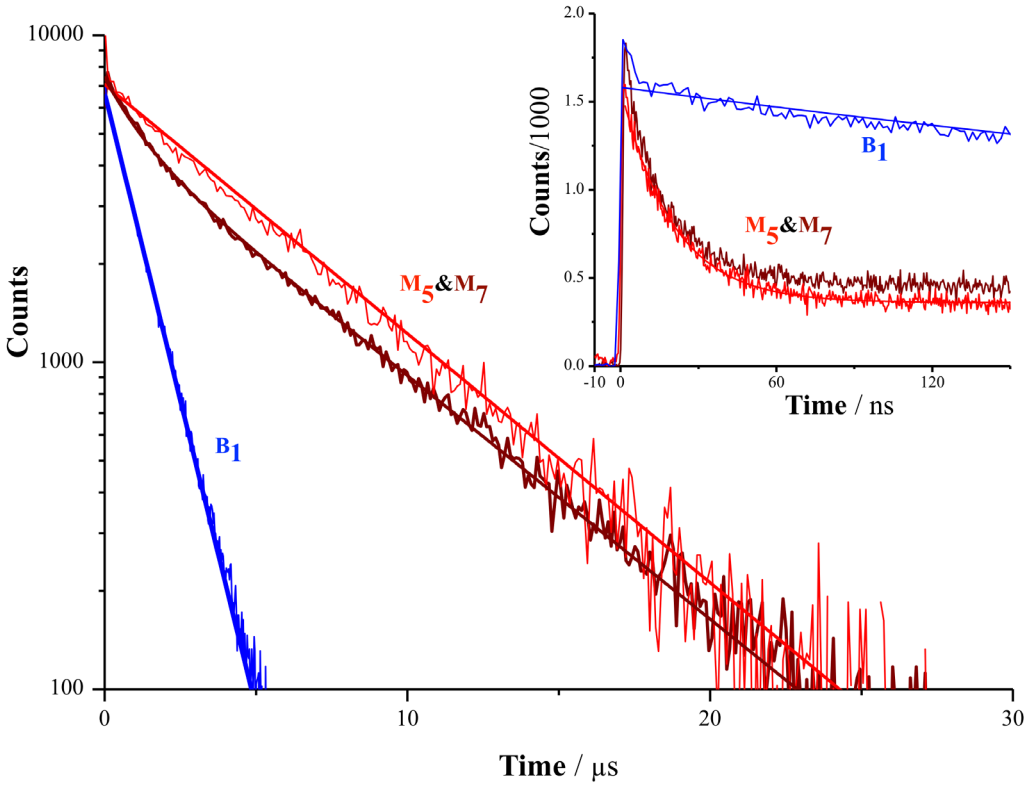

Figure 3.15 Luminescence decays of rotaxane $\mathbf{M_5}$&$\mathbf{M_7}$ and thread $\mathbf{B_1}$ in degassed acetonitrile (λ_{ex} = 450 nm, λ_{em} = 620 nm).

3.3.5 DFT calculations of rotaxanes M_7 and discussions of intercomponent interactions of M_5&M_7

DFT calculations were performed for rotaxane $\mathbf{M_7}$. As shown in Fig. 3.16, the ring encircles the triazole moiety close to the Ru complex in position **3** while it encircles the triazole moiety close to the trityl group in position **4**. In this case, the conformation in which the ring is on the side of the Ru complex turns out to be 8.88 kcal/mol more stable.

A 8.88 kcal/mol difference in energy between position **3** and **4** of rotaxane $\mathbf{M_7}$ is sufficient to ensure much more than 95% occupancy of position **3** at room temperature. This might explain why there is not a big difference of relevant optical measurements between rotaxanes $\mathbf{M_5}$ and $\mathbf{M_7}$.

From the preferred computational conformations of rotaxanes $\mathbf{M_5}$ and $\mathbf{M_7}$, the intercomponent interactions between the ring and different positions could mainly be associated with CH-π and

π-π bonds. Interactions of the pyrene with the stoppers were further investigated by performing single point calculations on the 4 studied conformations after replacement of the pyrene appendage of the ring by a hydrogen atom. Results show that, in absence of the pyrene unit, position **2** is 8.04 kcal/mol less stable than position **1** for $\mathbf{M_5}$ and position **4** is less stable than position **3** by 12.36 kcal/mol for $\mathbf{M_7}$ in absence of the pyrene unit, the macrocycle prefers closer to the Ru complex. While one should be cautious when comparing the energy values it appears the CH-π interaction stabilise the system by 3.21 kcal/mol for $\mathbf{M_5}$ and 3.48 kcal/mol for $\mathbf{M_7}$. Moreover, the computational analysis could help define the structures precisely, and allows the design of molecular machines and switches with better control over the sub-molecular motion.

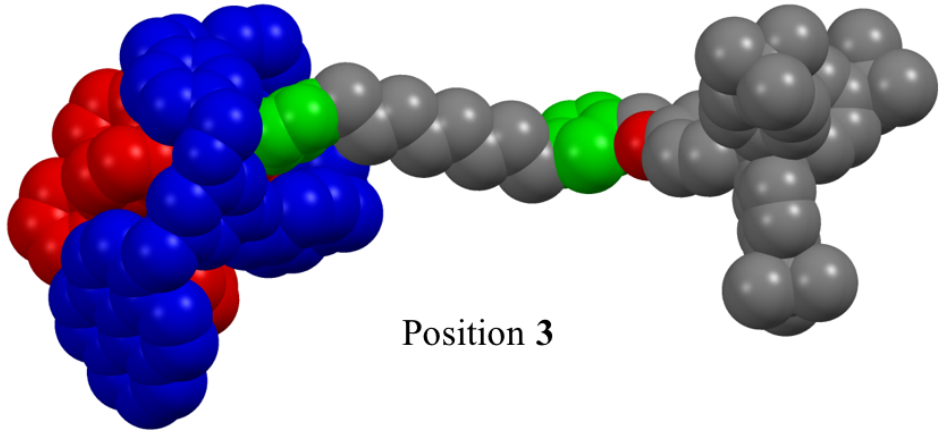

a)

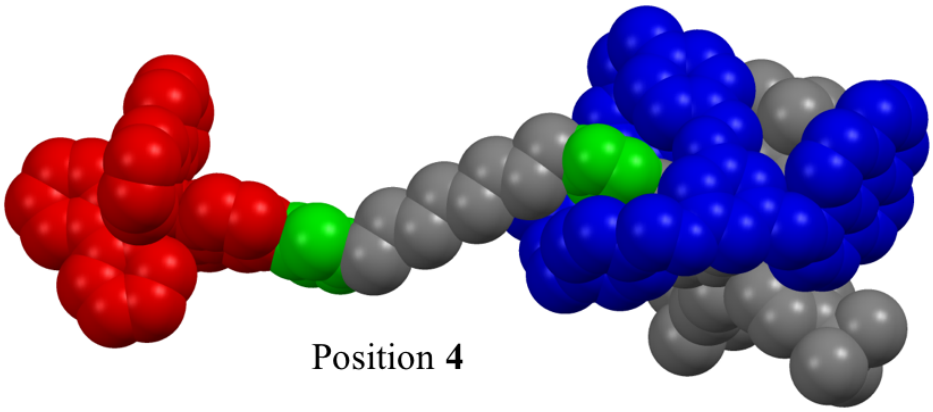

b)

Figure 3.16 DFT optimised geometries of rotaxane $\mathbf{M_7}$ in which a) the ring encircles the triazole moiety close to the Ru complex (position **3**), b) the ring encircles the triazole moiety close to the trityl group (position **4**).

3.4 Formation and spectroscopic studies of rotaxane M_8

3.4.1 Synthesis and characterization of rotaxane M_8

To get more information on the ring shuttling movement in such rotaxanes and REET processes during the shuttling movement, rotaxane **M_8** with a short thread (only a triazole moiety) was designed and synthesized, as shown in Fig. 3.17. After the normal work-up, the crude product was purified by GPC to afford the biggest fraction.

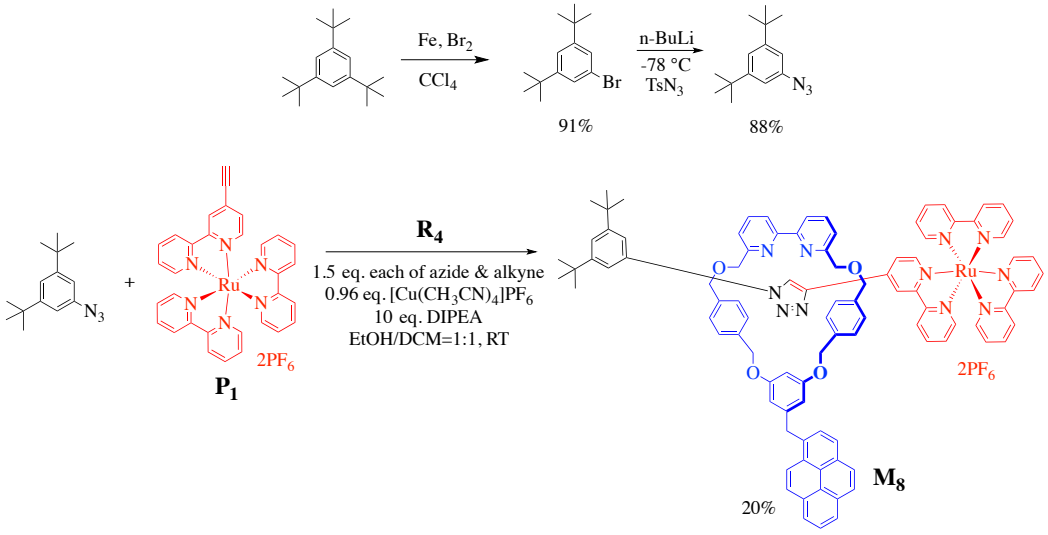

Figure 3.17 Schematic synthesis of rotaxane **M_8**.

On analyzing the ^{1}H NMR spectrum (Fig. 3.18), a singlet resonance at 9.90 ppm could be attributed to the specific triazole proton; a specific multiplet peak at 8.15 – 8.10 ppm could be attributed to the pyrene-moiety; two multiplets at 7.73 – 7.70 ppm and 7.13 – 7.07 ppm correspond to the Ru complex; a triplet peak at 5.96 ppm is associated to the proton of the benzene group, as a part of the macrocycle, which is attached to the methylene-pyrene group; several multiplets at 4.97 – 3.94 ppm belong to the macrocycle -CH_2- groups and so on; with the corresponding integral values. Taken in conjunction with ^{13}C NMR spectrum and HRMS, this fraction could be unambiguously identified as the target rotaxane.

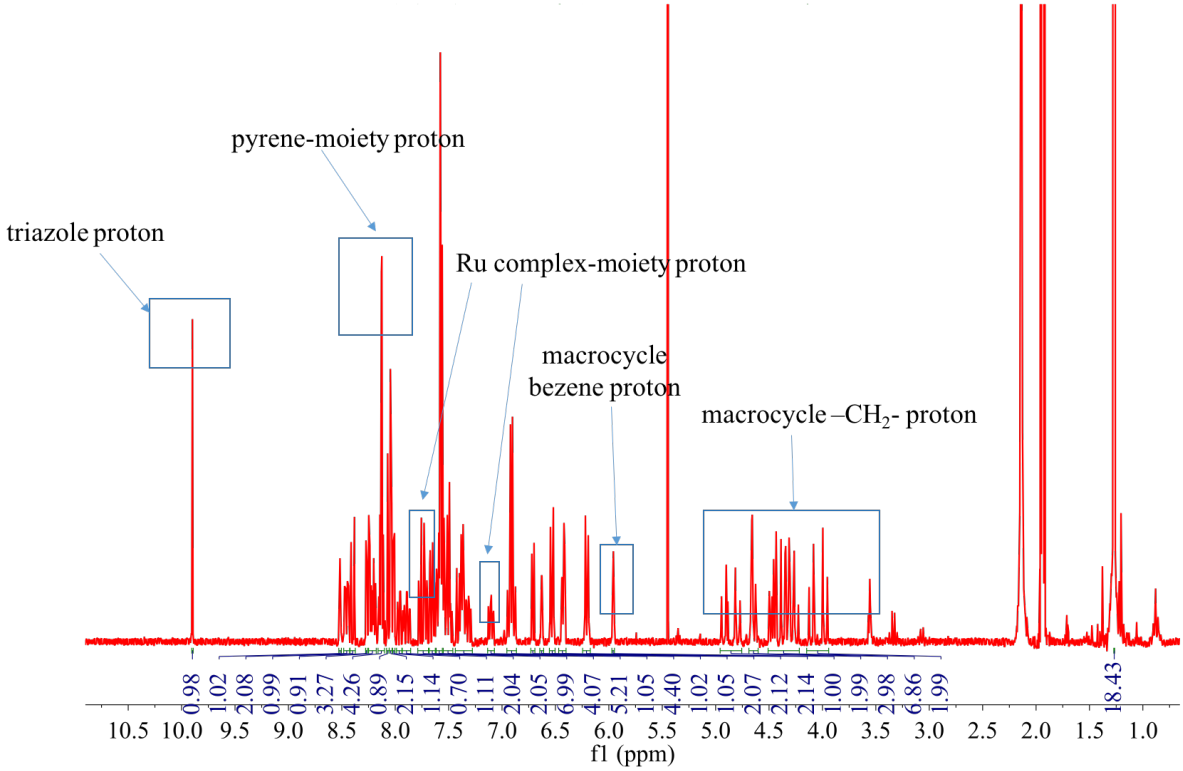

Figure 3.18 ^{1}H NMR of product **M_8** in CD_3CN.

3.4.2 UV-vis spectroscopy and luminescence spectroscopy of rotaxane M_8

The UV-vis absorption spectra of rotaxanes **M_5&M_8**, thread **B_1** and pyrene-containing macrocycle **R_4** in acetonitrile are shown in Fig. 3.19.a. In the visible region, compared with other rotaxanes, or the thread and the macrocycle, similar MLCT absorption bands and pyrene absorption bands for rotaxane **M_8** were observed. It is also concluded that there only exits a weak ground-state coupling between two chromophores in rotaxane **M_8**. Luminescence excitation and emission spectra of rotaxane **M_8** are also shown in Fig. 3.19.b.

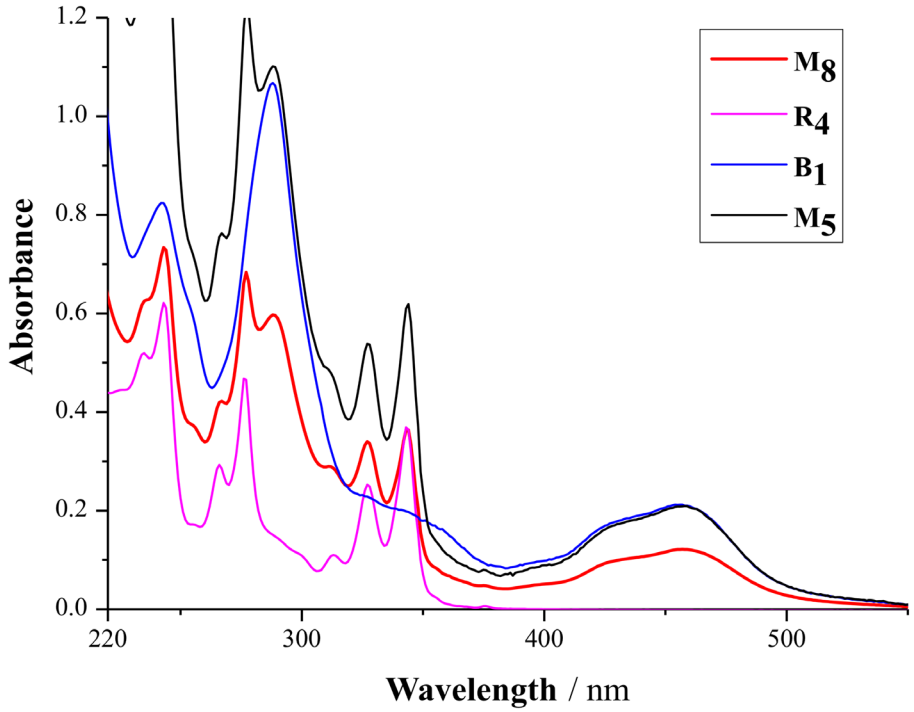

a)

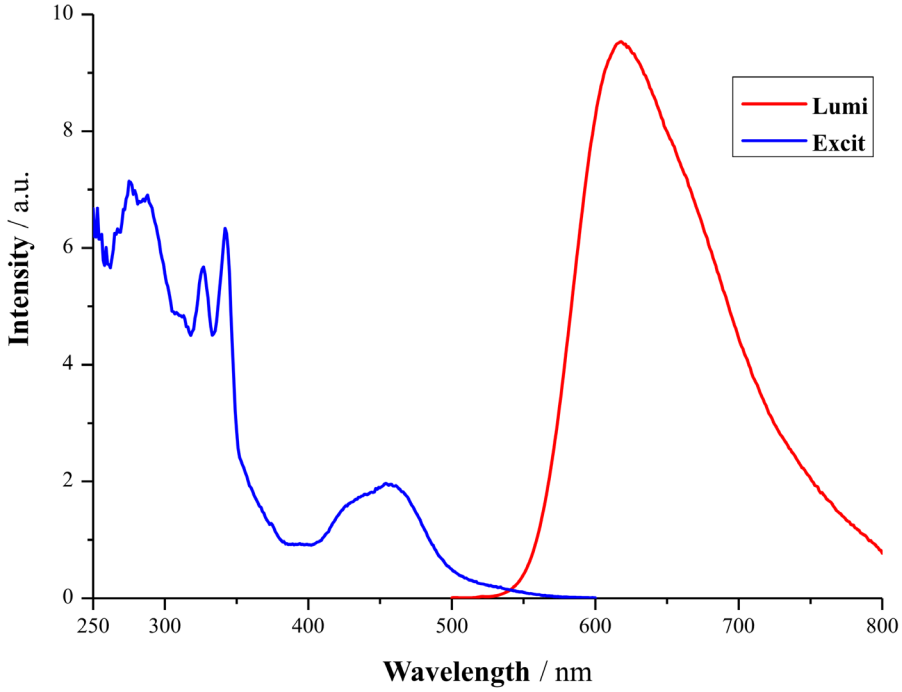

b)

Figure 3.19 a) UV-vis absorption spectra of rotaxanes **M$_5$**&**M$_8$**, thread **B$_1$** and pyrene-containing macrocycle **R$_4$** in acetonitrile; b) Luminescence excitation (λ_{em} = 620 nm) and emmission (λ_{ex} = 452 nm) spectra of rotaxane **M$_8$** in degassed acetonitrile.

3.4.3 Comparison of luminescence decays of rotaxanes M_5&M_8

Luminescence decays of rotaxanes **M_5&M_8** and thread **B_1** are shown in Fig. 3.20. REET processes are also instilled in rotaxane **M_8**, and the lifetime of decay is similar/slightly longer than that of **M_5** (6.3 μs *vs* 5.6 μs). From the structure analysis of **M_8**, there is almost no shuttling movement of the macrocycle because the thread is very short, and the distance between pyrene-moiety and Ru complex can be approximatively regarded as fixed. Spectra of luminescence decays of rotaxanes **M_5&M_8** are slightly different. This shows REET processes in **M_5** behave quite similar to the ones in **M_8**, which is consistent with non-shuttling movements of the macrocycle on the thread of **M_5**.

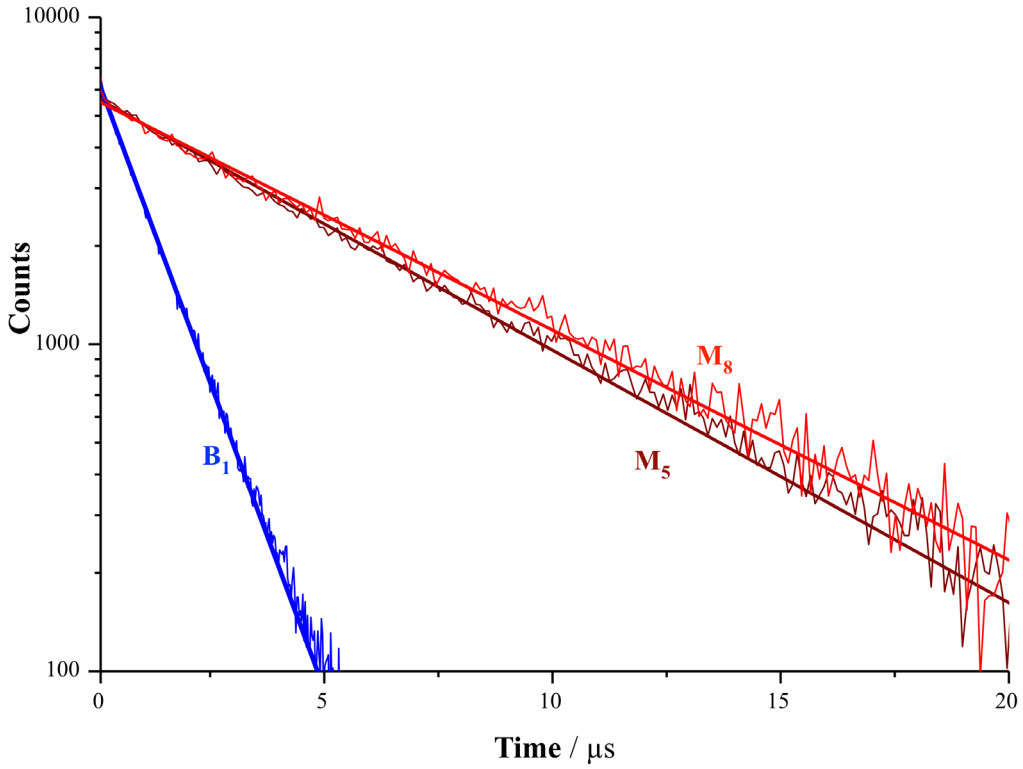

Figure 3.20 Luminescence decays of rotaxanes **M_5&M_8** and thread **B_1** in degassed acetonitrile (λ_{ex} = 450 nm, λ_{em} = 620 nm).

3.5 Formation and spectroscopic studies of rotaxanes M_9&M_{10} constructed by a templated Cadiot-Chodkiewicz method

In the meantime, to get more information of the interaction between triazole group and

bipyridine macrocycle, and the ring shuttling movement, two rotaxanes were constructed by Cadiot-Chodkiewicz templated method and the REET processes therein were investigated.

3.5.1 Synthesis and characterization of rotaxanes M_9&M_{10}

The synthesis scheme is shown in Fig. 3.21. Compound **II-4** was monosubstituted by a large excess of dibromododecane using a Williamson etherification mechanism to afford bromide **III-3**, which was reacted with propargyl alcohol, obtaining alkyne **III-5**. The following bromination of **III-5** alkyne hydrogen with NBS and silver nitrate afforded bromoalkyne $\mathbf{T_4}$. With the same method, bromoalkyne $\mathbf{T_5}$ was obtained from alkyne **III-2**. Through the Cadiot-Chodkiewicz active template method, bromoalkynes $\mathbf{T_4}$ and $\mathbf{T_5}$ were respectively reacted with the Ru^{2+}-complex and ring $\mathbf{R_3}$ to afford rotaxanes $\mathbf{M_9}$ and $\mathbf{M_{10}}$. After the normal work-up, the crude product was purified by column chromatography to obtain the desired rotaxanes $\mathbf{M_9}$&$\mathbf{M_{10}}$, and free-threads $\mathbf{B_2}$&$\mathbf{B_3}$, respectively. On analyzing the ^{1}H NMR spectra, ^{13}C NMR spectra and HRMS, products $\mathbf{M_9}$ and $\mathbf{M_{10}}$ were shown to be afforded successfully.

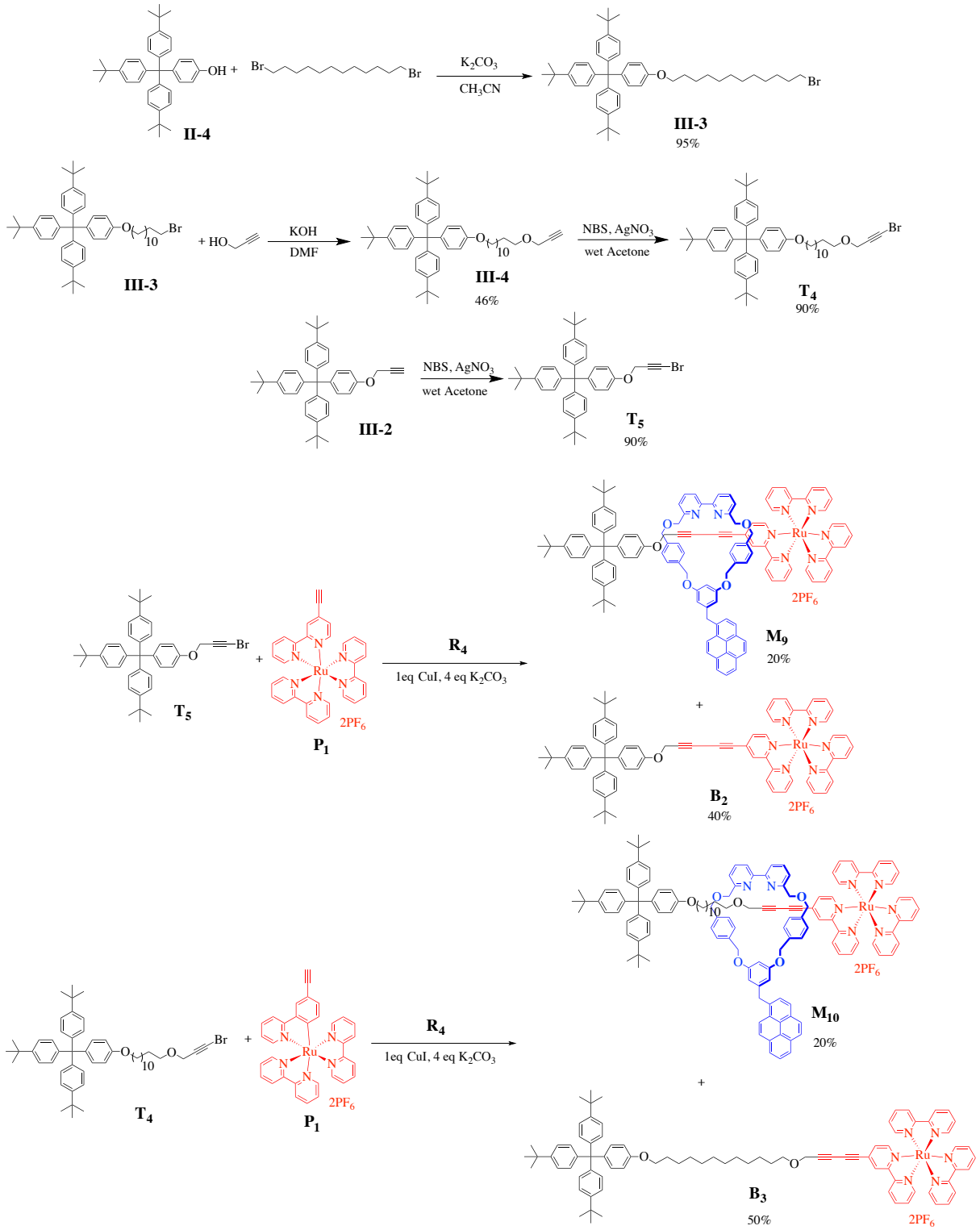

Figure 3.21 Schematic synthesis of rotaxanes **M$_9$&M$_{10}$** and threads **B$_2$&B$_3$**.

3.5.2 Electronic absorption spectroscopy of rotaxanes M$_9$&M$_{10}$

The UV-vis absorption spectra of rotaxanes **M$_9$&M$_{10}$**, threads **B$_1$&B$_2$** in acetonitrile are shown in Fig. 3.22. In the visible region, it is clear that rotaxanes **M$_9$&M$_{10}$** show MLCT absorption

bands and pyrene absorption bands in the range of 400 - 500 nm, 320 - 360 nm, respectively. It could be concluded that there only exists a weak ground-state coupling between the two chromophores in rotaxanes **M_9&M_{10}**. MLCT absorption bands of thread **B_2** were similar to the ones of rotaxanes **M_9&M_{10}**, while they were slightly different from the ones of thread **B_1**. This is because the ^{1}MLCT states of Ru complex on the thread differ from the ones of general $Ru(bpy)_3^{2+}$ complex derivatives, like thread **B_1**, due to a diynyl group directly connecting to the Ru complex.

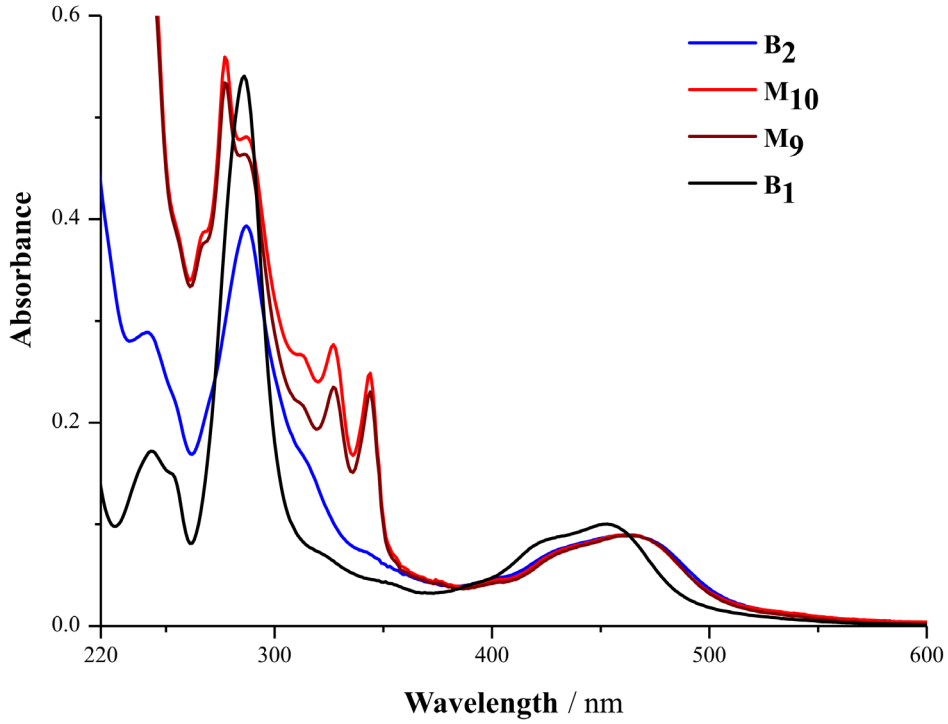

Figure 3.22 UV-vis absorption spectra of rotaxanes **M_9&M_{10}**, threads **B_1&B_2** in acetonitrile.

3.5.3 Luminescence spectroscopy of rotaxanes M_9&M_{10}

In Fig. 3.23, photoluminescence spectra of rotaxanes **M_9&M_{10}** and threads **B_2&B_3** in degassed acetonitrile at room temperature are shown. All four spectra were observed after photexcitation of λ_{ex} = 450 nm (**M_9** : $\lambda_{em.max}$ = 641 nm; **M_{10}** : $\lambda_{em.max}$ = 651 nm; **B_2** : $\lambda_{em.max}$ = 664 nm; **B_3** : $\lambda_{em.max}$ = 666 nm). Generally, MLCT energy levels depend on the ease of oxidation of the metal centre and the reduction of the ligands. If it is easier to oxidize the metal and reduce ligands, MLCT is of lower energy, which means MLCT emission shifts refer to a difference of MLCT

energy. Different alkyl chain lengths of threads **B₂&B₃** give similar MLCT emission because of sharing similar MLCT states energies. MLCT emissions of rotaxanes **M₉&M₁₀** have an obvious blue shift, compared with the relevant threads **B₂&B₃**. This is because the effective solvation-like effect of the macrocycle around the diynyl group of the thread in the rotaxane is completely different from the solvation of the free thread, causing MLCT states in rotaxanes to have higher energies. In **M₉** which has a short thread, **R₄** is always around the diynyl group; while in **M₁₀**, which has a much longer thread, parts **R₄** may be located away from the diynyl group, contributing less effective solvation effect on MLCT states in **M₁₀**. This is why **M₉** has a slight blue shift compared with **M₁₀**. It is noteworthy to indicate that luminescence emission spectrum of **M₁₀** is like a mix of luminescence emission spectra of **M₉** and **B₃**.

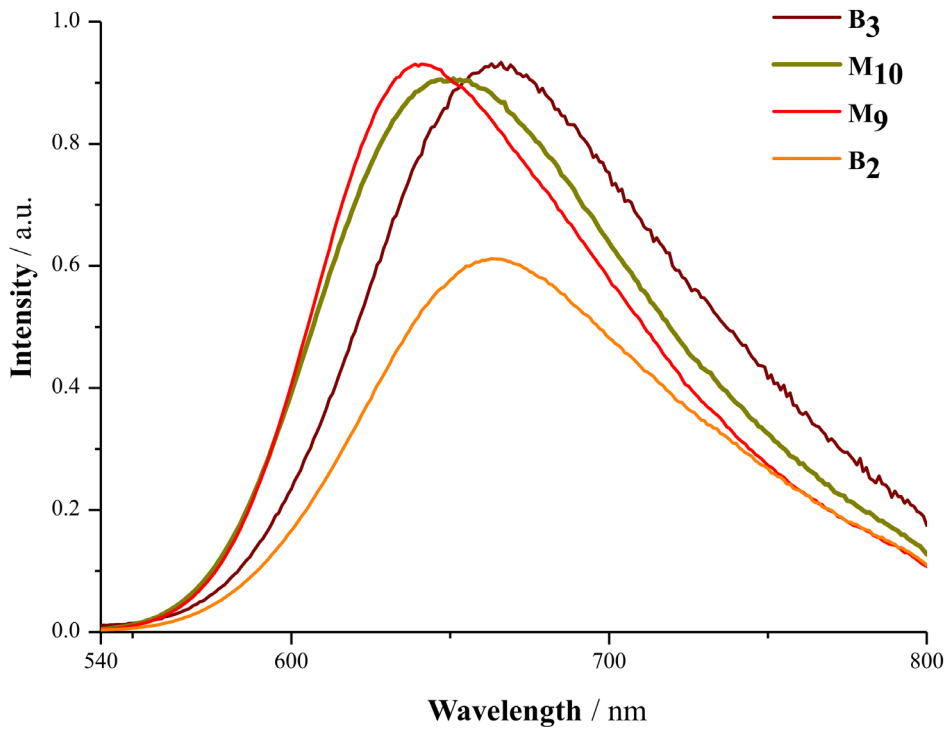

Figure 3.23 Luminescence (293 K) spectra of rotaxanes **M₉&M₁₀** and threads **B₂&B₃** in degassed acetonitrile (λ_{ex} = 450 nm).

Low temperature (77 K) phosphorescence measurements were undertaken to gain further insight into the energies of the pertinent states and relative energy levels of rotaxanes **M₉&M₁₀** and macrocycle **R₄**, as shown in Fig. 3.24. Indeed, the highest energy feature is taken as the energy of the excited state. At 77 K, ^{3}MLCT structured phosphorescence of **M₉&M₁₀** ($\lambda_{em.max}$ = 606 nm and 603 nm, respectively) could be observed. The energy of the lowest-lying ^{3}MLCT

of $\mathbf{M_9}$&$\mathbf{M_{10}}$ are calculated to be 2.056 and 2.060 eV, respectively, which are slightly different from the energy (2.070 eV) of the lowest-lying triplet pyrene in $\mathbf{R_4}$ ($\lambda_{em.max}$ = 600 nm). Such a small energy gap value ($\mathbf{M_9}$-$\mathbf{R_4}$: -0.014 eV; $\mathbf{M_{10}}$-$\mathbf{R_4}$: -0.010 eV) between two chromophores assumes the very efficient establishment of fast REET processes in $\mathbf{M_9}$&$\mathbf{M_{10}}$.

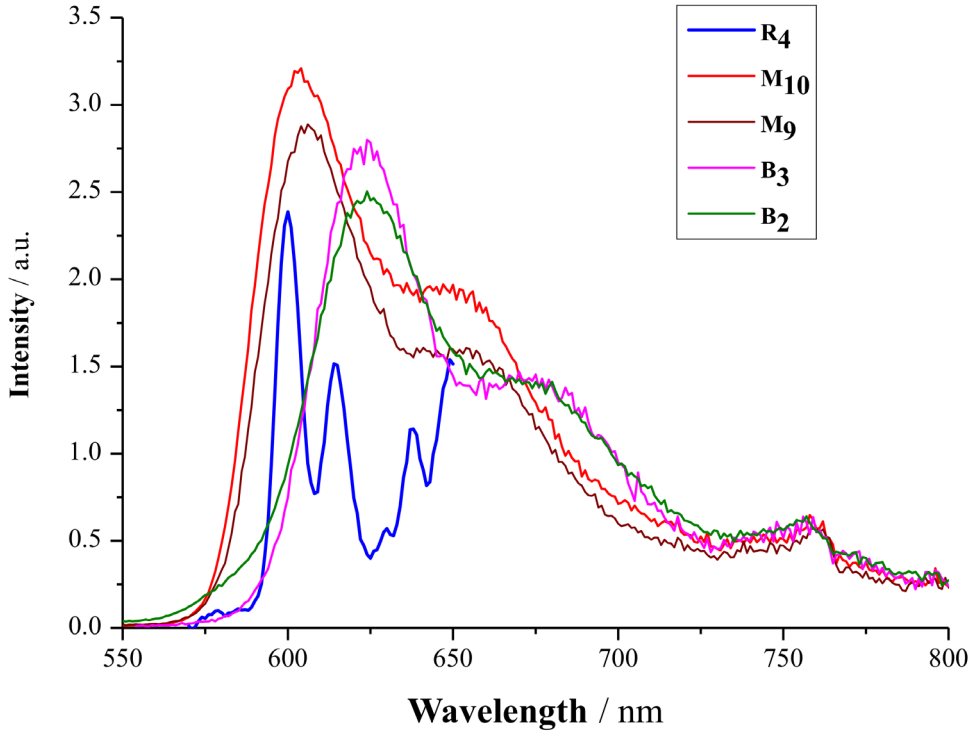

Figure 3.24 Phosphorescence spectra (77 K) of rotaxanes $\mathbf{M_9}$&$\mathbf{M_{10}}$ and threads $\mathbf{B_2}$&$\mathbf{B_3}$ (λ_{ex} = 450 nm), and macrocycle $\mathbf{R_4}$ (λ_{ex} = 342 nm) in degassed acetonitrile.

3.5.4 Luminescence decays of rotaxanes $\mathbf{M_9}$&$\mathbf{M_{10}}$

Fig. 3.25 shows luminescence decays of rotaxanes $\mathbf{M_9}$&$\mathbf{M_{10}}$ and thread $\mathbf{B_2}$ which are quite different. The lifetime of thread $\mathbf{B_2}$, in which there is only one chromophore, is 1.7 μs; the fit of luminescence decays spectrum of rotaxane $\mathbf{M_{10}}$ is a biexponential curve, 34% part of $\mathbf{M_{10}}$ behave as $\mathbf{B_2}$, 66% $\mathbf{M_{10}}$ show a longer average lifetime, 3.6 μs. While the fit of luminescence decays spectrum of rotaxane $\mathbf{M_9}$ is a monoexponential curve, showing an average lifetime of 3.6 μs. It could be concluded that in $\mathbf{M_{10}}$, the shuttling movement of the ring on the thread causes the distance change between Ru complex and pyrene moiety, 34% rotaxanes do not exhibit REET process because of the long distances between two chromophores; because of the short thread in $\mathbf{M_9}$, 100% rotaxanes show REET processes.

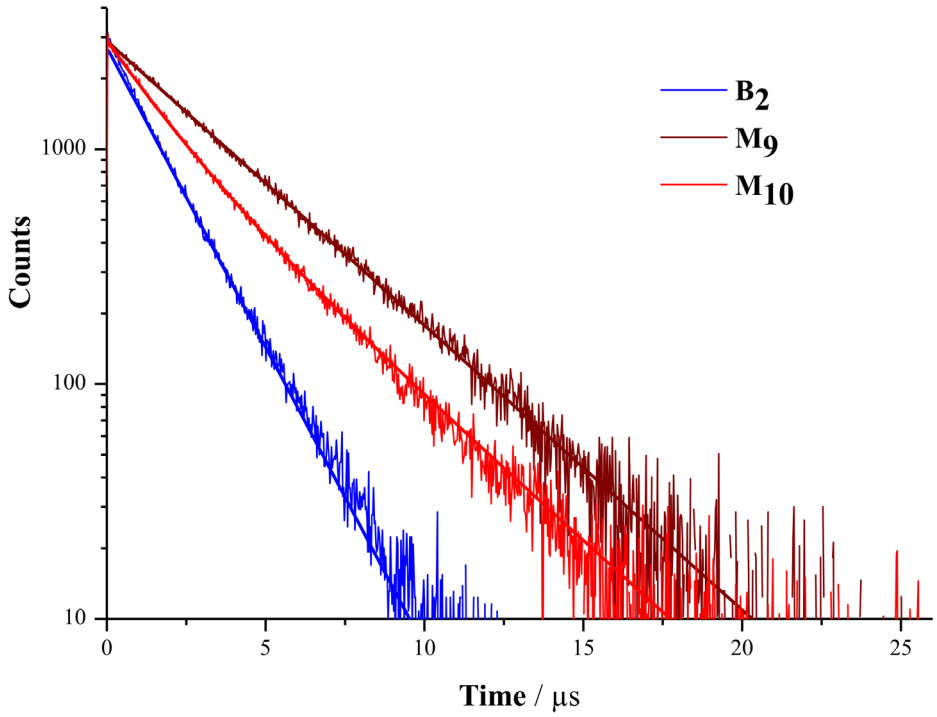

Figure 3.25 Luminescence decays of rotaxanes **M$_9$&M$_{10}$** and thread **B$_2$** in degassed acetonitrile (λ_{ex} = 450 nm, λ_{em} = 620 nm).

3.6 Conclusion

Three more rotaxanes **M$_6$&M$_7$&M$_8$** with REET processes were constructed by AT-CuAAC reactions and confirmed by NMR, HRMS. UV-vis spectroscopy, luminescence spectroscopy (steady-state and time-resolved) of rotaxanes **M$_6$&M$_7$&M$_8$** were performed. Compared with **M$_5$**, **M$_6$** has a shorter thread, while no difference could be seen from their luminescence decays spectra (τ = 5.6 μs). **M$_7$** has a slightly longer thread and one more triazole moiety than rotaxane **M$_5$**. From the luminescence decay spectra of **M$_5$&M$_7$**, they behave slightly differently; REET processes were not operational in 11% of **M$_7$**, which proved the ring was not fixed excusively at one single position, probably as a result of shuttling movement of the ring on the thread. **M$_8$** has a very short thread, one triazole moiety; from their luminescence decays spectra of **M$_5$&M$_8$**, **M$_8$** exhibit a slightly longer luminescence emission, which shows REET processes in two rotaxanes behave differently, implying the existence of shuttling movements of the macrocycle on the thread.

Another two Cadiot-type rotaxanes **M$_9$&M$_{10}$** were constructed and confirmed by NMR, HRMS,

UV-vis spectroscopy. To investigate REET processes, steady-state and time-resolved luminescence spectroscopy of **M_9&M_{10}** were further performed. Due to a diynyl group directly connected to the Ru complex, the MLCT absorption bands of **M_9&M_{10}** and thread **B_2** are different from the ones of thread **B_1**. The luminescence lifetime of **B_2** is 1.7 μs. Luminescence decays of rotaxanes **M_9&M_{10}** clearly behave differently, REET processes were no obtained in 34% of rotaxane **M_{10}**, 66% rest part shows a longer average lifetime, 3.6 μs, REET processes with an average lifetime 3.6 μs was built in 100% of rotaxane **M_9**. The results show that the Cadiot-type rotaxanes hold promise in the tracking of rings shuttling movement with REET process.

References

[1] Browne W. R., Feringa B. L. Making Molecular Machines Work. Nat. Nanotechnol., 2006, 1, 25-35.

[2] Gust D., Moore T. A., Moore A. L. Molecular Switches Controlled by Light. Chem. Commun., 2006, 1169-1178.

[3] Balzani V., Credi A., Venturi M. Molecular Devices and Machines Concepts and Perspectives for the Nanoworld, Wiley-VCH: Weinheim, 2008.

[4] Vukotic V. N., Zhu K., Baggi G., Loeb S. J. Optical Distinction between "Slow" and "Fast" Translational Motion in Degenerate Molecular Shuttles. Angew. Chem. Int. Ed., 2017, 56, 6136-6141.

[5] Gunbas D. D., Zalewskiz L., Brouwer A. M. Energy landscape of a hydrogen-bonded non-degenerate molecular shuttle. Chem. Commun., 2010, 46, 2061-2063.

[6] Gunbas D. D., Brouwer A. M. Degenerate Molecular Shuttles with Flexible and Rigid Spacers. J. Org. Chem. 2012, 77, 5724-5735.

[7] Young P. G., Hirose K., Tobe Y. Axle Length Does Not Affect Switching Dynamics in Degenerate Molecular Shuttles with Rigid Spacers. J. Am. Chem. Soc. 2014, 136, 7899-7906.

[8] Zheng X.-L., Yu S.-L., Pozzo J.-L., Pianet I., McClenaghan N. D., Qu D.-H. Extra Recognition Sites Accelerate Ring Shuttling in a Degenerate [2]Rotaxane.

[9] Berná J., Goldup S. M., Lee A.-L., Leigh D. A., Symes M. D., Teobaldi G., Zerbetto F. Cadiot-Chodkiewicz Active Template Synthesis of Rotaxanes and Switchable Molecular Shuttles with Weak Intercomponent Interactions. Angew. Chem. Int. Ed., 2008, 47, 4392-4396.

[10] Goldup S. M., Leigh D. A., Long T., McGonigal P. R., Symes M. D., Wu J. Active Metal Template Synthesis of [2]Catenanes. J. Am. Chem. Soc., 2009, 131, 15924-15929.

[11] Matsuoka Y., Mutoh Y., Azumaya I., Kikkawa S., Kasama T., Saito S. Synthesis and Shuttling Behavior of [2]Rotaxanes with a Pyrrole Moiety. J. Org. Chem. 2016, 81, 3479-3487.

[12] Movsisyan L. D., Franz M., Hampel F., Thompson A. L., Tykwinski R. R., Anderson H. L. Polyyne Rotaxanes: Stabilization by Encapsulation. J. Am. Chem. Soc., 2016, 138, 1366-1376.

[13] Frisch M. J., Trucks G. W., Schlegel H. B., Scuseria G. E., Robb M. A., Cheeseman J. R., Scalmani G., Barone V., Petersson G. A., Nakatsuji H., Li X., Caricato M., Marenich A. V., Bloino J., Janesko B. G., Gomperts R., Mennucci B., Hratchian H. P., Ortiz J. V., Izmaylov A. F., Sonnenberg J. L., Williams-Young D., Ding F., Lipparini F., Egidi F., Goings J., Peng B., Petrone A., Henderson T., Ranasinghe D., Zakrzewski V. G., Gao J., Rega N., Zheng G., Liang W., Hada M., Ehara M., Toyota K., Fukuda R., Hasegawa J., Ishida M., Nakajima T., Honda Y., Kitao O., Nakai H., Vreven T., Throssell K., Montgomery J. A., Jr., Peralta J. E., Ogliaro F., Bearpark M. J., Heyd J. J., Brothers E. N., Kudin K. N., Staroverov V. N., Keith T. A., Kobayashi R., Normand J., Raghavachari K., Rendell A. P., Burant J. C., Iyengar S. S., Tomasi J., Cossi M., Millam J. M., Klene M., Adamo C., Cammi R., Ochterski J. W., Martin R. L., Morokuma K., Farkas O., Foresman J. B., Fox D. J. Gaussian 16, Revision A.03. Gaussian, Inc., Wallingford CT, 2016.

[14] Grimme S., Antony J., Ehrlich S. and Krieg H. A consistent and accurate ab initio parameterization of density functional dispersion correction (DFT-D) for the 94 elements H-Pu. J. Chem. Phys., 2010, 132, 154104.

[15] Hay P. J., Wadt W. R. Ab Initio Effective Core Potentials for Molecular Calculations. Potentials for the Transition Metal Atoms Sc to Hg; Potentials for Main Group Elements Na to Bi; Potentials for K to Au Including the Outermost Core Orbitals. J. Chem. Phys. 1985, 82 (270), 284-299.

[16] Altieri A., Bottari G., Dehez F., Leigh D. A., Wong J. K. Y., Zerbetto F. Remarkable Positional Discrimination in Bistable Light- and Heat-Switchable Hydrogen-Bonded Molecular Shuttles. Angew. Chem. Int. Ed., 2003, 42, 2296-2300.

Chapter 4 REET Rotaxane as an Ionophore & Linear Reversible Electronic Energy Hopping

Chapter 4.1 REET rotaxane as an ionophore

4.1.1 Introduction

The assembly of interlocked molecules by employing metal ion binding to form mechanical bonds has been extensively studied for decades. Some rotaxanes and catenanes as metal-ion-binding fluorescence sensors have been investigated, while all such fluorescent responses rely on the binding station change of the macrocycle in rotaxanes or catenanes. In 2018, Goldup reported rotaxanes as fluorescence sensors, which rely on metal ion binding, and different metal ion bindings with interlocked molecules, e.g., as shown in Fig. 4.1.[1] Their [2]rotaxane **44** was afforded with high yield based on their classical macrocycle $\mathbf{R_0}$ and two short half threads, 3,5-di-*tert*-butyl-1-alkynebenzene and an azido-naphthalimides derivative by AT-CuAAC reaction. A titration of $Zn(ClO_4)_2 \cdot 6H_2O$ to a solution of the [2]rotaxane in CD_3CN showed that the rotaxane was capable of acting as a ligand. In Fig. 4.1.b, with addition of $Zn(ClO_4)_2 \cdot 6H_2O$ into a solution of the [2]rotaxane **44** in MeCN, the fluorescence emission (λ_{ex} = 343 nm) was getting weaker and weaker. Fig. 4.1.c shows the emission profiles of rotaxane in the presence of 5 equivalents different metal ions. This research reveals that such interlocked molecular machines may have some perspectives in fluorescent sensors and other optics fields.

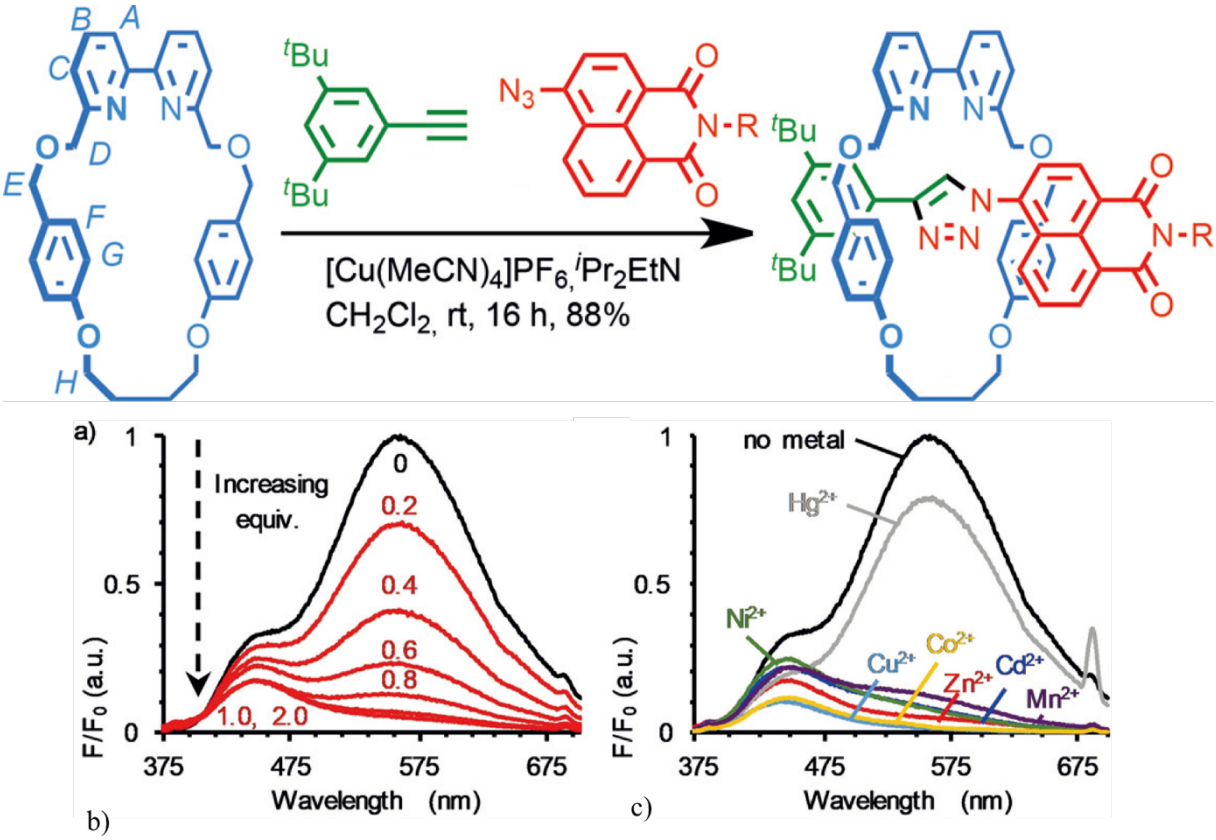

Figure 4.1 a) Synthesis of a fluorescent rotaxane **44** using the AT-CuAAC reaction, R=$CH_2C(H)Ph_2$, b) Emission profile of rotaxane (MeCN, 100 mm, λ_{ex}=343 nm) in the presence of varying amounts of $Zn(ClO_4)_2 \cdot 6H_2O$; (c) Emission profiles of rotaxane in the presence of 5 equivalents of different metal ions.

4.1.2 Strategy

From the aforementioned example, with addition of different specific metal ions, the fluorescence of the [2]rotaxane with one chromophore can be decreased to different degrees, acting as a fluorescent sensor. The response of guest complexation on interchromophore interactions of a bichromophoric [2]rotaxane, has never been investigated. When a metal ion coordinates with a bichromophoric [2]rotaxane, a significant interchromophore interaction modulation would result in a modulation of optical properties. Rotaxane **M_8** comprising a short thread can be a good candidate to give some information regarding this question. As discussed in Chapter 3, under photoexcitation of **M_8** at 450 nm, an efficient REET process was observed. The current work will focus on that how the REET process of **M_8** with a pyrene group and a Ru complex moiety is changed by addition of a metal ion, like Zn^{2+}, the scheme is shown in Fig. 4.2.

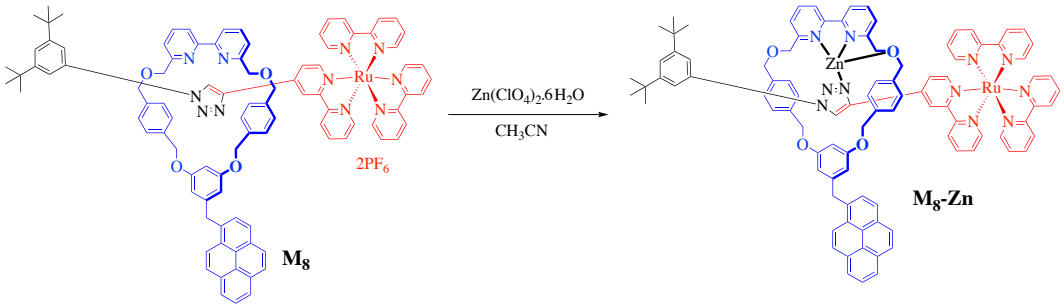

Figure 4.2 Schematic construction of bichromophoric chelating rotaxane ligand **M_8-Zn**.

4.1.3 Formation and ^{1}H NMR spectrum of bichromophoric chelating rotaxane ligand M_8-Zn

To a solution of rotaxane **M_8** in CD_3CN, a large excess of $Zn(ClO_4)_2 \cdot 6H_2O$ was added. Dramatic changes in the ^{1}H NMR spectrum of **M_8** were observed in Fig. 4.3, which showed the formation of chelator rotaxane **M_8-Zn**. The difference in ^{1}H NMR spectra of the solution of **M_8** before and after addition of $Zn(ClO_4)_2 \cdot 6H_2O$ is consistent with the binding of the metal ion into the cavity of the macrocycle, the binding of the metal ion to the macrocycle and the triazole moiety on the short thread. This ^{1}H NMR test confirms that **M_8** is a good candidate to act as a ligand.

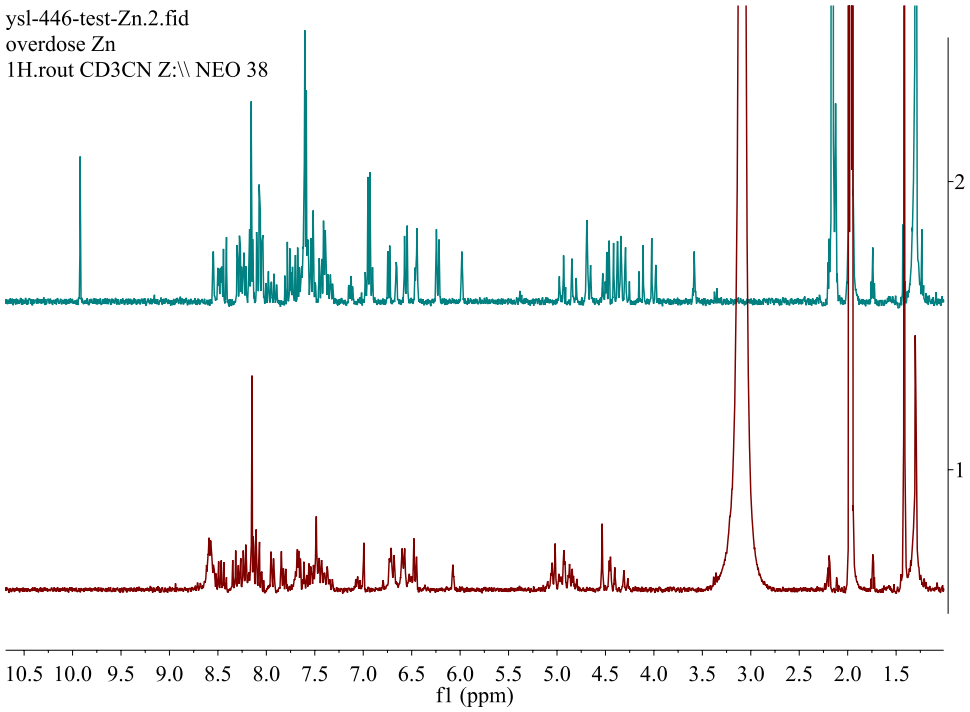

Figure 4.3 ^{1}H NMR spectra of rotaxane **M_8** (top) and chelator rotaxane **M_8-Zn** following addition of a large dose of $Zn(ClO_4)_2 \cdot 6H_2O$ to **M_8** (bottom) in CD_3CN.

4.1.4 Electronic absorption spectroscopy titrations of rotaxane M_8

Figure 4.4 shows UV/Vis titrations of rotaxane **M_8** in ACN with $Zn(ClO_4)_2 \cdot 6H_2O$. On adding $Zn(ClO_4)_2 \cdot 6H_2O$ in the solution, MLCT absorption bands in the range of 400 - 500 nm became less intense and broader. Several isosbestic points were observed at 477, 374, 325 nm. Conclusively, a further proof by UV/Vis titrations confirms the binding of the zinc ion into the cavity of the macrocycle, the coordination of the zinc ion and **M_8** occurs.

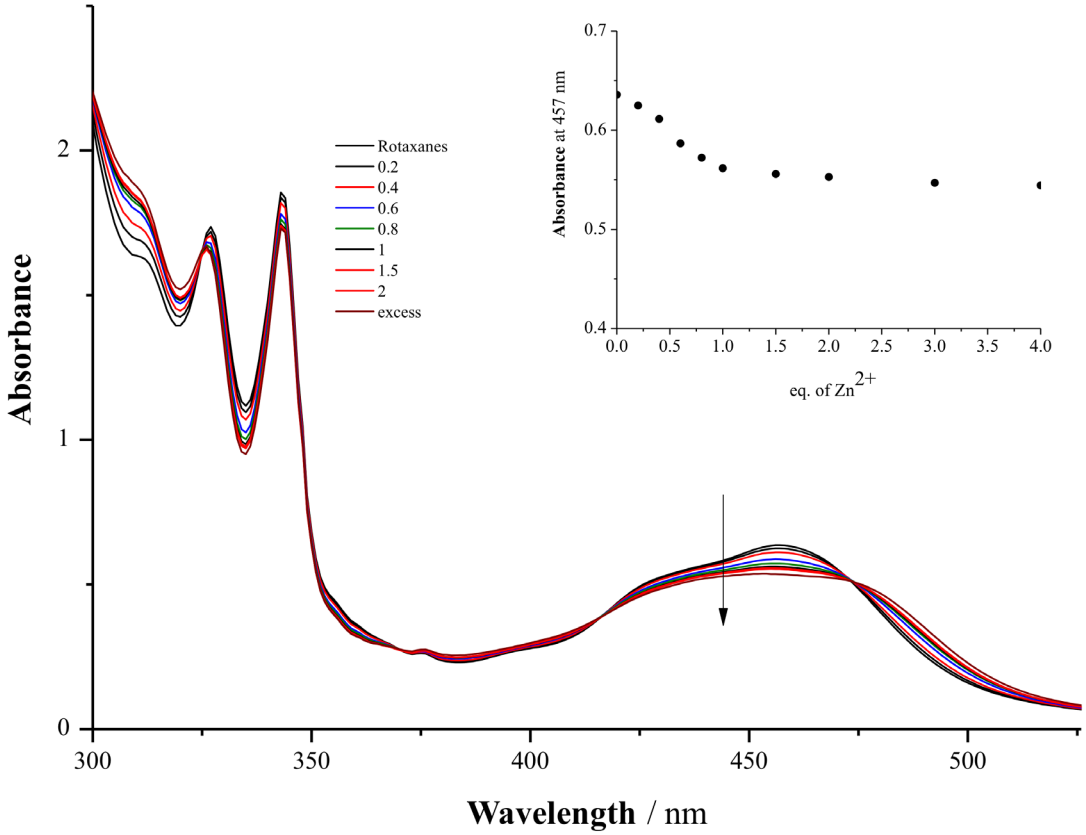

Figure 4.4 UV/Vis titrations of rotaxane **M_8** (3.19×10^{-5} M in MeCN) with $Zn(ClO_4)_2 \cdot 6H_2O$ (0, 0.2, 0.4, 0.6, 0.8, 1, 1.5, 2 eq, excess along the arrows). Inset: absorption of **M_8** solution at 457 nm with varying amounts of added Zn^{2+}.

4.1.5 Luminescence spectroscopy titrations rotaxane M_8

The titration of rotaxane **M_8** with $Zn(ClO_4)_2 \cdot 6H_2O$ in aerated MeCN solution was also followed by luminescence emission. Addition of Zn^{2+} resulted in a red shift and an intensity increase in the range of 550 – 800 nm, which was surprising. It should be mentioned that QY of luminescence of free threads in air solutions is about 3 times more than ones of relevant rotaxanes (Table 6.1), meaning that oxygen quenches the excited bichromophore more

efficiently than the ^{3}MLCT state of Ru-thread. As discussed in chapter 3, upon photoexcitation of **M$_8$** at 450 nm, REET processes are active. With the addition of Zn^{2+} into the aerated solution of **M$_8$**, the increase of MLCT emission seems to show that less and less triplet state of pyrene is quenched by oxygen, indicating more and more energy stays on MLCT states.

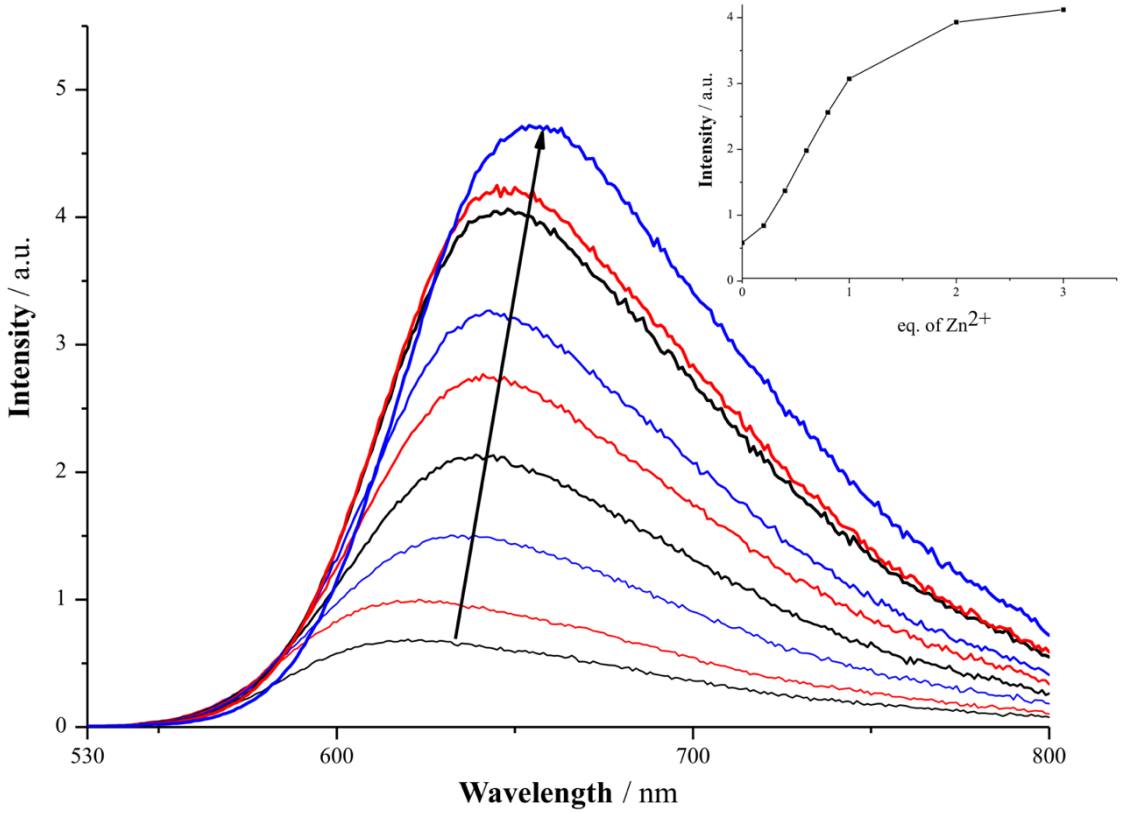

Figure 4.5 Luminescence emission titrations of rotaxane **M$_8$** (1.79×10^{-5} M in air MeCN, λ_{ex} = 477 nm) with $Zn(ClO_4)_2 \cdot 6H_2O$ (0, 0.2, 0.4, 0.6, 0.8, 1.0, 2.0, 3.0 eq, excess). Inset: Emission intensity of **M$_8$** solution at 640 nm with the equivalence of added Zn^{2+}.

The luminescence emission titration of rotaxane **M$_8$** with $Zn(ClO_4)_2 \cdot 6H_2O$ in degassed MeCN solution was also shown in Fig. 4.6. In the range of 550 – 800 nm, a red shift and an intensity increase was also observed by addition of Zn^{2+}, which also means more and more energy locates on MLCT states. An isoemissive point at 616 nm upon chelation between **M$_8$** and Zn^{2+} with variations on the red-side notably at 650 nm, also allows for ratiometric detection. Some luminescence decays comparisons of rotaxanes **M$_8$&M$_8$-Zn** and thread **B$_1$**, and the luminescence decays titration of **M$_8$** with $Zn(ClO_4)_2 \cdot 6H_2O$ in degassed solution (see below) were undertaken to gain further insight into how the coordination of Zn^{2+} to **M$_8$** influences MLCT excited states and REET process.

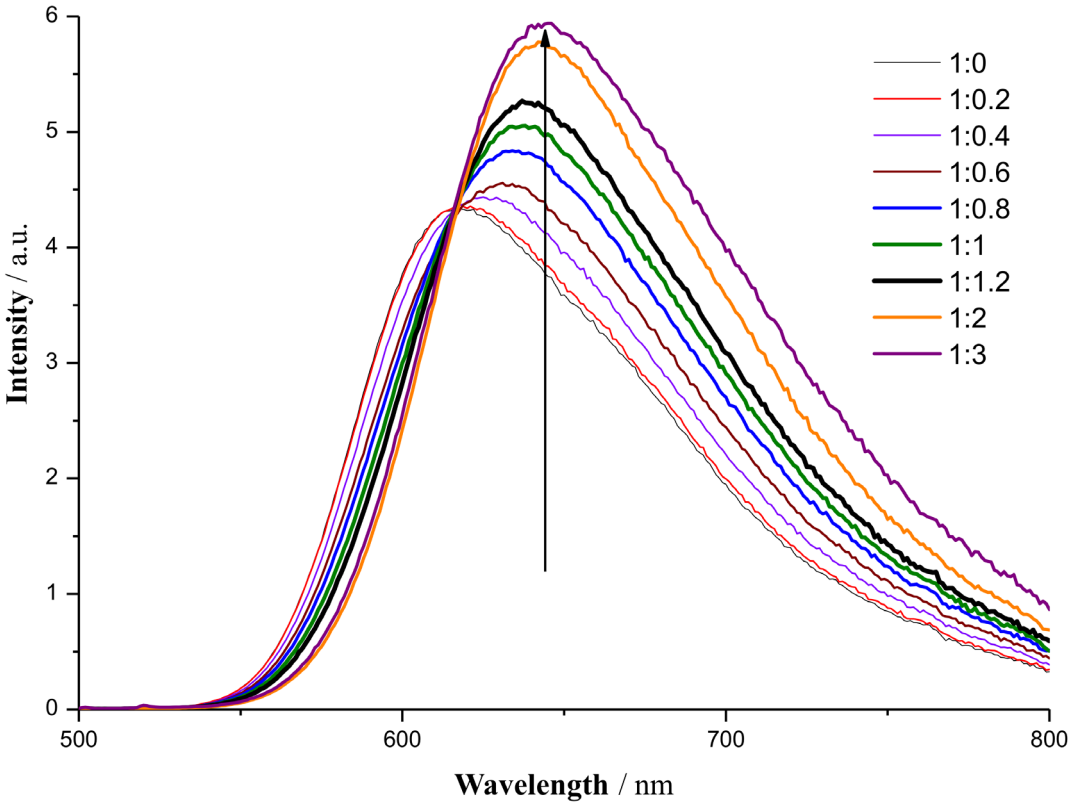

Figure 4.6 Luminescence emission titration of rotaxane **M_8** (1.18×10^{-5} M in degassed MeCN, λ_{ex} = 477 nm) with $Zn(ClO_4)_2 \cdot 6H_2O$ (0, 0.2, 0.4, 0.6, 0.8, 1.0, 1.2, 2.0, 3.0 eq).

4.1.6 Kinetics of chelator rotaxane M_8-Zn

Luminescence decays of rotaxanes **M_8**&**M_8-Zn** and thread **B_1** are shown in Fig. 4.7. The results show the lifetime of **M_8-Zn** (formed by excess Zn^{2+} addition into **M_8**) sharply decreased to 1.7 μs from 6.3 μs. While the decay lifetime of **M_8-Zn** is slightly longer than that of thread **B_1** (1.7 μs *vs* 1.2 μs). Combining the discussion about the luminescence emission titrations of Zn^{2+} to **M_8**, it is concluded that the coordination between **M_8** and Zn^{2+} occurs, and that this coordination changed the MLCT states in **M_8-Zn**. As a result the REET process is largely impededed by this coordination.

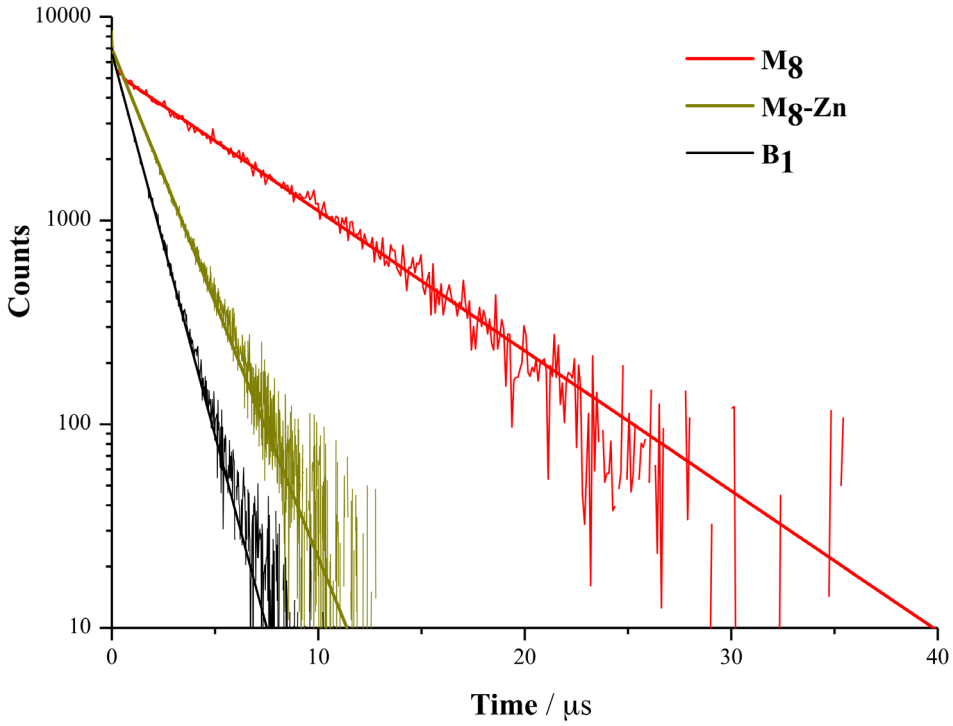

Figure 4.7 Luminescence decays of rotaxanes **M_8**&**M_8-Zn** and thread **B_1** in degassed acetonitrile (λ_{ex} = 450 nm, λ_{em} = 620 nm).

Transient absorption kinetics of rotaxane **M_8-Zn** at 370 nm and 410 nm (λ_{ex}=450 nm) were investigated to observe the energy transfer between the Ru^{2+} complex and pyrene, as shown in Fig.4.8. The kinetics at 370 nm corresponds to a superposition of bands corresponding to a decrease of ruthenium complex in ^{3}MLCT state and grow-in of pyrene triplet state ($T_1 \rightarrow T_n$ transition), the kinetics at 410 nm corresponds to grow-in of the pyrene triplet state. This result indicated that upon photoexcitation of the Ru complex, a small part of ^{3}MLCT energy transferred to the pyrene group, but energy distribution is different than the case of free **M_8**. The equilibrium between ^{3}MLCT and excited triplet states of pyrene is reached in 13 ns, the excited-state equilibrium constant is less than 1 (K=0.5), which is consistent with ^{3}MLCT states being extremely close or lower than triplet pyrene states.

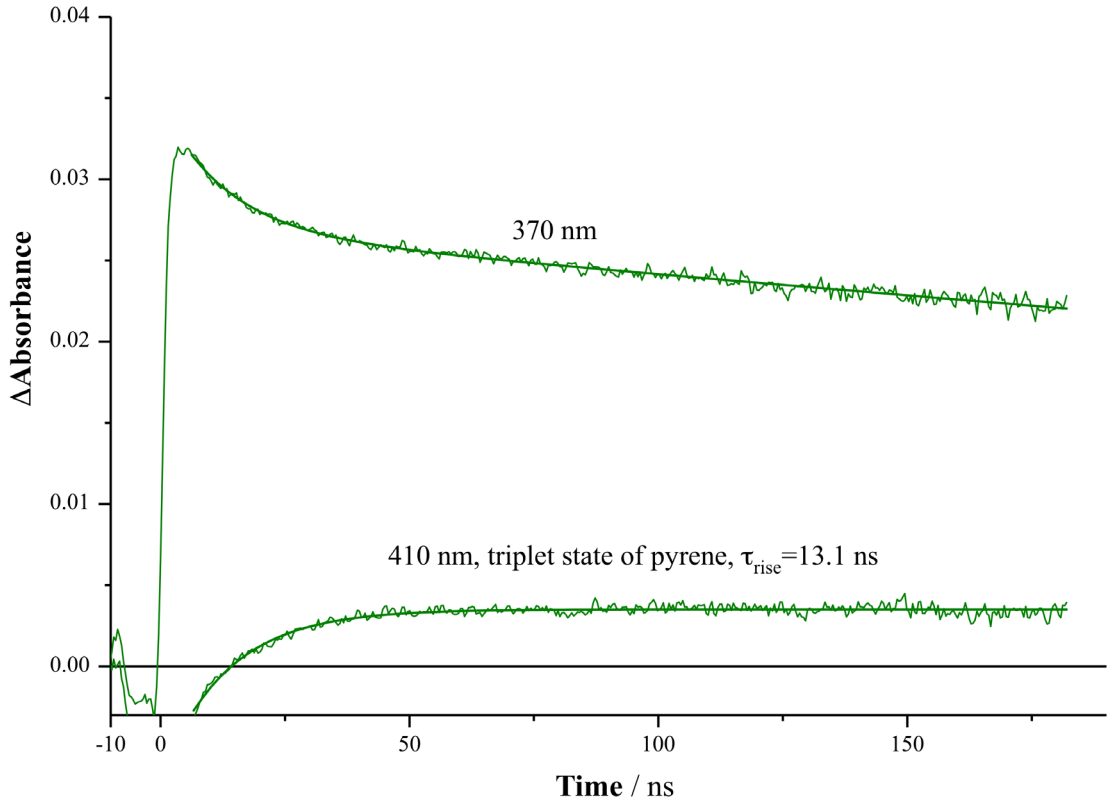

Figure 4.8 Transient absorption kinetics of rotaxane **M_8-Zn** at 370 and 410 nm in degassed acetonitrile (λ_{ex} = 450 nm).

The coordination of Zn^{2+} to rotaxane **M_8** lowers the ^{3}MLCT state energy with respect to pyrene triplet states, thus decreasing the proportion of energy which is temporarily stored on the pyrene group. As represented in Fig. 4.9, upon photoexcitation of **M_8**, where ^{3}MLCT states are higher that triplet pyrene states and where the energy gap is quite small, efficient reversible electronic energy transfer is instilled. Most of the stored excitation energy in the equilibrated system may be found in the pyrene reservoir for the overall population, the luminescence lifetime is prolonged, and luminescence intensity is decreased. When Zn^{2+} is bound in **M_8**, rotaxane **M_8-Zn** is afforded, the ^{3}MLCT states are decreased significantly with respect to pyrene triplet states. The energy transfer is less efficient, less energy is stored in the pyrene reservoir, MLCT luminescence lifetime is then shortened. In the presence of oxygen quencher the shorter MLCT luminescence intensity increases.

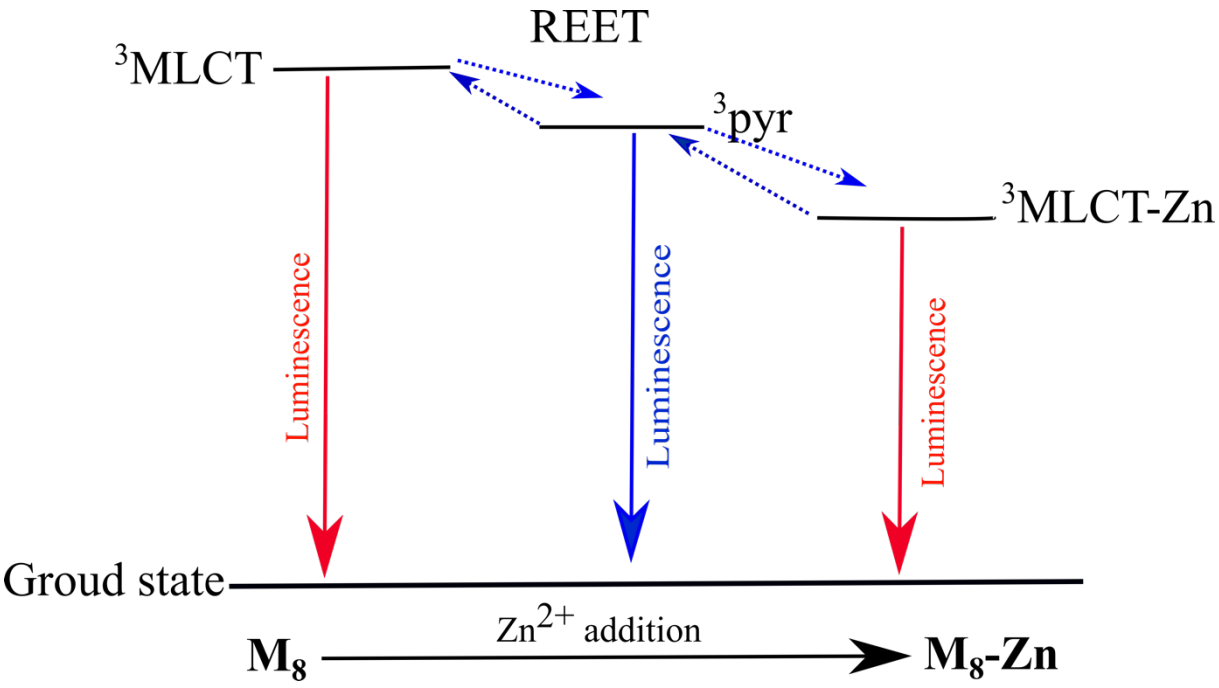

Figure 4.9 Schematic representation of electronic energy transfer between ^{3}MLCT of rotaxanes **M_8**&**M_8-Zn** and triplet pyrene.

4.1.7 Conclusions

Rotaxane **M_8-Zn** was formed by the coordination between rotaxane **M_8** and Zn^{2+}, and characterized by ^{1}H NMR. The change of electronic absorption and the luminescence emission spectra during titrations of Zn^{2+} with **M_8** further proved this coordination. From transient absorption and luminescence kinetics of **M_8-Zn**, it can be concluded that REET processes was still observed, but became much less efficient compared with free rotaxane on binding zinc. The shift of maximum of luminescence band (from 620 nm to 650 nm) and change of profile of luminescence kinetics shows that ^{3}MLCT states in **M_8-Zn** lies lower or close to pyrene triplet states. The excited-state equilibrium constant describing the energy distribution between chromophores is equal about 0.5, that is less than in case of free **M_8.** Luminescence lifetime of **M_8-Zn** is only slightly prolonged compared with thread **B_1**.

To summarize, pyrene in **M_8-Zn** cannot act as an efficient energy reservoir because the ion-induced perturbation of ^{3}MLCT energy results in a mismatch of the pertinent lowest-lying triplet states. The resulting complexation-induced optical change can be used for optical detection of analytes on varying luminescence lifetime by modulation of relative energy levels of energy donor and acceptor, or by intensity variations due to a diminished oxygen sensitivity.

Chapter 4.2 Linear reversible electronic energy hopping (varying number of acceptors at fixed distance)

4.2.1 Introduction

Reversible electronic energy transfer processes in bichromophoric molecule-based systems have been well studied, while there are only a few examples of REET processes in multichromophoric molecules which are reported. The presence of additional chromophores can have a significant effect on the excited-state properties. For example, a series of dyes, which are based on a bis-cyclometallated iridium core complex of the type Ir(2-(naphthalen-1-yl)pyridine)$_2$(bpy)$^+$ substituted with 0, 1 and 2 pyrene moieties, as shown in Fig. 4.10.a.[2] In Fig. 4.10.b, luminescence decays in the 580 – 620 nm range of dilute **45** (10 Mm, λ_{exc} = 465 nm), **46** and **47** (2 Mm, λ_{exc} = 355 nm) in the solution of degassed acetonitrile are shown. For Ir0, as there is only one chromophore, an emission lifetime of 8.3 μs was obtained according to the emission of ^{3}MLCT. the luminescence lifetime of **46** with a single appended pyrene in a micromolar solution is 225 ± 15 μs, is over 25-times longer. This is because REET process between two constituent chromophores stores most of the energy to pyrene-moiety, as an energy reservoir, after light irradiation. while for **47** which is doubly pyrene-grafted, the luminescence lifetime is 480 ± 15 μs, doubles to the one for Ir1, due to more energy storing in pyrene-moieties. This result simply shows increasing the number of energy reservoir (e.g., pyrene-moieties) units can increase the excited state lifetime linearly.

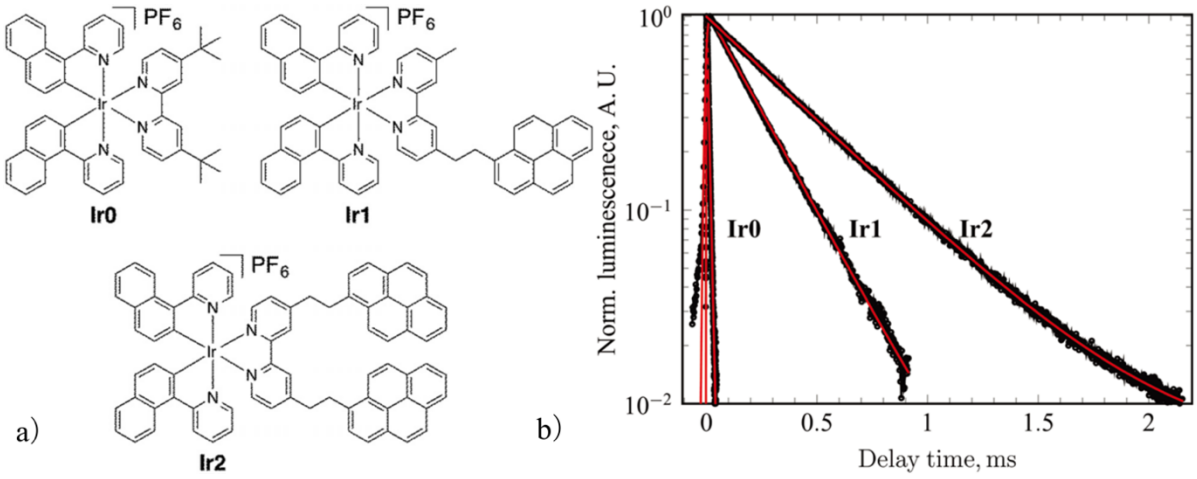

Figure 4.10 a) Series of iridium complexes studied in this work; b) Luminescence decays in the 580 – 620 nm range of dilute Ir0 (10 μM, λ_{exc} = 465 nm), Ir1 (2 μM, λ_{exc} = 355 nm) and Ir2 (2 μM, λ_{exc} = 355 nm) in degassed acetonitrile.

4.2.2 Concept and strategy of [3]rotaxane engineered with linear reversible electronic energy hopping

The aforementioned effect of chromophore degeneracy in REET systems inspired us to extend this investigation to multichromophore rotaxane systems, as illustrated in Fig. 4.11. Upon photoexcitation, REET will be instilled between metal complex (denoted by red ball; e.g, $Ru(bpy)_2$(phenanthroline) derivatives) and ring-Py_1 when the distance between two adjacent chromophores is short enough to be kinetically viable. It would be interesting to look at the real time energy migration across one or two rings, the excited state equilibration as energy redistributes itself across two or three chromophores and delayed deexcitation whose value depends on the influence of each ring. Such [3]rotaxane can be constructed by AT-CuAAC reaction with using some special short half-threads, following Goldup group's strategy to construct oligo[n]rotaxanes.

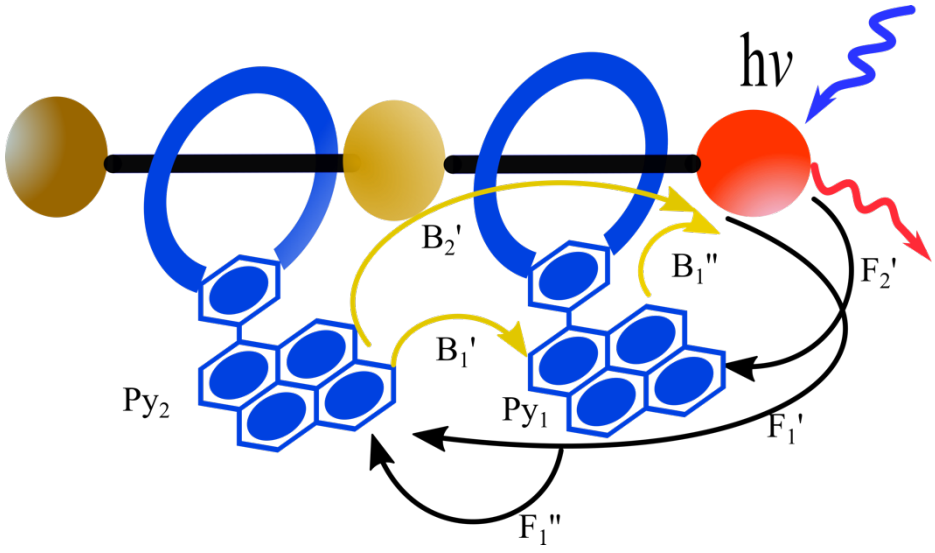

Figure 4.11 Illustration of reversible linear electronic energy hopping in rotaxane system.

To synthesize such a [3]rotaxane, some special half-thread components needs to be developed, and rotaxane formation by AT-CuAAC reaction can be considered. A research about the construction of oligo-[n]rotaxane by the group of Goldup could be instructive. As shown in Fig. 4.12, 1-azido-3-(TIPS-ethynyl)-5-*tert*-butylbenzene was used as a special half-thread to construct oligo-[n]rotaxane.[3] By AT-CuAAC reaction, [2]rotaxane was made based on the azide, 1,3-di-*tert*-butyl-5-azidobenzene and the macrocycle. After the deprotection of the TIPS group by the treatment of TBAF solution, a rotaxane alkyne **48** was obtained for the

construction of an oligo[n]rotaxane with 1-azido-3-(TIPS-ethynyl)-5-*tert*-butylbenzene and macrocycle. It is rational to use this strategy in the construction of our target rotaxanes.

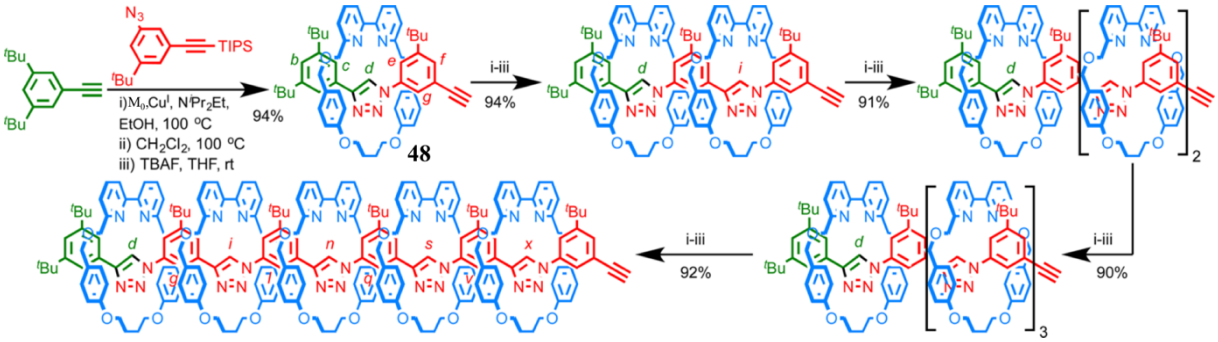

Fig. 4.12 Iterative AT-CuAAC synthesis of oligo[n]rotaxanes by Goldup et al.[3]

4.2.3 Synthesis and characterization of rotaxane M_{11}&M_{12}

In Fig. 4.13, half thread dialkyne **IV-2** was afforded in two steps: double Sonogashira coupling reaction of 3,5-dibromo-*tert*-butylbenzene and (trimethylsilyl)acetylene, and deprotection of the trimethylsilyl -group by treatment with K_2CO_3. Then rotaxane-alkyne **IV-7** was constructed based on macrocycle $\mathbf{R_3}$ and half threads **IV-2** and 1,3-di-*tert*-butyl-5-azidobenzene by mono-AT-CuAAC reaction. After the normal work-up, the crude product was purified by column chromatography and GPC to afford the biggest fraction, which proved to be the desired product. The complexation of commercially-available 5-bromo-phenanthroline with $Ru(bpy)_2Cl_2$, and workup offered the Ru complex $\mathbf{P_2}$ decorated by a bromo group. Following the Sonogashira coupling reaction with $\mathbf{P_2}$, rotaxane-alkyne was transformed into a REET [2]rotaxane $\mathbf{M_{11}}$. In the meantime, as a reference, another Ru complex $\mathbf{B_4}$ was also synthesized, considering a phenyl-alkynyl Ru complex probably has a slightly different excited state from the non-functionalized corresponding $Ru(bpy)_2$(phenanthroline) complex.

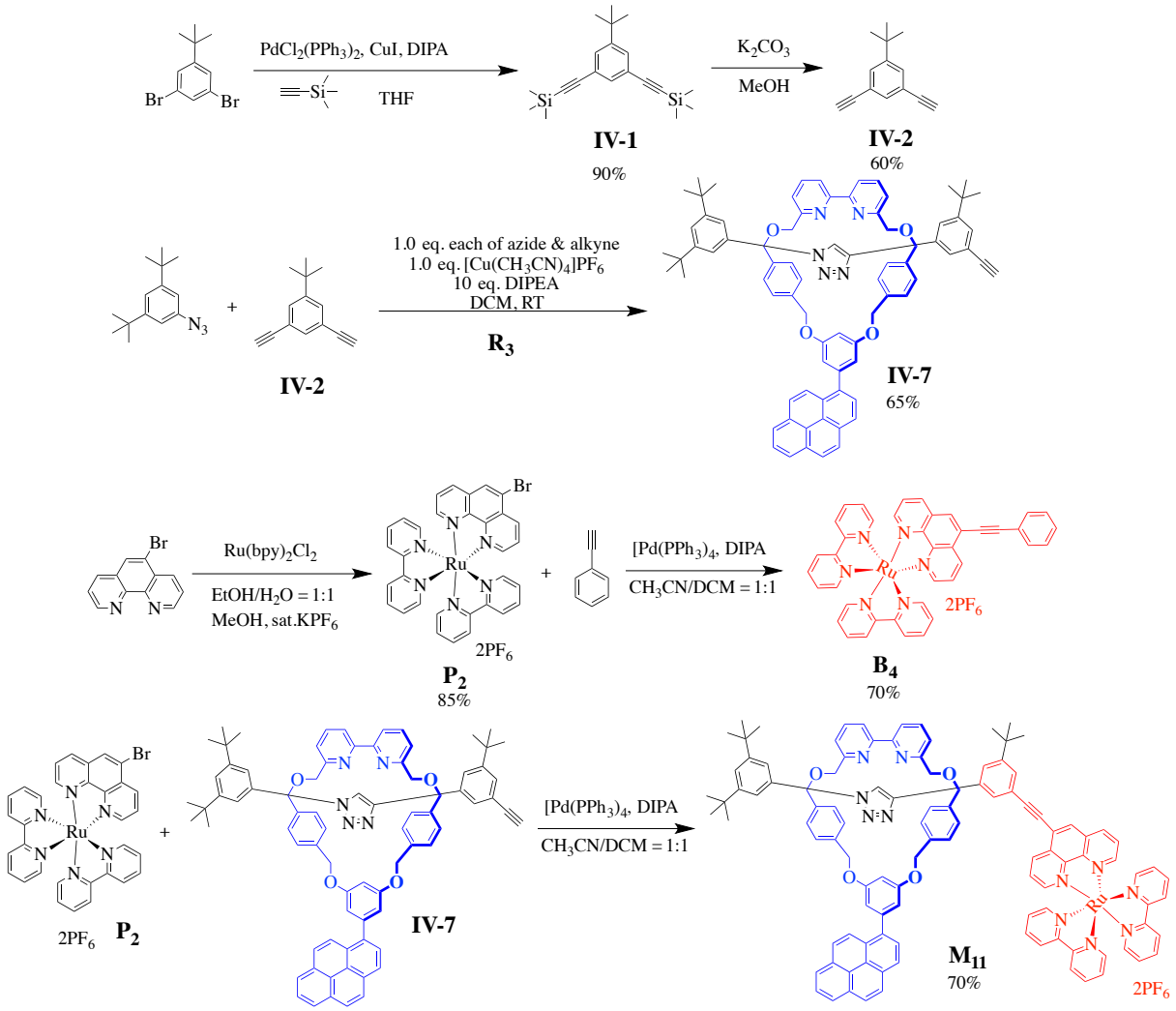

Figure 4.13 Synthesis of rotaxane **M$_{11}$**.

After the normal work-up, the crude product of **M$_{11}$** was purified by column chromatography and GPC to afford the biggest fraction, whose ^{1}H NMR spectrum is shown in Fig. 4.14. A singlet peak at 10.44 ppm could be attributed to the triazole proton; three specific multiplet peaks at 8.57 – 8.42, 7.22 – 7.13 and 7.14 – 7.08 ppm belong to Ru complex; A singlet peak at 8.21 ppm is associated to the pyrene-moiety proton; three multiplet peaks at region 5.21 – 4.00 ppm correspond to the macrocycle -CH_2- groups and so on; and the integration corresponds. Taken in conjunction with ^{13}C NMR spectrum and HRMS, it could be ascertained that this fraction is the desired rotaxane.

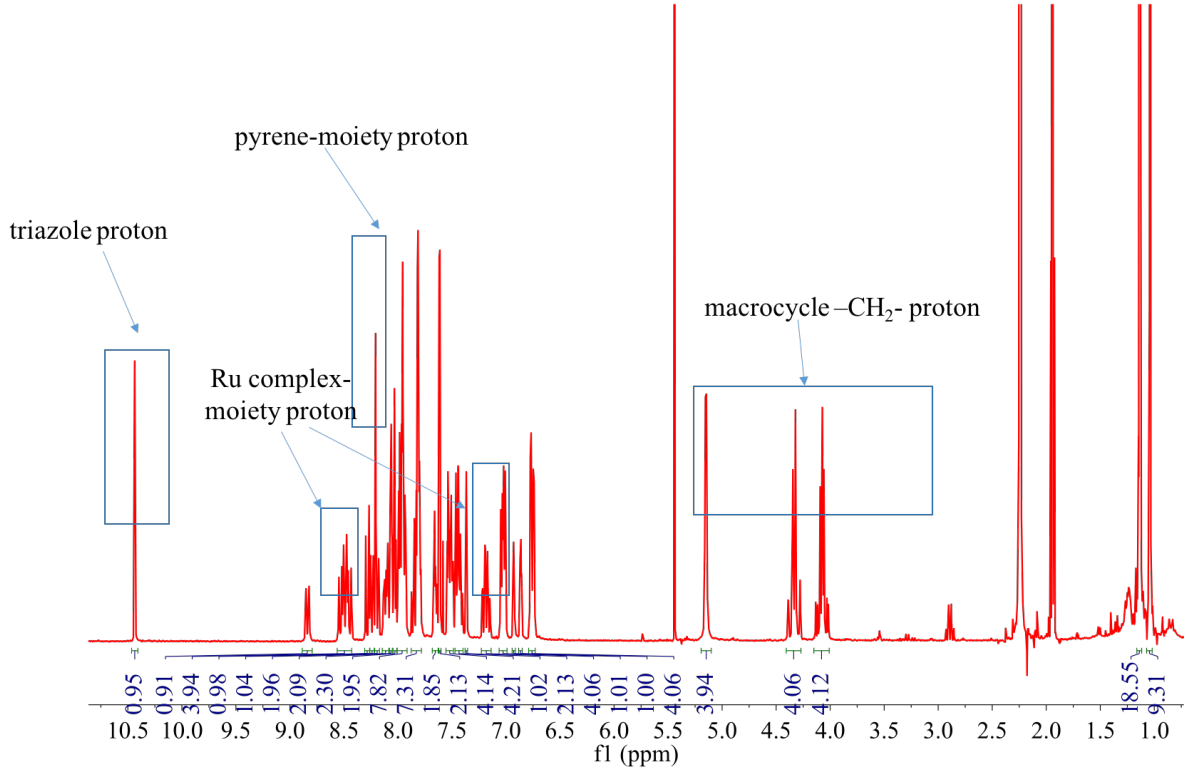

Figure 4.14 ^{1}H NMR of product **M$_{11}$** in CD_3CN.

Following Goldup group's strategy to construct [7]rotaxane step by step, half thread azide **IV-6** was afforded in four steps: single Sonogashira coupling reaction of 3,5-dibromo-*tert*-butylbenzene and 2-methyl-3-butyn-2-ol, deprotection of the acetone-group by treatment with NaOH, alkyne protection using TIPS group, and bromide-to-azide substitution by tosyl azide under strong base condition (Fig. 4.15). Then a precursor of rotaxane-alkyne **IV-8** was constructed based on macrocycle **R$_3$** and half threads **IV-2** and **IV-6** by AT-CuAAC reaction, before the deprotection of TIPS group with TBAF treatment. Following the Sonogashira coupling reaction with Ru^{2+} complex **P$_2$**, rotaxane-alkyne **IV-8** was transformed into a REET [3]rotaxane **M$_{12}$**. After the standard work-up, the crude product was purified by GPC.

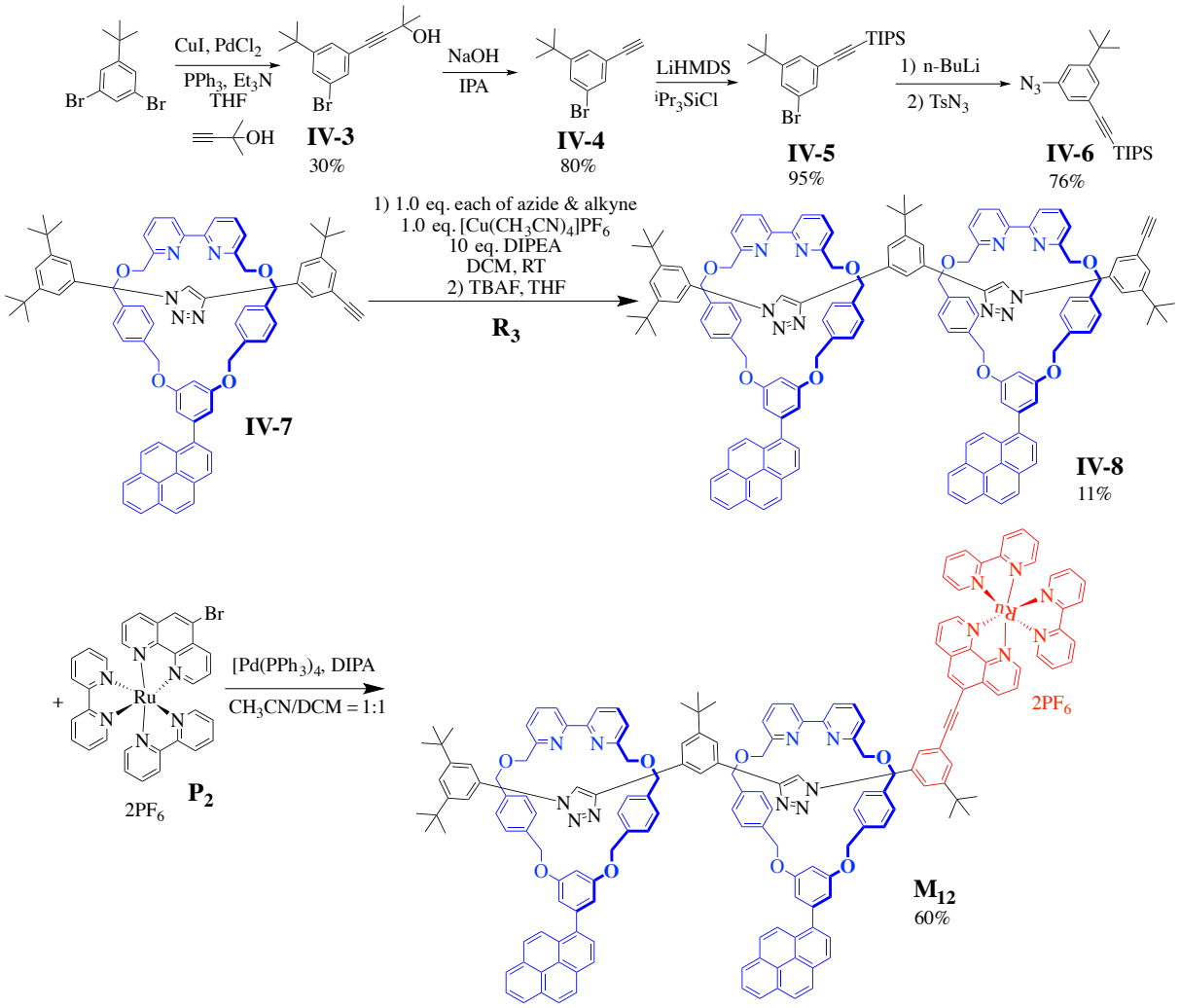

Figure 4.15 Synthesis of rotaxane **M_{12}**.

On analyzing this NMR spectrum (Fig. 4.16), a singlet peak at 10.44 ppm could be attributed to two triazole protons; three specific multiplet peaks at 7.12 – 7.03 and 6.85 – 6.78 ppm correspond to the Ru^{2+} complex; some multiplet peaks at region 5.41 – 4.06 ppm belong to the macrocycle -CH_2- groups and so on; and the integration is as anticipated. Taken in conjunction with ^{13}C NMR spectrum and HRMS, it could be ascertained that this fraction is the desired rotaxane.

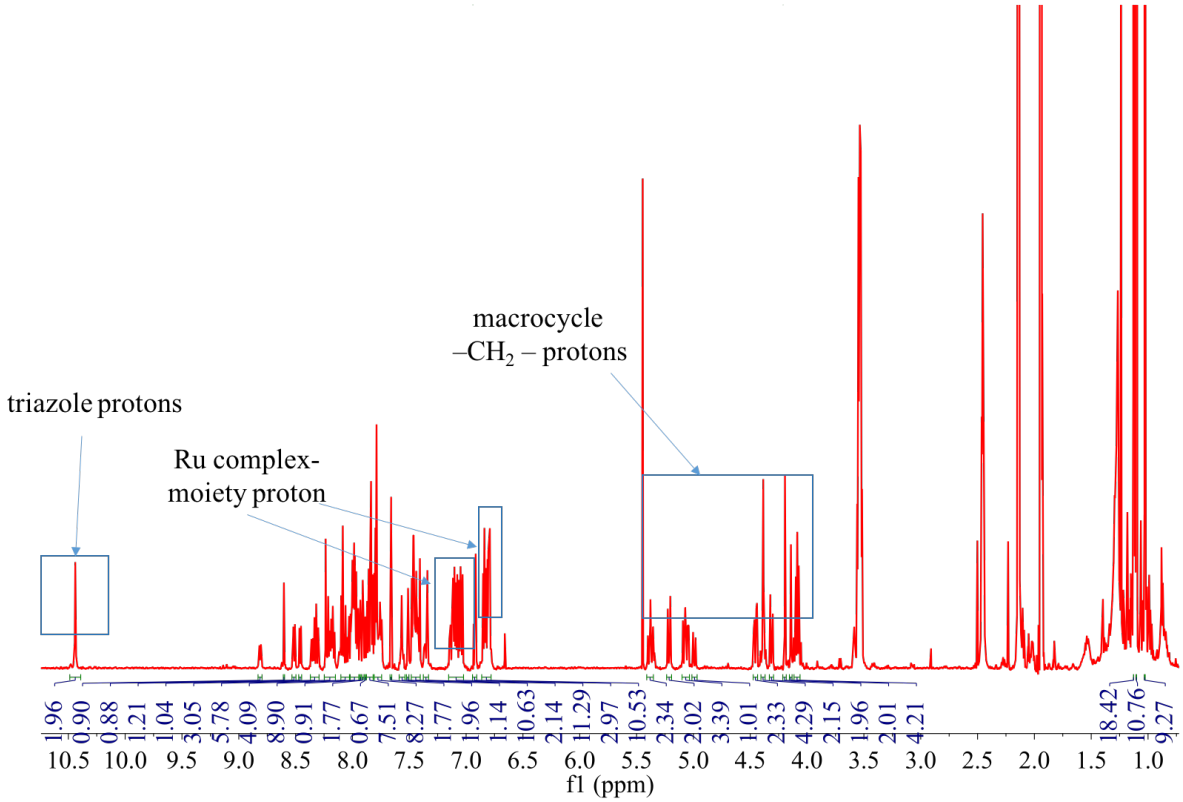

Figure 4.16 ^{1}H NMR of product **M$_{12}$** in CD_3CN.

4.2.4 Electronic absorption spectroscopy of rotaxane M_{11}

The electronic absorption spectra of rotaxane **M$_{11}$** in acetonitrile, with pyrene-appended macrocycle **R$_3$** and Ru complex components **B$_1$**&**B$_4$** as references, are shown in Fig. 4.17. In the range of 400 - 500 nm, rotaxane **M$_{11}$** and thread **B$_4$** share similar MLCT absorption bands, which behave slightly different thread **B$_1$**; similar phenyl-pyrene absorption bands for rotaxane **M$_{11}$** and macrocycle **R$_3$** were found in the range of 320 - 360 nm, which implies that there is only a weak ground-state coupling between two chromophores in rotaxane **M$_{11}$**. The establishment of REET processes between chromophores phenyl-pyrene (e.g., macrocycle **R$_3$**) and decorated Ru(bpy)$_2$(phenanthroline) derivative (e.g., Ru complex component **B$_4$**) has not been studied, so further spectroscopic studies (see below) were undertaken to gain further information about rotaxane **M$_{11}$**.

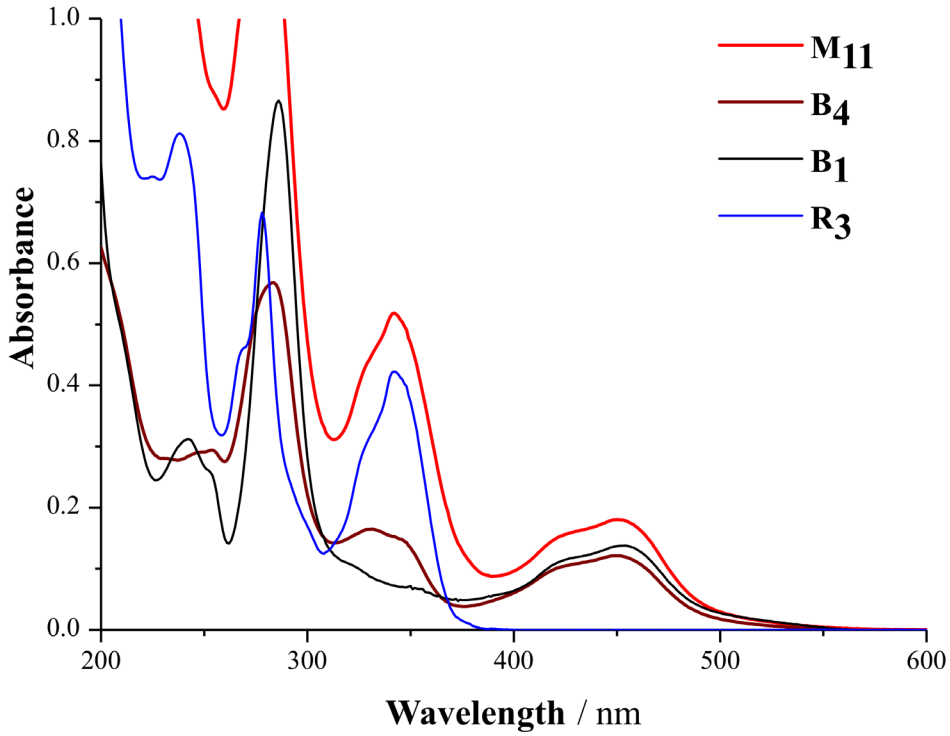

Figure 4.17 UV-vis absorption spectra of rotaxane **M$_{11}$**, threads **B$_1$**&**B$_4$** and pyrene-containing macrocycle **R$_3$** in acetonitrile.

4.2.5 Luminescence spectroscopy of rotaxane M$_{11}$

In Fig. 4.18, the photoluminescence spectra of rotaxane **M$_{11}$** and thread **B$_4$** are presented, at room temperature and 77 K. At room temperature, a broad structureless red MLCT-based emission for **M$_{11}$** ($\lambda_{em.max}$ = 620 nm, λ_{ex} = 450 nm) in degassed acetonitrile is measured. Low temperature phosphorescence measurements were undertaken to gain further insight into the energies of the pertinent states and relative energy levels of **M$_{11}$** and **R$_3$**. Interestingly, luminescence spectra of **M$_{11}$** and **B$_4$** (λ_{ex} = 450 nm) are quite similar, unlike the luminescence spectra of rotaxanes **M$_9$**&**M$_{10}$** compared with threads **B$_2$**&**B$_3$**. This could be ascribed to the structure design of **M$_{11}$**, in which the the tert-butyl phenyl group assures a certain distance between **M$_{11}$** and **B$_4$**. Indeed, the highest energy feature is taken as the energy of the excited state. At 77 K, slightly blue-shifted ^{3}MLCT structured phosphorescence ($\lambda_{em.max}$ = 582 nm) could be observed with respect to room temperature for rotaxane **M$_{11}$**. The energy of the lowest-lying ^{3}MLCT ($\lambda_{em.max}$ = 582 nm) is calculated to be 2.014 eV, and the energy of the lowest-lying triplet phenyl-pyrene ($\lambda_{em.max}$ = 608 nm, λ_{ex} = 342 nm) is 1.928 eV. The energy difference

(ΔE) between these two chromophores is 0.056 eV < 0.1 eV, assuming the possible establishment of REET processes in rotaxane **M**$_{11}$.

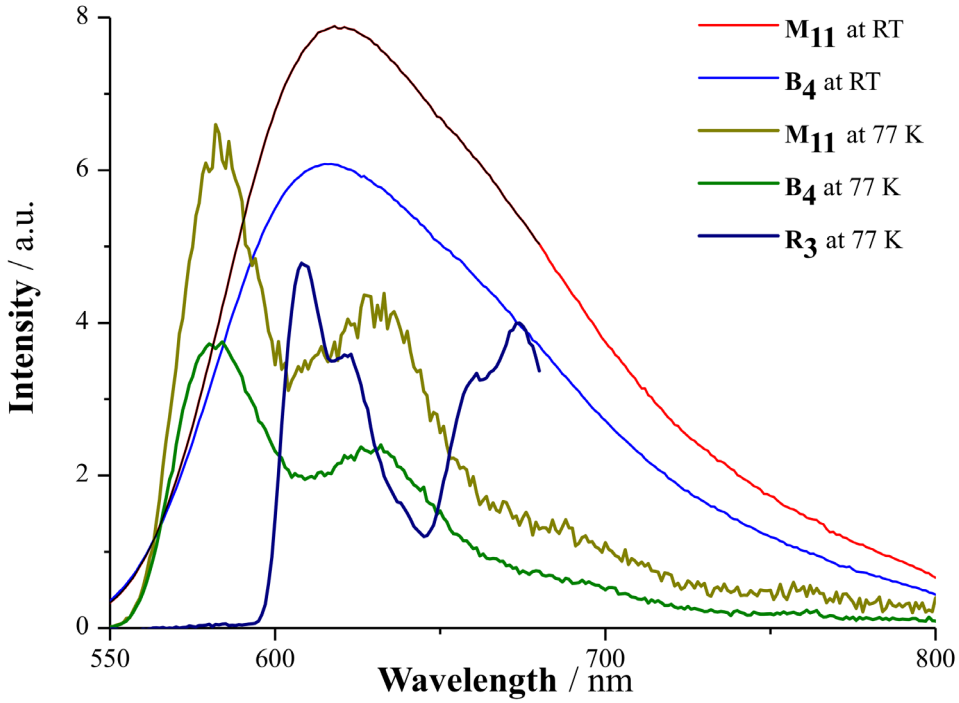

Figure 4.18 Luminescence (293 K) and phosphorescence (77 K) spectra of rotaxane **M**$_5$ and thread **B**$_4$ (λ_{ex} = 450 nm), phosphorescence (77 K) spectrum of macrocycle **R**$_3$ (λ_{ex} = 342 nm) in degassed acetonitrile.

4.2.6 Luminescence decays of rotaxane M$_{11}$

Fig. 4.19 shows luminescence decays of rotaxane **M**$_{11}$ and thread **B**$_4$ which are quite different. Free thread **B**$_4$ shows typical MLCT luminescence in degassed acetonitrile, from the monoexponential curve fit of its luminescence decays, its lifetime is about 1.0 μs. Rotaxane **M**$_{11}$ shows a much longer average lifetime 35.6 μs (share 0.97), from the biexponential curve fit of luminescence decays. But it is surprising that a certain amount (3%) of Ru complex components behave as a thread. **M**$_{11}$ has a very short thread (only a triazole-moiety), the distance between the Ru complex and phenyl-pyrene group should be short enough for the REET establishment without any hindrance. This is probably because of the conformations of

phenyl-pyrene group, slow forward energy transfer or rotaxane disociation, as discussed previously in the case of related **M4**.

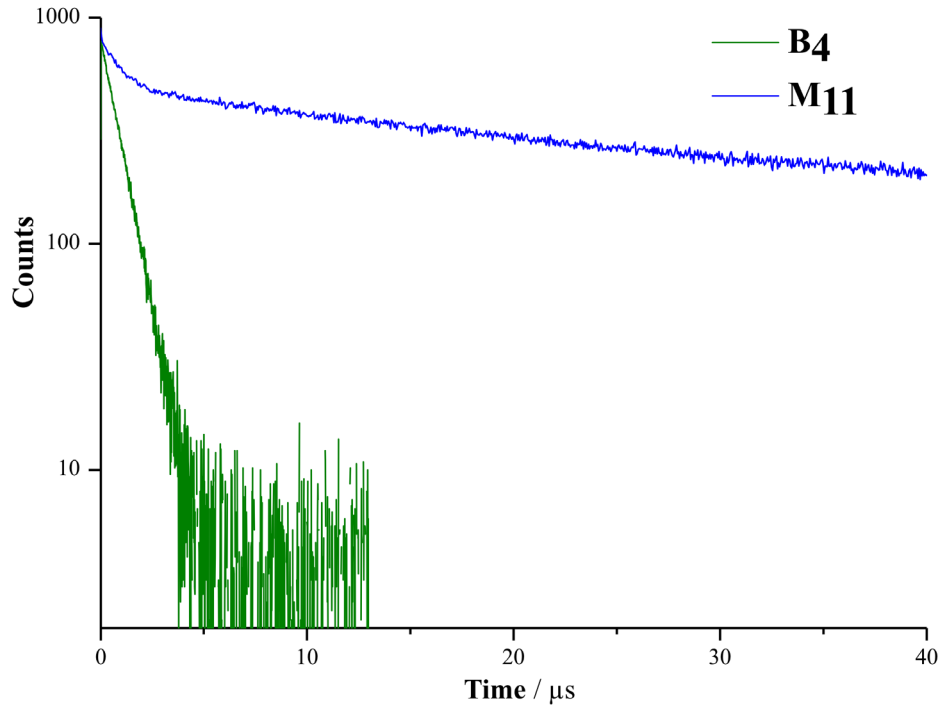

Figure 4.19 Luminescence decays of rotaxane **M11** and thread **B4** in degassed acetonitrile (λ_{ex} = 450 nm, λ_{em} = 620 nm).

4.2.9 Outlook

Increased unquenched phenyl-pyrene emission spectra and luminescence decays of rotaxane **M11** after the laser irradiation (λ_{ex} = 450 nm) may be consistent with macrocycle **R3** moving off the thread. This could possibly result from a ligand photodissocation followed by re-association. This hypothesis warrants further investigation. Several measurements need to be done in the near future: transient absorption studies on rotaxane **M11** after the laser irradiation will tell us how much of this type of Ru^{2+} complex is dissociating.

4.2.10 Conclusion

Two rotaxanes **M11**&**M12** were synthesized and characterized by ^{1}H NMR, ^{13}C NMR, HRMS. Variable temperature dependant ^{1}H NMR experiments suggest that rotaxane-alkyne is very stable, and the stopper 3,5-di-*tert*-butylphenyl is big enough to block the macrocycle. UV-vis

spectroscopy of rotaxane $\mathbf{M_{11}}$ shows distinct phenyl-pyrene and phenyl-alkynyl-$Ru(bpy)_2$(phenanthroline) absorption bands, implying a weak ground-state coupling between these two chromophores. Luminescence spectroscopy of $\mathbf{M_{11}}$ was also investigated, and the energy gap between the two chromophores was found to be less than 5 kT (i.e. 3.36 kT), suggesting a possible establishment of REET processes in $\mathbf{M_{11}}$. REET process was instilled in $\mathbf{M_{11}}$ with a well prolonged luminescence lifetime. Several extra experiments are currently in progress in order to understand better the results shown in this chapter.

References

[1] Denis M., Pancholi J., Jobe K., Watkinson M., Goldup S. M. Chelating rotaxane ligands as fluorescent sensors for metal ions. Angew. Chem. Int. Ed. 2018, 57, 5310-5314.

[2] Rodríguez S. M., Denisov S. A., Cudré Y., Male L., Suárez M. M., Gutiérrez A. F., Sánchez J. F., Tron A., Jonusauskas G., McClenaghan N. D., Baranoff E. High performance optical oxygen sensors based on iridium complexes exhibiting interchromophore energy shuttling. Analyst, 2016, 141, 3090-3097.

[3] Lewis J. E. M., Winn J., Cera L., Goldup S. M. Iterative synthesis of oligo[n]rotaxanes in excellent yield. J. Am. Chem. Soc. 2016, 138, 16329-16336.

Chapter 5 General Conclusion

The main objective of this thesis was to engineer and study new photo-induced processes in interlocked molecules, specifically reversible electronic energy transfer. In this goal a matched pair of chromophores are required and the benchmark chromophores, pyrene and ruthenium(II) tris(bipyridine), were chosen to for the bichromophoric dyads as they were anticipated to offer matched energetic levels and appropriate kinetics.

In chapter 2, to realize the construction of a rotaxane engineered with REET processes, an alkynyl-functionalised $Ru(bpy)_3^{2+}$ complex $\mathbf{P_1}$, as a stopper and a donor group of REET process, was synthesized. A strategy of synthesis of bipyridine-containing macrocycles with a pyrene group appendage was developed. Four different pyrene-macrocycles ($\mathbf{R_1}$, $\mathbf{R_2}$, $\mathbf{R_3}$, $\mathbf{R_4}$) were successfully designed and synthesized. Two symmetrical pyrene-macrocycles (phenyl pyrene $\mathbf{R_3}$, and methylene pyrene $\mathbf{R_4}$) were found to be good candidates for rotaxane formation. Two rotaxanes ($\mathbf{M_4}$, $\mathbf{M_5}$) were constructed with different symmetrical pyrene-macrocycles ($\mathbf{R_3}$, $\mathbf{R_4}$) by active template Cu-catalyzed alkyne-azide cycloaddition reaction, and confirmed by NMR, HRMS. Here the metal ion plays the dual role of catalyst and templating/structuring agent. Electronic absorption spectroscopy implies that there is only a weak ground-state coupling between chromophores. Time-resolved spectroscopy and steady state spectroscopy showed that unprecedented reversible electronic energy transfer processes were instilled in rotaxane systems ($\mathbf{M_4}$, $\mathbf{M_5}$) and prolonged luminescence lifetimes were observed. Luminescence decays showed MLCT luminescence lifetime (14 μs) of $\mathbf{M_4}$ was much longer than the one (5.6 μs) of $\mathbf{M_5}$, due to the different energy gaps of excited pyrene-$\mathbf{P_1}$ (1.4 kT) and phenylpyrene-$\mathbf{P_1}$ (2.4 kT). Transient absorption spectroscopy of $\mathbf{M_5}$ elucidated the management of energy by excited molecules before emission occurred, confirming the presence of quasi-isoenergetic excited states on the two adjacent chromophores, thus permitting rapid REET.

In chapter 3, the relationship between REET processes and shuttling movements of the macrocycle on threads in rotaxanes was studied. Three more REET rotaxanes ($\mathbf{M_6}$, $\mathbf{M_7}$, $\mathbf{M_8}$) based on macrocycle $\mathbf{R_4}$ with different thread lengths were afforded by AT-CuAAC. These rotaxanes were characterised by NMR, HRMS and electronic absorption spectra. From comparisons of related spectroscopic measurements among rotaxanes $\mathbf{M_6}$&$\mathbf{M_6}$&$\mathbf{M_7}$&$\mathbf{M_8}$, REET processes were elucidated, but with slight differences. $\mathbf{M_8}$ having the shortest thread showed a slightly longer luminescence lifetime (6.3 μs); $\mathbf{M_5}$&$\mathbf{M_6}$ with only 4 $-CH_2-$ difference on the thread exhibited no difference (5.6 μs); in $\mathbf{M_7}$ which has the longest thread, 11% of the

population did not give REET processes. DFT calculations of **M_5&M_7** gave some insights into specific interactions macrocycle and **R_4**, including CH-π interactions. REET processes are not very sensitive to the differences of the shuttling movements of the macrocycle on the threads with different lengths in these 4 rotaxanes. Two Cadiot-type REET rotaxanes **M_9&M_{10}** comprising a diyne linkage with different thread lengths were also synthesized and characterized by NMR, HRMS, UV-vis spectroscopy. Steady-state and time-resolved luminescence spectroscopy showed establishment of REET processes with an average lifetime 3.6 μs in **M_9**, which has a shorter thread; 34% of **M_{10}** exhibited a MLCT emission with a luminescence lifetime 1.7 μs, which is equal to the one of free thread **B_3**, and the rest part showed an average lifetime of 3.6 μs, suggesting different ring locations. These results imply that the Cadiot-type rotaxanes hold promise in the tracking of rings shuttling movement with REET process.

In chapter 4, rotaxane **M_8** was chosen as a rotaxane chelating ligand to investigate how the photophysical properties of a REET rotaxane change upon coordination of a metal ion. Coordination of Zn^{2+} by rotaxane **M_8** (giving **M_8-Zn**) was confirmed using NMR, electronic absorption and luminescence emission spectra. Luminescence decays of **M_8-Zn** revealed a much shorter luminescence lifetime (1.7 μs) than rotaxane **M_8** (6.3 μs) when degassed. The shift of maximum of luminescence band (from 620 nm to 650 nm) and change of profile of luminescence kinetics showed that ^{3}MLCT states in **M_8-Zn** lies lower in energy than triplet pyrene states. Transient absorption of **M_8-Zn** disclosed that REET processes still exist, but were less efficient compared with free rotaxane. This result indicates that the complexation between REET rotaxane and a metal ion can be used as a new method for optical detection of analytes on varying luminescence lifetime by modulation of relative energy levels of energy donor and acceptor. One approach to reversible linear electronic energy hopping with varying number of acceptors at fixed distance in rotaxane systems is considered. [2]Rotaxane **M_{11}** and [3]rotaxane **M_{12}** were synthesized and characterized by ^{1}H NMR, ^{13}C NMR, HRMS. Spectroscopic studies proved that REET process was instilled in **M_{11}** with a prolonged luminescence lifetime (37 μs). In future, detailed photophysical experiments & kinetic modelling will be carried out on [3]rotaxane **M_{12}**.

In summary, REET processes were successfully introduced into rotaxane systems: the relationship between REET processes and molecular structure was investigated. The

coordination between REET [2]rotaxane and Zn^{2+} significantly changed MLCT excited state energies and dramatically influenced the REET process. More sophisticated multicomponent REET rotaxanes have been designed and constructed. This research opens the way towards more performant multicomponent systems and extends photochemistry applications with rotaxane architectures.

Chapter 6 Experimental

6.1 Solvents

Solvents of technical grade were distilled and dried prior to utilization. All manipulations were performed under a nitrogen atmosphere using standard techniques. Toluene was distilled over sodium, acetonitrile and dichloromethane were distilled over calcium hydride, THF and diethyl ether were distilled over sodium/benzophenone and acetone ExtraDry 99.8%, chloroform ExtraDry 99.9%, dimethylformamide ExtraDry 99.8% (DMF), ethyl acetate ExtraDry 99.9%, absolute ethanol (99.8%) and anhydrous methanol (99.8%) were purchased from Sigma Aldrich and stored over molecular sieves. Deuterated solvents for NMR analysis were bought from Sigma-Aldrich. Deionized water was obtained by purification over an ion exchange column and a membrane filter of 0.45 μm (Micron separation, Inc.). Solvents for spectroscopy without the addition of stabilizing agents or other absorbing material were employed as received.

6.2 Thin layer chromatography, silica, alumina columns and gel permeation chromatography

Thin layer chromatography was performed on silica gel 60 F254 sheets on aluminium produced by Merck. Spots on the TLC plate were observed under UV lamp (254 nm / 365 nm), while an appropriate staining agent, $KMnO_4$ solution, was employed for non-absorbing compounds. Column chromatography for the separation of organic compounds was performed using silica gel from Merck with a particle size of 40 - 63 μm (230 - 400 mesh). Flash column chromatography was performed using a puriFlash®430 automated chromatography system from *Interchim*, employing PF-dry load empty F0004-0040 flash columns. Alumina was prepared with 7% of water and stirred for 2h in a closed flask. Organic compounds for separation were dissolved in a minimum amount of chromatography solvent, a deposited on top of the column and subsequently eluted. Gel permeation chromatography (GPC) was performed on a set of 1H, 1.5H, 2.5H and 3H columns (JAIGEL 20 × 600 mm) JAIGEL 20*600 mm columns (Japan Analytical Industry) in chloroform/0.5~1% ethanol, as mobile phase, with a flow rate of 3.5 mL/min. The monitoring UV detector is UV-600 NEXT.

6.3 Nuclear magnetic resonance spectroscopy (NMR)

^{1}H and ^{13}C-NMR spectra were recorded at 600, 400, and 300 MHz at 295 K on a Bruker Avance

300 (1H: 300 MHz, 13C: 75 MHz), Avance II 400 (1H: 400 MHz, 13C: 100 MHz), and an Avance III 600 (1H: 600 MHz, 13C: 150 MHz) spectrometer. Chemical shifts are reported in ppm (δ) and are referenced to the NMR solvent residual peaks (CD_2Cl_2, $CDCl_3$, Tetrahydrofuran-d_8, CD_3OD, CD_3CN, $(CD_3)_2SO$) residual peak. Abbreviations used are s = singlet, d = doublet, t = triplet, q = quartet, dd = doublet of doublets, dt = doublet of triplets, td = triplet of doublets and m = multiplet. The coupling constants (J) are reported in Hertz (Hz).

6.4 Mass spectrometry

Mass spectrometry was performed by the "Centre d'Etude Structurale et d'Analyse des Molecules Organique" (CESAMO) at the University of Bordeaux, on a QStar Elite mass spectrometer (Applied Biosystems). ESI-QTOF mass spectra (including all HRMS) were performed on an instrument equipped with an ESI source and spectra were recorded in the positive mode. The electrospray needle was maintained at 5000 V and operated at room temperature. Samples were introduced by injection through a 20 µL sample loop into a 4500 µL/min flow of methanol from the LC pump. ESI-MS experiments were performed on an ion trap spectrometer equipped with an electrospray ion source (ESI) and spectra were recorded in the positive mode. Field desorption (FD) spectra were recorded on a TOF mass spectrometer using an FD emitter with an emitter voltage of 10 kV. One to two microliters solution of the compound is deposited on a 13 µm emitter wire.

6.5 DFT calculations

DFT calculations for rotaxanes **M_5**, **M_5-N**, **M_7** and **M_7-N** were performed by Dr. Claire Tonnelé and Pr. Frédéric Castet (ISM) using with the Gaussian (G16) program package. Geometries were optimized at the b3lyp/6-311g(d) level, including Grimme's D3 dispersion correction, with the LanL2DZ pseudopotential and basis set to describe the Ru^{2+} atom.

6.6 Electronic absorption (UV-Vis) and fluorescence spectroscopy

Electronic absorption spectra were measured on a spectrophotometer Cary 5G UV-Vis-NIR (Varian) using 10 and 1 mm synthetic quartz (Suprasil) quartz cells. The wavelengths observed ranged from 200 – 800 nm. Sample solutions were measured in matched quartz cells with a pathlength of 10 mm. Before each measurement a baseline of pure solvent was recorded, which

was subtracted from the measured spectra. Fluorescence emission spectra were measured on a HORIBA Jobin-Yvon Fluorolog-3 equipped with a xenon lamp (450 W), with Hamamatsu R2658P and R928P photomultiplier (PMT) detection. Quartz cells of 10 mm length were employed for study of optically dilute samples with fluorescence emission being measured at a right angle with respect to the excitation beam.

6.7 Fluorescence quantum yield

Fluorescence quantum yields of rotaxanes and threads for optical diluted solutions in CH_3CN were determined by comparing to an optically dilute standard of known quantum yield. The fluorescence quantum yield of the sample solution (Φ) was then calculated using Equation 6-1 where Φ_{ref} is the fluorescence quantum yield of the reference compound $[Ru(bpy)_3]Cl_2$ in H_2O (0.028), I is the integral of the fluorescence emission of the sample solution, I_{ref} is the integral of the fluorescence emission of the reference, A is the absorption at the excitation wavelength and η is the refractive index of the used solvent. For our measurements the correction factor $\frac{\eta^2}{\eta_{ref}^2}$ is equal to 1.079. QYs of all studied rotaxanes and threads in degassed and air-equilibrated solution are shown in Table 6-1. Experimental error is about 10 %.

$$\Phi = \Phi_{ref} \times \frac{I}{I_{ref}} \times \frac{A_{ref}}{A} \times \frac{\eta^2}{\eta_{ref}^2} \qquad \text{Equation 6-1}$$

Table 6-1 Summary of QY of all studied rotaxanes and threads, in degassed and air solution.

compounds	Φ in degassed solution	Φ in air solution
M_4	0.10	0.005
B_1	0.10	0.017
M_5	0.11	0.006
M_6	0.11	0.006
M_7	0.11	0.006
M_8	0.11	0.006
M_9	0.13	0.001
M_{10}	0.12	0.002
B_2	0.07	0.011
B_3	0.09	0.013
M_8-Zn	0.17	0.032
M_{11}	0.07	0.002
B_4	0.07	0.010

6.8 Transient absorption / time-resolved luminescence

The transient absorption / time-resolved luminescence set-up was built as follows: a frequency tripled Nd:YAG amplified laser system (30 ps, 30 mJ @1064 nm, 20 Hz, Ekspla model PL 2143) output was used to pump an optical parametric generator (Ekspla model PG 401) producing tunable excitation pulses in the range 410 – 2300 nm. The residual fundamental laser radiation was focused in a high pressure Xe filled breakdown cell where a white light pulse for sample probing was produced. All light signals were analyzed by a spectrograph (Princeton Instruments Acton model SP2300) coupled with a high dynamic range streak camera (Hamamatsu C7700, 1ns-1ms). Accumulated sequences (sample emission, probe without and with excitation) of pulses were recorded and treated by HPDTA (Hamamatsu) software to produce two-dimensional maps (wavelength vs delay) of transient absorption intensity in the range 300 – 800 nm. Typical measurement error was better than 10^{-3} O.D. Data were analysed using home-written software developed in LabVIEW 2014 system-design platform and development environment. The trust-region dogleg algorith (supported by LabVIEW 2014) was applied to determine the set of parameters that best fit the set of input data. The trust-region dogleg algorithm was used instead of Levenberg-Marquardt algorithm, the latter being less stable in most cases during optimization process, because trust region methods are robust, and can be applied to ill-conditioned problems.

6.9 Synthesis

p-tert-Butylbromobenzene, methyl *p-tert*-butylbenzoate, phenol, dibromoalkane, sodium azide, 2,2'-bipyridine, trifluoroacetic acid, acetyl bromide, phosphorus tribromide, dichlorobis(triphenylphosphine) palladium (II), copper iodide, diisopropylamine, (trimethylsilyl)acetylene, Ru(bipyridine)$_2$Cl$_2$, tetrakis(triphenylphosphine) palladium(0), 1-pyreneboronic acid, 4-bromoveratrole, boron tribromide, 3-bromopropanol, 4-toluenesulfonyl chloride, triethylamine, 4-methoxyphenylboronic acid, 2,6-dibromopyridine, triphenylphosphine, dibromobis(triphenylphosphine) nickel(II), tetraethylammonium iodide, tetrakis(acetonitrile)copper(I) hexafluorophosphate, DIPEA, (chloromethyl)benzyl chloride, ethyl-6-bromopicolinate, sodium borohydride, sodium hydride, 3,5-dimethoxy-1-bromobenzene, n-butyllithium solution, 3,5-dimethoxybenzaldehyde, dimethylmonochlorosilane, indium(III) chloride, propargyl bromide, prop-2-yn-1-ol, N-bromosuccinimide, silver nitrate, 5-bromo-phenanthroline, 1-tert-butyl-3,5- dibromobenzene,

palladium chloride, LiHMDS, iPr_3SiCl, Bromine, tosyl azide and phenylacetylene were purchased from the Sigma Aldrich TCI Europe, Alfa Aesar and Acros Chemicals, and were used as received.

Tris(4-(*tert*-butyl)phenyl)methanol (II-3)

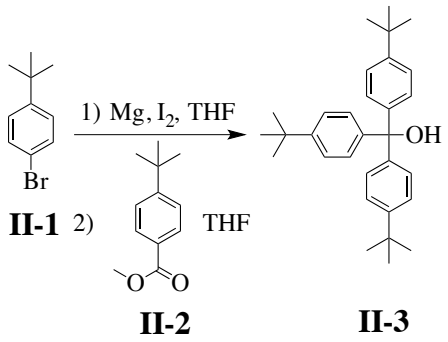

In an oven-dried 500-mL three-necked flask equipped with a condenser, dropping funnel stirrer, under a nitrogen atmosphere were placed magnesium turnings (1.97 g, 82 mmol, 2.3 eq) and a catalytic amount of iodine in dry THF (130 mL), *p-tert*-butylbromobenzene **II-1** (16.39 g, 77 mmol, 2.1 eq) in dry THF (200 mL) was added dropwise over 1 h with gentle heating. The reaction was stirred for 1h and the reaction mixture became brown. Methyl *p-tert*-butylbenzoate **II-2** (6.94 g, 36 mmol, 1 eq) in dry THF (17 mL) was added dropwise over 1h during heating, then the mixture was stirred overnight at reflux under nitrogen. The solution was cooled to room temperature and neutralized with 10% HCl. The product was extracted with n-hexane (2 × 50 mL). The combined organic phase was washed with water (3 × 80 mL) and dried with Na_2SO_4. The solvents were removed and the crude product was recrystalized in methanol twice, affording 12 g of the desired product tris(4-(*tert*-butyl)phenyl)methanol **II-3**, as a white solid (yield = 89%).

^{1}H NMR ($CDCl_3$, 300 MHz): δ 7.34 – 7.28 (m, 6H), 7.21 – 7.16 (m, 6H), 2.72 (s, 1H), 1.30 (s, 27H). Analysis is in agreement with literature data.[2]

4-(Tris(4-(*tert*-butyl)phenyl)methyl)phenol (II-4)

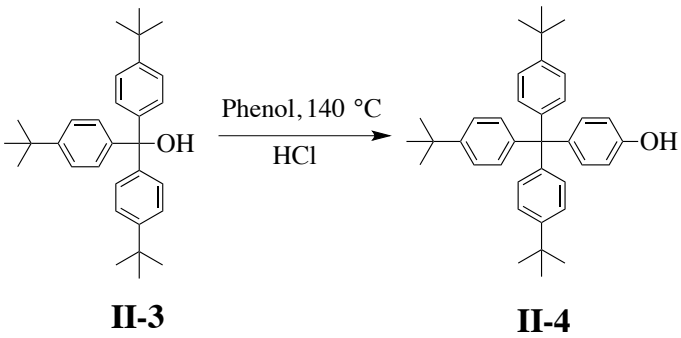

Methanol **II-3** (12.0 g, 28.0 mmol, 1 eq) was dissolved in phenol (50.0 g) on warming. 0.5 mL concentrated HCl was added as a catalyst. A deep reddish-brown colour was observed immediately, then the mixture was heated 24 h at 140 °C. After cooling to room temperature, toluene (200 mL) was added into the mixture and the mixture was washed with 20 g/L aqueous NaOH solution (3 × 150 mL) and dried with Na_2SO_4. A white solid was obtained after the organic solution was decolourized with activated carbon and the solvent was evaporated *in vacuo*. The solid was boiled in n-hexane for 30 min, filtered and recrystallized in 1:1 toluene/hexane, affording 5 g of the pure product 4-(tris(4-(*tert*-butyl)phenyl)methyl)phenol **II-4**, as a white solid. (yield = 73%).

^{1}H NMR ($CDCl_3$, 300 MHz): δ 7.25 – 7.19 (m, 6H), 7.11 – 7.01 (m, 8H), 6.72 – 6.67 (m, 2H), 4.62 (br, 1H), 1.30 (s, 27H). Analysis is in agreement with literature data.[2]

1,1',1'-[[4-(n-Bromoalkyl)phenyl]methylidyne]tris[4-(*tert*-butyl)benzene]

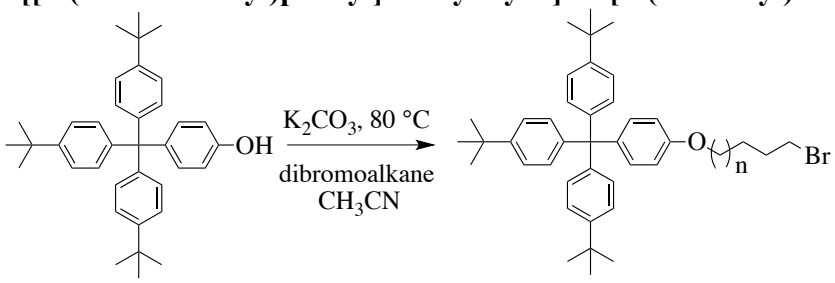

II-4 **II-5:** n = 1
II-6: n = 5

To a solution of **II-4** (1.5 g, 4.95 mmol, 1 eq), potassium carbonate (1.82 g, 14.85 mmol, 3 eq) and dibromoalkane (3 eq) in CH_3CN (60 mL). The suspension was heated at reflux overnight. After cooling, the mixture was filtered and the filtrate was concentrated *in vacuo*. The crude product was purified by column chromatography (SiO_2, cyclohexane/DCM, 8:1, v/v), affording **II-5** or **II-6** as a white solid.

II-5(yield = 95 %): **^{1}H NMR** ($CDCl_3$, 300 MHz): δ 7.25 – 7.20 (m, 6H), 7.11 – 7.04 (m, 8H), 6.78 – 6.72 (m, 2H), 3.97 (t, *J* = 6.0 Hz, 2H), 3.49 (t, *J* = 6.5 Hz, 2H), 2.12 – 1.87 (m, 4H), 1.30 (s, 27H). Analysis is in agreement with literature data.[3]

II-6(yield = 95 %): **^{1}H NMR** ($CDCl_3$, 300 MHz): δ 7.25 – 7.19 (m, 6H), 7.11 – 7.04 (m, 8H), 6.78 – 6.72 (m, 2H), 3.92 (t, *J* = 6.5 Hz, 2H), 3.41 (t, *J* = 6.6 Hz, 2H), 1.72 – 1.48 (m, 4H), 1.47 – 1.34 (m, 8H), 1.30 (s, 27H). Analysis is in agreement with literature data.[3]

1,1',1'-[[4-(n-Azidoalkyl)phenyl]methylidyne]tris[4-(*tert*-butyl)benzene]

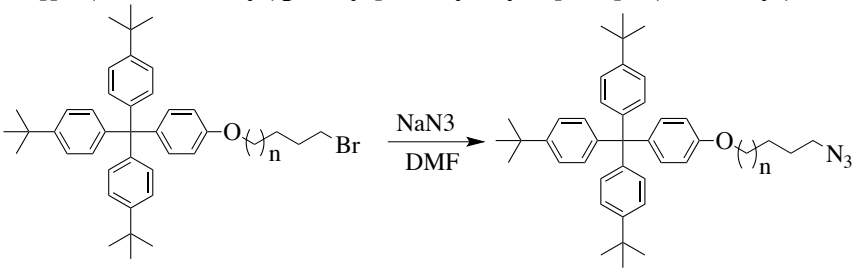

II-5: n = 1 **T$_1$:** n = 1
II-6: n = 5 **T$_2$:** n = 5

To a solution of bromide **II-5** or **II-6** (1 eq) in DMF (60 mL), sodium azide (3 eq) was added. The mixture was heated at 80 °C overnight. After cooling, the solvent was removed. Water (40 mL) was added into the mixture and extracted with AcOEt (3 × 50 mL). The organic layer was dried with Na_2SO_4 and the solvent was removed. The crude product was purified by column chromatography (SiO_2, cyclohexane/AcOEt, 6:4, v/v), affording of azide **II-7** or **II-8** as a white solid.

II-7 (yield = 94 %): **^{1}H NMR** ($CDCl_3$, 300 MHz): δ 7.25 – 7.20 (m, 6H), 7.11 – 7.05 (m, 8H), 6.78 – 6.72 (m, 2H), 3.96 (t, *J* = 5.6 Hz, 2H), 3.36 (t, *J* = 6.6 Hz, 2H), 1.90 – 1.72 (m, 4H), 1.30 (s, 27H). Analysis is in agreement with literature data.[3]

II-8 (yield = 94 %): **^{1}H NMR** ($CDCl_3$, 300 MHz): δ 7.25 – 7.19 (m, 6H), 7.11 – 7.04 (m, 8H), 6.78 – 6.72 (m, 2H), 3.92 (t, *J* = 6.5 Hz, 2H), 3.26 (t, *J* = 6.7 Hz, 2H), 1.81 – 1.54 (m, 4H), 1.47 – 1.34 (m, 8H), 1.30 (s, 27H). Analysis is in agreement with literature data.[3]

2,2'-Bipyidine-1-oxide (II-8)

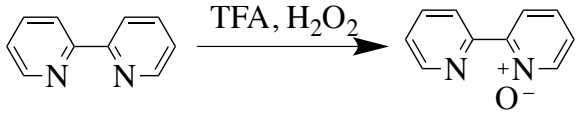

To a solution of 2,2'-bipyridine (5.1 g, 33 mmol, 1 eq) in trifluoroacetic acid (37.6 g, 330 mmol, 10 eq) was added 30% H_2O_2 (1.7 g, 50 mmol, 1.5 eq). After stirring at room temperature for 3 h, the reaction mixture was neutralized by addition of 6 M NaOH and extracted with chloroform (3 × 60 mL). The combined organic layers were washed with sat. NaCl, dried over Na_2SO_4 and concentrated to afford a colorless oil **II-8** (4.3 g, 88%).

4-Nitro-2,2'-bipyridine-1-oxide (II-9)

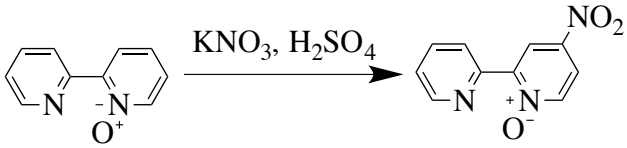

A mixture of 2,2'-bipyidine-1-oxide (4.3 g, 0.025 mol, 1 eq), KNO_3 (12.5 g, 0.125 mol) in 30 mL of concentrated sulfuric acid was stirred over 30 h at 80 °C. Then the mixture was poured onto ice (200 g) and neutralized with 25 % NaOH to pH 9.0. The precipitate formed was filtered off, washed with plenty of cold water, the solid residue was dissolved in dichloromethane and washed with water, dried over $MgSO_4$, and concentrated to afford a yellow powder **II-9** (2.9 g, yield 54%).

^{1}H NMR (300 MHz, $CDCl_3$): δ 9.17 (d, *J* = 3.3 Hz, 1H), 8.89 (dt, *J* = 8.1, 1.0 Hz, 1H), 8.79 (ddd, *J* = 1.0, 1.9, 4.8 Hz, 1H), 8.36 (d, *J* = 7.3 Hz, 1H), 8.07 (dd, *J* = 3.3, 7.2 Hz, 1H), 7.88 (td, *J* = 7.7, 1.8 Hz, 1H), 7.44 (ddd, *J* = 1.1, 4.7, 5.9 Hz, 1H). Analysis is in agreement with literature data.[4]

4-Bromo-2,2'-bipyridine-1-oxide (II-10)

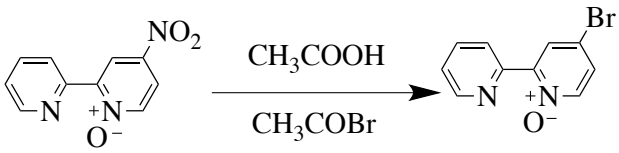

4-Nitro-2,2'-bipyridine-1-oxide (2 g, 9.21 mmol, 1 eq) and 1.7 mL of acetyl bromide was dissolved in 12.5 mL of glacial acetic acid. the mixture was heated overnight under nitrogen atmosphere at 60 °C. After then the mixture was poured onto ice (100 g) and tuned the solution to pH 11 with NaOH solution. The product was extracted with chloroform (3 × 70 mL), the combined organic layer was washed with water (100 mL) and sat. NaCl (100 mL), dried over Na_2SO_4 and evaporated to give 2.16 g of white solid **II-10** (yield = 94%) without any further purifications.

^{1}H NMR (300 MHz, $CDCl_3$): δ 8.95 (dt, *J* = 1.0, 8.1 Hz, 1H), 8.74 (ddd, *J* = 1.0, 1.8, 2.8 Hz, 1H), 8.40 (d, *J* = 2.9 Hz, 1H), 8.15 (dd, *J* = 0.5, 7.0 Hz, 1H), 7.85 (ddd, *J* = 1.8, 7.6, 8.1 Hz, 1H), 7.42 – 7.35 (m, 2H). Analysis is in agreement with literature data.[4]

4-Bromo-2,2'-bipyridine (II-11)

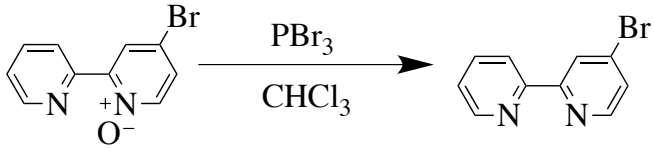

To a solution of 4-bromo-2,2'-bipyridine-1-oxide (0.852 g, 3.40 mmol, 1 eq) in 70 mL of chloroform, PBr_3 (1.1 mL, 11.93 mmol, 3.5 eq) was added dropwise. The mixture was heated at reflux under N_2 overnight. The mixture obtained was poured onto 50 g of ice and based to pH 11 with 20% NaOH solution. The organic phase was separated and the water layer was

extracted with dichloromethane (3 × 100 ml). The combined organic extracts were dried over Na_2SO_4 and evaporated. The crude product was purified by flash column chromatography on silica gel with a mobile phase of hexane and 0 – 10% of mixture (EtOAc/triethylamine = 40:1, v/v), yielding **4-bromo-2,2'-bipyridine (II-11)** (0.716 g, yield = 90%).

^{1}H NMR (300 MHz, $CDCl_3$): δ 8.68 (ddd, *J* = 0.9, 1.8, 2.8 Hz, 1H), 8.62 (dd, *J* = 0.6, 2.0 Hz, 1H), 8.47 (d, *J* = 5.2 Hz, 1H), 8.38 (dt, *J* = 8.0, 8.0 Hz, 1H), 7.82 (td, *J* = 7.6, 7.6 Hz, 1H), 7.47 (dd, *J* = 1.9, 5.2 Hz, 2H), 7.33 (ddd, *J* = 1.2, 4.8, 6.0 Hz, 1H). Analysis is in agreement with literature data.[4]

4-(Trimethylsilyl)ethynyl-2,2'-bipyridine (II-12)

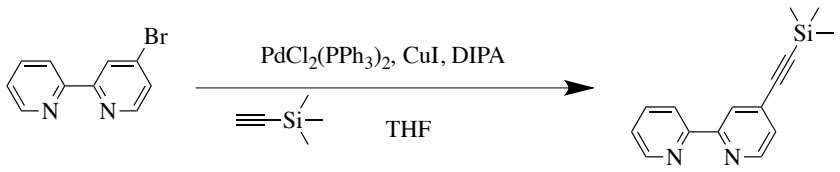

To a mixture of 4-bromo-2,2'-bipyridine (550 mg, 2.35 mmol, 1 eq), $PdCl_2(PPh_3)_2$ (49.5 mg, 0.07 mmol, 0.03 eq), copper iodide (44.7 mg, 0.23 mmol, 0.1 eq), nitrogen-degassed dry THF (40 mL), diisopropylamine (7.70 g, 58.75 mmol, 25 eq) and (trimethylsilyl)acetylene (0.50 mL, 3.53 mmol, 1.5 eq) were added under nitrogen atmosphere. The reaction mixture was stirred at room temperature for 14 hours, then heated at reflux for 3 hours. During that time the color of the solution turned black. The reaction mixture was concentrated and dissolved in DCM (40 mL), washed with water (40 mL) and sat. NaCl (40 mL), the combined extracts were dried over Na_2SO_4 and concentrated. The crude product was purified by flash column chromatography on silica gel with a mobile phase of hexane and 0 – 10% of mixture (EtOAc/triethylamine = 40:1, v/v), yielding **4-(trimethylsilyl)ethynyl-2,2'-bipyridine (II-12)** 504 mg (yield = 85%), as a brown oil.

^{1}H NMR (300 MHz, CDCl3): δ 8.69 (d, *J* = 4.8 Hz, 1H), 8.62 (d, *J* = 5.0 Hz, 1H), 8.46 (s, 1H), 8.38 (d, *J* = 8.0 Hz, 1H), 7.83 (td, *J* = 7.6, 1.8 Hz, 1H), 7.38 – 7.29 (m, 2H). Analysis is in agreement with literature data.[5]

4-Ethynyl-2,2'-bipyridine (II-13)

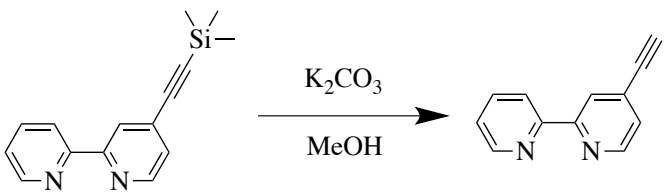

A solution of 4-(trimethylsilyl)ethynyl-2,2'-bipyridine (180 mg, 0.71 mmol, 1 eq) in CH_3OH (15 mL) was treated with K_2CO_3 (118 mg, 0.86 mmol, 1.2 eq) at room temperature. After 16 h, the reaction mixture was quenched with H_2O (30 mL) and the organic solvent evaporated under vacuum. The residue was extracted with CH_2Cl_2 (3 × 30 mL), and the organic layers washed with brine, dried over $MgSO_4$ and concentrated. The crude product was purified by flash column chromatography on silica gel with a mobile phase of hexane and 0 – 10% of mixture (EtOAc/triethylamine = 40:1, v/v), yielding **4-ethynyl-2,2'-bipyridine(II-13)** 85 mg (yield = 68%), as a beige solid.

^{1}H NMR (300 MHz, $CDCl_3$): δ 8.67 (ddd, *J* = 1.0, 1.8, 2.8 Hz, 1H), 8.63 (dd, *J* = 0.9, 5.0 Hz, 1H), 8.48 (dd, *J* = 0.9, 1.6 Hz 1H), 8.37 (dt, *J* = 8.0, 1.0 Hz, 1H), 7.80 (ddd, *J* = 1.8, 4.9, 7.5 Hz, 1H), 7.36 – 7.28 (m, 2H), 3.31 (s, 1H). Analysis is in agreement with literature data.[5]

Ruthenium (bipyridine)$_2$-(bipyridine-CCH) hexafluorophosphate (P_1)

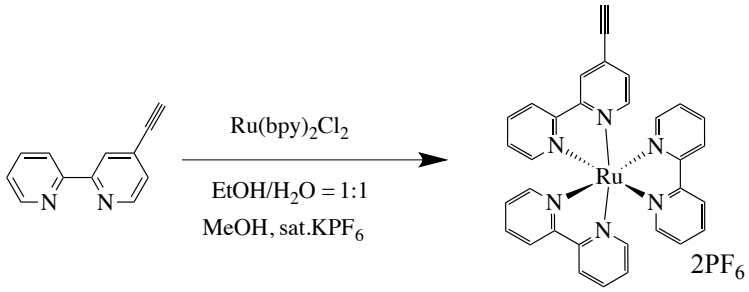

To a solution of Ru(bipyridine)$_2$Cl$_2$ (549 mg, 1.05 mmol, 1 eq) in 1:1 EtOH/H_2O (20 mL) at room temperature, 4-ethynyl-2,2'-bipyridine (190 mg, 1.05 mmol, 1 eq) was added. The solution was heated overnight under nitrogen atmosphere at 90 °C. The reaction mixture was allowed to reach room temperature and the solvent was evaporated. The mixture was redissolved in DCM (30 mL), and washed with sat. KPF_6 solution, the organic layer was dried over Na_2SO_4 and the solvent was removed. The crude product was purified by column chromatography (SiO_2, acetonitrile/water /$KNO_{3\ (sat.\ aq.)}$ = 95:4.9:0.1, v/v/v), the product was collected and the solvent was removed. The solid was solubilized in small quantity of DCM and filtered with a syringe filter, the solution was collected and diluted with DCM (5 mL), and washed with sat. NH_4PF_6 aqueous solution, and dried over Na_2SO_4 and concentrated to obtain a red solid **P_1** (746 mg, 80% yield).

^{1}H NMR (300 MHz, CD_3CN): δ 8.62 – 8.60 (m, 1H), 8.58 – 8.51 (m, 5 H), 8.13 – 8.03 (m, 5 H), 7.79 – 7.70 (m, 6H), 7.47 – 7.38 (m, 6H), 4.04 (s, 1H). Analysis is in agreement with literature data.[5]

4-(1-Pyrene)veratrole (II-16)

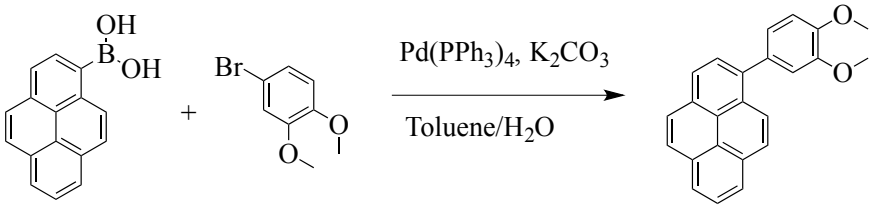

Tetrakis(triphenylphosphine)palladium(0) (188 mg, 0.035 mmol, 0.02 eq) was added to a degassed solution of 1-pyreneboronic acid (2.0 g, 8.13 mmol, 1 eq), 4-bromoveratrole (1.76 g, 8.13 mmol, 1 eq) and K_2CO_3 (3.36 g, 24.3 mmol, 3 eq) in toluene/water (50 mL, 1/1, v/v) and the mixture was heated overnight at 110 °C. The aqueous layer was extracted with toluene (2 × 50 mL). The combined organic layer was washed with water (50 mL) and dried over Na_2SO_4 and the solvent was removed. The crude product was purified by flash column chromatography (SiO_2, cyclohexane/AcOEt = 3:1, v/v), affording **II-16** (1.72 g) as a yellow solid (yield = 83%).
^{1}H NMR (300 MHz, $CDCl_3$): δ 8.23 – 8.16 (m, 4H), 8.10 (s, 2H), 8.05 – 7.98 (m, 3H), 7.20 - 7.16 (m, 2H), 7.08 (d, *J* = 8.1 Hz, 1H), 4.01 (s, 3H), 3.95 (s, 3H). **HRMS (ESI+):** calcd for $C_{24}H_{19}O_2$ *m/z* = 339.1307, found *m/z* = 339.1378.

4-(1-Pyrene)catechol (II-17)

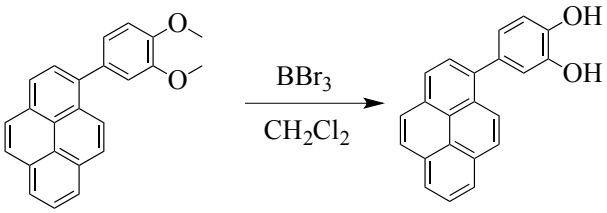

Boron tribromide (4.2 g, 16.8 mmol, 2.7 eq) was added slowly to a solution of **II-16** (2.1 g, 6.2 mmol, 1 eq) in dichloromethane (60 mL) at 0°C. The mixture was stirred 2 h at 0 °C, and stirred overnight at room temperature. Methanol (6 mL) followed by water (50 mL) was added slowly to a mixture and stirred for a further 2 h at room temperature. The mixture was washed with a saturated aqueous solution of $NaHCO_3$ (100 mL) and extracted with dichloromethane (2 × 75 mL). The organic layer was dried with Na_2SO_4 and the solvent was removed. The crude product was purified by flash column chromatography (SiO_2, cyclohexane/AcOEt = 8:2, v/v), affording of **II-17** (1.54 g) as a yellow solid (yield = 80%).
^{1}H NMR (300 MHz, $CDCl_3$): δ 8.23 – 8.15 (m, 4H), 8.08 (s, 2H), 8.03 – 7.92 (m, 3H), 7.15 (m, 1H), 7.07 (m, 2H), 5.4 (br, 2H). **^{13}C NMR**(300 MHz, Tetrahydrofuran-d_8): δ 146.1, 145.9, 139.2, 133.3, 132.4, 131.9, 131.0, 129.2, 128.2, 128.0, 127.6, 127.5, 126.5, 126.3, 125.8, 125.7, 125.4,

125.2, 122.5, 118.2, 115.8. **HRMS (ESI+):** calcd for *m/z* = 309.0921 ($[M-H]^+$), found *m/z* = 309.0928.

Alcohol II-18

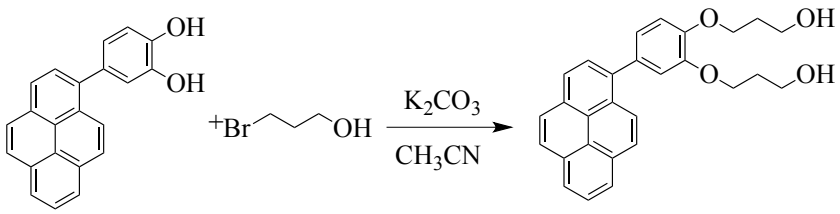

3-Bromopropanol (1.88 g, 13.53 mmol, 2.5 eq) was added to a solution of **II-17** (1.68 g, 5.41 mmol, 1 eq) and K_2CO_3 (4.48 g, 32.5 mmol, 6 eq) in acetonitrile (60 mL) and the mixture was heated overnight at reflux. The white suspension was filtered and washed with acetonitrile (40 mL) and the solvent was removed. The crude product was purified by flash column chromatography (SiO_2, cyclohexane/AcOEt = 65:35 to 4:6, v/v), affording **II-18** (1.82 g) as a yellow solid (yield = 79%).

^{1}H NMR (300 MHz, CD_2Cl_2): δ 8.27 – 8.17 (m, 4H), 8.11 (s, 2H), 8.08 – 7.97 (m, 3H), 7.22 – 7.17 (m, 2H), 7.14 – 7.08 (m, 1H), 4.29 (t, *J* = 5.7 Hz, 2H), 4.26 (t, *J* = 5.7 Hz, 2H), 3.93 – 3.80 (m, 4H), 2.74 (br, 2H), 2.15 – 1.99 (m, 4H). **HRMS (ESI+):** calcd for $C_{28}H_{27}O_4$ *m/z* = 427.1831, found *m/z* = 427.1792.

Tosylate II-19

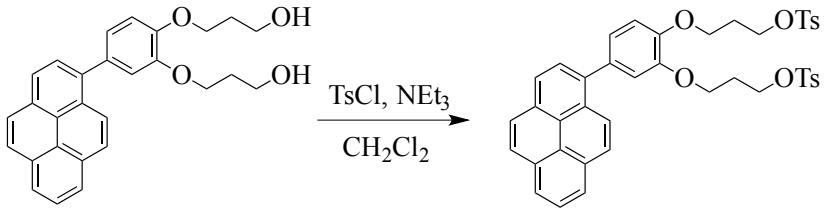

4-Toluenesulfonyl chloride (1.38 g, 7.25 mmol, 2.4 eq) was added to a solution of **II-18** (1.29 g, 3.02 mmol, 1 eq) and Et_3N (3.9 mL, 28.0 mmol, 10 eq) in DCM (80 mL) and the solution was stirred overnight at room temperature. The reaction was quenched with water (50 mL) and extracted with AcOEt (2 × 75 mL). The organic layer was dried over Na_2SO_4 and the solvent was evaporated. The crude product was purified by flash column chromatography (SiO_2, cyclohexane/AcOEt, 8:2 to 1:1, v/v), affording of **II-19** (1.8 g) as a yellow solid (yield = 87%).

^{1}H NMR (300 MHz, $CDCl_3$): δ 8.22 – 8.16 (m, 4H), 8.09 (s, 2H), 8.04 – 7.95 (m, 3H), 7.82 (d, *J* = 8.2 Hz, 2H), 7.74 (d, *J* = 8.2 Hz, 2H), 7.31 (d, *J* = 8.2 Hz, 2H), 7.18 (d, *J* = 8.2 Hz, 2H), 7.20 – 7.17 (m, 2H), 7.08 (d, *J* = 8.1 Hz, 1H), 4.32 (t, *J* = 6.1 Hz, 2H), 4.28 (t, *J* = 6.1 Hz, 2H),

4.09 (t, *J* = 6.0 Hz, 2H), 4.01 (t, *J* = 6.0 Hz, 2H), 2.41 (s, 3H), 2.28 (s, 3H), 2.23 – 2.10 (m, 4H). **HRMS (ESI+):** calcd for $C_{42}H_{39}O_8S_2$ *m/z* = 735.2008, found *m/z* = 735.2074.

6-Bromo-2-(4-methoxyphenyl)pyridine (II-14)

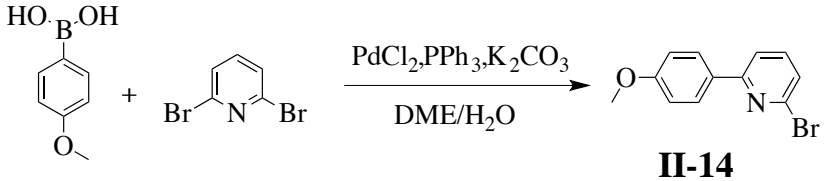

II-14

4-Methoxyphenylboronic acid (2.52 g, 16.60 mmol, 1.4 eq), 2,6-dibromopyridine (2.81 g, 11.85 mmol, 1 eq), K_2CO_3 (6.54 g, 47.40 mmol, 4 eq), $PdCl_2$ (19 mg, 0.11 mmol, 0.009 eq) and triphenylphosphine (63 mg, 0.24 mmol, 0.02 eq) were dissolved in degassed DME/water (50 mL, 2:1, v/v), and the mixture was heated for 3 d at 60°C. AcOEt (100 mL) and water (100 mL) were then added to the mixture. The aqueous layer was further extracted with AcOEt (2 × 600 mL) and the combined organic layers were washed with brine (200 mL). The organic layer was dried with $MgSO_4$ and the solvent was removed. The crude product was purified by flash column chromatography (SiO_2, cyclohexane/AcOEt = 8:2, v/v), affording 6-bromo-2-(4-methoxyphenyl)pyridine **II-14** (2.65 g) as a white solid (yield = 85%).

^{1}H NMR (300 MHz, CD_2Cl_2): δ 7.98 - 7.92 (m, 2H), 7.66 (dd, *J* = 1.0, 7.8 Hz, 1H), 7.58 (t, *J* = 7.6 Hz, 1H), 7.35 (dd, *J* = 0.9, 7.6 Hz, 1H), 7.02 - 6.96 (m, 2H), 3.86 (s, 3H). Analysis is in agreement with literature data.[6]

2-Bromo-6-(4-phenol)pyridine (II-15)

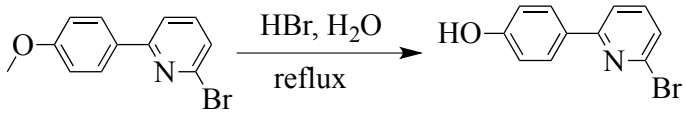

Hydrogen bromide (0.5 g, 6.2 mmol, 1.2 eq) was added to a solution of 2-bromo-6-(4-methoxyphenyl)pyridine (1.4 g, 5.3 mmol, 1 eq) in dichloromethane (40 mL) at room temperature. The mixture was heated overnight at reflux. The mixture was washed with a saturated aqueous solution of $NaHCO_3$ (100 mL) and extracted with dichloromethane (2 × 75 mL). The organic layer was dried with Na_2SO_4 and the solvent was removed. The crude product was purified by flash column chromatography (SiO_2, cyclohexane/AcOEt = 9:1, v/v), affording 2-bromo-6-(4-phenolic)pyridine **II-15** (1.06 g) as a white solid (yield = 80%).

^{1}H NMR (300 MHz, $CDCl_3$): δ 7.92 - 7.88 (m, 2H), 7.59 - 7.51 (m, 2H), 7.35 (dd, *J* = 1.2, 7.2 Hz, 1H), 6.94 - 6.90 (m, 2H). Analysis is in agreement with literature data.[6]

Macrocycle Precursor II-20

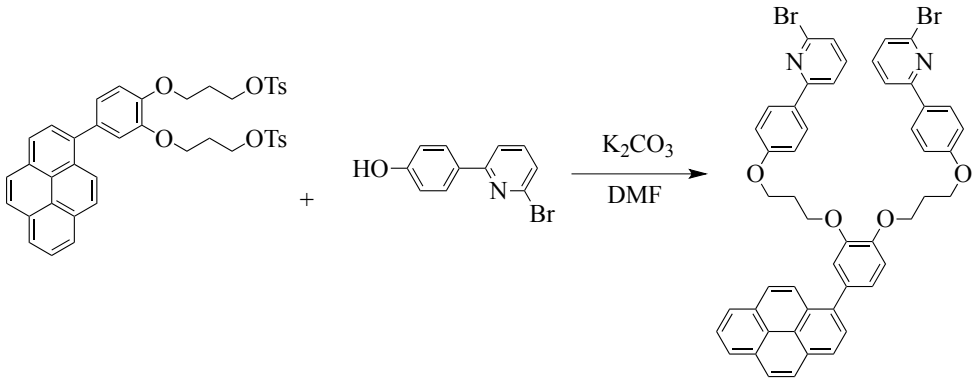

II-19 (353 mg, 0.48 mmol, 1 eq), **II-15** (265 g, 1.06 mmol, 2.2 eq) and K_2CO_3 (663 mg, 4.80 mmol, 10 eq) were heated overnight in DMF (40 mL) at 80 °C. the mixture was diluted with dichloromethane (40 mL), and washed with sat. NH_4Cl solution (2 × 50 mL). The organic layer was dried over Na_2SO_4 and the solvent was evaporated. The crude product was purified by flash column chromatography (SiO_2, CH_2Cl_2/AcOEt = 1:0 to 1:1, v/v), affording **II-20** (427 mg) as a yellow solid (yield = 95%).

^{1}H NMR (300 MHz, CD_2Cl_2): δ 8.25 – 8.15 (m, 4H), 8.09 (s, 2H), 8.05 – 7.95 (m, 3H), 7.93 – 7.88 (m, 2H), 7.86 – 7.79 (m, 2H), 7.60 – 7.48 (m, 4H), 7.35 – 7.28 (m, 2H), 7.23 (d, *J* = 2.1 Hz, 1H), 7.20 –7.10 (m, 2H), 7.04 – 6.98 (m, 2H), 6.95 – 6.89 (m, 2H), 4.37 – 4.13 (m, 8H), 2.42 – 2.23 (m, 4H). **^{13}C NMR** (300 MHz, $CDCl_3$): 160.4, 158.3, 158.2, 148.8, 148.4, 142.1, 139.0, 137.5, 134.6, 131.6, 131.1, 130.5, 130.3, 130.2, 128.7, 128.5, 128.4, 127.7, 127.5, 127.4, 126.1, 125.6, 125.5, 125.4, 125.2, 125.1, 125.0, 124.9, 124.7, 123.6, 118.2, 116.8, 115.8, 114.8, 114.7, 114.1, 77.4, 65.9, 64.7, 29.6. **HRMS (ESI+):** calcd for *m/z* = 889.1271 (M+H), found *m/z* = 889.1264.

Macrocycle R_1

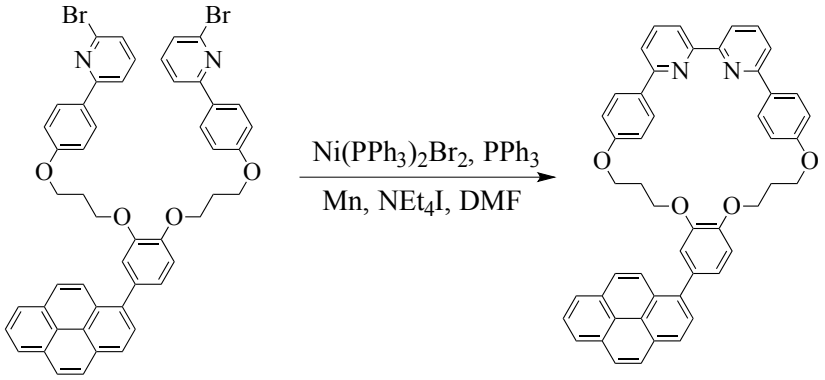

Dibromobis(triphenylphosphine)nickel(II) (227 mg, 0.304 mmol, 1 eq), triphenylphosphine (162 mg, 0.608 mmol, 2 eq), manganese(0) (167 mg, 3.040 mmol, 10 eq) and

tetraethylammonium iodide (78 mg, 0.304 mmol, 1 eq) were dissolved in DMF (3 mL) and sonicated for 10 min followed by heating for 1 h at 50 °C. **II-20** (270 mg, 0.304 mmol, 1 eq) was dissolved in DMF (3 mL) and added to the reaction mixture via a syringe pump over 4 h at 50 °C. The mixture was then heated for a further 1 h. A solution of EDTA/NH_4OH(aq) (50 mL) was added and the mixture was stirred at room temperature for 4 min. The aqueous layer was extracted with dichloromethane (2 × 30 mL), the combined organic layer was washed with water (50 mL) and brine (50 mL). The solvent was removed. The crude product was purified by flash column chromatography (SiO_2, DCM/MeOH = 100:1, v/v), affording macrocycle $\mathbf{R_1}$ (135 mg) (yield = 61%).

^{1}H NMR (300 MHz, CD_2Cl_2): δ 8.25 – 8.09 (m, 7H), 8.08 (s, 2H), 8.06 – 7.97 (m, 3H), 7.92 – 7.83 (m, 2H), 7.81 – 7.68 (m, 4H), 7.18 – 7.06 (m, 7H), 4.44 (t, *J* = 6.9 Hz, 2H), 4.37 (t, *J* = 6.9 Hz, 2H), 4.25 (t, *J* = 6.6 Hz, 2H), 4.18 (t, *J* = 6.6 Hz, 2H), 2.48 – 2.31 (m, 4H). **^{13}C NMR** (300 MHz, $CDCl_3$): δ 147.8, 147.4, 137.1, 132.8, 131.0, 130.4, 129.8, 128.9, 127.7, 127.5, 127.4, 127.2, 126.4, 125.2, 124.8, 124.2, 124.1, 122.6, 115.0, 114.8, 112.6, 64.8, 64.5, 64.4, 31.3, 31.1, 29.8, 29.0, 28.7, 27.8, 22.1, 13.9. **HRMS (ESI+):** calcd for *m/z* = 731.2904 (M+H), found *m/z* = 731.2893.

Rotaxane $\mathbf{M_1}$

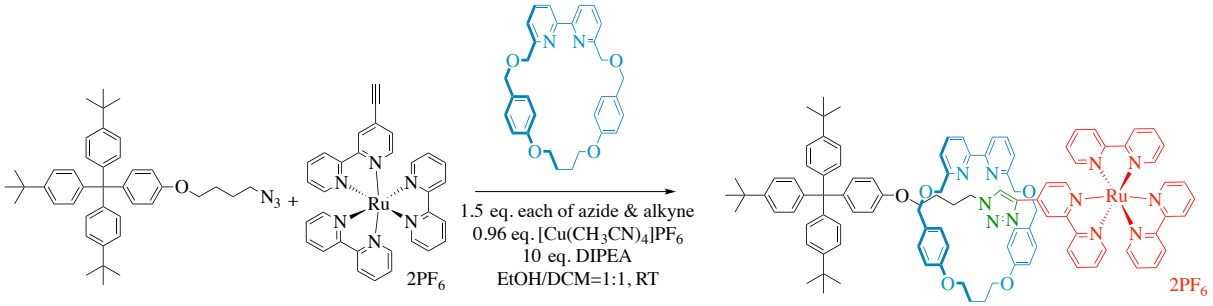

A CEM vial was charged with macrocycle $\mathbf{R_0}$ (24.1 mg, 0.050 mmol, 1 eq), $[Cu(MeCN)_4](PF_6)$ (17.9 mg, 0.075 mmol, 0.96 eq), azide $\mathbf{T_1}$ (45.1 mg, 0.075 mmol, 1.5 eq) and alkyene $\mathbf{P_1}$ (44.6 mg, 0.075 mmol, 1.5 eq), in 1:1 EtOH/DCM (5.0 mL). A solution of DIPEA (84 µL, 10 eq) was added to the reaction mixture. The deep red solution was stirred overnight at room temperature. The reaction mixture was then diluted with DCM (40 mL) and washed EDTA/NH_4OH(aq) (50 mL). The aqueous layer was extracted with dichloromethane (2 × 40 mL), the combined organic layer was washed with water (50 mL) and brine (50 mL). The organic layer was dried with $MgSO_4$ and the solvent was removed. The crude product was purified by flash column chromatography (SiO_2, petrol/DCM/MeOH = 75:75:1, v/v) to afford a red solid. The solid was

dissolved in DCM (5 mL), and washed with sat. NH_4PF_6 aqueous solution, and dried over Na_2SO_4 and concentrated to obtain **M_1** as a red solid (49.2 mg).

^{1}H NMR (300 MHz, CD_3CN): δ 9.07 (s, 1H), 9.06 (d, *J* = 0.9 Hz, 1H), 8.67 (d, *J* = 6.3 Hz, 2H), 8.54 (dd, *J* = 2.7, 2.4 Hz, 2H), 8.24 – 8.06 (m, 5H), 7.94 – 7.86 (m, 2H), 7.81 – 7.74 (m, 3H), 7.67 – 7.58 (m, 4H), 7.57 – 7.50 (m, 3H), 7.47 – 7.38 (m, 4H), 7.36 – 7.31 (m, 6H), 7.25 – 7.17 (m, 7H), 7.13 – 7.09 (m, 3H), 6.87 (dd, *J* = 1.2, 0.9 Hz, 1H), 6.81 (d, *J* = 6.3 Hz, 2H), 6.63 (dd, *J* = 6.6, 6.6 Hz, 4H), 6.32 (d, *J* = 6.3 Hz, 2H), 5.71 (d, *J* = 6.3 Hz, 2H), 4.52 (d, *J* = 9.0 Hz, 2H), 4.32 – 4.26 (m, 2H), 4.25 – 4.08 (m, 8H), 3.89 – 3.82 (m, 2H), 3.74 (t, *J* = 1.8 Hz, 2H), 1.93 – 1.83 (m, 4H), 1.70 – 1.63 (m, 2H), 1.54 – 1.46 (m, 2H), 1.30 (s, 27 H).

Chloride II-22

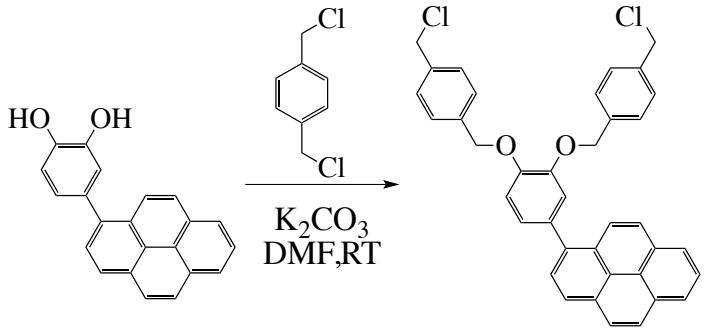

II-17 (0.897 g, 2.89 mmol, 1 eq) in DMF (40 mL) was slowly added dropwise into the solution of 4 (chloromethyl)benzyl chloride (2.26 g, 13.02 mmol, 4.5 eq) and K_2CO_3 (1.66 g, 12.05 mmol, 3 eq) in acetonitrile (30 mL) and the mixture was heated overnight at reflux. The white suspension was filtered and washed with acetonitrile (40 mL) and the solvent was removed. The crude product was purified by flash column chromatography (SiO_2, cyclohexane/AcOEt = 95:5, v/v), affording **II-22** (1.05 g) as a yellow solid (yield = 62%).

^{1}H NMR (300 MHz, $CDCl_3$): δ 8.21 – 8.14 (m, 3H), 8.08 (s, 2H), 8.07 – 7.90 (m, 4H), 7.56 – 7.51 (m, 2H), 7.48 – 7.38 (m, 6H), 7.22 – 7.09 (m, 3H), 5.29 (s, 2H), 5.24 (s, 2H), 4.63 (d, *J* = 2.1 Hz, 4H). **MS (ESI+):** calcd for $C_{38}H_{28}Cl_2O_2$ *m/z* = 586.15, found *m/z* = 586.2.

6-Bromo-2-pyridine-methanol (II-21)

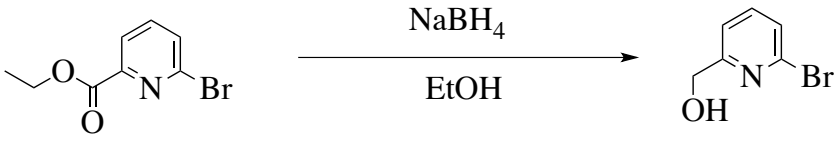

II-21

To a solution of ethyl-6-bromopicolinate (25.7 g, 0.112 mol, 1 eq) in EtOH (200 mL) in an ice water bath was added $NaBH_4$ (6.4 g, 0.168 mol, 1.5 eq) portionwise over 1 h. The solution was

stirred for 18 h then H_2O (50 mL) was added slowly to quench the reaction before the EtOH was removed *in vacuo*. The suspension was extracted with CH_2Cl_2 (3 × 500 mL), dried over Na_2SO_4 and concentrated *in vacuo* to afford **II-21** (19.9 g, 95%) as a white, low-melting solid that was used without further purification.

^{1}H NMR (300 MHz, $CDCl_3$): δ 7.49 (t, *J* = 7.7 Hz, 1H), 7.34 – 7.26 (m, 2H), 4.69 (s, 2H), 3.94 – 3.57 (br, 1H). Analysis is in agreement with literature data.[7]

Macrocycle Precursor II-23

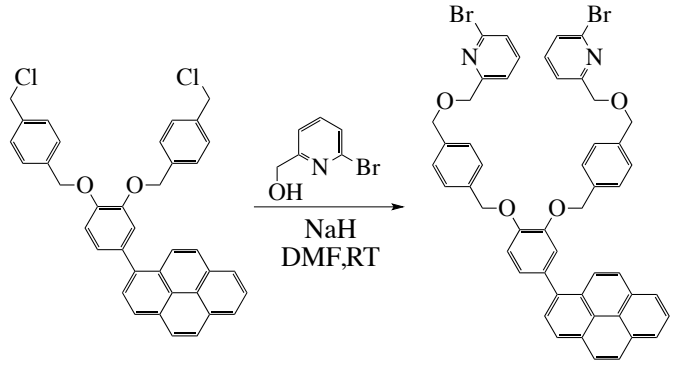

NaH (98 mg, 4.08 mmol, 2.6 eq) was added to a solution of 6-bromo-2-pyridinemethanol (641 mg, 3.41 mmol, 2.2 eq) in dry DMF (40 mL). **II-22** (914 mg, 1.56 mmol, 1 eq) was then added to the mixture at 0 °C and the solution was stirred overnight at room temperature. The mixture was then diluted with H_2O (500 mL) and extracted with CH_2Cl_2 (3 × 50 mL). The organic layer was dried over Na_2SO_4), and the solvent was removed. The crude product was purified by flash column chromatography (SiO_2, cyclohexane/AcOEt = 8:2, v/v), affording **II-23** (596 mg) as a yellow oil (yield = 64%).

^{1}H NMR (300 MHz, $CDCl_3$): δ 8.18 (d, *J* = 7.1 Hz, 2H), 8.14 – 8.10 (m, 1H), 8.07 (s, 2H), 8.05 – 7.90 (m, 4H), 7.59 – 7.33 (m, 14H), 7.22 (d, *J* = 17.2, 1.5 Hz, 1H), 7.16 – 7.08 (m, 2H), 5.28 (d, *J* = 7.5 Hz, 4H), 4.70 – 4.64 (m, 8H). **^{13}C NMR** (300 MHz, $CDCl_3$): δ 160.4, 148.5, 148.4, 141.4, 139.1, 137.5, 137.4, 137.2, 137.0, 134.6, 131.6, 131.1, 130.5, 128.6, 128.2, 127.7, 127.6, 127.5, 127.4, 126.8, 126.7, 126.1, 125.3, 125.2, 125.1, 125.0, 124.9, 124.7, 123.8, 120.1, 117.8, 114.9, 77.3, 73.0, 72.5, 71.2, 71.1, 32.1, 29.8, 29.5, 22.8, 14.3. **HRMS (ESI+):** calcd for $C_{50}H_{38}N_2O_4NaBr_2$ *m/z* = 911.1090, found *m/z* = 911.1108.

Macrocycle R_2

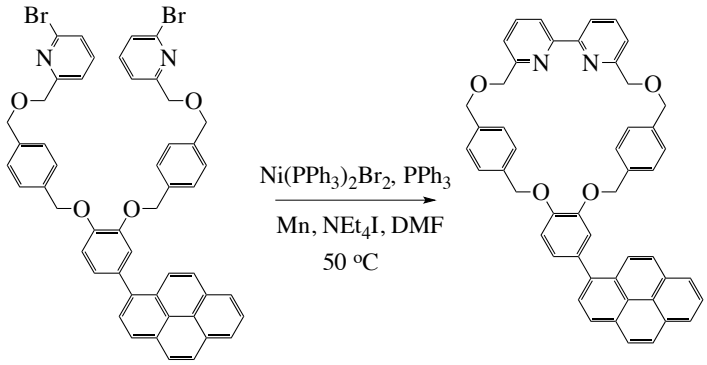

Dibromobis(triphenylphosphine)nickel(II) (375 mg, 0.505 mmol, 1 eq), triphenylphosphine (265 mg, 1.010 mmol, 2 eq), manganese(0) (278 mg, 5.05 mmol, 10 eq) and tetraethylammonium iodide (130 mg, 0.505 mmol, 1 eq) were dissolved in DMF (5 mL) and sonicated for 10 min followed by heating for 1 h at 50 °C. **II-23** (450 mg, 0.505 mmol, 1 eq) was dissolved in DMF (5 mL) and added to the reaction mixture via a syringe pump over 4 h at 50 °C. The mixture was then heated for further 1 h. A solution of EDTA/NH_4OH(aq) (100 mL) was added and the mixture was stirred at room temperature for 4 min. The aqueous layer was extracted with dichloromethane (2 × 30 mL), the combined organic layer was washed with water (50 mL) and brine (50 mL). The solvent was removed. The crude product was purified by flash column chromatography (SiO_2, petrol with a 0 to 100% gradient of ether), affording macrocycle $\mathbf{R_2}$ (260 mg, yield = 70%).

^{1}H NMR (300 MHz, $CDCl_3$): δ 8.22 – 8.15 (m, 4H), 8.09 (s, 2H), 8.04 – 7.96 (m, 5H), 7.74 (t, J = 6.2 Hz, 2H), 7.47 – 7.37 (m, 6H), 7.35 – 7.28 (m, 5H), 7.20 – 7.18 (m, 2H), 5.22 (s, 2H), 5.16 (s, 2H), 4.78 (d, J = 3.0 Hz, 4H), 4.75 (s, 2H), 4.73 (s, 2H). **^{13}C NMR** (300 MHz, $CDCl_3$): δ 158.3, 148.6, 148.4, 137.9, 137.7, 137.6, 137.5, 136.8, 136.7, 134.6, 132.3, 131.6, 131.1, 130.6, 128.9, 128.7, 128.5, 127.7, 127.6, 127.5, 127.4, 126.1, 125.5, 125.2, 125.1, 125.0, 124.9, 124.7, 123.7, 122.7, 120.9, 117.0, 114.2, 77.4, 72.6, 72.5, 72.4, 70.8, 31.1, 29.8. **HRMS (ESI+):** calcd for $C_{50}H_{39}N_2O_4$ m/z = 731.2915, found m/z = 731.2910.

Rotaxane M_3

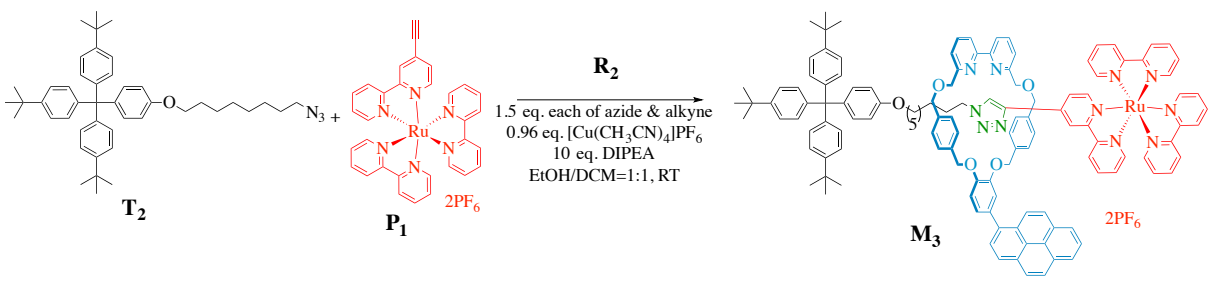

A CEM vial was charged with macrocycle **R_4** (31.0 mg, 0.0423 mmol, 1 eq), $[Cu(MeCN)_4](PF_6)$ (15.1 mg, 0.0406 mmol, 0.96 eq), azide **T_1** (41.7 mg, 0.0635 mmol, 1.5 eq) and alkyne **P_1** (56.1 mg, 0.0635 mmol, 1.5 eq), in 1:1 EtOH/DCM (4.2 mL). A solution of DIPEA (73 µL, 10 eq) was added to the reaction mixture. The deep red solution was stirred overnight at room temperature. The reaction mixture was then diluted with DCM (40 mL) and washed EDTA/NH_4OH(aq) (50 mL). The aqueous layer was extracted with dichloromethane (2 × 40 mL), the combined organic layer was washed with water (50 mL) and brine (50 mL). The organic layer was dried with $MgSO_4$ and the solvent was removed. The crude product was purified by flash column chromatography (SiO_2, petrol/DCM/MeOH = 75:75:1, v/v) and gel permeation chromatography (GPC) yielded a red solid. The solid was dissolved in DCM (5 mL), and washed with sat. NH_4PF_6 aqueous solution, and dried over Na_2SO_4 and concentrated to obtain rotaxane **M_3** (32.6 mg) as a red solid (Yield = 37%).

HRMS (ESI+): calcd for *m/z* = 990.9292 ($[M - 2PF_6]^{2+}$)/2, found *m/z* = 990.9322.

(3,5-Dimethyoxylbenzene)pyrene (II-25)

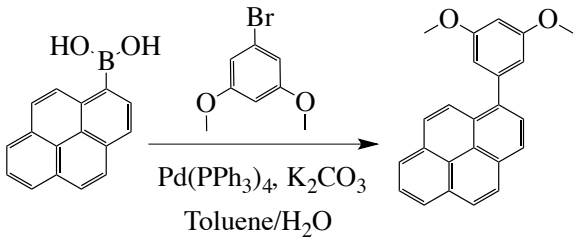

Tetrakis(triphenylphosphine)palladium(0) (141 mg, 0.012 mmol, 0.02 eq) was added to a degassed solution of 1-pyreneboronic acid (1.5 g, 6.09 mmol, 1 eq), 3,5-dimethoxy-1-bromobenzene (1.45 g, 6.7 mmol, 1.1 eq) and K_2CO_3 (2.77 g, 20.1 mmol, 3.3 eq) in toluene/water (50 mL, 1/1, v/v) and the mixture was heated overnight at 110 °C. The aqueous layer was extracted with toluene (2 × 50 mL). The combined organic layer was washed with water (50 mL) and dried with Na_2SO_4 and the solvent was removed. The crude product was purified by column chromatography (SiO_2, cyclohexane/AcOEt = 95:5, v/v), affording **II-25** (1.24 g) as a yellow solid (yield = 60 %).

^{1}H NMR (300 MHz, $CDCl_3$): δ 8.25 – 8.15 (m, 4H), 8.10 (s, 2H), 8.05 – 7.97 (m, 3H), 6.78 (d, *J* = 2.4 Hz, 2H), 6.61 (t, *J* = 3.2 Hz, 1H), 3.88 (s, 6H). **^{13}C NMR** (300 MHz, $CDCl_3$): δ 160.8, 143.3, 137.8, 131.1, 130.8, 128.6, 127.6, 127.5, 127.4, 126.2, 125.5, 125.3, 125.0, 124.7, 108.9, 99.6, 77.4, 55.6. **HRMS (ESI+):** calcd for $C_{24}H_{19}O_2$ *m/z* = 339.1379, found *m/z* = 339.1379.

(3,5-Dimethanolbenzene)pyrene (II-26)

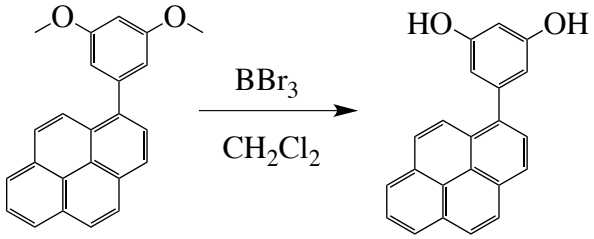

Boron tribromide (0.64 mL, 6.6 mmol, 2.7 eq) was added slowly to a solution of **II-25** (823 mg, 2.2 mmol, 1 eq) in dichloromethane (40 mL) at 0 °C. The mixture was stirred 2 h at 0 °C, and stirred overnight at room temperature. Methanol (6 mL) followed by water (50 mL) was added slowly to a mixture and stirred for further 2 h at room temperature. The mixture was washed with a saturated aqueous solution of $NaHCO_3$ (100 mL) and extracted with dichloromethane (2 × 75 mL). The organic layer was dried with Na_2SO_4 and the solvent was removed. The crude product was purified by flash column chromatography (SiO_2, cyclohexane/AcOEt = 6:4, v/v), affording of **II-26** (634 mg) as a yellow solid (yield = 84%).

^{1}H NMR (300 MHz, d_8-THF): 6.56 (s, 2H), 6.46 (d, J = 9.3 Hz, 1H), 6.36 – 6.27 (m, 3 H), 6.22 – 6.20 (m, 2H), 6.19 – 6.07 (m, 3H), 4.66 (d, J = 2.4Hz, 2H), 4.52 (t, J = 2.2Hz, 1H). **^{13}C NMR** (300 MHz, $CDCl_3$): δ 159.8, 143.8, 139.5, 132.5, 132.1, 131.4, 129.3, 128.2, 128.0, 127.8, 126.7, 126.4, 125.8, 125.5, 125.4, 109.8, 102.5. **HRMS (ESI+):** calcd for $C_{22}H_{15}O_2$ *m/z* = 311.1066, found *m/z* = 311.1070.

2-Bromo-6-((4-chloromethyl-benzyloxy)methyl)pyridine (II-24)

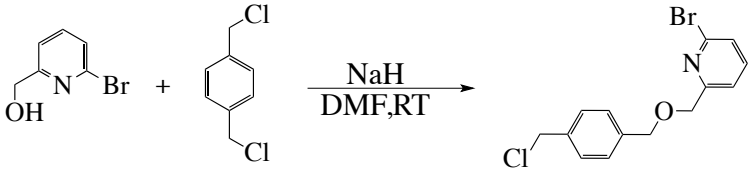

6-Bromo-2-pyridine-methanol (1 g, 5.35 mmol, 1 eq) in DMF (40 mL) was slowly added dropwise into the solution of 4-(chloromethyl) benzyl chloride (2.79 g, 16.05 mmol, 3 eq) and NaH (0.26 g, 11.05 mmol, 2 eq) in DMF (30 mL) and the mixture was stirring overnight at room temperature. The mixture was washed with a saturated aqueous solution of NH_4Cl (80 mL) and extracted with dichloromethane (2 × 75 mL). The organic layer was dried with $MgSO_4$ and the solvent was removed. The crude product was purified by column chromatography (SiO_2, cyclohexane/AcOEt = 90:10, v/v), affording **II-24** (0.94 g) as a yellow solid (yield = 54%).

^{1}H NMR (300 MHz, $CDCl_3$): δ 7.56 (t, J = 7.2Hz, 1H), 7.48 - 7.44 (m, 1H), 7.41 - 7.34 (m, 5H), 4.67 - 4.33 (m, 4H), 4.59 (s, 2H). **^{13}C NMR** (300 MHz, $CDCl_3$): δ 160.2, 141.3, 139.0,

138.0, 137.1, 128.8, 128.6, 128.1, 126.7, 120.0, 72.6, 72.4, 46.0. **HRMS (ESI+):** calcd for $C_{14}H_{13}NaBrClNO$ *m/z* = 347.9761, found *m/z* = 349.9746.

Phenyl-Macrocycle Precursor II-27

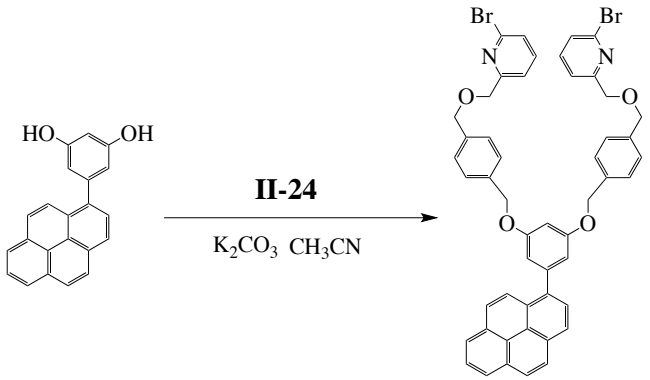

II-24 (1.14 g, 3.51 mmol, 2 eq) was added to a solution of **II-26** (0.54 g, 1.76 mmol, 1 eq) and K_2CO_3 (1.45 g, 10.8 mmol, 6 eq) in acetonitrile (45 mL) and the mixture was heated overnight at reflux. The white suspension was filtered and washed with acetonitrile (40 mL) and the solvent was removed. The crude product was purified by column chromatography (SiO_2, cyclohexane/AcOEt = 3:1, v/v), affording **II-27** (1 g) as a yellow solid (yield = 64%).

^{1}H NMR (300 MHz, $CDCl_3$): δ 8.22 – 8.11 (m, 4H), 8.08 (s, 2H), 8.03 – 7.97 (m, 3H), 7.57 – 7.34 (m, 14H), 6.86 (d, *J* = 2.4 Hz, 2H), 6.75 (t, *J* = 2.2 Hz, 1H), 5.12(s, 4H), 4.66(s, 4H), 4.65(s, 4H). **^{13}C NMR** (300 MHz, CDCl3): δ 160.4, 159.8, 143.4, 141.4, 139.1, 137.7, 137.6, 136.7, 131.6, 131.1, 130.8, 128.5, 128.2, 127.9, 127.6, 127.5, 127.4, 126.8, 126.1, 125.4, 125.0, 124.7, 120.1, 110.1, 101.4, 77.4, 72.9, 72.4, 70.1, 68.1, 25.7. **HRMS (ESI+):** calcd for $C_{50}H_{38}Br_2N_2O_4$ *m/z* = 888.1198, found *m/z* = 888.1237.

Phenyl-Macrocycle R_3

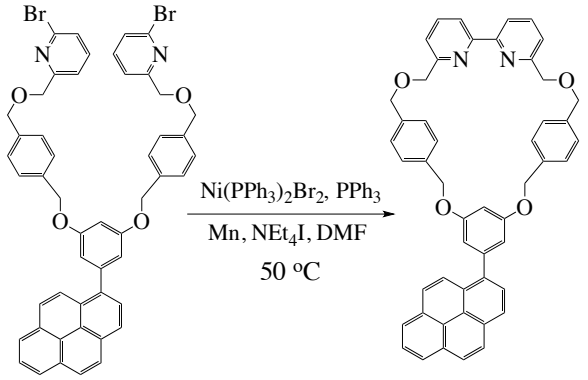

Dibromobis(triphenylphosphine)nickel(II) (516 mg, 0.696 mmol, 1 eq), triphenylphosphine (366 mg, 1.392 mmol, 2 eq), manganese(0) (382 mg, 6.959 mmol, 10 eq) and

tetraethylammonium iodide (179 mg, 0.696 mmol, 1 eq) were dissolved in DMF (7 mL) and sonicated for 10 min followed by heating for 1 h at 50 °C. **II-27** (618 mg, 0.696 mmol, 1 eq) was dissolved in DMF (7 mL) and added to the reaction mixture via a syringe pump over 4 h at 50 °C. The mixture was then heated for further 1 h. A solution of EDTA/NH_4OH(aq) (100 mL) was added and the mixture was stirred at room temperature for 4 min. The aqueous layer was extracted with dichloromethane (2 × 35 mL), the combined organic layer was washed with water (50 mL) and brine (50 mL). The solvent was removed. The crude product was purified by flash column chromatography (SiO_2, petrol with a 0 to 100% gradient of ether), affording macrocycle $\mathbf{R_3}$ (356 mg, yield = 70%).

^{1}H NMR (300 MHz, $CDCl_3$): δ 8.24 – 8.15 (m, 4H), 8.10 (s, 2H), 8.06 – 8.00 (m, 3H), 7.89 – 7.85 (m, 2H), 7.67 (t, J = 7.8 Hz, 2H), 7.38 – 7.27(m, 10H), 6.85 (d, J = 2.4 Hz, 2H), 6.42 (t, J = 2.4 Hz, 1H), 5.10(s, 4H), 4.74(s, 4H), 4.69(s, 4H). **^{13}C NMR** (300 MHz, $CDCl_3$): δ 159.8, 158.5, 155.6, 143.2, 137.7, 137.6, 137.3, 136.7, 131.5, 131.1, 130.7, 128.8, 128.5, 127.6, 127.5, 127.4, 127.2, 127.1, 126.1, 125.5, 125.0, 124.7, 121.6, 120.5, 110.2, 101.7, 77.4, 72.9, 72.7, 70.1, 41.0, 28.5, 24.0. **HRMS (ESI+):** calcd for $C_{50}H_{38}N_2O_4Na$ *m/z* = 753.2723, found *m/z* = 753.2720.

Rotaxane M_4

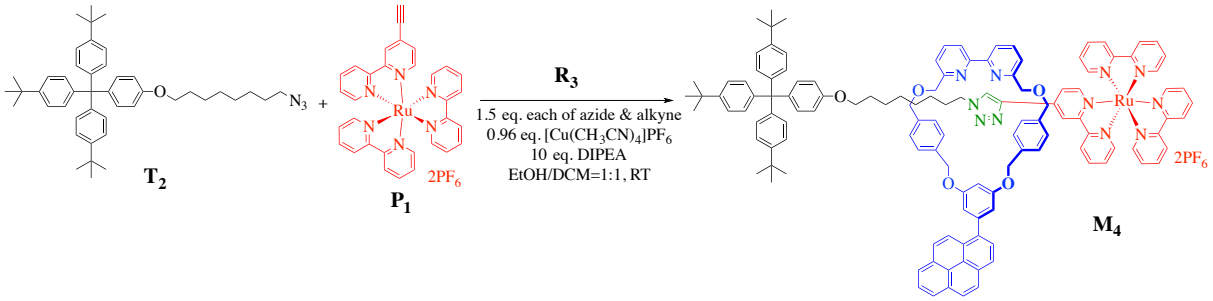

A CEM vial was charged with macrocycle $\mathbf{R_3}$ (26.9 mg, 0.0367 mmol, 1 eq), $[Cu(MeCN)_4](PF_6)$ (13.1 mg, 0.0352 mmol, 0.96 eq), azide $\mathbf{T_2}$ (36.2 mg, 0.0551 mmol, 1.5 eq) and alkyene **II-7** (48.7 mg, 0.0551 mmol, 1.5 eq), in 1:1 EtOH/DCM (3.7 mL). A solution of DIPEA (64 µL, 10 eq) was added to the reaction mixture. The deep red solution was stirred overnight at room temperature. The reaction mixture was then diluted with DCM (40 mL) and washed EDTA/NH_4OH(aq) (50 mL). The aqueous layer was extracted with dichloromethane (2 × 40 mL), the combined organic layer was washed with water (50 mL) and brine (50 mL). The organic layer was dried with $MgSO_4$ and the solvent was removed. The crude product was purified by flash column chromatography (SiO_2, petrol/DCM/MeOH = 75:75:1, v/v) and gel permeation chromatography (GPC) yielded a red solid. The solid was dissolved in DCM (5

mL), and washed with sat. NH_4PF_6 aqueous solution, and dried over Na_2SO_4 and concentrated to obtain rotaxane **M_4** (32.7 mg) as a red solid (yield = 40%).

^{1}H NMR (300 MHz, CD_3CN): δ 8.87 (s, 1H), 8.64 (s, 1H), 8.59 – 8.50 (m, 4H), 8.31 – 8.23 (m, 3H), 8.20 – 8.15 (m, 3H), 8.13 – 7.99 (m, 8H), 7.87 – 7.75 (m, 4H), 7.74 – 7.66 (m, 5H), 7.61 – 7.56 (m, 2H), 7.51 – 7.32 (m, 6H), 7.30 – 7.24 (m, 6H), 7.20 – 7.09 (m, 10H), 7.06 – 6.97 (m, 4H), 6.95 – 6.89 (m, 2H), 6.79 – 6.68 (m, 5H), 6.63 – 6.57 (m, 2H), 6.27 (t, J = 2.2 Hz, 1H), 5.19 – 5.12 (m, 1H), 5.02 (d, J = 13.3 Hz, 2H), 4.84 – 4.77 (m, 1H), 4.55 – 4.37 (m, 6H), 4.27 – 4.15 (m, 2H), 3.71 (t, J = 7.1 Hz, 2H), 3.63 (t, J = 4.3 Hz, 2H), 3.14 (q, J = 7.3 Hz, 1H), 1.48 – 1.25 (m, 39 H). **^{13}C NMR** (600 MHz, CD_3CN): δ 157.9, 152.6, 152.5, 149.4, 145.6, 138..8, 138.5, 132.5, 131.1, 129.1, 129.0, 128.8, 128.7, 128.6, 128.5, 128.4, 128.3, 127.7, 126.0, 125.4, 125.3, 125.2, 114.2, 73.8, 73.0, 68.4, 34.9, 31.5, 29.9, 29.6, 29.4, 29.3, 26.5, 26.2, 9.1. **HRMS (ESI+):** calcd for *m/z* = 990.9292 $([M - 2PF_6]^{2+})/2$, found *m/z* = 990.9251.

Thread Ru-complex B_1

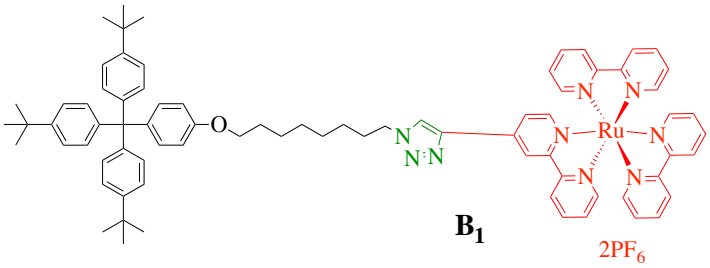

B_1

During the purification of rotaxane **M_4**, the thread as a side product was yielded as a red solid (50%).

^{1}H NMR (300 MHz, CD_3CN): δ 8.95 – 8.93 (m, 1H), 8.70 (dt, *J* = 8.4, 1.1 Hz, 1H), 8.60 (s, 1 H), 8.54 -8.48 (m, 4 H), 8.09 - 8.00 (m, 5 H), 7.84 - 7.68 (m, 7 H), 7.43 - 7,34 (m, 5 H), 7.33 - 7.27 (m, 6 H), 7.18 – 7.07 (m, 8 H), 6.79 – 6.72 (m, 2 H), 4.44 (t, *J* = 7.0 Hz, 2 H), 3.90 (t, *J* = 6.5 Hz, 2 H), 1.98 – 1.90 (m, 4 H), 1.74 - 1.63 (m, 2 H), 1.44 - 1.22 (m, 33 H). **^{13}C NMR** (600 MHz, CD_3CN): δ 157.9, 152.8, 152.6, 145.5, 138.7, 132.6, 131.1, 128.6, 128.5, 125.4, 125.2, 114.2, 68.6, 55.3, 51.4, 34.9, 31.5, 30.6, 29.8, 29.7, 29.4, 26.8, 26.5. **HRMS (ESI+):** calcd for *m/z* = 625.7876 $([M - 2PF_6]^{2+})/2$, found *m/z* = 625.7898.

(3,5-Dimethyoxylphenyl)Pyren-1-ylmethanol (II-28)

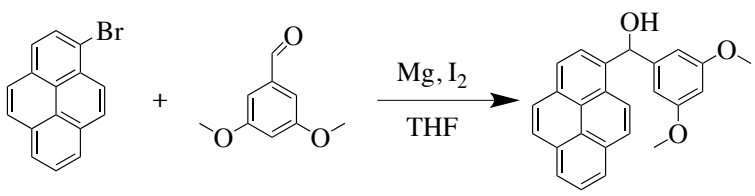

6.7 mL of 2.4 M n-BuLi in hexane was slowly added dropwise into a solution of 1-bromopyrene (3.0 g, 10.7 mmol, 1 eq) in THF (10 mL) under N_2 atmosphere at -78 °C, (pyrene-1-yl)-magnesium bromide was prepared after 30 min. 3,5-Dimethoxybenzaldehyde (1.8 g, 10.7 mmol, 1 eq) was added to the solution slowly. The reaction mixture was stirred for 2 h at room temperature and then quenched by the addition of an aqueous solution of NH_4Cl. The organic layer was extracted with ether and washed with water and brine. The solution was dried over Na_2SO_4. The solvent was removed *in vacuo*. The crude product was purified by column chromatography (SiO_2, cyclohexane/AcOEt = 3:1, v/v), affording **II-28** (3.3 g) as a white solid (yield = 84%).

^{1}H NMR (300 MHz, $CDCl_3$): δ 8.41 (d, *J* = 12 Hz, 1H), 8.26 - 8.18 (m, 4H), 8.15 - 8.02 (m, 4H), 6.86 (d, *J* =3.9 Hz, 1H), 6.67 (d, *J* = 1.8 Hz, 2H), 6.42 (t, *J* = 2.4 Hz, 1H), 3.77(s, 6H), 2.50 (d, *J* = 3.9 Hz, 1H). **^{13}C NMR** (300 MHz, $CDCl_3$): δ 160.9, 146.2, 136.4, 131.3, 131.0, 130.6, 128.2, 127.8, 127.5, 127.4, 126.0, 125.3, 125.2, 125.0, 124.9, 124.8, 123.0, 105.1, 99.4, 73.4, 55.3. **HRMS (ESI+):** calcd for $C_{25}H_{20}O_3Na$ *m/z* = 391.1304, found *m/z* = 391.1310.

1-(3,5-Dimethyoxylbenzyl)pyrene (II-29)

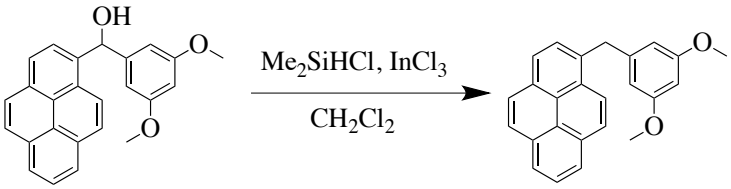

To a solution of **II-28** (2.50 g, 6.8 mmol, 1 eq) and $InCl_3$ (75 g, 0.05 eq) in 30 mL of CH_2Cl_2 was added Me_2SiHCl (1.53 g, 16.2 mmol, 2.4 eq). The solution was stirred for 6 h at room temperature. The reaction mixture was diluted with CH_2Cl_2 and washed with water and brine. After being dried over Na_2SO_4, the solvent was removed *in vacuo*. The residue was purified by a silica column (cyclohexane/AcOEt = 95:5, v/v) to give the white solid **II-29** (2.06 g, 86%).

^{1}H NMR (300 MHz, $CDCl_3$): δ 8.25 (d, *J* = 12 Hz, 1H), 8.19 - 8.12 (m, 3H), 8.08 - 7.96 (m, 4H), 7.88 (d, *J* = 7.8 Hz, 1H), 6.38 (d, *J* = 2.1 Hz, 2H), 6.30 (t, *J* = 2.4 Hz, 1H), 4.68 (s, 2H), 3.69(s, 6H). **^{13}C NMR** (300 MHz, $CDCl_3$): δ 160.9, 143.7, 134.2, 131.4, 130.9, 130.3, 129.3, 128.2, 127.5, 126.9, 125.9, 125.2, 125.0, 124.9, 123.7, 107.1, 97.9, 55.2, 39.6. **HRMS (ESI+):** calcd for $C_{25}H_{20}O_2Na$ *m/z* = 375.1355, found *m/z* = 375.1356.

1-(3,5-Dimethanolbenzyl)-pyrene (II-30)

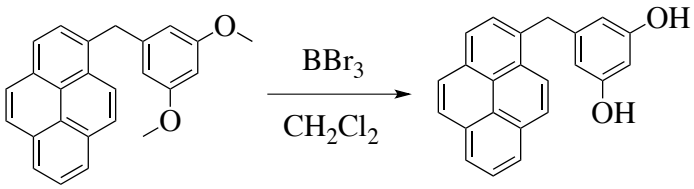

Boron tribromide (0.50 mL, 4.9 mmol, 2.7 eq) was added slowly to a solution of **II-29** (653 mg, 1.8 mmol, 1 eq) in dichloromethane (40 mL) at 0°C. The mixture was stirred 2 h at 0°C, and stirred overnight at room temperature. Methanol (6 mL) followed by water (50 mL) was added slowly to a mixture and stirred for further 2h at room temperature. The mixture was washed with a saturated aqueous solution of $NaHCO_3$ (100 mL) and extracted with dichloromethane (2 × 75 mL). The organic layer was dried with Na_2SO_4 and the solvent was removed. The crude product was purified by column chromatography (SiO_2, cyclohexane/AcOEt = 6:4, v/v), affording of **II-30** (515 mg) as a white solid (yield = 86%).

^{1}H NMR (300 MHz, $CDCl_3$): δ 8.22 - 8.13 (m, 4 H), 8.10 – 7.96 (m, 3 H), 8.00 (t, *J* = 7.5 Hz, 1 H), 6.23 (dt, *J* = 2.1, 0.9 Hz, 2 H), 6.17 (t, *J* = 2.3 Hz, 1 H), 4.62 (s, 2H), 4.60 (s, 2 H). **^{13}C NMR** (300 MHz, Tetrahydrofuran-d_8): δ 158.9, 143.1, 135.0, 131.5, 131.0, 130.2, 129.4, 128.4, 127.3, 127.0, 126.5, 125.7, 125.0, 124.8, 124.7, 124.6, 124.1, 106.7, 100.2, 38.9. **HRMS (ESI+):** calcd for $C_{23}H_{17}O_2$ *m/z* = 325.1223, found *m/z* = 325.1228.

Phenyl-methylene-macrocycle precursor (II-31)

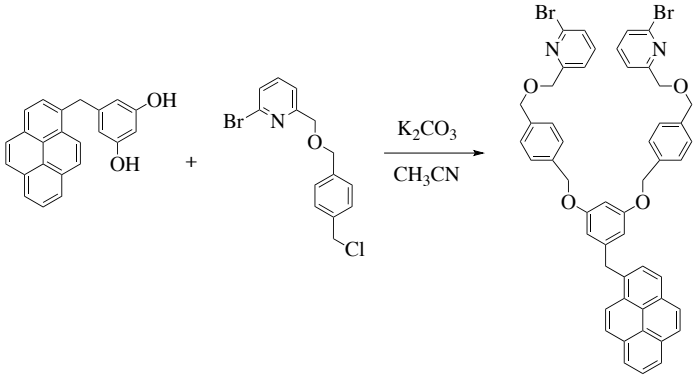

II-24 (813 mg, 2.50 mmol, 2 eq) was added to a solution of **II-30** (405 mg, 1.25 mmol, 1 eq) and K_2CO_3 (1.04 g, 7.50 mmol, 6 eq) in acetonitrile (45 mL) and the mixture was heated overnight at reflux. The white suspension was filtered and washed with acetonitrile (40 mL) and the solvent was removed. The crude product was purified by column chromatography (SiO_2, cyclohexane/AcOEt = 3:1, v/v), affording **II-31** (721 mg) as a yellow solid (yield = 64%).

^{1}H NMR (300 MHz, $CDCl_3$): δ 8.11 – 8.01 (m, 4H), 7.97 – 7.86 (m, 4H), 7.77 (d, *J* = 6.9 Hz, 2H), 7.43 (t, *J* = 7.8 Hz, 2H), 7.36 – 7.24 (m, 4H), 7.20 – 7.13 (m, 8H), 6.35 (s, 3H), 4.82(s,

4H), 4.55 (s, 2H), 4.53 (s, 4H), 4.45 (s, 4H). **^{13}C NMR** (300 MHz, $CDCl_3$): δ 160.3, 160.0, 143.7, 141.3, 139.0, 137.4, 136.5, 134.0, 131.4, 130.9, 129.3, 128.3, 127.9, 127.6, 127.5, 126.9, 126.6, 125.9, 125.2, 125.1, 124.9, 123.8, 120.0, 108.1, 99.9, 72.7, 72.3, 69.7, 39.5, 27.0. **HRMS (ESI+):** calcd for $C_{51}H_{40}NaBr_2N_2O_4$ *m/z* = 925.1247, found *m/z* = 927.1229.

Phenyl-methylene-macrocycle R_4

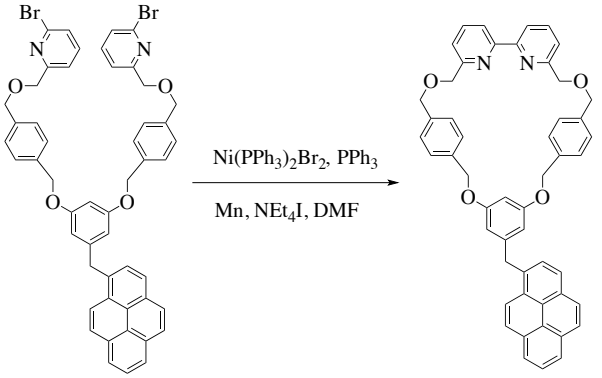

Dibromobis(triphenylphosphine)nickel(II) (421 mg, 0.566 mmol, 1 eq), triphenylphosphine (297 mg, 1.132 mmol, 2 eq), manganese(0) (312 mg, 5.66 mmol, 10 eq) and tetraethylammonium iodide (146 mg, 0.566 mmol, 1 eq) were dissolved in DMF (5 mL) and sonicated for 10 min followed by heating for 1 h at 50°C. **II-31** (511 mg, 0.566 mmol, 1 eq) was dissolved in DMF (5 mL) and added to the reaction mixture via a syringe pump over 4 h at 50°C. The mixture was then heated for further 1 h. A solution of EDTA/NH_4OH(aq) (100 mL) was added and the mixture was stirred at room temperature for 4 min. The aqueous layer was extracted with dichloromethane (2 × 15 mL), the combined organic layer was washed with water (50 mL) and brine (50 mL). The solvent was removed. The crude product was purified by flash column chromatography on silica gel with a mobile phase of petrol and 0 – 100% Et_2O yielded macrocycle **R_4** (295 mg) as a white solid (yield = 70%).

^{1}H NMR (300 MHz, $CDCl_3$): δ 8.27 - 8.14 (m, 4H), 8.09 - 7.09 (m, 4H), 7.89 (d, *J* = 6.9 Hz, 2H), 7.82 (d, *J* = 8.7 Hz, 2H), 7.54 (t, *J* = 7.8 Hz, 2H), 7.18 - 7.06 (m, 10H), 6.43 (d, *J* = 2.1 Hz, 2H), 6.12 (t, *J* = 2.1 Hz, 1H), 4.89 (s, 4H), 4.66 (s, 2H), 4.64 (s, 4H), 4.59 (s, 4H). **^{13}C NMR** (300 MHz, $CDCl_3$): δ 159.9, 158.2, 155.5, 143.5, 137.5, 137.2, 136.5, 134.1, 131.4, 130.9, 130.3, 129.3, 128.6, 128.4, 127.6, 127.5, 127.0, 125.9, 125.2, 125.1, 124.9, 123.8, 121.6, 120.3, 108.0, 100.3, 77.3, 72.8, 72.6, 69.7, 39.5. **HRMS (ESI+):** calcd for $C_{51}H_{40}N_2O_4Na$ *m/z* = 767.2880, found *m/z* = 767.2881.

Rotaxane M_5

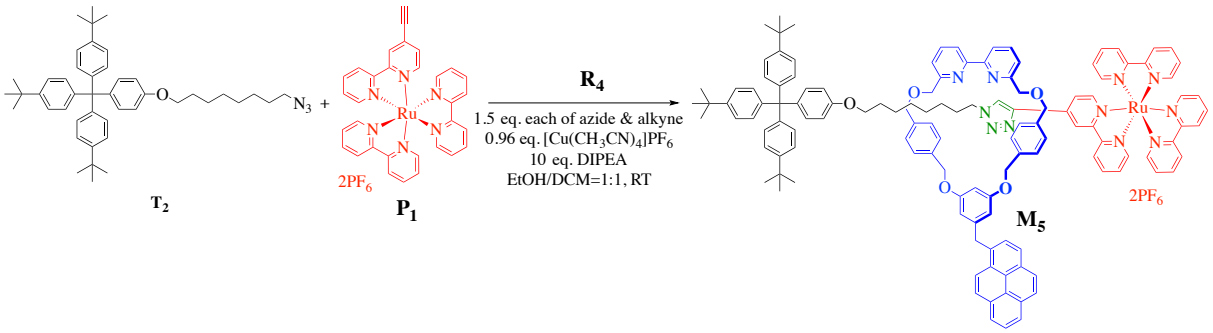

A CEM vial was charged with macrocycle **R_4** (27.3 mg, 0.0367 mmol, 1 eq), $[Cu(MeCN)_4](PF_6)$ (13.1 mg, 0.0352 mmol, 0.96 eq), azide **T_2** (36.2 mg, 0.0551 mmol, 1.5 eq) and alkyne **P_1** (48.7 mg, 0.0551 mmol, 1.5 eq), in 1:1 EtOH/DCM (3.7 mL). A solution of DIPEA (64 µL, 10 eq) was added to the reaction mixture. The deep red solution was stirred overnight at room temperature. The reaction mixture was then diluted with DCM (40 mL) and washed EDTA/NH_4OH(aq) (50 mL). The aqueous layer was extracted with dichloromethane (2 × 40 mL), the combined organic layer was washed with water (50 mL) and brine (50 mL). The organic layer was dried with $MgSO_4$ and the solvent was removed. The crude product was purified by flash column chromatography (SiO_2, petrol/DCM/MeOH = 75:75:1, v/v) and gel permeation chromatography (GPC) yielded a red solid. The solid was dissolved in DCM (5 mL), and washed with sat. NH_4PF_6 aqueous solution, and dried over Na_2SO_4 and concentrated to obtain rotaxane **M_5** (36.6 mg) as a red solid (yield = 45%).

^{1}H NMR (300 MHz, CD_3CN): δ 8.64 - 8.60 (m, 2H), 8.52 (dd, *J* = 8.1, 3.9 Hz, 2 H), 8.39 (d, *J* = 9.3 Hz, 1 H), 8.35 -8.28 (m, 1 H), 8.27 - 8.20 (m, 3 H), 8.15 - 7.93 (m, 9 H), 7.81 (t, *J* = 7.6 Hz, 1 H), 7.74 - 7,34 (m, 14 H), 7.28 - 7.22 (m, 6 H), 7.21 - 7.18 (m, 1H), 7.15 – 7.09 (m, 6 H), 7.07 – 7.01 (m, 2 H), 6.98 – 6.88 (m, 5 H), 6.74 (dd, *J* = 6.0, 1.8 Hz, 1H), 6.67 – 6.60 (m, 4 H), 6.57 (s, 1H), 6.46 – 6.40 (m, 3 H), 5.94 (t, *J* = 2.2 Hz, 1 H), 4.83 (q, *J* = 13.2 Hz, 2 H), 4.74 - 4.62 (m, 3 H), 4.51 - 4.34 (m, 7 H), 4.13 (q, *J* = 12.3 Hz, 2 H), 3.84 (t, *J* = 6.9 Hz, 2 H), 3.70 (t, *J* = 6.4 Hz, 2 H), 2.02 - 1.97 (m, 4 H), 1.33 - 1.25 (m, 35 H). **^{13}C NMR** (600 MHz, CD_3CN): δ 158.6, 157.1, 156.8, 156.0, 155.8, 155.7, 155.6, 155.4, 154.5, 150.6, 150.4, 150.3, 150.2, 150.0, 148.8, 147.3, 143.5, 143.0, 142.2, 138.7, 138.1, 136.8, 136.7, 136.3, 136.0, 135.8, 135.3, 133.8, 130.4, 130.2, 130.0, 129.1, 127.9, 127.4, 127.1, 126.7, 126.5, 126.4, 126.3, 126.1, 125.9, 125.1, 124.4, 124.1, 124.0, 123.9, 123.8, 123.4, 123.3, 123.2, 123.1, 122.9, 122.8, 122.7, 121.5, 121.1, 120.5, 120.4, 120.2, 112.1, 106.3, 106.1, 100.1, 71.6, 71.3, 71.1, 70.9, 68.1, 67.8, 66.3, 65.0, 61.8, 48.5, 37.8, 32.8, 32.4, 29.4, 29.0, 28.8, 28.2, 27.9, 27.5, 27.4, 27.3, 24.5, 24.3. **HRMS (ESI+):** calcd for *m/z* = 997.9370 $([M - 2PF_6]^{2+})/2$, found *m/z* = 997.9420.

Rotaxane M_6

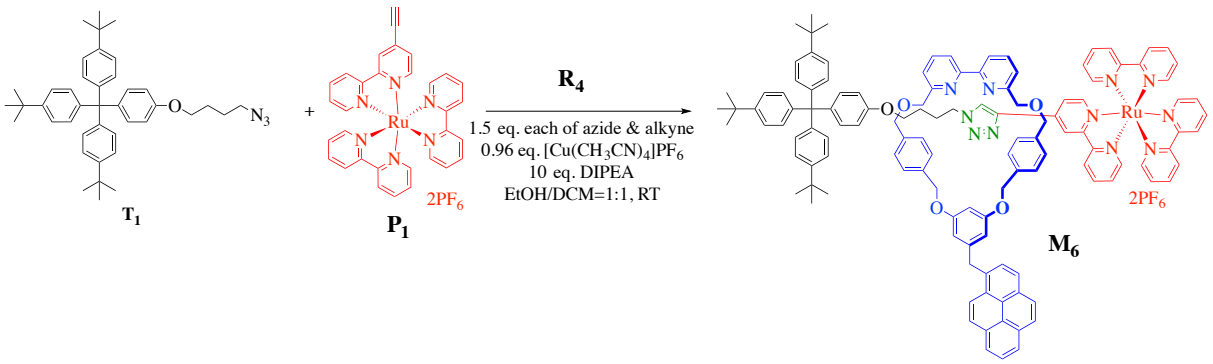

A CEM vial was charged with macrocycle **R_4** (31.1 mg, 0.0418 mmol, 1 eq), $[Cu(MeCN)_4](PF_6)$ (14.9 mg, 0.0401 mmol, 0.96 eq), azide **T_1** (37.7 mg, 0.0627 mmol, 1.5 eq) and alkyne **P_1** (52.9 mg, 0.0627 mmol, 1.5 eq), in 1:1 EtOH/DCM (4.2 mL). A solution of DIPEA (73 µL, 10 eq) was added to the reaction mixture. The deep red solution was stirred overnight at room temperature. The reaction mixture was then diluted with DCM (40 mL) and washed EDTA/NH_4OH(aq) (50 mL). The aqueous layer was extracted with dichloromethane (2 × 40 mL), the combined organic layer was washed with water (50 mL) and brine (50 mL). The organic layer was dried with $MgSO_4$ and the solvent was removed. The crude product was purified by flash column chromatography (SiO_2, petrol/DCM/MeOH = 75:75:1, v/v) and gel permeation chromatography (GPC) yielded a red solid. The solid was dissolved in DCM (5 mL), and washed with sat. NH_4PF_6 aqueous solution, and dried over Na_2SO_4 and concentrated to obtain rotaxane **M_6** (32.6 mg) as a red solid (yield = 37%).

^{1}H NMR (300 MHz, CD_3CN): δ 8.59 (s, 1H), 8.56 (d, *J* = 1.5 Hz, 1H), 8.50 – 8.44 (m, 2H), 8.37 (d, *J* = 9.3 Hz, 1H), 8.30 – 8.18 (m, 5H), 8.13 – 8.03 (m, 5H), 8.02 – 7.91 (m, 5H), 7.72 – 7.60 (m, 5H), 7.52 – 7.42 (m, 7H), 7.40 – 7.29 (m, 4H), 7.28 – 7.22 (m, 6H), 7.21 – 7.08 (m, 7H), 7.03 – 6.97 (m, 2H), 6.95 – 6.83 (m, 5H), 6.66 (dd, *J* = 1.7, 2.9 Hz, 1H), 6.62 – 6.54 (m, 3H), 6.51 – 6.54 (m, 2H), 6.40 – 6.33 (m, 3H), 5.91 (t, *J* = 2.0 Hz, 1H), 4.83 (q, *J* = 16.9 Hz, 2H), 4.68 – 4.58 (m, 3H), 4.47 – 4.29 (m, 7H), 4.10 (q, *J* = 15.5 Hz, 2H), 3.82 – 3.75 (m, 2H), 3.49 (t, *J* = 6.2 Hz, 2H), 1.30 – 1.20 (m, 31H). **^{13}C NMR** (600 MHz, CD_3CN): δ 160.6, 158.0, 157.8, 157.7, 157.4, 152.5, 152.4, 152.3, 151.9, 149.4, 145.6, 145.1, 143.2, 140.4, 138.9, 138.7, 138.4, 138.0, 137.9, 137.4, 135.8, 132.4, 132.3, 131.8, 131.2, 131.1, 129.9, 129.5, 129.3, 128.8, 128.6, 128.5, 128.1, 127.9, 127.6, 127.2, 126.2, 126.1, 126.0, 125.8, 125.5, 125.4, 125.2, 125.0, 124.8, 124.7, 123.6, 122.4, 114.2, 108.4, 108.1, 102.1, 73.4, 73.2, 70.1, 69.8, 67.6, 67.0, 64.0, 56.0, 50.2, 39.8, 39.7, 34.9, 34.5, 31.5, 31.1, 30.3, 29.6, 26.9, 26.4, 25.2, 24.5, 23.6, 23.4, 18.7, 17.3, 14.3, 12.9, 11.3. **HRMS (ESI+):** calcd for *m/z* = 969.9057 $([M - 2PF_6]^{2+})/2$, found *m/z* = 969.9062.

1,8-Diazidoctane (III-1)

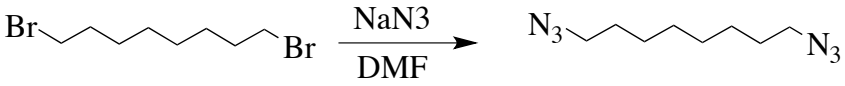

To a solution of 1,8-dibromooctane (4.2 g, 15.44 mmol, 1 eq) in DCM (10 mL), sodium azide (3.0 g, 46.32 mmol, 3 eq) was added. The mixture was heated overnight at 80 °C before being diluted with DCM. The mixture was washed with sat. NH_4Cl aqueous solution, dried over Na_2SO_4. Volatiles were removed under reduced pressure to afford the desired compounds **III-1** as a colourless oil (2.7 g, 88 %).

^{1}H NMR (300 MHz, $CDCl_3$): δ 3.26 (t, *J* = 6.9 Hz, 4H), 1.66 – 1.54 (m, 4H), 1.43 – 1.30 (m, 8H).

3-(4-(Tris(4-(*tert*-butyl)phenyl)methyl)phenoxy)-prop-1-yne (III-2)

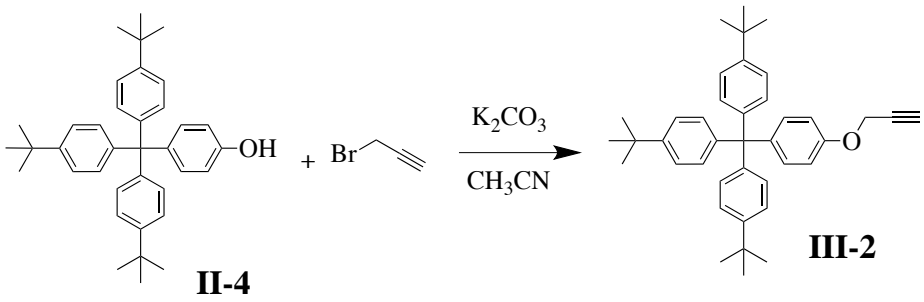

II-4 **III-2**

To a solution of **II-4** (1.5 g, 4.95 mmol, 1 eq), potassium carbonate (1.82 g, 14.85 mmol, 3 eq) in DMF (50 mL), propargyl bromide (0.65 mL, 80 % solution in toluene, 5.94 mmol, 1.5 eq). The suspension was heated at 80 °C overnight. After cooling, the solvent was removed, water (50 mL) was added and extracted with AcOEt (3 × 50 mL). The organic layer was dried with Na_2SO_4 and the solvent was removed. The crude product was purified by column chromatography (SiO_2, cyclohexane/AcOEt, 95:5, v/v), affording of 3-(4-(tris(4-(*tert*-butyl)phenyl)methyl)phenoxy)-prop-1-yne **III-2** as a white solid (1.3 g, 85%).

^{1}H NMR ($CDCl_3$, 300 MHz): δ 7.25 – 7.20 (m, 6H), 7.13 – 7.03 (m, 8H), 6.87 – 6.81 (m, 2H), 4.66 (d, *J* = 2.4 Hz, 2H), 2.51 (t, *J* = 2.4 Hz, 1H), 1.30 (s, 27H). Analysis is in agreement with literature data.[8]

Azide T_3

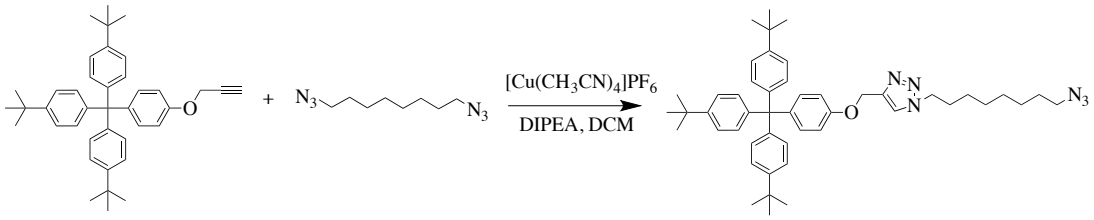

III-2 **III-1** **T_3**

To a solution of 1,8-diazidooctane **III-1** (543 mg, 2.76 mmol, 5 eq) in DCM (10 mL), **III-2** (300 mg, 0.55 mmol, 1 eq) was added dropwise, followed by the addition of a freshly prepared tetrakis(acetonitrile)copper(I) hexafluorophosphate (41 mg, 0.11 mmol, 0.2 eq). The mixture was stirred overnight at room temperature. Volatiles were removed under reduced pressure. The crude product was purified by column chromatography (SiO_2, DCM/MeOH = 200:1, v/v) to afford the desired compound **T_3** as white powder (276 mg, 68%).

^{1}H NMR (300 MHz, $CDCl_3$): δ 7.59 (s, 1H), 7.25 – 7.20 (m, 6H), 7.13 – 7.04 (m, 8H), 6.90 – 6.82 (m, 2H), 5.19 (s, 2H), 4.36 (t, J = 10.2 Hz, 2H), 3.25 (t, J = 6.8 Hz, 2H), 1.98 – 1.85 (m, 2H), 1.64 – 1.53 (m, 2H), 1.39 – 1.26 (m, 35H). **^{13}C NMR** (300 MHz, $CDCl_3$): δ 156.4, 148.7, 144.6, 144.3, 140.5, 132.6, 131.0, 124.3, 122.8, 113.5, 77.5, 63.4, 62.4, 51.7, 50.8, 34.6, 31.7, 30.5, 30.0, 29.2, 29.1, 26.9, 26.7. **HRMS (ESI+):** calcd for m/z = 761.4877 ($[M + Na]^+$), found m/z = 761.4880 ($[M + Na]^+$).

Rotaxane M_7

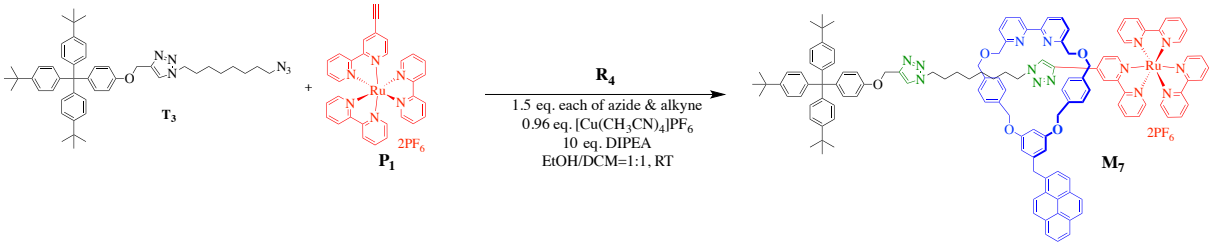

A CEM vial was charged with macrocycle **R_4** (23.6 mg, 0.032 mmol, 1 eq), $[Cu(MeCN)_4](PF_6)$ (11.4 mg, 0.030 mmol, 0.96 eq), azide **T_3** (35.2 mg, 0.048 mmol, 1.5 eq) and alkyne **P_1** (42.1 mg, 0.048 mmol, 1.5 eq), in 1:1 EtOH/DCM (3.2 mL). A solution of DIPEA (56 µL, 10 eq) was added to the reaction mixture. The deep red solution was stirred overnight at room temperature. The reaction mixture was then diluted with DCM (40 mL) and washed EDTA/NH_4OH(aq) (50 mL). The aqueous layer was extracted with dichloromethane (2 × 40 mL), the combined organic layer was washed with water (50 mL) and brine (50 mL). The organic layer was dried with Na_2SO_4 and the solvent was removed. The crude product was purified by gel permeation chromatography (GPC) yielded a red solid. The solid was dissolved

in DCM (5 mL), and washed with sat. NH_4PF_6 aqueous solution, and dried over Na_2SO_4 and concentrated to obtain rotaxane **M_7** (36.6 mg) as a red solid (yield = 70%).

^{1}H NMR (300 MHz, CD_3CN): δ 8.63 (d, *J* = 2.0 Hz, 1H), 8.62 (s, 1H), 8.45 (dd, *J* = 3.7, 7.9 Hz, 2H), 8.40 – 8.33 (m, 1H), 8.29 – 8.16 (m, 5H), 8.11 – 7.88 (m, 10H), 7.77 (t, *J* = 7.8 Hz, 1H), 7.71 – 7.58 (m, 8H), 7.57 – 7.29 (m, 8H), 7.26 – 7.19 (m, 6H), 7.18 – 7.03 (m, 9H), 6.96 – 6.77 (m, 8H), 6.64 – 6.60 (m, 2H), 6.54 (t, *J* = 1.5 Hz, 1H), 6.46 – 6.39 (m, 3H), 5.92 (t, *J* = 2.3 Hz, 1H), 5.01 (s, 2H), 4.80 (q, *J* = 13.2 Hz, 2H), 4.71 – 4.58 (m, 3H), 4.49 – 4.30 (m, 7H), 4.13 (q, *J* = 12.4 Hz, 2H), 4.00 (t, *J* = 7.1 Hz, 2H), 3.84 (t, *J* = 7.0 Hz, 2H), 3.54 (q, *J* = 6.9 Hz, 2H), 1.48 – 1.36 (m, 2H), 1.29 – 1.18 (m, 33H). **^{13}C NMR** (600 MHz, CD_3CN): δ 106.6, 158.0, 157.9, 157.8, 152.6, 152.5, 149.4, 145.4, 145.1, 141.0, 140.8, 138.8, 138.7, 138.6, 137.9, 132.5, 132.3, 131.7, 131.2, 131.1, 130.9, 129.9, 129.4, 129.1, 128.6, 128.5, 127.9, 127.2, 126.2, 126.1, 126.0, 125.8, 125.6, 125.5, 125.4, 125.2, 125.2, 125.1, 124.8, 123.7, 122.6, 120.8, 108.3, 108.2, 101.9, 73.1, 69.8, 63.9, 55.3, 50.7, 39.7, 34.9, 31.5, 30.5, 30.3, 29.2, 27.8, 26.7, 23.4, 14.4. **HRMS (ESI+):** calcd for *m/z* = 1038.4534 ($[M - 2PF_6]^{2+}$)/2, found *m/z* = 1038.4551.

1,3-Di-*tert*-butyl-5-bromobenzene

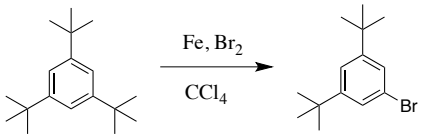

To a 100 mL round bottomed flask, 1,3,5-tri-*tert*-butylbenzene (5 g, 20.3 mmol, 1 eq) was dissolved in 20 mL of CCl_4, finely powdered iron (1.4 g, 24.8 mmol, 1.22 eq) was added. Bromine (0.87 mL, 42.4 mmol, 2.09 eq) was dissolved in 5 mL of CCl_4 and added dropwise into the mixture over 20 minutes. The reaction was stirred for 16 h at room temperature. The mixture was washed with water (40 mL), and the aqueous layer was extracted with DCM (40 mL). The combined organic layers were washed with 10% Na_2SO_3 aqueous solution (40 mL), dried over Na_2SO_4. The solvent was evaporated *in vacuo* to yield 1,3-di-*tert*-butyl-5-bromobenzene, as an oily solid (4.9 g, 91%) without further purification.

1,3-Di-*tert*-butyl-5-azidobenzene

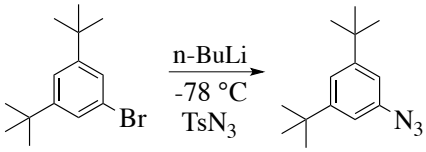

To a 100 mL two-neck round flask, 1,3-di-*tert*-butyl-5-bromobenzene (500 mg, 1.86 mmol, 1 eq) was dissolved in THF (40 mL), and cooled to -78 °C. The colourless solution was treated

with 2.5 M n-BuLi in hexane (3.60 mL, 5.60 mmol, 3 eq) and stirred at -78 °C for 25 minute before a solution of tosyl azide (1.103 g, 5.60 mmol, 3 eq) in THF (5 mL) was added over a 2 min period. The deep red solution was stirred for a 25 min before being warmed to 25 °C followed by further stirring for 16 h. The mixture was poured onto water (40 mL) and extracted with Et_2O (2 x 50 mL). The organic extracts were combined, washed with water (50 mL) and brine (50 mL) then dried over Na_2SO_4 and reduced *in vacuo*. The crude product was purified by column chromatography (SiO_2, hexane) to yield 1,3-di-*tert*-butyl-5-azidobenzene, as a yellow oil (378 mg, 88%). **^{1}H NMR** (300 MHz, $CDCl_3$): δ 7.20 (t, J = 1.7 Hz, 1H), 6.86 (d, J = 1.6 Hz, 2H), 1.32 (s, 9H). Analysis is in agreement with literature data.[9]

Rotaxane M_8

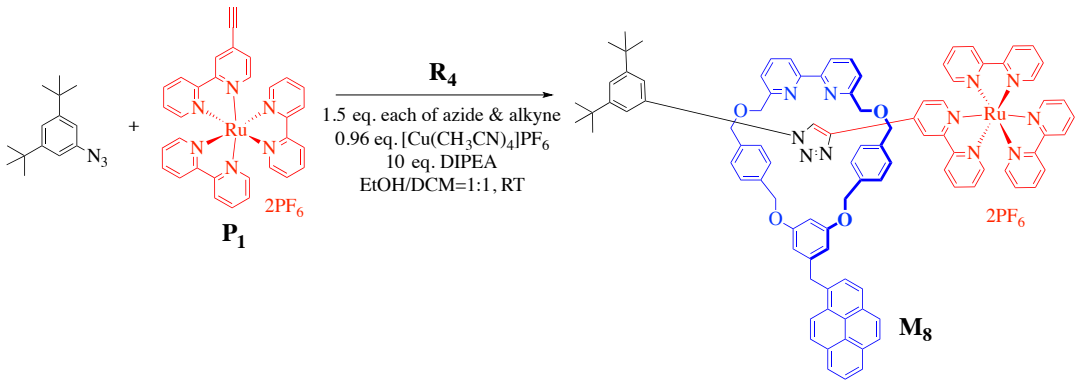

A CEM vial was charged with macrocycle **R_4** (22.4 mg, 0.030 mmol, 1 eq), $[Cu(MeCN)_4](PF_6)$ (10.7 mg, 0.029 mmol, 0.96 eq), azide **T_1** (6.9 mg, 0.0627 mmol, 1.5 eq) and alkyene **P_1** (40.0 mg, 0.045 mmol, 1.5 eq), in 1 : 1 EtOH/DCM (3.1 mL). A solution of DIPEA (52 µL, 10 eq) was added to the reaction mixture. The deep red solution was stirred overnight at room temperature. The reaction mixture was then diluted with DCM (40 mL) and washed EDTA/NH_4OH(aq) (50 mL). The aqueous layer was extracted with dichloromethane (2 × 40 mL), the combined organic layer was washed with water (50 mL) and brine (50 mL). The organic layer was dried with $MgSO_4$ and the solvent was removed. The crude solid was further purified by column chromatography (SiO_2, acetonitrile/water /$KNO_{3\ (sat.\ aq.)}$ = 90:9.8:0.2, v/v/v) and gel permeation chromatography (GPC) yielded a red solid. The solid was dissolved in DCM (5 mL), and washed with sat. NH_4PF_6 aqueous solution, and dried over Na_2SO_4 and concentrated to obtain **M_8** as a red solid (yield = 20%).

^{1}H NMR (300 MHz, CD_3CN): δ 9.90 (s, 1H), 8.52 (d, J = 1.7 Hz, 1H), 8.48 – 8.38 (m, 3H), 8.28 – 7.86 (m, 14H), 7.79 – 7.46 (m, 15H), 7.43 – 7.28 (m, 5H), 7.13 – 7.07 (m, 1H), 6.96 – 6.87 (m, 4H), 6.71 (dd, J = 0.8, 5.9 Hz, 1H), 6.64 – 6.62 (m, 1H), 6.56 – 6.51 (m, 2H), 6.45 –

6.40 (m, 2H), 6.23 – 6.18 (m, 2H), 5.96 (t, *J* = 1.9 Hz, 1H), 4.96 – 4.76 (m, 2H), 4.68 – 4.62 (m, 3H), 4.52 – 4.21 (m, 7H), 4.14 – 3.95 (m, 2H), 1.27 (s, 18H). **^{13}C NMR** (600 MHz, CD_3CN): δ 160.8, 160.7, 159.4, 158.8, 158.1, 158.0, 157.8, 157.7, 157.6, 157.3, 156.1, 154.0, 152.5, 152.4, 152.2, 151.5, 150.5, 145.2, 143.8, 140.2, 139.1, 138.9, 138.7, 138.3, 138.2, 138.1, 137.7, 137.5, 137.3, 135.9, 132.3, 131.7, 131.2, 129.8, 129.4, 128.8, 128.6, 128.5, 128.4, 128.3, 128.0, 127.9, 127.2, 126.2, 126.1, 125.9, 125.8, 125.5, 125.2, 124.9, 124.8, 124.2, 123.9, 123.5, 123.1, 122.7, 122.3, 122.2, 115.1, 108.6, 108.3, 102.2, 73.8, 73.6, 72.8, 70.6, 70.0, 39.7, 35.8, 31.4. **HRMS (ESI+):** calcd for *m/z* = 784.7909 ($[M - 2PF_6]^{2+}$)/2, found *m/z* = 784.7934.

1,1',1'-[[4-(12-Bromododecyl)phenyl]methylidyne]tris[4-(*tert*-butyl)benzene] (III-3)

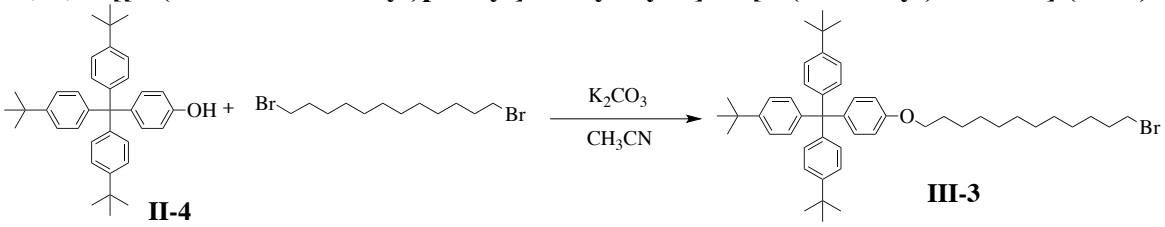

II-4 **III-3**

To a solution of **II-4** (1.5 g, 4.95 mmol, 1 eq), potassium carbonate (1.82 g, 14.85 mmol, 3 eq) and dibromododecane (4.84 g, 14.85 mmol, 3 eq) in CH_3CN (60 mL). The suspension was heated at reflux overnight. After cooling, the mixture was filtered and the filtrate was concentrated *in vacuo*. The crude product was purified by column chromatography (SiO_2, cyclohexane/DCM, 8:1, v/v), affording bromide **III-3** as a white solid(3.5 g, 95%).

^{1}H NMR ($CDCl_3$, 300 MHz): δ 7.25 – 7.19 (m, 6H), 7.11 – 7.03 (m, 8H), 6.78 – 6.72 (m, 2H), 3.91 (t, *J* = 6.5 Hz, 2H), 3.40 (t, *J* = 6.9 Hz, 2H), 1.90 – 1.69 (m, 4H), 1.46 – 1.36 (m, 4H), 1.31 – 1.24 (m, 39H). Analysis is in agreement with literature data.[3]

Alkyne III-4

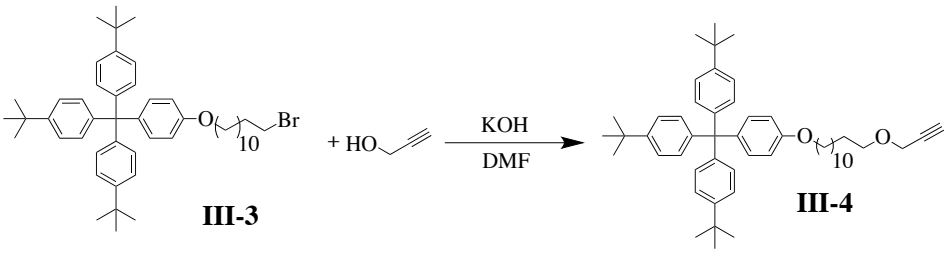

III-3 **III-4**

To a solution of **III-3** (1.0 g, 1.33 mmol, 1 eq) and prop-2-yn-1-ol (0.4 g, 6.66 mmol, 5 eq) in 30 mL of dry DMF, KOH (1.68 g, 30 mmol) was added. The temperature was gradually raised to 70 °C, after being stirred for 8 h, the mixture was subjected to H_2O/ethyl acetate. The organic layer was washed with water for 5 times, and further concentrated in vacuum. The crude product was purified by column chromatography (SiO_2, cyclohexane/DCM, 95:5, v/v), affording **III-4**

as a white solid(446 mg, 46%).

^{1}H NMR ($CDCl_3$, 300 MHz): δ 7.25 – 7.20 (m, 6H), 7.11 – 7.04 (m, 8H), 6.78 – 6.73 (m, 2H), 4.13 (d, *J* = 2.4 Hz, 2H), 3.92 (t, *J* = 6.5 Hz, 2H), 3.51 (t, *J* = 6.6 Hz, 2H), 2.41 (t, *J* = 2.4 Hz, 1H), 1.82 – 1.67 (m, 2H),1.64 – 1.57 (m, 2H), 1.37 – 1.23 (m, 43H). **^{13}C NMR** ($CDCl_3$, 300 MHz): δ 157.1, 148.4, 144.3, 139.5, 132.3, 130.9, 124.2, 113.1, 80.2, 77.4, 74.2, 70.5, 68.0, 63.2, 58.2, 34.4, 31.5, 29.7, 29.6, 29.5, 26.3, 26.2. **HRMS (ESI+):** calcd for *m/z* = 749.5268 ($[M + Na]^+$), found *m/z* = 749.5269.

Bromoalkyne T_4

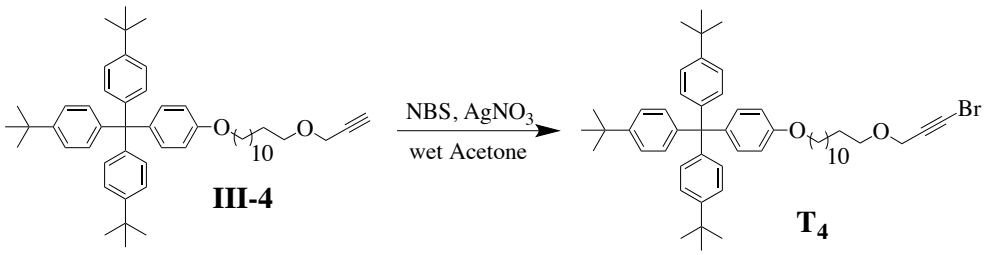

III-4 **T_4**

To a solution of **III-4** (200 mg, 0.28 mmol, 1 eq) in wet acetone (10 mL) was added NBS (59 mg, 0.34 mmol, 1.2 eq) and $AgNO_3$ (5 mg, 0.03 mmol, 0.1 eq). When the the reaction was completed after 1h, the mixture was diluted with water (40 mL), extracted with EtOAc (2 × 50 mL). The organic layer was dried with Na_2SO_4 and the solvent was removed to afford **T_4** as a white solid (199 mg, 90%).

^{1}H NMR ($CDCl_3$, 300 MHz): δ 7.25 – 7.20 (m, 6H), 7.11 – 7.04 (m, 8H), 6.78 – 6.72 (m, 2H), 4.15 (s, 2H), 3.92 (t, *J* = 6.4 Hz, 2H), 3.49 (t, *J* = 6.6 Hz, 2H), 1.81 – 1.70 (m, 2H),1.64 – 1.53 (m, 2H), 1.50 – 1.24 (m, 43H). **^{13}C NMR** ($CDCl_3$, 300 MHz): δ 156.9, 148.4, 148.3, 144.2, 144.0, 139.3, 132.3, 132.2, 130.7, 124.1, 124.0, 113.3, 112.9, 77.2, 70.5, 67.8, 63.1, 63.0, 59.0, 45.5, 34.3, 31.4, 29.6, 29.5, 29.4, 26.1. **MS (ESI+):** calcd for $C_{51}H_{40}N_2O_4$ *m/z* = 804.4, found *m/z* = 804.5.

1,1',1'-[[4-[(3-Bromo-2-propyn-1-yl)oxy]phenyl]methylidyne]tris[4-(*tert*-butyl)benzene] (T_5)

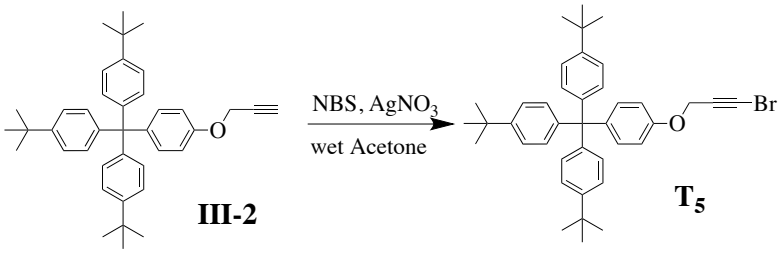

III-2 **T_5**

To a solution of **III-2** (300 mg, 0.55 mmol, 1 eq) in wet acetone (10 mL) was added NBS (117

mg, 0.66 mmol, 1.2 eq) and $AgNO_3$ (9 mg, 0.06 mmol, 0.1 eq). When the the reaction was completed after 1 h, the mixture was diluted with water (40 mL), extracted with EtOAc (2 × 50 mL). The organic layer was dried with Na_2SO_4 and the solvent was removed to afford **T_5** as a white solid (309 mg, 90%).

^{1}H NMR ($CDCl_3$, 300 MHz): δ 7.25 – 7.20 (m, 6H), 7.13 – 7.05 (m, 8H), 6.84 – 6.80 (m, 2H), 4.68 (s, 2H), 1.30 (s, 27H). Analysis is in agreement with literature data.[10]

Rotaxane M_9

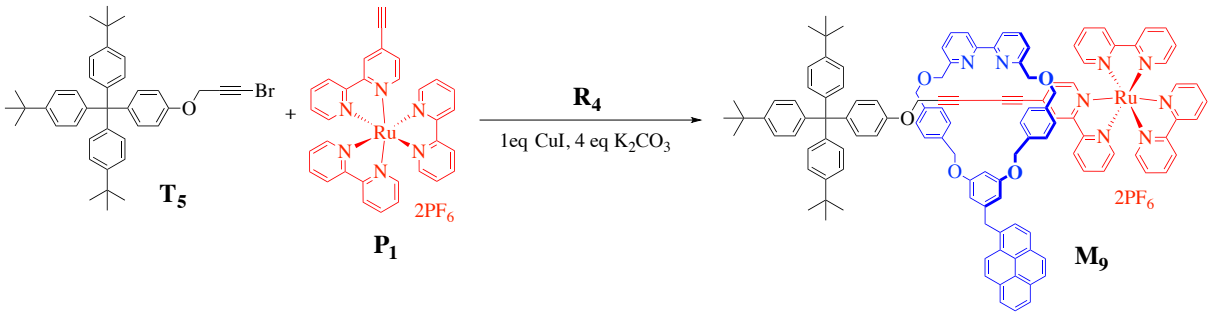

A solution of CuI (4.4 mg, 23 μmol, 1 eq) in CH_3CN (1.5 mL) was added to a solution of macrocycle **R_3** (14.7 mg, 23.0 μmol, 1 eq) in CH_2Cl_2 (1.5 mL) the mixture was stirred for 1 h at 20 °C. This mixture was then added to a mixture of alkyne **P_1** (22 mg, 23 μmol, 1 eq), bromoalkyne **T_5** (25 mg, 35 μmol, 1 eq), and K_2CO_3 (13 mg, 92 μmol, 4 eq) in CH_3CN (2 mL), degassed through freeze-pump-thaw cycles, flushed with nitrogen, and stirred at 60 °C for 3 d. After cooling to 20 °C, the reaction was quenched by the addition of KCN (20 mg, 0.30 mmol, in 1 mL H_2O), diluted with CH_2Cl_2 (1 mL), CH_3CN (1 mL), and stirred at 20 °C for 2 h. CH_2Cl_2 (10 mL) was added, the organic phase separated, washed with H_2O (10 mL), brine (10 mL), and the solvents were removed. The crude product was purified by flash column chromatography (SiO_2, petrol/DCM/MeOH = 75:75:1, v/v) to afford a crude red solid. The crude solid was further purified by column chromatography (SiO_2, acetonitrile/water /$KNO_{3\,(sat.\,aq.)}$ = 95:4.9:0.1, v/v/v), the product was collected and the solvent was removed. The solid was solubilized in small quantity of DCM and filtered with a syringe filter, the solution was collected and diluted with DCM (5 mL), and washed with sat. NH_4PF_6 aqueous solution, and dried over Na_2SO_4 and concentrated to obtain **M_9** as a red solid (yield = 20%).

^{1}H NMR (300 MHz, CD_3CN): δ 8.55 (dd, J = 3.7, 8.2 Hz, 2H), 8.42 – 8.28 (m, 4H), 8.25 – 8.15 (m, 5H), 8.14 – 7.96 (m, 8H), 7.88 – 7.76 (m, 3H), 7.74 - 7.60 (m, 6H), 7.56 (t, J = 7.7 Hz, 1H), 7.49 – 7.38 (m, 4H), 7.36 – 7.26 (m, 3H), 7.21 – 7.14 (m, 8H), 7.12 (s, 1H), 7.10 – 7.04 (m, 6H), 6.89 (d, J = 8.8 Hz, 2H), 6.83 – 6.71 (m, 5H), 6.58 (d, J = 7.9 Hz, 2H), 6.39 – 6.23 (m, 4H), 5.75 (t, J = 2.1 Hz, 1H), 5.34 (dd, J = 1.6, 5.8 Hz, 1H), 4.88 (s, 2H), 4.76 (s, 2H), 4.67 –

4.54 (m, 6H), 4.42 (s, 1H), 4.37 – 4.34 (m, 2H), 4.32 – 4.22 (m, 3H), 1.23 (s, 27H). **^{13}C NMR** (600 MHz, CD_3CN): δ 160.7, 159.0, 158.9, 158.4, 158.3, 158.2, 158.0, 157.3, 156.7, 156.4, 152.8, 152.2, 151.0, 149.8, 145.7, 145.4, 142.1, 139.7,139.4, 139.3, 139.1, 138.7, 137.8, 137.4, 135.6, 133.2, 132.8, 132.2, 131.6, 130.8, 130.4, 130.2, 130.0, 129.4, 129.3, 129.1, 129.0, 128.9, 128.8, 128.4, 128.3, 128.1, 127.7, 126.7, 126.6, 126.5, 126.2, 125.9, 125.8, 125.6, 125.1, 123.5, 123.4, 122.6, 115.1, 108.3, 108.0, 103.0, 84.2, 81.6, 74.8, 73.8, 72.8, 72.2, 71.7, 70.2, 70.0, 57.1, 55.7, 40.0, 35.3, 33.0, 31.9, 30.7, 23.8, 14.8. **HRMS (ESI+):** calcd for *m/z* = 939.3737 ($[M - 2PF_6]^{2+}$)/2, found *m/z* = 939.3709.

Thread Ru-complex B_2

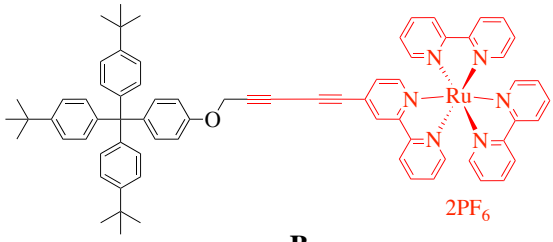

B_2

During the purification of rotaxane **M_9**, the thread **B_2** as a side product was yielded as a red solid (40%).

^{1}H NMR (300 MHz, CD_3CN): δ 8.53 – 8.42 (m, 5H), 8.09 – 8.00 (m, 5H), 7.75 – 7.65 (m, 6H), 7.42 – 7.33 (m, 6H), 7.33 – 7.27 (m, 6H), 7.21 – 7.08 (m, 8H), 6.78 – 6.72 (m, 2H), 4.92 (s, 2H), 1.64 (s, 27H). **^{13}C NMR** (600 MHz, CD_3CN): δ 158.4, 157.8, 153.0, 152.7, 152.6, 152.5, 149.4, 146.9, 145.6, 140.3, 139.0, 138.9, 132.6, 131.2, 130.2, 128.9, 128.6, 127.7, 125.5, 125.4, 125.3, 114.3, 71.4, 68.7, 59.1, 34.9, 31.5, 30.4, 30.3, 30.2, 30.1, 30.0, 29.9, 26.7. **HRMS (ESI+):** calcd for *m/z* = 567.2249 ($[M - 2PF_6]^{2+}$)/2, found *m/z* = 567.2290.

Rotaxane M_{10}

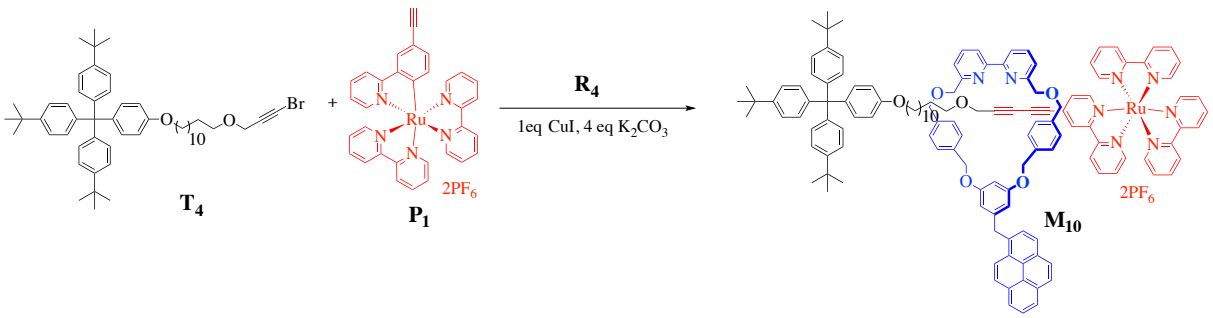

T_4 **P_1** **M_{10}**

To a solution of macrocycle **R_4** (14.7 mg, 23.0 µmol) in CH_2Cl_2 (1.5 mL) a solution of CuI (4.4 mg, 23 µmol) in CH_3CN (1.5 mL) was added and the mixture was stirred for 1 h at 20 °C. This mixture was then added to a mixture of alkyne **P_1** (22 mg, 23 µmol), bromoalkyne **T_4** (25 mg,

35 μmol), and K_2CO_3 (13 mg, 92 μmol) in CH_3CN (2 mL), degassed through freeze-pump-thaw cycles, flushed with nitrogen, and stirred at 60 °C for 3 d. After cooling to 20 °C, the reaction was quenched by the addition of KCN (20 mg, 0.30 mmol, in 1 mL H_2O), diluted with CH_2Cl_2 (1 mL), CH_3CN (1 mL), and stirred at 20 °C for 2 h. CH_2Cl_2 (10 mL) was added, the organic phase separated, washed with H_2O (10 mL), brine (10 mL), and the solvents were removed. The crude product was purified by flash column chromatography (SiO_2, petrol/DCM/MeOH = 75:75:1, v/v/v) to afford a crude red solid. The crude solid was further purified by column chromatography (SiO_2, acetonitrile/water /$KNO_{3\ (sat.\ aq.)}$ = 90:9.8:0.2, v/v/v), the product was collected and the solvent was removed. The solid was solubilized in small quantity of DCM and filtered with a syringe filter, the solution was collected and diluted with DCM (5 mL), and washed with sat. NH_4PF_6 aqueous solution, and dried over Na_2SO_4 and concentrated to obtain **M_{10}** as a red solid (yield = 20%).

^{1}H NMR (300 MHz, CD_3CN): δ 8.52 (dd, *J* = 3.6, 8.2 Hz, 2H), 8.39 – 8.28 (m, 3H), 8.27 – 8.17 (m, 4H), 8.16 – 8.11 (m, 4H), 8.10 – 8.01 (m, 3H), 7.96 (t, *J* = 7.9 Hz, 2H), 7.92 – 7.85 (m, 2H), 7.70 – 7.64 (m, 2H), 7.64 – 7.55 (m, 5H), 7.45 – 7.32 (m, 6H), 7.29 – 7.21 (m, 7H), 7.16 – 7.04 (m, 9H), 6.86 – 6.76 (m, 4H), 6.74 – 6.67 (m, 3H), 6.61 (d, *J* = 8.0 Hz, 2H), 6.41 – 6.25 (m, 4H), 5.73 (t, *J* = 2.6 Hz, 1H), 5.41 (dd, *J* = 1.7, 5.9 Hz, 1H), 4.82 – 4.70 (m, 2H), 4.63 (d, *J* = 3.4 Hz, 1H), 4.58 (d, *J* = 3.0 Hz, 1H), 4.52 (s, 2H), 4.50 – 4.41 (m, 2H), 4.39 – 4.31 (m, 3H), 4.28 – 4.22 (m, 3H), 3.81 (t, *J* = 6.5 Hz, 2H), 3.38 (t, *J* = 6.7 Hz, 2H), 1.64 -0.80 (m, 47H).

^{13}C NMR (600 MHz, CD_3CN): δ 159.4, 159.3, 157.6, 157.1, 157.0, 156.9, 156.8, 156.7, 156.0, 155.4, 151.5, 151.4, 150.9, 149.8, 148.4, 144.6, 144.0, 139.3, 138.3, 138.1, 138.0, 137.9, 137.8, 137.7, 137.3, 136.5, 136.1, 134.2, 131.6, 131.4, 131.2, 130.8, 130.3, 130.2, 129.8, 129.0, 128.9, 128.7, 128.6, 128.0, 127.9, 127.8, 127.7, 127.6, 127.5, 127.0, 126.9, 126.7, 126.3, 125.3, 125.1, 124.9, 124.6, 124.5, 124.4, 124.2, 123.7, 122.1, 122.0, 121.3, 121.2, 113.3, 107.0, 106.7, 101.7, 84.8, 80.6, 72.8, 72.4, 71.4, 70.9, 70.3, 69.2, 68.9, 68.6, 67.7, 63.0, 58.1, 54.3, 38.6, 33.9, 30.6, 29.9, 29.2, 29.1, 29.0, 28.9, 28.8, 25.7, 25.6. **HRMS (ESI+):** calcd for *m/z* = 1031.4651 ([M – $2PF_6$]$^{2+}$)/2, found *m/z* = 1031.4683.

Thread Ru-complex B_3

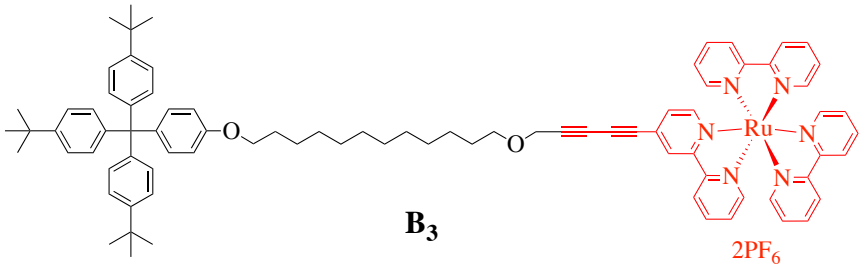

B_3

During the purification of rotaxane **M_{10}**, the thread **B_3** as a side product was yielded as a red solid (50%).

^{1}H NMR (300 MHz, CD_3CN): δ 8.56 (dd, *J* = 0.8, 1.8 Hz, 1H), 8.51 – 8.44 (m, 5H), 8.09 – 8.00 (m, 5H), 7.74 – 7.65 (m, 2H), 7.42 – 7.33 (m, 6H), 7.33 – 7.27 (m, 6H), 7.19 – 7.08 (m, 8H), 6.78 – 6.72 (m, 2H), 4.30 (s, 2H), 3.88 (t, *J* = 6.5 Hz, 2H), 3.50 (t, *J* = 6.4 Hz, 2H), 1.64 - 0.80 (m, 47H). **^{13}C NMR** (600 MHz, CD_3CN): δ 158.4, 157.8, 153.0, 152.7, 152.6, 152.5, 149.4, 146.9, 145.6, 140.3, 139.0, 138.9, 132.6, 131.2, 130.2, 128.9, 128.6, 127.7, 125.5, 125.4, 125.3, 114.3, 71.4, 68.7, 59.1, 34.9, 31.5, 30.4, 30.3, 30.2, 30.1, 30.0, 29.9, 26.7. **HRMS (ESI+):** calcd for *m/z* = 659.3157 ($[M - 2PF_6]^{2+}$)/2, found *m/z* = 659.3173.

Ruthenium (bipyridine)$_2$-(5-bromo-phenanthroline) hexafluorophosphate (P_2)

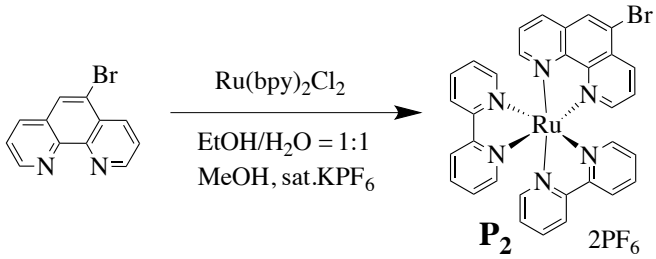

P_2

To a solution of Ru(bipyridine)$_2$Cl$_2$ (200 mg, 0.38 mmol, 1 eq) in 1:1 EtOH/H_2O (20 mL) at room temperature, 5-bromo-phenanthroline (100 mg, 0.38 mmol, 1 eq) was added. The solution was heated overnight under nitrogen atmosphere at 90 °C. The reaction mixture was allowed to reach room temperature and the solvent was evaporated. The mixture was redissolved in DCM (30 mL), and washed with sat. KPF_6 solution, the organic layer was dried over Na_2SO4 and the solvent was removed. The crude product was purified by column chromatography (SiO_2, acetonitrile/water /$KNO_{3\ (sat.\ aq.)}$ = 95:4.9:0.1, v/v/v), the product was collected and the solvent was removed. The solid was solubilized in small quantity of DCM and filtered with a syringe filter, the solution was collected and diluted with DCM (5 mL), and washed with sat. NH_4PF_6 aqueous solution, and dried over Na_2SO_4 and concentrated to obtain the Ru^{2+} complex stopper **P_2**, as a red solid (818 mg, 85% yield).

^{1}H NMR (300 MHz, CD_3CN): δ 8.81 (dd, *J* = 1.2, 8.6 Hz, 1H), 8.63 (s, 1H), 8.55 – 8.46 (m, 5H), 8.15 – 8.06 (m, 4H), 8.03 – 7.96 (m, 2H), 7.85 – 7.78 (m, 3H), 7.73 (dd, *J* =5.2, 8.2 Hz, 1H), 7.55 – 7.49 (m, 2H), 7.47 – 7.41 (m, 2H), 7.25 – 7.18 (m, 2H). Analysis is in agreement with literature data.[11]

3,5-Bisethynyl-*tert*-butylbenzene (IV-2)

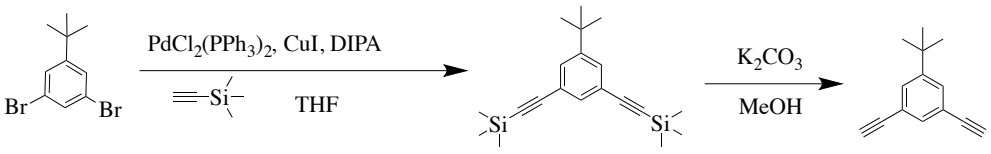

IV-1 **IV-2**

To a mixture of 3,5-dibromo-*tert*-butylbenzene (2 g, 6.90 mmol, 1 eq), $Pd(PPh_3)_4$ (399 mg, 0.34 mmol, 0.05 eq), copper iodide (40 mg, 0.21 mmol, 0.03 eq), nitrogen-degassed dry THF (40 mL), TEA (10 mL) and (trimethylsilyl)acetylene (2.029 g, 20.70 mmol, 3 eq) were added under nitrogen atmosphere. The reaction mixture was stirred at room temperature for 14 hours, then heated at reflux for 3 hours. The reaction mixture concentrated and redissolved in DCM (40 mL), washed with water (40 mL) and sat. NaCl (40 mL), the combined extracts were dried over Na_2SO_4 and concentrated. The crude product was purified by column chromatography (SiO_2, hexane), as a yellow oil (2.025 g, 90%).

The oil (2.025 g, 6.21 mmol, 1 eq) was dissolved in CH_3OH (15 mL), to which was added K_2CO_3 (1.028 g, 7.45 mmol, 1.2 eq) at room temperature. After 16 h, the reaction mixture was quenched with H_2O (30 mL) and the organic solvent evaporated under vacuum. The residue was extracted with CH_2Cl_2 (3 × 30 mL), and the organic layers washed with brine, dried over $MgSO_4$ and concentrated. The crude product was purified by column chromatography (SiO_2, hexane) to yield bisethynyl **IV-2**, as a yellow oil (679 mg, 60%).

^{1}H NMR (300 MHz, $CDCl_3$): δ 7.50 (d, *J* = 1.5 Hz, 2H), 7.44 (t, *J* = 1.5 Hz, 1H), 3.06 (s, 2H), 1.30 (s, 9H). Analysis is in agreement with literature data.[12]

4-[3-Bromo-5-(*tert*-butyl)phenyl]-2-methyl-3-butyn-2-ol (IV-3)

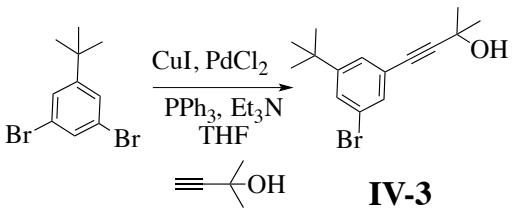

IV-3

To a dry 100 mL round bottomed flask with stirrer bar, 1-*tert*-butyl-3,5- dibromobenzene (5.00 g, 17.2 mmol, 1 eq), copper iodide (164 mg, 0.86 mmol, 0.05 eq), palladium chloride (92 mg,

0.62 mmol, 0.04 eq) and triphenylphosphine (270 mg, 1.03 mmol, 0.06 eq) were added followed by a solution of tetrahydrofuran (45 mL) and triethylamine (15 mL). The brown solution was stirred at room remperature for 5 mins before being treated with 2-methyl-3-butyn-2-ol (1.67 mL, 17.2 mmol, 1eq), the solution immediately turned black. The reaction stirred at 70 °C for 16 h. The mixture was concentrated, redissolved in DCM (50 mL) and was washed with water (150 mL) and then brine (150 mL), dried over Na_2SO_4 and reduced in vacuo. The crude product was purified by flash column chromatography (SiO_2, cyclohexane/EtOAc = 1:1, v/v), yielded **IV-3** as a black oil (1.5 g, yield = 29.6%).

^{1}H NMR (300 MHz, $CDCl_3$): δ 7.45 (t, *J* = 1.8 Hz, 1H), 7.38 (t, *J* = 1.4 Hz, 1H), 7.35 (t, *J* = 1.6 Hz, 1H), 1.98 (br, 1H), 1.62 (s, 6H), 1.29 (s, 9H). Analysis is in agreement with literature data.[13]

1-Bromo-3-(*tert*-butyl)-5-ethynylbenzene (IV-4)

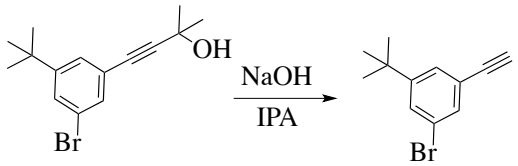

IV-3 **IV-4**

To a 100 mL round bottomed flask with stirrer bar, alcohol **IV-3** (1 g, 3.40 mmol, 1eq), finely powdered sodium hydroxide (1.4 g, 34.0 mmol, 10 eq) was added followed by a solution of 2-propanol (50 mL). the mixture was heated at 90 °C for 1 h before being cooled to room temperature, diluted with CH_2Cl_2 and washed with water (50 mL). The organic extract was dried over Na_2SO_4 and reduced *in vacuo*. The crude product was purified by column chromatography (SiO_2, hexane), yielded acetylene **IV-4** as a black oil (642 mg, yield = 80%).

^{1}H NMR (300 MHz, $CDCl_3$): δ 7.50 (t, *J* = 1.8 Hz, 1H), 7.45 (t, *J* = 1.5 Hz, 1H), 7.43 (t, *J* = 1.6 Hz, 1H), 3.08 (s, 1H), 1.30 (s, 9H). Analysis is in agreement with literature data.[13]

1-Bromo-3-*tert*-butyl-5-[(2-trisisopropylsilyl)ethynyl]benzene (IV-5)

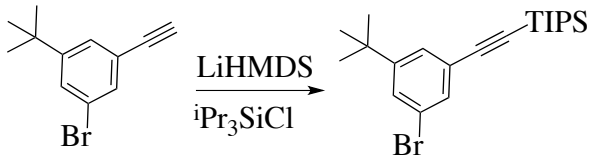

IV-4 **IV-5**

To a 100 mL two-neck round flask, acetylene **IV-4** (292 mg, 1.24 mmol, 1 eq) and THF (40 mL) were added, the temperature was cooled to -78 °C. The colorless solution was treated with

LiHMDS (1.33 mL, 1.0 M solution in THF, 1.24 mmol, 1.4 eq) and stirred at -78 °C for 25 minutes before *i*Pr_3SiCl (0.37 mL, 1.24 mmol, 1.4 eq) was added. The pale yellow solution was stirred for a 25 min before being warmed to 25 °C followed by further stirring for 2 h. The mixture was diluted with EtOAc (30 ml) and washed with an NH_4Cl(aq) solution (50 mL), water (50 mL) and brine (50 mL). The organic extracts were dried over Na_2SO_4 and reduced *in vacuo*. The crude product was purified by column chromatography (SiO_2, hexane) to give bromobenzene **IV-5** as a yellow oil (462 mg, 95%).

^{1}H NMR (300 MHz, $CDCl_3$): δ 7.45 (t, *J* = 1.8 Hz, 1H), 7.43 (t, *J* = 1.5 Hz, 1H), 7.37 (t, *J* = 1.6 Hz, 1H), 1.30 (s, 9H), 1.13 (s, 21H). Analysis is in agreement with literature data.[13]

1-Azido-3-*tert*-butyl-5-[(2-trisisopropylsilyl)ethynyl]benzene (IV-6)

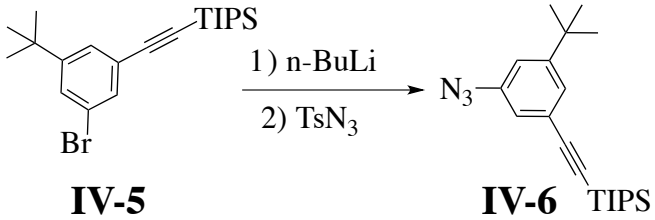

IV-5 **IV-6**

To a 100 mL two-neck round flask, bromobenzene **IV-5** (215 mg, 0.55 mmol, 1 eq) was dissolved in THF (30 mL), and cooled to -78 °C. The colourless solution was treated with 2.5 M n-BuLi in hexane (0.70 mL, 1.64 mmol, 3 eq) and stirred at -78 °C for 25 minutes before a solution of tosyl azide (324 mg, 1.64 mmol, 3 eq) in THF (5 mL) was added over a 2 min period. The deep red solution was stirred for a 25 min before being warmed to 25 °C followed by further stirring for 16 h. The mixture was poured onto water (50 mL) and extracted with Et_2O (2 × 50 mL). The organic extracts were combined, washed with water (60 mL) and brine (60 mL) then dried over Na_2SO_4 and reduced *in vacuo*. The crude product was purified by column chromatography (SiO_2, hexane) to yield azide **IV-6**, as a yellow oil (346 mg, 76%).

^{1}H NMR (300 MHz, $CDCl_3$): δ 7.24 (t, *J* = 1.5 Hz, 1H), 6.96 (d, *J* = 1.5 Hz, 2H), 1.30 (s, 9H), 1.14 (s, 21H). Analysis is in agreement with literature data.[13]

Rotaxane-alkyne IV-7

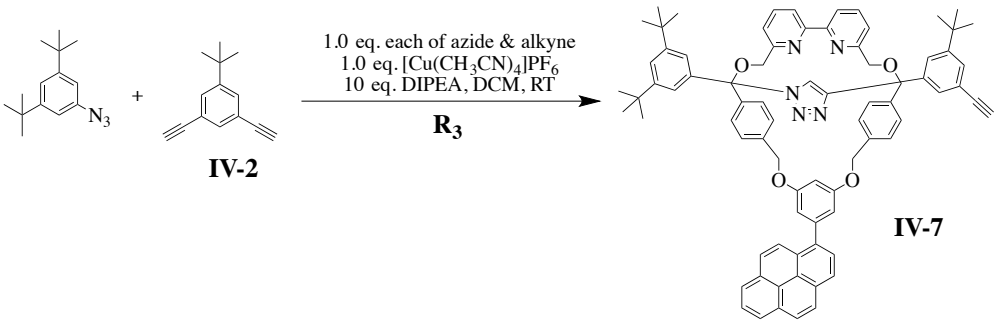

A CEM vial was charged with macrocycle **R_3** (83.0 mg, 0.113 mmol, 1 eq), $[Cu(MeCN)_4](PF_6)$ (42.2 mg, 0.108 mmol, 0.96 eq), 1,3-di-*tert*-butyl-5-azidobenzene (26.2 mg, 0.113 mmol, 1.0 eq) and dialkyne **IV-2** (20.7 mg, 0.113 mmol, 1.0 eq), in 1:1 EtOH/DCM (3.2 mL). A solution of DIPEA (198 μL, 1.130 mmol, 10 eq) was added to the reaction mixture. The deep red solution was stirred overnight at room temperature. The reaction mixture was then diluted with DCM (40 mL) and washed with EDTA/NH_4OH(aq) (50 mL). The aqueous layer was extracted with dichloromethane (2 × 40 mL), the combined organic layer was washed with water (50 mL) and brine (50 mL). The organic layer was dried with Na_2SO_4 and the solvent was removed. The crude product was purified by flash column chromatography (SiO_2, petrol/DCM/MeOH = 75:75:1, v/v) and gel permeation chromatography (GPC) to afford [2]rotaxane **IV-7** (84.0 mg) as a light yellow solid (yield = 65%).

^{1}H NMR (300 MHz, $CDCl_3$): δ 10.24 (s, 1H), 8.47 (d, J = 9.5 Hz, 1H), 8.29 – 8.18 (m, 3H), 8.16 – 8.08 (m, 4H), 8.03 (t, *J* = 7.6 Hz, 1H), 7.84 (t, *J* = 2.2 Hz, 1H), 7.78 (t, *J* = 7.7 Hz, 2H), 7.72 – 7.64 (m, 4H), 7.54 (d, *J* = 1.6 Hz, 2H), 7.46 (d, *J* = 7.4 Hz, 2H), 7.29 – 7.23 (m, 2H), 7.05 (d, *J* = 7.9 Hz, 4H), 6.96 (d, *J* = 2.2 Hz, 2H), 6.78 (d, *J* = 8.0 Hz, 4H), 5.26 – 5,14 (m, 4H), 4.38 (s, 4H), 4.13 – 4.02 (m, 4H), 2.96 (s, 1H), 1.14 (s, 18H), 1.00 (s, 9H). **^{13}C NMR** (600 MHz, $CDCl_3$): δ 160.8, 159.3, 156.0, 151.5, 150.9, 145.5, 142.6, 138.2, 137.3, 137.0, 135.7, 131.9, 131.5, 131.1, 130.6, 128.6, 127.5, 127.4, 127.3, 127.1, 127.0, 126.4, 126.0, 125.9, 125.0, 124.8, 124.6, 124.3, 121.0, 120.8, 120.5, 114.8, 110.1, 103.9, 84.5, 77.3, 76.1, 72.7, 71.2, 70.5, 35.0, 34.5, 31.3, 31.2, 31.0, 29.7. **HRMS (ESI+):** calcd for *m/z* = 1144.5711 ($[M + Na]^+$), found *m/z* = 1144.5750 ($[M + Na]^+$).

REET [2]Rotaxane M_{11}

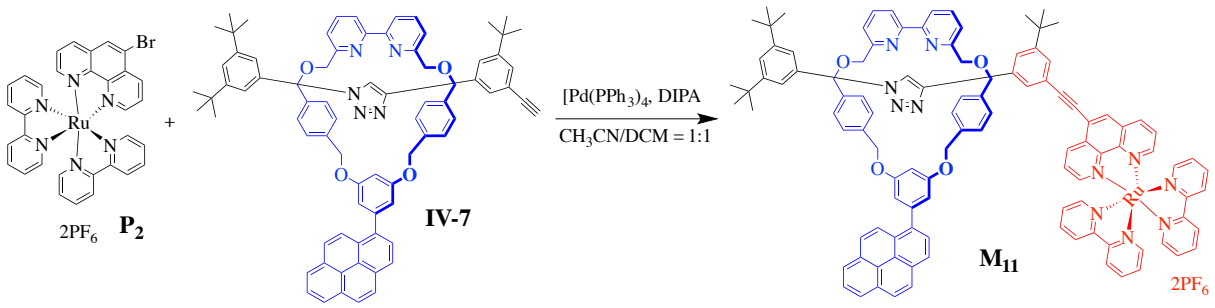

To a mixture of rotaxane-alkyne **IV-7** (15 mg, 0.013 mmol, 1 eq), ruthenium (bipyridine)2-(5-bromo-phenanthroline) hexafluorophosphate (13 mg, 0.013 mmol, 1 eq), $Pd(PPh_3)_4$ (0.7 mg, 0.65 μmol, 0.05 eq), nitrogen-degassed 1:1 DCM/CH_3CN (40 mL) and DIPA (15 μL) were added under nitrogen atmosphere. The reaction mixture was stirred at room temperature for 14 hours. The reaction mixture was diluted with DCM (20 mL), washed with water (20 mL) and sat. NaCl (20 mL), the combined extracts were dried over Na_2SO_4 and concentrated. The crude product was purified by gel permeation chromatography (GPC) yielded a red solid. The solid was dissolved in DCM (5 mL), and washed with sat. NH_4PF_6 aqueous solution, and dried over Na_2SO_4 and concentrated to obtain [2]rotaxane **M_{11}** (18 mg) as a red solid (yield = 70%).

^{1}H NMR (300 MHz, $CDCl_3$): δ 10.44 (s, 1H), 8.84 (dd, *J* = 1.2, 8.4 Hz, 1H), 8.57 – 8.42 (m, 4H), 8.28 (d, *J* = 9.3 Hz, 1H), 8.24 (dd, *J* = 1.2, 8.5 Hz, 1H), 8.21 – 8.17 (m, 2H), 8.14 – 8.01 (m, 6H), 8.00 – 7.92 (m, 8H), 7.88 – 7.77 (m, 7H), 7.68 – 7.63 (m, 2H), 7.61 (d, *J* = 1.7 Hz, 2H), 7.55 – 7.48 (m, 4H), 7.47 – 7.40 (m, 4H), 7.37 (t, J = 1.7 Hz, 1H), 7.23 – 7.14 (m, 2H), 7.06 – 6.99 (m, 4H), 6.94 – 6.91 (m, 1H), 6.87 – 6.85 (m, 1H), 6.76 (dd, *J* = 2.4, 8.2 Hz, 4H), 5.15 (d, *J* = 2.8 Hz, 4H), 4.40 – 4.26 (m, 4H), 4.14 – 4.00 (m, 4H), 1.13 (s, 18H), 1.04 (s, 9H).

^{13}C NMR (600 MHz, $CDCl_3$): δ 161.7, 161.6, 159.9, 158.1, 157.9, 157.0, 153.7, 153.6, 152.9, 152.8, 152.7, 148.4, 148.0, 145.9, 143.5, 138.8, 138.7, 138.6, 138.2, 137.8, 137.7, 137.1, 136.2, 133.4, 132.3, 131.8, 131.5, 131.4, 131.3, 129.1, 128.5, 128.4, 128.3, 128.2, 128.0, 127.9, 127.4, 127.3., 127.2, 127.1, 126.3, 126.2, 125.9, 125.8, 125.5, 125.4, 125.2, 125.1, 124.0, 122.8, 122.4, 122.3, 122.1, 121.8, 115.6, 111.1, 111.0, 104.7, 99.5, 84.2, 73.2, 72.3, 72.2, 71.1, 55.2, 35.6, 35.3, 31.4, 31.1. **HRMS (ESI+):** calcd for *m/z* = 867.8300 $([M - 2PF_6]^{2+})/2$, found *m/z* = 867.8319.

Ruthenium (bpy)$_2$-(5-phenylethynyl-1,10-phenanthroline) hexafluorophosphate (B_4)

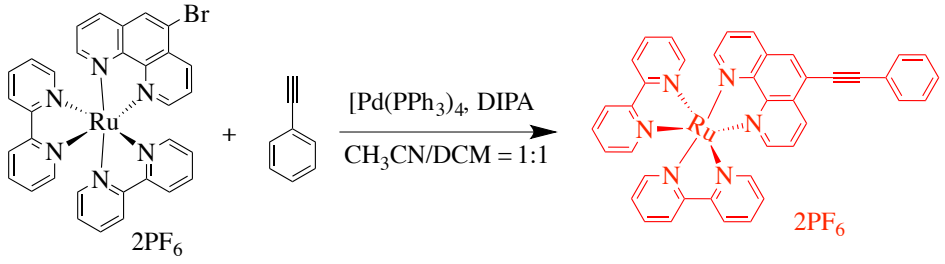

P_2 **B_4**

To a mixture of phenylacetylene (9.7 mg, 0.095 mmol, 2 eq), ruthenium (II) bis(bipyridine)-(5-bromo-1,10-phenanthroline) hexafluorophosphate **P_2** (39.0 mg, 0.048 mmol, 1 eq), $Pd(PPh_3)_4$ (2.8 mg, 2.38 μmol, 0.05 eq), nitrogen-degassed 1:1 DCM/CH_3CN (20 mL) and DIPA (15 μL) were added under nitrogen atmosphere. The reaction mixture was stirred at room temperature for 14 hours. The reaction mixture was diluted with DCM (20 mL), washed with water (20 mL) and sat. NaCl (20 mL), the combined extracts were dried over Na_2SO_4 and concentrated. The crude product was purified by gel permeation chromatography (GPC) yielded a red solid. The solid was dissolved in DCM (5 mL), and washed with sat. NH_4PF_6 aqueous solution, and dried over Na_2SO_4 and concentrated to give **B_4** (18 mg) as a red solid (yield = 70%).

^{1}H NMR (300 MHz, $CDCl_3$): δ 9.02 (dd, *J* = 1.3, 8.4 Hz, 1H), 8.62 – 8.50 (m, 5H), 8.49 (s, 1H), 8.17 – 8.07 (m, 4H), 8.00 (dddd, 2H), 7.87 – 7.72 (m, 6H), 7.57 (dddd, 2H), 7.54 – 7.49 (m, 3H), 7.45 (ddt, 2H), 7.23 (dddd, 2H). **^{13}C NMR** (600 MHz, $CDCl_3$): δ 158.2, 157.9, 154.0, 153.9, 153.0, 152.9, 148.6, 148.3, 138.9, 138.7, 137.5, 136.4, 132.9, 132.4, 131.7, 131.5, 130.8, 129.9, 128.5, 128.4, 127.5, 125.3., 125.2, 122.6, 98.4, 84.9. **HRMS (ESI+):** calcd for *m/z* = 347.0703 ($[M - 2PF_6]^{2+}$)/2, found *m/z* = 347.0713.

Rotaxane-alkyne IV-8

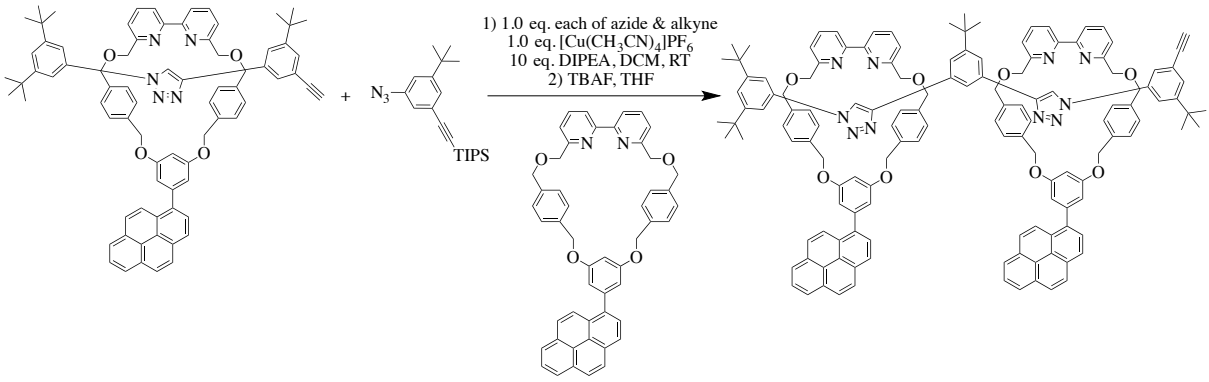

A CEM vial was charged with macrocycle **R_3** (33.2 mg, 0.046 mmol, 1 eq), $[Cu(MeCN)_4](PF_6)$ (16.2 mg, 0.045 mmol, 0.96 eq), azide **IV-6** (16.2 mg, 0.046 mmol, 1.0 eq) and rotaxane-alkyne

M_{11} (52.2 mg, 0.046 mmol, 1.0 eq), in 1:1 EtOH/DCM (3.2 mL). A solution of DIPEA (27 µL, 0.460 mmol, 10 eq) was added to the reaction mixture. The deep red solution was stirred overnight at room temperature. The reaction mixture was then diluted with DCM (40 mL) and washed with EDTA/NH_4OH(aq) (50 mL). The aqueous layer was extracted with dichloromethane (2 × 40 mL), the combined organic layer was washed with water (50 mL) and brine (50 mL). The organic layer was dried with Na_2SO_4 and the solvent was removed. The residue was dissolved in THF (2.5 mL) and n-Bu_4NF (1.0 M, 2 eq) was added. The mixture was stirred at room temperature for 2 h. Sat. aqueous NH_4Cl solution (20 mL) was added and extracted with DCM (2 × 30 mL). The organic layer was dried with Na_2SO_4 and the solvent was removed. The crude product was purified by flash column chromatography (SiO_2, petrol/DCM/MeOH = 75:75:1, v/v) and gel permeation chromatography (GPC) to afford [2]rotaxane alkyne **IV-8** (10.0 mg) as a light yellow solid (yield = 10.6%).

^{1}H NMR (300 MHz, $CDCl_3$): δ 10.33 (s, 1H), 10.07 (s, 1H), 8.55 (t, J = 1.6 Hz, 1H), 8.47 (dd, J = 4.6, 9.3 Hz, 2H), 8.27 – 7.96 (m, 20H), 7.80 – 7.39 (m, 19H), 7.23 – 7.17 (m, 3H), 7.12 – 7.07 (m, 4H), 7.05 – 7.00 (m, 4H), 6.99 (d, J = 2.2 Hz, 2H), 6.93 (d, J = 2.2 Hz, 2H), 6.92 – 6.88 (m, 4H), 6.84 – 6.79 (m, 4H), 5.31 (s, 2H), 5.27 (s, 2H), 5.08 – 4.95 (m, 4H), 4.52 – 4.36 (m, 8H), 4.32 – 4.22 (m, 4H), 4.18 (s, 4H), 2.89 (s, 1H), 1.11 (s, 18H), 0.94 (s, 9H), 0.85 (s, 9H). **^{13}C NMR** (600 MHz, $CDCl_3$): δ 158.8, 158.3, 158.2, 157.7, 156.6, 155.8, 154.3, 153.3, 153.0, 152.8, 152.5, 152.3, 152.0, 150.9, 149.6, 148.8, 148.5, 148.4, 145.7, 144.1, 140.4, 139.8, 139.5, 139.3, 139.2, 139.0, 138.7, 138.5, 138.4, 138.3, 138.2, 136.8, 132.9, 132.5, 131.7, 131.3, 131.1, 130.0, 129.9, 129.8, 129.4, 128.8, 128.7, 128.6, 128.3, 128.2, 128.0, 127.7, 127.5, 127.4, 126.3, 126.2, 126.1, 125.4, 125.2, 125.0, 124.6, 124.5, 124.1, 123.8, 123.7, 124.2, 121.8, 120.9, 115.4, 114.3, 74.8, 74.1, 74.0, 71.7, 71.5, 71.4, 68.4, 63.9, 50.8, 34.9, 31.5, 30.5, 30.3, 30.0, 29.8, 29.7, 29.6, 29.5, 26.8, 26.5. **HRMS (ESI+):** calcd for *m/z* = 2074.9715 $[M + H]^+$, found *m/z* = 2074.9766.

REET [3]rotaxane M_{12}

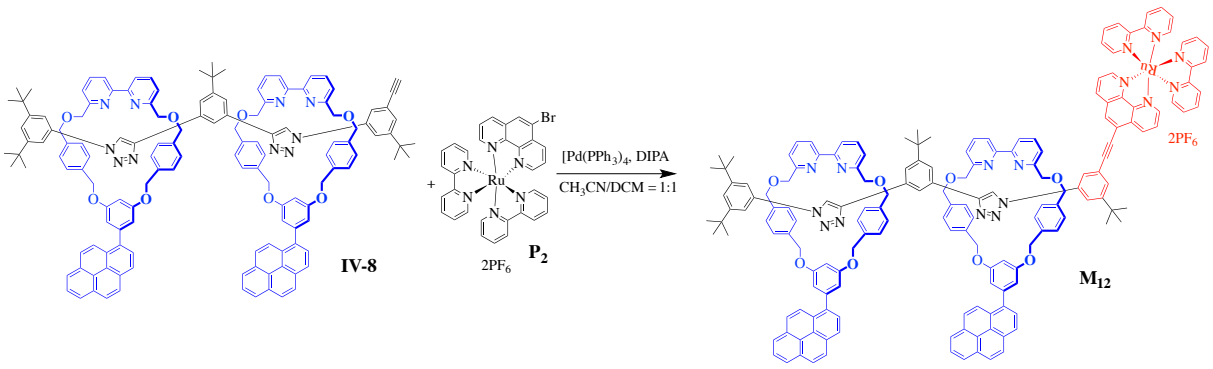

To a mixture of rotaxane-alkyne **IV-8** (10.0 mg, 4.82 μmol, 1 eq), ruthenium (II) bis(bipyridine)-(5-bromo-phenanthroline) hexafluorophosphate **P_2** (4.6 mg, 4.82 μmol, 1 eq), $Pd(PPh_3)_4$ (1.0 mg, 0.24 μmol, 0.05 eq), nitrogen-degassed 1:1 DCM/CH_3CN (40 mL) and DIPA (9 μL) were added under nitrogen atmosphere. The reaction mixture was stirred at room temperature for 14 hours. The reaction mixture was diluted with DCM (20 mL), washed with water (20 mL) and sat. NaCl (20 mL), the combined extracts were dried over Na_2SO_4 and concentrated. The crude product was purified by gel permeation chromatography (GPC) yielded a red solid. The solid was dissolved in DCM (5 mL), and washed with sat. NH_4PF_6 aqueous solution, and dried over Na_2SO_4 and concentrated to obtain rotaxane **M_{12}** (8.5 mg) as a red solid (yield = 60%).

^{1}H NMR (600 MHz, CD_3CN): δ 10.44 (s, 2H), 8.81 (d, *J* = 4.2 Hz, 1H), 8.60 (d, *J* = 0.8 Hz, 1H), 8.51 (d, *J* = 4.1 Hz, 1H), 8.46 (d, *J* = 4.1 Hz, 1H), 8.37 – 8.30 (m, 3H), 8.24 – 8.15 (m, 5H), 8.10 – 8.03 (m, 4H), 8.02 – 7.94 (m, 9H), 7.93 (t, *J* = 1.1 Hz, 1H), 7.92 – 7.90 (m, 2H), 7.89 (t, *J* = 0.7 Hz, 1H), 7.88 – 7.82 (m, 7H), 7.81 – 7.74 (m, 8H), 7.66 (d, *J* = 0.9 Hz, 2H), 7.57 – 7.56 (m, 1H), 7.51 (t, *J* = 1.1 Hz, 1H), 7.48 – 7.41 (m, 9H), 7.40 (t, *J* = 0.8 Hz, 1H), 7.38 – 7.33 (m, 2H), 7.15 – 7.02 (m, 11H), 6.94 – 6.91 (m, 3H), 6.86 – 6.79 (m, 10H), 5.38 (t, *J* = 6.8 Hz, 2H), 5.21 (d, *J* = 6.5 Hz, 2H), 5.10 – 5.04 (m, 3H), 4.99 (d, *J* = 6.6 Hz, 1H), 4.45 (dd, *J* = 1.8, 6.4 Hz, 2H), 4.41 – 4.36 (m, 4H), 4.31 (dd, *J* = 0.9, 6.4 Hz, 2H), 4.19 (s, 2H), 4.14 (d, *J* = 0.9 Hz, 2H), 4.12 – 4.05 (m, 4H), 1.13 (s, 27H), 1.10 (s, 9H), 1.03 (s, 9H). **^{13}C NMR** (600 MHz, CD_3CN): δ 160.1, 159.1, 158.4, 158.3, 158.2, 157.8, 156.5, 154.2, 153.1, 153.0, 152.7, 152.6, 152.4, 152.1, 150.7, 149.4, 148.9, 148.7, 148.6, 145.5, 144.3, 140.3, 139.7, 139.6, 139.4, 139.1, 139.0, 138.7, 138.6, 138.5, 138.3, 138.2, 136.3, 132.6, 132.5, 131.9, 131.5, 131.1, 130.0, 129.9, 129.7, 129.2, 128.9, 128.8, 128.7, 128.5, 128.4, 128.1, 128.0, 127.9, 127.6, 127.4, 126.3, 126.2, 126.1, 125.9, 125.6, 125.4, 125.2, 125.0, 124.6, 124.2, 124.1, 124.0, 123.8, 123.7, 123.2, 121.8, 120.8, 115.4, 114.2, 74.8, 74.1, 74.0, 71.7, 71.5, 71.4, 68.4, 63.9, 50.8, 34.9, 31.5, 30.5, 30.3, 30.0, 29.8, 29.7, 29.6, 29.5, 26.8, 26.5. **HRMS (ESI+):** calcd for *m/z* = 1333.0301 ($[M - 2PF_6]^{2+}$)/2, found *m/z* = 1333.0345.

6.10 Single crystal X-ray crystallographic information

The crystal of compound **R_4** was mounted on a short glass fibre attached to a tapered copper pin. A full hemisphere of data was collected on a Brüker Nonius Kappa diffractometer fitted with a CCD based detector using MoKα radiation (0.71073 Å). The structure was solved by direct methods, completed by subsequent Fourier syntheses and refined with full-matrix least-squares methods against $|F^2|$ data. All non-hydrogen atoms were refined anisotropically. All hydrogen atoms were treated as idealized contributions. A summary of crystal data collection, solution and structure refinement parameters are listed in Table 6-2.

Table 6-2 A summary of crystal data collection of compound **R_4**

Compound	**R_4**
Formula	C51 H40 N2 O4
Formula weight	744.85
Space group Crystal system	monoclinic
Space group	P 2_1
Cell measurement temperature (K)	293(2)
Cell length a (Å)	12.2254 (10)
Cell length b (Å)	22.067 (2)
Cell length c (Å)	13.8371 (10)
Cell angle alpha (°)	90
Cell angle beta (°)	95.357 (10)
Cell angle gamma (°)	90
Cell volume	3716.64(5)
Cell formula units (Z)	4
Crystal density ρ ($g.cm^{-3}$)	1.331
Absorption coefficient μ (mm^{-1})	0.664
F (000)	1568
Index ranges	-15 <=h<=14, -27<=k<=27, 16<=l<=16
Reflections collected	28722

References

[1] Ishida H., Tobita S., Hasegawa Y., Katoh R., Nozaki K. Recent Advances in Instrumentation for Absolute Emission Quantum Yield Measurements. Coord. Chem. Rev. 254, 2449-2458, 2010.

[2] Gibson H. W., Lee S. H., Engen P. T., Lecavalier P., Sze J., Shen Y. X., Bheda M. New Triarylmethyl Derivatives, Blocking Groups for Rotaxanes and Polyrotaxanes. J. Org. Chem. 1993, 58, 3748-3756.

[3] Li H.-G., Wang G.-W. Liquid-Assisted One-Pot Mechanosynthesis and Properties of Neutral Donor-Acceptor [2]Rotaxanes. J. Org. Chem., 2017, 82 (12), 6341-6348.

[4] Kodama K., Kobayashi K., Hirose T. Synthesis and Spectral Properties of Ruthenium(II) Complexes based on 2,2'-Bipyridines Modified by a Perylene Chromophore. Tetrahedron Letters, 2013, 54(40), 5514-5517.

[5] Baron A., Herrero C., Quaranta H., Charlot M.-F., Leibl W., Vauzeilles B., Aukauloo A. Click Chemistry on a Ruthenium Polypyridine Complex. An Efficient and Versatile Synthetic Route for the Synthesis of Photoactive Modular Assemblies. Inorg. Chem., 2012, 51, 5985-5987.

[6] Bordoli R. J., Goldup S. M. An Efficient Approach to Mechanically Planar Chiral Rotaxanes. J. Am. Chem. Soc. , 2014 , 136 , 4817.

[7] Lewis J. E. M., R. Bordoli J., Denis M., Fletcher C. J., Galli M., Neal E. A., Rochettea E. M., Goldup S. M. High Yielding Synthesis of 2,2'-Bipyridine Macrocycles, Versatile Intermediates in the Synthesis of Rotaxanes. Chem. Sci., 2016, 7, 3154-3161.

[8] Aucagne, V.; Hanni, K. D.; Leigh, D. A.; Lusby, P. J.; Walker, D. B. Catalytic "Click" Rotaxanes: A Substoichiometric Metal-Template Pathway to Mechanically Interlocked Architectures. J. Am. Chem. Soc. 2006, 128, 2186.

[9] Bakka T. A., Strøm M. B., Andersen J. H., Gautun O. R. Synthesis and Antimicrobial Evaluation of Cationic Low Molecular Weight Amphipathic 1,2,3-Triazoles. Bioorganic & Medicinal Chemistry Letters, 2017, 27(5), 1119-1123.

[10] Berná J., Goldup S. M., Lee A.-L., Leigh D. A., Symes M. D., Teobaldi G., Zerbetto F. Cadiot-Chodkiewicz Active Template Synthesis of Rotaxanes and Switchable Molecular Shuttles with Weak Intercomponent Interactions. Angew. Chem. Int. Ed., 2008, 47, 4392-4396.

[11] Tang L. L., Qi, Z. J., Hong M. X., Li N., Shen W., Yang F., Ji X., Hu A J. Comparison Study of Oxygen Quenching of Ru(II) Phenanthroline Complexes with Different Functional Groups. Huaxue Xuebao, 2012, 70(9), 1081-1087.

[12] Hua Y. R., Ramabhadran R. O., Uduehi E. O., Karty J. A., Raghavachari K., Flood A. H. Aromatic and Aliphatic CH Hydrogen Bonds Fight for Chloride while Competing Alongside Ion Pairing within Triazolophanes. Chem. Eur. J., 2011, 17, 312- 321.

[13] Lewis J. E. M., Winn J., Cera L., Goldup S. M. Iterative Synthesis of Oligo[n]rotaxanes in Excellent Yield. J. Am. Chem. Soc., 2016, 138, 16329-16336.

Annexes

Abbreviations

ACMMs	Artificial Constructed Molecular Machines
AT-CuAAC	Active Template Cu-mediated Alkyne-Azide Cycloaddition reaction
BBr_3	Boron Tribromide
bpy	2,2'–bipyridine
CuAAC	Copper(I)-Catalyzed Terminal Alkyne-Azide Cycloaddition
CB[n]	Cucurbit[n]uril
$CBPQT^{4+}$	Cyclobis(paraquat-p-phenylene)
α-CD	Cyclodextrin
DAA	Dialkylammonium
DB24C8	Dibenzo-24-crown-8 macrocycle
DBA	Dibenzylamine
EET	Electronic Energy Transfer
FRET	Förster Resonance Energy Transfer
GPC	Gel Permeation Chromatography
HOMO	Highest Occupied Molecular Orbital
HRMS	High Resolution Mass Spectrometry
IC	Vibrational Relaxation
ICD	Induced Circular Dichroism Spectrum
ISC	Intersystem Crossing
LUMO	Lowest Unoccupied Molecular Orbital
MIMs	Mechanically Interlocked Molecules
MLCT	Metal-to-Ligand Charge Transfer
MTA	Methyltriazolium
NMR	Nuclear Magnetic Resonance Spectra
REET	Reversible Electronic Energy Transfer
S_0	Singlet State
T_1	Triple State
TEA	Triethylamine
TsCl	4-Toluenesulfonyl Chloride
ΔE	Energy Difference
QY (Φ)	Quantum Yield

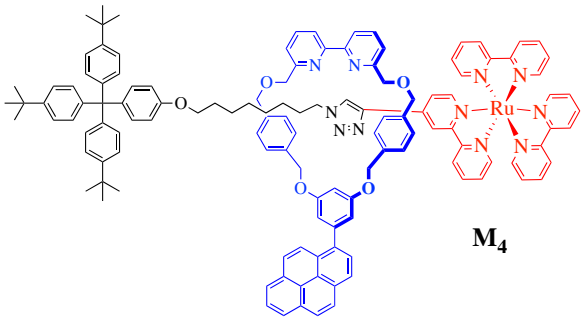

M$_4$

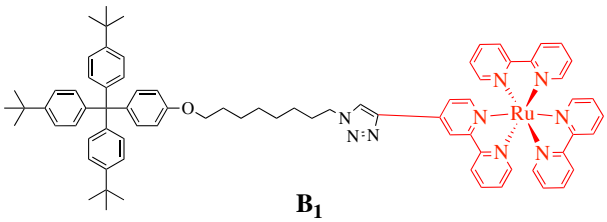

B$_1$

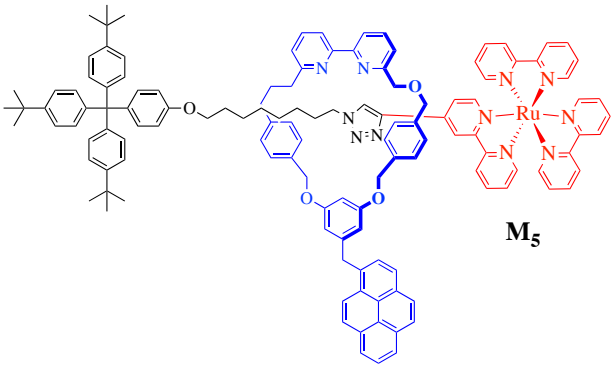

M$_5$

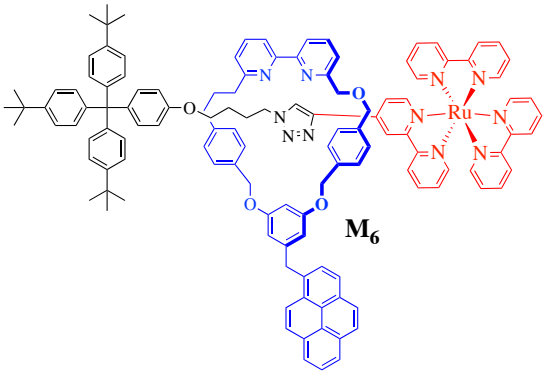

M$_6$

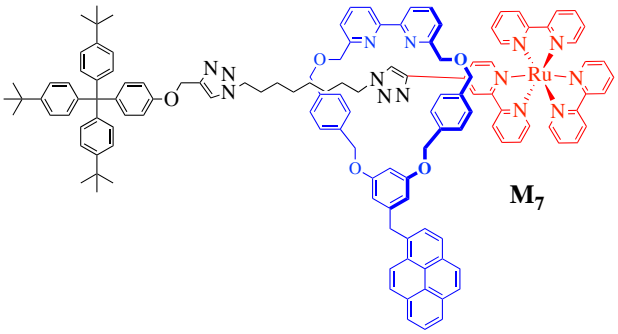

M$_7$

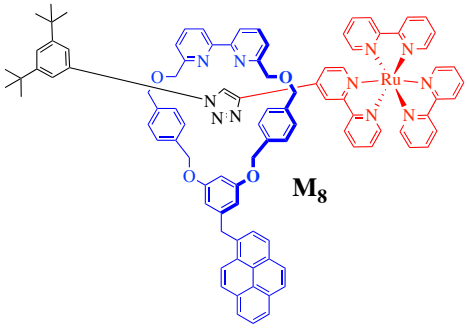

M$_8$

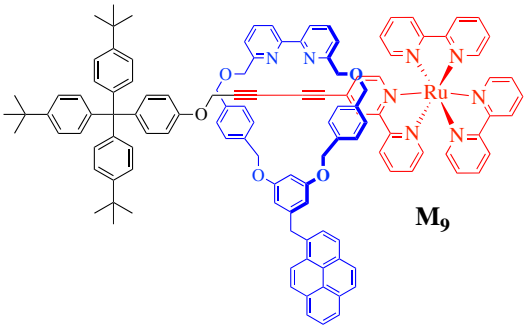

M$_9$

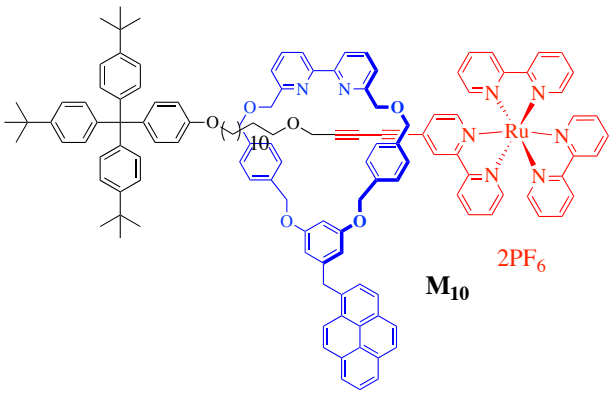

M$_{10}$ $2PF_6$

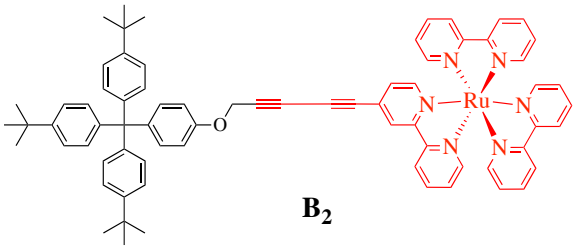

B_2

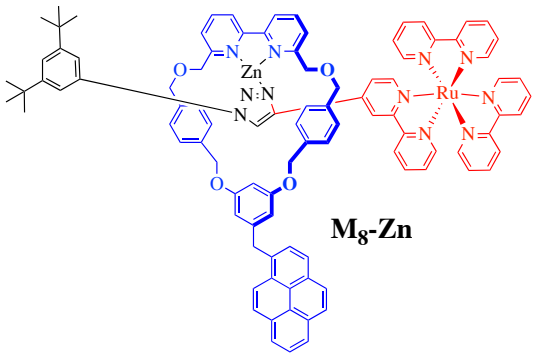

M_8-Zn

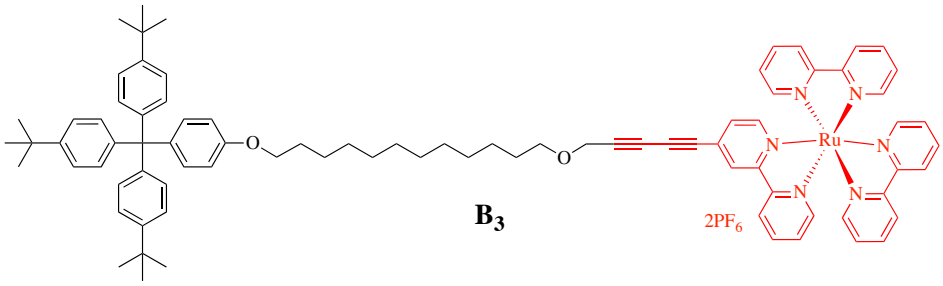

B_3

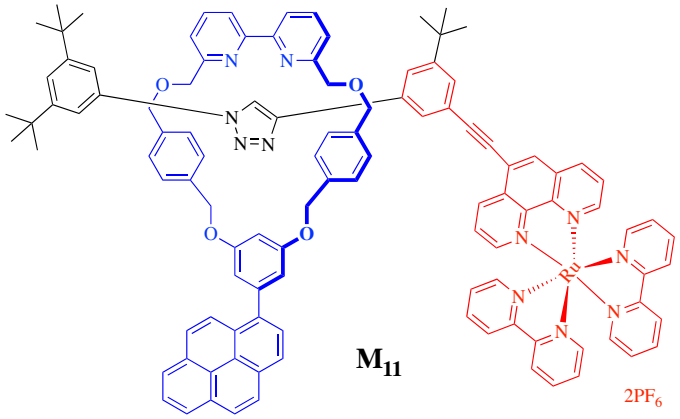

M_{11}

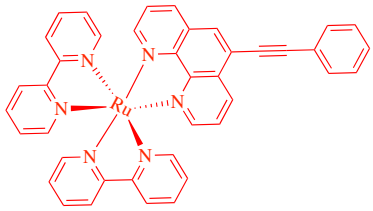

B_4

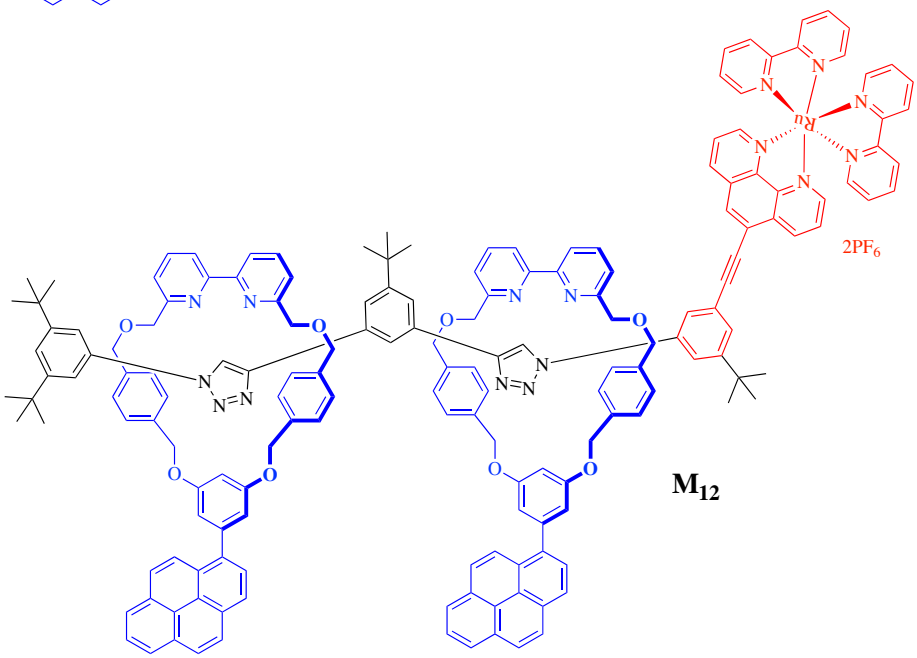

M_{12}

Résumé de thèse:

Transfert Réversible d'Energie Electronique au sein d'Architectures de Type Rotaxane

Shilin Yu

1 Introduction

1.1 Introduction de l'architecture rotaxane

La chimie supramoléculaire est un domaine assez récent de la recherche en chimie. Les concepts de chimie supramoléculaire, ou plus spécifiquement les interactions hôte-invité, ont d'abord été décrits pour expliquer certains phénomènes biologiques. Ce type d'approche a commencé à émerger comme nouveau domaine d'étude à la fin des années 1960 et a été reconnu par le grand public suite au prix Nobel décerné en 1987 à trois de ses pionniers, Donald J. Cram, Jean-Marie Lehn et Charles J. Pedersen, «Pour leur développement et leur utilisation de molécules présentant des interactions spécifiques à la structure de haute sélectivité, récompensées pour la synthèse de molécules mimant d'importants processus biologiques». La chimie supramoléculaire vise à étudier les structures, les fonctions et les propriétés de ces entités chimiques [1]. Pour cela elle prend en compte deux ou plusieurs entités chimiques, qui se combinent par des interactions moléculaires et deviennent une entité chimique hautement sophistiquée et bien organisée. Leur principale caractéristique est que tous les composants se combinent par des interactions moléculaires non covalentes. Comme le dit Lehn, l'interaction entre les molécules en chimie supramoléculaire est comme les atomes et les liaisons covalentes dans la molécule. Il a décrit la chimie supramoléculaire comme une «chimie au-delà de la molécule» [2].

Avec le développement de la chimie supramoléculaire, le domaine des machines moléculaires construites artificiellement et basées sur l'auto-assemblage supramoléculaire a

beaucoup attiré l'attention au cours des dernières décennies. Le discours fondateur de Richard Feynman (Prix Nobel de physique) intitulé «There's plenty of room at the bottom» au California Institute of Technology en 1959 [3] a incité les scientifiques à utiliser une approche ascendante pour construire des machines nanométriques avec des atomes ou molécules, au lieu d'utiliser une approche de miniaturisation descendante traditionnelle. Alors qu'avant ce discours, les moteurs et les machines moléculaires se trouvaient déjà dans toute une gamme de processus biologiques: l'exploitation de l'énergie solaire, le stockage de l'énergie, le transport ionique dans la cellule [4]. De plus en plus de chimistes se consacrent à la recherche de constructions artificielles de machines moléculaires pour des applications biologiques ou médicales. Le fort intérêt potentiel dans ce domaine s'est concrétisé par le prix Nobel de chimie attribué conjointement en 2016 à Jean-Pierre Sauvage, Sir J. Fraser Stoddart et Bernard L. Feringa «pour la conception et la synthèse de machines moléculaires». Les machines moléculaires sont de taille nanoscopique (1-100 nm). Il s'agit typiquement d'un assemblage moléculaire associant deux composants (ou plus) par des interactions de liaison non covalentes ou des liaisons covalentes réversibles. Un assemblage moléculaire pourrait produire un mouvement mécanique (sortie) comme des machines macroscopiques, en réponse à un stimulus externe approprié (entrée). Les mouvements mécaniques entraînent souvent des changements physiques ou chimiques dans le système et certains signaux peuvent être détectés pour effectuer des recherches sur le mouvement de la machine moléculaire. À l'heure actuelle, l'étude des machines moléculaire comprend principalement:

1. types de stimulus externes qui font fonctionner ou déclenchent des machines moléculaires;
2. types de mouvements relatifs des composants de la machine moléculaire;
3. méthodes pour détecter ou contrôler les mouvements relatifs des composants;
4. différentes méthodes de synthèse de machines moléculaires;
5. fonctions des machines moléculaires;
6. approches du calcul avec des machines moléculaires.

Les machines moléculaires artificielles sont généralement basées sur des molécules à verrouillage mécanique, telles que les rotaxanes, comme représenté sur la figure I. Les rotaxanes comprennent un composant en forme d'anneau et un composant en forme d'haltère, qui pénètre dans la cavité interne du composant en forme d'anneau. Deux bouchons aux extrémités du composant en forme d'haltère empêchent la dissociation de l'anneau du fil. Sous un stimulus spécifique externe, le composant annulaire peut avancer / reculer le long du fil du composant en forme d'haltère, sans séparation.

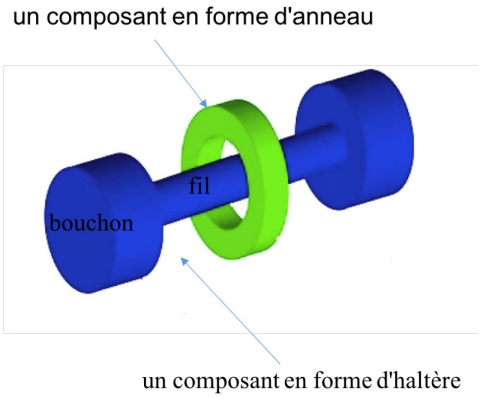

Figure I. Schematic representation of mechanically-interlocked rotaxane molecules.

1.2 Une courte introduction du processus transfert d'énergie electronique réversible

En revanche, dans un système moléculaire bichromophorique, lorsque les états excités les plus bas en énergie sur les deux chromophores sont quasi-isoénergétiques ($\Delta E \leq 5$ kT) et que la distance interchromophore est suffisamment courte, un transfert d'énergie électronique réversible (TEER) peut se produire entre chromophores. [5] Le processus TEER est illustré en utilisant des chromophores pyrène et un complexe Ru^{2+} comme exemple (Fig. II): lors de la photoexcitation, l'état ^{1}MLCT est initialement peuplé; puis, sur l'échelle temporelle inférieure à la picoseconde, un changement de spin électronique se produit en peuplant l'état excité: ^{3}MLCT, qui est énergétiquement plus stable. Si l'écart énergétique entre les chromophores ≤ 5 kT et la distance interchromophore est suffisamment court, il se produit un transfert d'énergie électronique entre ^{3}MLCT et le triplet pyrène. La distribution moyenne pondérée de l'énergie entre chaque chromophore et les taux de décroissance des chromophores intrinsèques régit la durée de vie observée, selon l'équation 1 (τ_{Ru}: durée de vie de l'émission MLCT; τ_{pyr}: durée de vie de l'émission pyrène-fragment α: pourcentage d'énergie résidant sur le complexe Ru^{2+}.

$$\frac{1}{\tau} = \alpha \left(\frac{1}{\tau_{Ru}}\right) + (1 - \alpha) \left(\frac{1}{\tau_{pyr}}\right) \qquad \text{Equation 1}$$

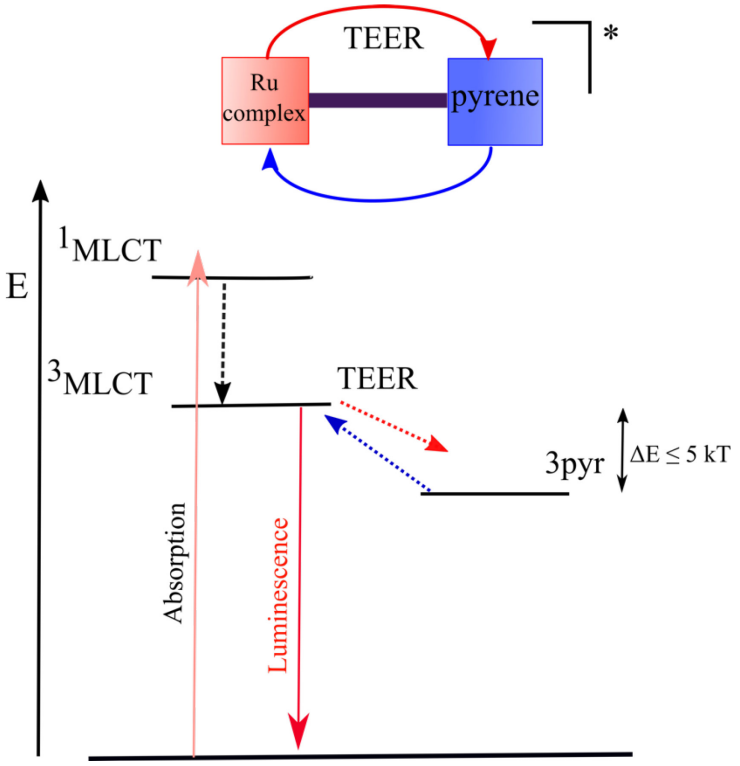

Figure II. Représentation schématique du transfert d'énergie électronique réversible entre le complexe Ru^{2+} et le fragment pyrène.

Le transfert d'énergie électronique peut prolonger la durée de vie de la luminescence, changer la nature de l'état excité. Les processus TEER, dans le cadre des études de photochimie, ont été bien étudiés dans les dyades covalentes. Cependant, peu d'exemples de processus TEER ont été trouvés dans les systèmes supramoléculaires, en particulier dans les systèmes rotaxane. À travers cette thèse, les principaux objectifs sont de concevoir et de construire des systèmes rotaxane conçus avec des processus de transfert d'énergie électronique réversibles. Les principaux résultats de cette thèse sont généralisés dans les sections suivantes:

2 Prototype [2]rotaxanes conçus avec des procédés de transfert d'énergie électroniques réversibles

Le chapitre 2 porte sur l'établissement de processus TEER dans les architectures rotaxanes. « Active metal template synthesis » ou le métal joue le rôle double de catalyseur et agent structurant (réactions de Huisgen et Cadiot-Chodkiewicz) est choisie pour la formation du rotaxane. Dans ce scénario, l'ion métallique, qui est le cuivre dans le cas présent, garantit que

la réaction de couplage se produit au sein de la cavité macrocyclique. Le pyrène et le ruthénium (II) tris(bipyridine) ont été choisis afin que les dyades bichromophores puissent établir un processus REET, offrant des niveaux énergétiques et une cinétique appropriés. Tout d'abord, comme le montre la figure III, un complexe **P1** de $Ru(bpy)_3^{2+}$ fonctionnalisé par un alcyne, en tant que bouchon et groupe de donneurs de processus REET, a été synthétisé; deux groupes trityles fonctionnalisés par des azotures classiques en tant que bouchon ont été choisis; une stratégie de synthèse de macrocycles **R1**, **R2**, **R3**, **R4** contenant des bipyridines avec un groupe pyrène a été conçu. Deux macrocycles de pyrène symétriques (phénylpyrène **R3** et méthylène pyrène **R4**) se sont avérés être de bons candidats pour la formation de rotaxanes par réactions AT-CuAAC ou Cadiot-Chodkiewicz.

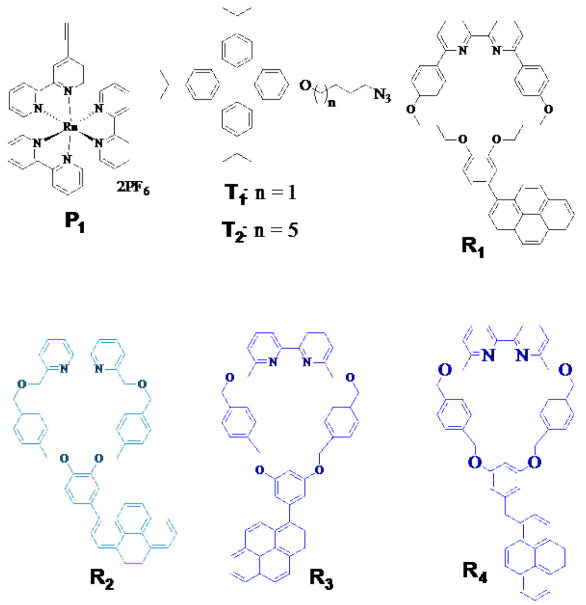

Figure III. Structures des demi-fils **P1&Tn** et macrocycles **R1&R2&R3&R4**.

Deux rotaxanes (**M4**, **M5**) et le fil **B1** ont été synthétisés avec succès, comme le montre la figure IV. Les déclins de luminescence ont clairement montré que les durées de vie de luminescence MLCT étaient considérablement prolongées, et des processus de transfert d'énergie électronique réversible et sans précédent ont été instillés dans les rotaxanes. Il est à noter que la durée de vie de luminescence MLCT (14 µs) de **M4** était beaucoup plus longue que celle (5,6 µs) de **M5**, ceci étant attribué en grande partie aux différents écarts énergétiques de ^{3}MLCT-**M4** vs ^{3}pyr-**R3** et ^{3}MLCT-**M5** vs ^{3}pyr -**R4**.

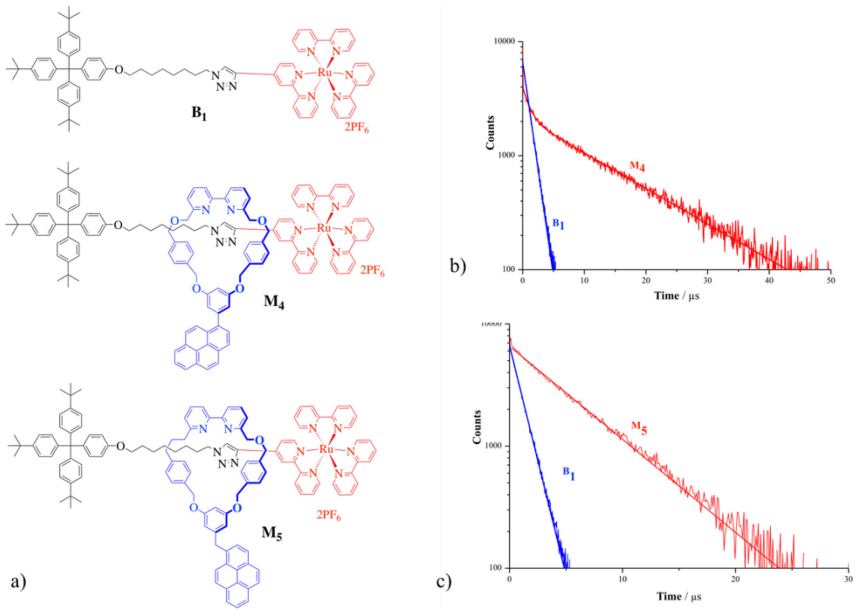

Figure IV. a) Structures des rotaxanes **M4**&**M5** and thread **B1**; Déclins de luminescence de b) Rotaxane **M4** & fil **B1**; c) Rotaxane **M5** & fil **B1** (λ_{ex} = 450 nm, λ_{em} = 620 nm) dans le MeCN dégazé.

3. TEER dans les navettes moléculaires avec des natures de fils variables

3.1 TEER dans les navettes moléculaires synthesisées par AT-CuAAC

Dans le chapitre 3, la relation entre les processus REET et les mouvements de navette du macrocycle sur les fils dans les rotaxanes a été étudiée. AT-CuAAC a fourni trois rotaxanes REET (**M6**, **M7**, **M8**) basés sur le macrocycle **R4** avec différentes longueurs de fil, comme le montre la figure V. Ces rotaxanes ont été étudiés en utilisant des spectres de RMN, des spectres spectroscopie à l'état stable. Les déclins de luminescence de ces rotaxanes ont montré: **M8** partageait une durée de vie de luminescence légèrement plus longue (τ = 6,3 µs); **M5** et **M6** ne présentaient aucune différence (τ = 5,6 µs); 11% des parties de **M7** n'ont pas donné de processus REET (τ = 1,2 µs = τ_{B1}), 89% des parties partageaient la plus longue durée de vie de la luminescence (τ = 5,6 µs). Ces résultats montrent que le pyrène reste proche de la fraction Ru^{2+}, suggérant qu'il n'y a pas de mouvements de navette de l'anneau sur les fils de quatre rotaxanes différents (**M5** - **M8**).

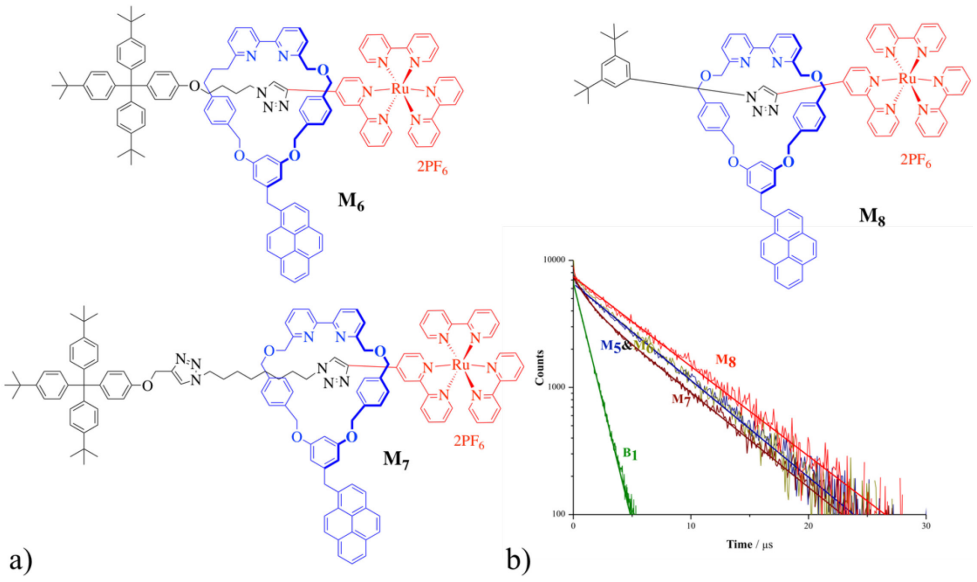

Figure V. a) Structures des rotaxanes **M6**-**M8**; b) Déclins de luminescence de rotaxanes **M5**-**M8** et fil **B1**.

3.2 TEER dans les navettes moléculaires synthesizé par AT-CuAAC Cadiot-Chodkiewicz

Deux autres rotaxanes possédant un processus REET, **M9** et **M10** comprenant une liaison diyne avec différentes longueurs de fil ont également été construits par une réaction de Cadiot-Chodkiewicz qui en premet le contrôle et ont été étudiés en utilisant les spectroscopies stationnaire et résolue dans le temps. Les déclins de luminescence ont montré: l'établissement à 100% de processus REET avec une durée de vie moyenne de 3,6 µs dans **M9**; 34% de **M10** présentaient une émission de MLCT avec une durée de vie de luminescence de 1,7 µs, qui est égale à celle du fil libre **B2**, et la partie restante présentait une durée de vie moyenne de 3,6 µs. Ces résultats impliquent que les rotaxanes de type Cadiot sont prometteurs dans le suivi du mouvement des anneaux avec les processus TEER.

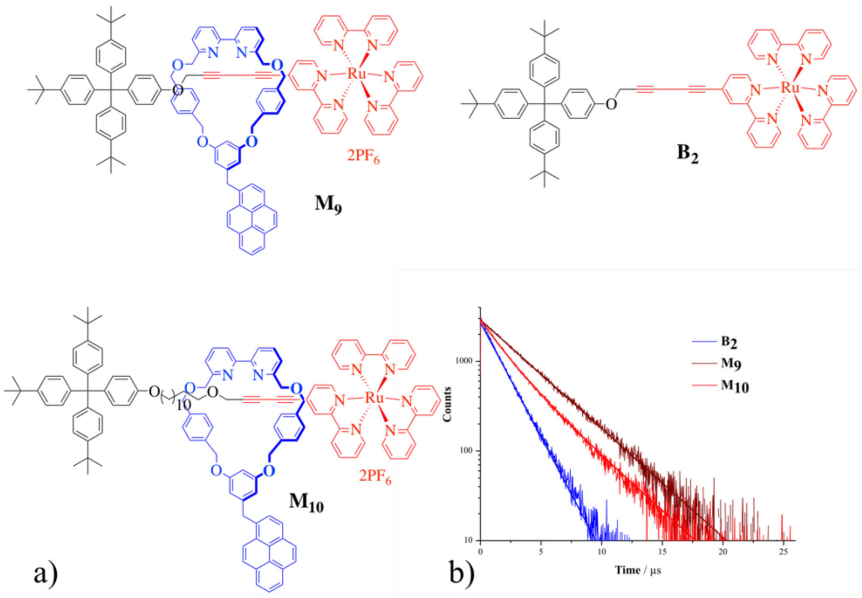

Figure VI. a) Structures des rotaxanes **M9&M10** et fil **B2**; b) Déclins de luminescence des rotaxanes **M9&M10** et fil **B2**.

4 REET Rotaxanes Comme Ligands Chélatants & Transfert d'Énergie Electronique Linéaire

4.1 REET rotaxanes comme ligands chélatants

Rotaxane **M8** a été choisi comme ligand chélatant pour étudier comment les propriétés photophysiques d'un rotaxane montrant REET changent par la coordination avec un ion métallique. La coordination entre Zn^{2+} et **M8** a été étudiée par spectres de RMN, spectres d'absorption électronique, spectroscopies stationnaire et résolue dans le temps. Le résultat a montré que **M8**-Zn^{2+} présentait une durée de vie de luminescence beaucoup plus courte (1,7 µs) que le rotaxane **M8**, que l'intensité de luminescence était augmentée, que les processus REET étaient grandement influencés. Le pyrène dans **M8**-Zn^{2+} ne peut pas agir comme un réservoir d'énergie efficace car la perturbation induite par les ions de l'énergie de ^{3}MLCT entraîne une discordance des états de triplet les plus bas en énergie. Le changement optique induit par la complexation résultant peut être utilisé pour la détection optique d'analytes sur différentes durées de luminescence par modulation des niveaux d'énergie relative du donneur et de l'accepteur d'énergie ou par variations d'intensité dues à une sensibilité réduite au dioxygène.

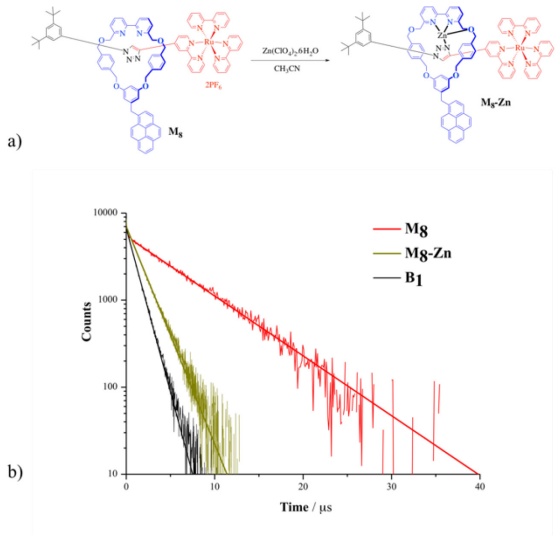

Figure VII. a) Illustration de la coordination entre le Zn^{2+} et **M8**; b) Déclins de luminescence des rotaxanes **M8**&**M8**-Zn^{2+} et fil **B1**.

4.2 Transfert d'Énergie Electronique Linéaire Réversible au sein des Rotaxanes

Une approche vers l'étude de sauts d'énergie électronique réversible linéaire avec un nombre variable d'accepteurs à distance fixe dans les systèmes rotaxane est envisagée. [2]Rotaxane **M11** et [3]rotaxane **M12** (Fig. VII) ont été conçus et synthétisés avec succès. Les études spectroscopiques ont prouvé que le processus REET était instillé dans **M11** avec une durée de vie de luminescence bien prolongée de 35,6 μs. Par la suite, des expériences photophysiques détaillées et une modélisation cinétique seriont réalisées sur [3]rotaxane **M12**.

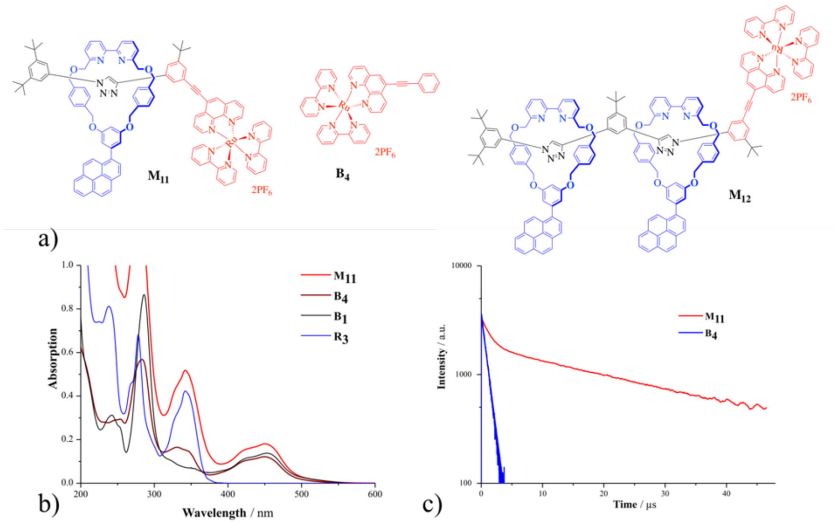

Figure VIII. a) Structures des rotaxanes **M11&M12** et fil **B4**; b) Spectres d'absorption électronique de **M11**, **B1**, **B4** et **R3** dans l'acetonitrile; c) Déclins de luminescence de **M11** et **B2**.

5 Conclusions

En résumé, le processus REET a d'abord été introduit dans les systèmes rotaxane et les possibilités de suivre le mouvement des anneaux par les processus REET dans les navettes moléculaires ont été principalement étudiées. La coordination entre le [2]rotaxane montrant REET et le Zn^{2+} a légèrement modifié les états excités MLCT et influencé de manière spectaculaire les processus REET et réponse optique. Des rotaxanes REET plus sophistiqués ont été conçus et construits ou sont en cours de réalisation. Les recherches ouvrent la voie à des systèmes multicomposants plus performants et étendent les applications de la photochimie aux architectures rotaxanes.

Références

[1] Lehn J. M. Supramolecular Chemistry: Concepts and Perspectives. Wiley-VCH: Weinheim, 1995.

[2] Lehn J. M. Nobel Lecture. December 8, 1987.

[3] Feynman, R. P. Eng. Sci., 1960, 23, 22.

[4] Noji, H.; Yasuda, R.; Yoshida, M.; Kinosita Jr, K. Direct Observation of the Rotation of F_1-ATPase. Nature, 1997, 386, 299.

[5] Praveen V. K., Ranjith C., Bandini E., Ajayaghosh A., Armaroli N. Oligo(phenylenevinylene) Hybrids and Self-assemblies: Versatile Materials for Excitation Energy Transfer. Chem. Soc. Rev., 2014, 4222–4242.